

Emilio Chuvieco
Editor

Earth Observation of Global Change

*The Role of Satellite Remote Sensing in
Monitoring the Global Environment*



Springer



Earth Observation of Global Change

Earth Observation of Global Change

The Role of Satellite Remote Sensing
in Monitoring the Global Environment

Emilio Chuvieco
Editor

Department of Geography, University of Alcalá, Spain



Springer

Editor

Emilio Chuvieco
Department of Geography
University of Alcalá
Colegios 2, 28801, Alcalá
de Henares, Spain
emilio.chuvieco@uah.es

ISBN: 978-1-4020-6357-2 e-ISBN: 978-1-4020-6358-9

Library of Congress Control Number: 2007935798

© 2008 Springer Science + Business Media B.V.

No part of this work may be reproduced, stored in a retrieval system, or transmitted in any form or by any means, electronic, mechanical, photocopying, microfilming, recording or otherwise, without written permission from the Publisher, with the exception of any material supplied specifically for the purpose of being entered and executed on a computer system, for exclusive use by the purchaser of the work.

Cover Illustration: Synthetic image of the Earth generated from GOES, SeaWiFS and AVHRR data, as well as digital terrain information. This image was created by Reto Stockli with the help of Alan Nelson, under the leadership of Fritz Hasler. Laboratory for Atmospheres at NASA's Goddard Space Flight Center, Greenbelt, MD (Source: http://visibleearth.nasa.gov/view_rec.php?id = 174)

Printed on acid-free paper.

9 8 7 6 5 4 3 2 1

springer.com

*Then I saw a new heaven and a new earth.
The former heaven and the former earth had passed
away,
and the sea was no more (Apocalypse 21:1)*

Contents

1 International Efforts on Global Change Research	1
Beatriz Alonso and Fernando Valladares	
2 NASA Earth Observation Satellite Missions for Global Change Research	23
Emilio Chuvieco and Chris Justice	
3 The Role of the European Space Agency in Global Change Observations	49
Olivier Arino	
4 Ozone in the Atmosphere	59
Abel Calle and Jose Luis Casanova	
5 Remote Sensing of Land-Cover and Land-Use Dynamics	85
Philippe Mayaux, Hugh Eva, Andreas Brink, Frédéric Achard and Alan Belward	
6 Satellite Observation of Biomass Burning	109
Emilio Chuvieco	
7 Satellites Oceans Observation in Relation to Global Change	143
Manuel Cantón-Garbín	
8 Observing Surface Waters for Global Change Applications	169
Richard G. Lawford	
9 Remote Sensing of Terrestrial Snow and Ice for Global Change Studies	189
Richard Kelly and Dorothy K. Hall	
Index	221
CD–Rom included inside back cover	

Preface

The earth environment has always been affected by change, since all forces interacting to shape world landscapes are intrinsically dynamic. However, the pace of change varies widely between processes: from slow moving plate tectonics and erosion, to fast changing wind or temperature conditions. Considering phenomenon at the human time scale, weather and vegetation changes are the most noticeable. Along with temporal change, spatial variations are also evident over a range of scales from the very local to thousands of kilometres, depending on the process being considered.

Both temporal and spatial transformations are considered in terms of Global Change, although the expression has a broad range of meanings. Some authors use it as synonym of climatic change, while others refer to broad planetary changes, including human land use transformations. This latter sense has been used throughout this book, which includes both climate related changes, as well as direct human landscape conversion.

Concern about global change has greatly increased in the last two decades, and particularly in the last five years, when it has become a controversial issue in daily newspapers and other media. The impact of human activities on climate through extensive consumption of fossil fuels is a main factor of concern for decision makers, because of the economic and geopolitical implications. Other critical factors, such as tropical deforestation, biodiversity loss, water pollution or soil erosion are often less reported on, perhaps because they have a less direct impact on the developed economies. However, they are the most evident signals of global change, and are – unlike global warming- clearly beyond scientific dispute as to whether or not they are human caused.

The identification of any type of global change involves having the means to observe global environmental processes. To be confident that changes are occurring, a baseline and repeated observations are needed. This requires access to long-term and global data that are acquired systematically and calibrated enough to be fully comparable and capable of measuring long-term changes. Means of observing environmental processes are very diverse: weather probes, water gauges, vertical profile balloons, tree rings, pollen records, ice core drills, sediments fossils, etc. Satellite observation is particularly useful for the study of global change processes, since satellite data provide one of the most systematic ways of collecting data worldwide, in a fully comparable and repeatable way. For this reason, the use of satellite

observations in global change studies have been very significant in the last decades, from weather surveys and forecast to vegetation, ice and water monitoring.

This book aims to present the main contributions of satellite Earth Observation for the study of global-scale environmental processes. Although a great number of books have addressed the implications of global change, a small number have been focused on the means to monitor that change. Some previous books have used satellite images to display global processes, but few have dealt with analyzing the actual contribution of satellite images to global change projects, and the key global variables that can currently be derived from satellite data. This is the main purpose of this book.

The book should be useful to those studying global change processes, particularly those interested on how data are acquired and processed. The book has an environmental scope, and therefore should be valuable for a diverse collection of scientists, such as ecologist, geographers, foresters, land use planners, geologists, oceanographers, and physics.

The origin of this book was an international symposium on Earth Observation of Global Change that I organized in Madrid (Spain) in 2006, under the auspices of the Fundacion Areces and the Spanish Royal Academy of Sciences. The experts gathered there recognized the need of a textbook providing an overview on how satellite remotely sensed data have been used in different disciplines, from oceanography to land use, from forest fires to water, ice and snow. A review of current missions to observe global processes was also desirable, since information of space missions is much dispersed and needs critical assessment. A brief introduction to institutions and networks of scientist working on global change was also recommended. As a result of this interaction, the scheme of this book was finally agreed on.

We favored a textbook style, rather than a collection of specialized chapters. Therefore, the sections of the book were generally conceived to provide a state of the art review on the different topics, instead of just presenting everyone's own research on the field. The reader should judge if we succeeded in this comprehensive view. Since displaying satellite information in black and white limits their information content, a CD-ROM with color plates of the same figures has been attached to the book. The reader should find there additional material to explore actual applications of satellite data to global change studies.

We finally acknowledge the Fundacion Areces and the Spanish Royal Academy of Sciences for their support to organize the meeting, and the Springer editors for their favorable response to convert the presentations from that meeting into a textbook. We hope that the final result will be worth the effort, and will make a sound contribution to emphasizing the importance of global change studies, and particularly to the support of long-term satellite observations of global processes.

Emilio Chuvieco
College Park (1st April 2007)

Contributors

Frédéric Achard

Institute for Environment and Sustainability,
Joint Research Centre,
European Commission, TP 440; I-21020 Ispra
(VA); Italy
E-mail: frederic.achard@jrc.it

Beatriz Alonso

Instituto de Recursos Naturales,
Centro de Ciencias Medioambientales
(CSIC), Serrano 115 dpdo.
E-28006 Madrid
E-mail: beatriz.alonso@ccma.csic.es

Olivier Arino

ESA-ESRIN Data Users Program
Via Galileo Galilei
Casella Postale 64
00044 Frascati, Italy
E-mail: oliver.arino@esa.int

Alan Belward

Institute for Environment and Sustainability,
Joint Research Centre,
European Commission,
TP 440; I-21020 Ispra (VA); Italy
E-mail: alan.belward@jrc.it

Andreas Brink

Institute for Environment and Sustainability,
Joint Research Centre,
European Commission,
TP 440; I-21020 Ispra (VA); Italy
E-mail: andreas.brink@jrc.it

Abel Calle

LATUV – Edificio I+D
Paseo de Belén 1
47005 Valladolid, Spain
E-mail: abel@latuv.uva.es

Manuel Cantón-Garbín

Dpto. De Lenguajes y Computación,
Universidad de Almería.
04120 Almería, Spain
E-mail: mcanton@ual.es

Jose Luis Casanova

LATUV – Edificio I+D
Paseo de Belén 1
47005 Valladolid, Spain
E-mail: jois@latuv.uva.es

Emilio Chuvieco

Department of Geography,
University of Alcalá,
Colegios 2, 28801, Alcalá
de Henares, Spain
E-mail: emilio.chuvieco@uah.es

Hugh Eva

Institute for Environment and Sustainability,
Joint Research Centre,
European Commission,
TP 440; I-21020 Ispra (VA); Italy
E-mail: hugh.eva@jrc.it

Dorothy K. Hall

Hydrospheric and Biospheric Processes
Laboratory, NASA Goddard Space
Flight Center, Greenbelt, Maryland,
20771, USA
E-mail: dorothy.k.hall@nasa.gov

Chris Justice

Department of Geography, University
of Maryland, 2181 Lefrak Hall,
College Park, MD 20742, USA
E-mail: justice@hermes.geog.umd.edu

Richard Kelly

Department of Geography, University
of Waterloo, Waterloo, Ontario,
Canada, N2L 2W1
E-mail: rejkelly@fes.uwaterloo.ca

Richard G. Lawford

Director, International GEWEX Project
Office, 1010 Wayne Avenue,
Suite 450, Silver Spring, Maryland 20910
E-mail: gewex@gewex.org
and lawford@umbc.edu

Philippe Mayaux

Institute for Environment and Sustainability,
Joint Research Centre,
European Commission,
TP 440; I-21020 Ispra (VA); Italy
E-mail: philippe.mayaux@jrc.it

Fernando Valladares

Instituto de Recursos Naturales, Centro
de Ciencias Medioambientales
(CSIC), Serrano 115 dpdo. E-28006 Madrid
E-mail: valladares@ccma.csic.es

Chapter 1

International Efforts on Global Change Research

Beatriz Alonso and Fernando Valladares

1.1 Global Change: An Overview

The Earth's environment is a dynamic system including many interacting components (physical, chemical, biological and human) that are constantly changing. The interactions and feedbacks among these components are complex and register high variability in time and space. Changes have always been present within the functioning of our planet. But during the last decades, human activities have produced an important impact in the Earth system (land surface, oceans, coasts, atmosphere, biological diversity, water cycle and biogeochemical cycles) causing changes well beyond natural variability (Vitousek 1992, Foley et al. 2005, Levitus et al. 2000). And the magnitude of these changes is increasing throughout the years due to the growth of the population and the extension in scale of activities such as industry or agriculture. Over the past 50 years, the ecosystems have been modified by humans more rapidly and extensively than in any other comparable time period. Since 1950, more land has been converted to cropland than between 1700 and 1850, so approximately a quarter of the Earth's terrestrial surface is currently occupied by cultivated systems; in the last decades it is estimated that about 20% of the world's coral reefs were lost and 20% were degraded; since 1960 the amount of water stored behind dams is four times bigger (Millennium Ecosystem Assessment 2005). And these are just some examples. These changes have contributed to an economic development in some regions of our planet, but it has been achieved with a parallel degradation of many ecosystem services, an increase of the risks of nonlinear changes (e.g.: disease emergence, species losses) and the intensification of poverty in some other regions. (Millennium Ecosystem Assessment 2005).

Although global change is now a big issue of international concern, scientists have been interested on it for over a hundred of years. As early as 1827, Fourier was the first who compared the atmosphere functioning to a greenhouse. Some years later, Tyndall discovered the main so-called "greenhouse gases" (GHGs) and proposed a relationship between their concentration and past changes in the climate (O'Neill et al. 2001). And finally in 1896, Arrhenius predicted the potential of CO₂ to alter the climate, as it has been proved today (Arrhenius 1896, Hansen et al. 2005, Harries et al. 2001).

In spite of the growing concern over the last climate change evidences, global change is not restricted to climate, nor can it be understood in terms of a simple cause-effect process. Actually, the most important direct drivers of change are five: habitat change, overexploitation, invasive species, pollution, and climate change (Millennium Ecosystem Assessment 2005). And each of them has a different effect and trend in each specific ecosystem (Fig. 1.1).

The concept of global change brings together a big spectrum of changes suffered by the Earth's ecosystems. But they have basically three characteristics in common. First, they have an anthropogenic origin. Second, they have an exponential increase rate (Fig. 1.2). And finally they occur in a global scale (Fig. 1.3).

The assessment of the consequences of each separate driver of change in the ecosystems becomes difficult due to the fact that they interact with each other and are affected by feedbacks from the ecosystem impacts (Vitousek 1992). For example, land use change is the most important cause of species loss, but the loss of diversity itself can produce effects on land use (Ehrlich and Wilson 1991). Time scale is also an additional complex factor that must be taken into account to

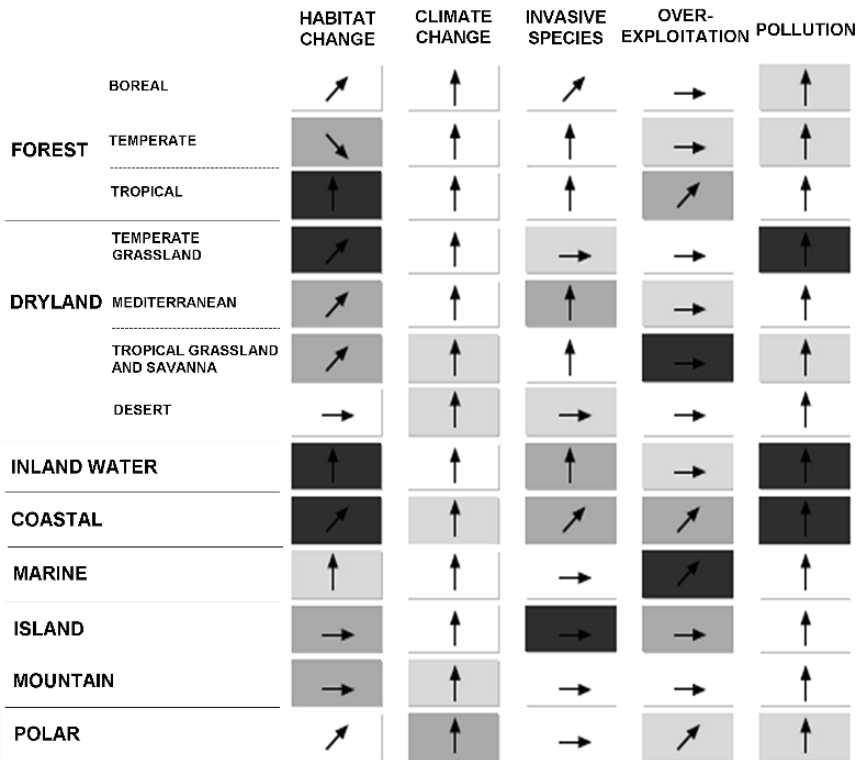


Fig. 1.1 Main direct drivers of global change in main ecosystem types. The grey scale represents the importance of the impacts on biodiversity over the last century in each ecosystem type (dark being large impact) and arrows indicate the temporal trend of these impacts. Source: Millennium Ecosystem Assessment 2005

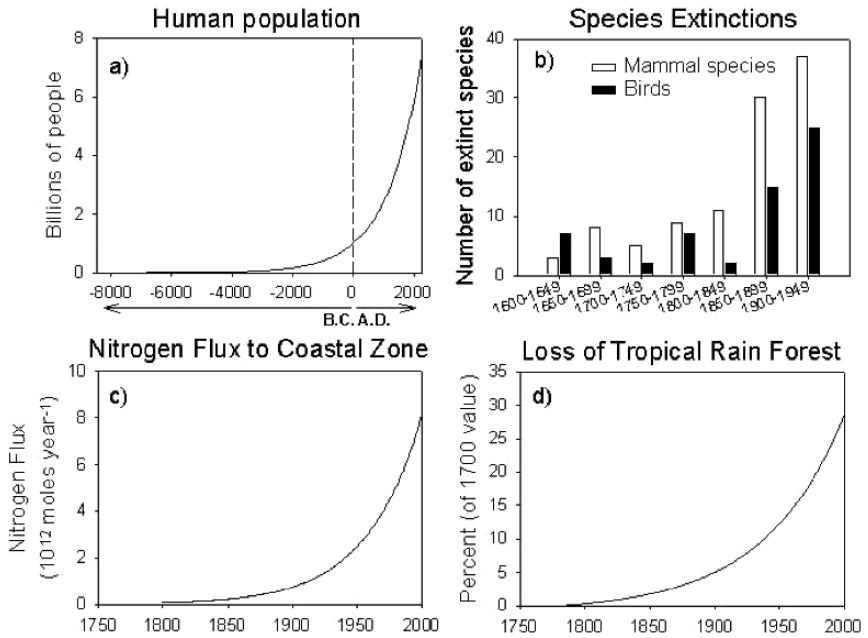


Fig. 1.2 Examples of global changes with exponential increase rates: a) Human population (International Database, U.S. Bureau of Census) b) Species extinctions (Reid and Miller 1989) c) Nitrogen flux to coastal zones (Mackenzie et al. 2002) d) Loss of tropical rain forest (Richards 1991)

evaluate and understand global change (Vitousek 1992). An increase or decrease in a parameter can be considered as a punctual discontinuity or as a trend according to the length of the event. Equally, the drivers of change can produce direct and immediate ecosystem responses but also direct and indirect effects on the long term.

Global change is one of the greatest challenges that humanity faces today. The increasing human transformation of the environment is not sustainable and new strategies for its management are urgently required. Policy makers need a good understanding of the global system to be able to take good decisions. And to get this knowledge it is essential to implement a new research approach based on two key concepts. First of all, multidisciplinary; it is indispensable a greater integration across disciplines and a closer contact among specialists from different fields in order to understand the complex behaviour of our planet's environment. Second, long-term perspective; observations in the long term are essential to interpret the experimental results, to analyse the behaviour of models and to propose hypotheses about the effects and trends of global change. Following these principles, numerous efforts have been invested throughout the last decades and ecologists have had to change their traditional focus on organisms, to study the Earth as an integrated ecosystem (Schlesinger 2006).

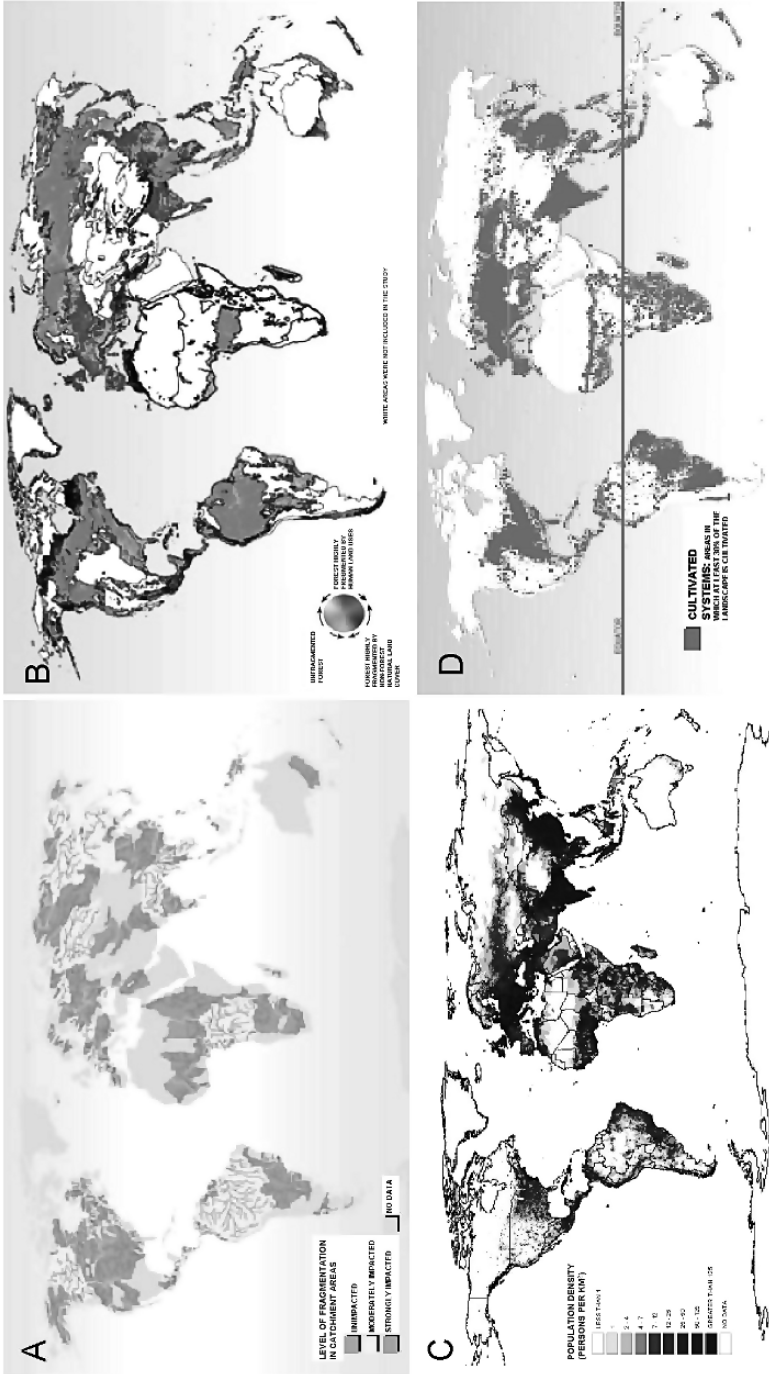


Fig. 1.3 Examples of the large spatial scale of human activity impacts. A) Impact due to water flow regulation and river channel fragmentation of the main river systems (Source: CBD 2006). B) Forest fragmentation with anthropogenic origin (Source: CBD 2006). C) Global population density (Source: WRI 2000 based on CENSIN 2000). D) Terrestrial surface covered by cultivated systems in 2000 (Source: Millennium Ecosystem Assessment 2005)

1.2 The Time Dimension of Global Change and the Notion of “Long term”

Our perception of a given phenomenon is directly related to the scale in space of the ecosystem that we are taking into account. This perception is also different if a variable is analysed just at one specific moment or if the same variable is monitored throughout a period of time. Ecologists agree that carrying out long-term experiments is the only way to detect trends and to make predictions for the future. But what is exactly considered as “long term”? There is not only one answer to this question. Actually, the notion of “long term” will depend on the behaviour of the process we are interested to study. This concept may be easier to understand if we think of one of the global change drivers as for example climate. It is well known that the structure and the functioning of the ecosystems are largely determined by the regularities of our planet’s climate (Parmesan et al. 2000). But this climate regularity suffers frequent nonlinear changes that gives more complexity to the system and introduces uncertainty in ecological research. For this reason, the assessment of how ecosystems respond to climate change depend strongly on the time scale (Greenland et al. 2003): effects will be different according to the type of climatic event and, at the same time, each type of climatic event will produce effects on the ecosystems that will last a different time in the future. From this point of view it is possible to classify them in the following four time scales:

- Short-term climatic events (e. g.: unusual repeated frequency of floods, hurricanes, drought conditions) that may produce important short and long-term ecosystem responses (Foster et al. 1998) determined also by the timing of the event (Gage 2003).
- The Quasi-Quintennial Timescale, a term used to recognize climatic events that reoccur every 2–7 years as for example the El Niño-Southern Oscillation (ENSO), phenomenon with a worldwide influence (Greenland 2003).
- The Interdecadal Timescale that includes patterns in the global circulation system occurring with recurring cycles (from 10 to 50 years). They are characterized by a variety of indexes as the Pacific Decadal Oscillation (PDO) or the North Atlantic Oscillation (NAO). They usually have a large spatial scale impact (McHugh and Gooding 2003).
- The Century to Millennial Timescale that includes long-term changes that have occurred over centuries (e.g. Little Ice Age) to thousands of years (e.g. Last Glacial Maximum) and that have shaped current ecosystems (Elias 2003).

It is uncommon that an ecosystem suffers the effects of climate variability at one determinate time scale. On the contrary, ecosystems are usually reacting to climate variability happening at several time scales (Greenland et al. 2003). Moreover, the overlapping of climate events at different time scales may reinforce their separate effects because of the possibility of interactions between them (Goodin et al. 2003).

Currently available information suggests that the only way to understand the patterns and behaviour of our planet's climate is trying to extend the scale on time and space of our observations and experiments (Greenland et al. 2003). And the same principle can be applied to the rest of global change drivers and to responses of the ecosystems to global processes as the increase of CO₂, nitrogen or ozone (Schlesinger 2006).

1.3 International Research in Global Change

It has been well proved that human activities are responsible for big impacts in the Earth's environment during the last decades (Rojstaczer et al. 2001, Postel et al. 1996) and all the predictions point out that the ecosystems will continue suffering serious changes during at least several more decades in the near future (Millennium Ecosystem Assessment 2005, IPCC 2001). Global change has thus become an issue of international concern and there is an increasing social interest in finding strategies to deal with it.

The classical science system has been characterised by the specialisation of researchers. Scientists have usually focused their efforts, knowledge and experience in very specific and concrete topics studied by very small groups of people around the world but with few links to other disciplines. The situation now is different. Researchers have realized the need for a science based on integration and cooperation in order to face the changes that our planet is experimenting. It is time to bring together contributions from natural scientists (ecologists, climatologists, oceanographers, etc.) as well as from social scientists (economists, anthropologists, sociologists) working at every spatial scale (Wessman 1992). This global approach has been possible with the help of new tools that allow the development of a better science, as for example the measurements of net carbon exchange of wide areas by the use of Eddy covariance methods (Schlesinger 2006, Ciais et al. 2005). In addition, the combination of tools such as geographic information systems, remote sensing technologies and simulation modelling has permitted to extrapolate information from individual organisms or processes observed at a given site to a regional or global scale (Roughgarden et al. 1991).

To advance in this new global perspective and communication level, the research community needs to be encouraged beyond the national boundaries on the basis of sharing data and infrastructure. And this is actually one of the main goals of several programmes and organizations involved in global change research (Table 1.1). Most of these programmes and organizations are often collaborating in joint projects and activities. But the exact objectives of all these initiatives and their interrelationships are sometimes unclear and difficult to understand particularly in a first approach or when a complete view of international efforts on global change is looked after. In order to clarify this "soup of acronyms" corresponding to all these programmes and organizations, the main activities in global change research will be reviewed in the next lines, grouped according to their activities.

Table 1.1 Programmes and organizations involved in global change research

ACRONYM	PROGRAMMES/ORGANIZATIONS	WEB SITE
AIACC	Assessment of impacts and Adaptation to Climate Change in Multiple Regions and Sectors	www.aiccproject.org
AIMES	Analysis, Integration and Modelling of the Earth System	www.aimes.ucar.edu
ALTERNET	A Long-Term Biodiversity, Ecosystem and Awareness Research Network	www.alter-net.info
APN	Asia-Pacific Network of Global Change Research	www.apn-gcr.org
BRIM	Biosphere Reserve Integrated Monitoring	-
CACGP	Commission on Atmospheric Chemistry and Global Pollution	http://croc.gsfc.nasa.gov/cacgp/
CAN	Climate Action Network	www.climnet.org
CEOS	Committee on Earth Observations	www.ceos.org
CLIC	The Climate and Cryosphere Project	http://clic.npolar.no/
CLICK	USGS Center for LIDAR Information Coordination and Knowledge	http://lidar.cr.usgs.gov/index.php
CLIVAR	Climate Variability and Predictability	www.clivar.org
CPWC	Co-operative Programme on Water and Climate	www.waterandclimate.org
DIVERSITAS	An International Programme of Biodiversity Science	www.diversitas-international.org
ENRICH	European Network for Research in Global Change	http://mediasfrance.org/Reseau/Lettre/09/en/Internat/enrich/enrich.html
ESSP	Earth System Science Partnership	www.essp.org
FAO	Food and agriculture Organization	www.fao.org
GAIM	Global Analysis, Interpretation and Modelling	http://gaim.unh.edu/
GBIF	Global Biodiversity Information Facility	www.gbif.org
GCOS	Global Climate Observation System	www.wmo.ch/web/gcos/gcoshome.html
GCP	Global Carbon Project	www.globalcarbonproject.org
GCRIO	US Global Change Research Information Office	www.gcrio.org
GECAFS	Global Environmental Change and Food Systems	www.gecafs.org
GEC&HH	Global Environmental Change and Human Health	-
GECHS	Global Environmental Change and Human Security	www.gechs.org
GEO	Global Earth Observations	www.earthobservations.org
GEOSS	Global Earth Observation System of Systems	http://www.epa.gov/geoss/
GEWEX	Global Energy and Water Cycle Experiment	www.gewex.org
GISP	The Global Invasive Species Programme	www.gisp.org
GOF-C-GOLD	Global Observation for Forest & Land Cover Dynamics	www.fao.org/gtos/gofc-gold
GLOBEC	Global Ocean Ecosystem Dynamics	www.globec.org
GLP	Global Land Project	www.globallandproject.org

(continued)

Table 1.1 (continued)

ACRONYM	PROGRAMMES/ORGANIZATIONS	WEB SITE
GMBA	Global Mountain Biodiversity Assessment	http://gmba.unibas.ch/index/index.htm
GOOS	Global Ocean Observing Systems	www.ioc-goos.org
GTOS	Global Terrestrial Observing Systems	www.fao.org/GTOS
GWSP	Global Water System Project	www.gwsp.org
IAI	Inter-American Institute for Global Change Research	www.iai.int
ICSU	International Council for Science	www.icsu.org
IDGEC	International Dimensions of Global Change Environmental Change	http://www2.bren.ucsb.edu/~idgec/
IGAC	International Global Atmospheric Chemistry	www.igac.noaa.gov
IGBP	International Geosphere-Biosphere Programme	www.igbp.net
IGFA	International Group of Funding Agencies for Global Change Research	www.igfagcr.org
IGOS	The Integrated Global Observing Strategy	www.igospartners.org
IHDP	International Human Dimensions Programme on Global Environmental Change	www.ihdp.org
ILEAPS	Integrated Land Ecosystem-Atmosphere Processes Study	www.atm.helsinki.fi/ILEAPS
ILTER	The International Long Term Ecological Research Network	www.ilternet.edu
IMBER	Integrated Marine Biogeochemistry and Ecosystem Research	www.imber.info
IOC	Intergovernmental Oceanographic Commission	http://ioc.unesco.org/iocweb/index.php
IPCs	International Cooperative Programmes	www.unece.org/env/wge/icps.htm
IPCC	International Panel on Climate Change	www.ipcc.ch
IRI	International Research Institute for Climate Prediction	www.iri.columbia.edu
IT	Industrial Transformation	www.ihdp-it.org
IUCN	The World Conservation Union	www.iucn.org
JGOFS	Joint Global Ocean Flux Study	http://www1.whoi.edu/
LOICZ	Land Ocean Interactions in Coastal Zones	www.loicz.org
LUCC	Land Use and Cover Change	www.geo.ucl.ac-be/LUCC/
MAIRS	Monsoon Asia Integrated Regional Study	www.mairs-essp.org
MEA	Millennium Ecosystem Assessment	www.maweb.org
MRI	Mountain Research Initiative	http://mri.scnatweb.ch/
NASA	National Aeronautic and Space Administration	www.nasa.gov
NGDC	NOAA National Geophysical Data Center	www.ngdc.noaa.gov
NOAA	National Oceanic & Atmospheric Administration (U.S. Department of commerce)	www.noaa.gov
PAGES	Past Global Changes	www.pages.unibe.ch
PERN	Population Environment Research Network	www.populationenvironmentresearch.org/

(continued)

Table 1.1 (continued)

ACRONYM	PROGRAMMES/ORGANIZATIONS	WEB SITE
REDOTE	Spanish Long Term Ecological Research Network	www.redote.org
ROSELT	Long Term Ecological Monitoring Observatories Network	www.roselt-oss.org
SCOPE	Scientific Committee on the problems of the Environment	www.icsu-scope.org
SCOR	Scientific Committee on Oceanic Research	www.jhu.edu/~scor
SOLAS	Surface Ocean-Lower Atmospheric Study	www.solas-int.org
SPARC	Stratospheric Processes and their role in Climate	www.atmosph.physics.utoronto.ca/SPARC/index.html
START	System for Analysis, Research and Training	www.start.org
TBA	Tropical Biology Association	www.tropical-biology.org
UNEP	United Nations Environment Programme	www.unep.org
UNFCCC	UN Framework Convention for Climate Change	www.unfccc.int
USGS	U.S. Geological Survey	www.usgs.gov
US-LTER	The US Long Term Ecological Research Network	www.lternet.edu
WCRP	World Climate Research Programme	http://wcrp.wmo.int/
WMO	World Meteorological Organization	www.wmo.int
YHDR	Young Human Dimensions Researchers	www.ihdp.uni-bonn.de/html/initiatives/i-yhdr.html

1.4 Global Observing Systems

To understand the impact of human activities on the ecosystems it has long been recognized the need to obtain detailed data at a global scale (Sanderson et al. 2002). During the 1990s, the use of satellite technology applied to Earth observation made this goal more and more feasible. For this purpose, NASA and other agencies launched the Earth Observing System (EOS) satellites that are currently monitoring many of the characteristics of our planet like temperature or land cover (Schlesinger 2006). The analysis of this extensive data set allows for modelling and predictions that provide valuable information for decision making.

1.4.1 *The Integrated Global Observing Strategy (IGOS)*

The Integrated Global Observing Strategy (**IGOS**) aims to provide a framework to harmonize the activities of the systems for global observation of the Earth. It is an over-arching strategy for guiding the execution of observations related to climate, oceans and land surface, making an effort to integrate the existing international global observing programmes. Within IGOS, there are partners involved in link

research, long-term monitoring and operational programmes. The goal is to build a structure that permits to identify observation gaps. Some of the IGOS partners are:

- The Global Climate Observing System (**GCOS**). It was established to ensure the achievement of climate observations and to facilitate their access to all potential users. GCOS does not make observations directly itself but it encourages and gives support to national and international organizations in this purpose.
- The Global Ocean Observing System (**GOOS**). It is a global system for continuous observation of the ocean. As GCOS, GOOS does not make observations but it is a framework for international cooperation and a forum for interaction between research and user communities.
- The Global Terrestrial Observation System (**GTOS**). It is a framework that promotes observations and analysis of terrestrial ecosystems and facilitates interactions between research programmes, monitoring networks and policy makers in order to manage global change affecting terrestrial ecosystems.
- The Committee on Earth Observation Satellites (**CEOS**). It is an international mechanism for the coordination of the international Earth Observation satellite programs. The main CEOS goal is to ensure the remote coverage of the main issues related to Earth observation and global change and to prevent overlapping between satellite missions.

1.4.2 The Global Earth Observation System of Systems (GEOSS)

The Global Earth Observation System of Systems (**GEOSS**) is a large national and international cooperative initiative that envisages coordinating the existing Earth Observation Systems. GEOSS will identify gaps and will support data sharing improving the delivery of information to users. The intergovernmental Group on Earth Observations (GEO) was established in February 2005 to carry out a 10-Year Implementation Plan of GEOSS. GEO includes 66 member countries, the European Commission, and 43 participating organizations.

1.5 International Collaborative Programmes: The Earth System Science Partnership (ESSP)

The Earth System Science Partnership (**ESSP**) is a joint initiative that brings together researchers from different disciplines, and from across the globe, to carry out an integrated study of the Earth System, the changes that are occurring in it and their implications for global sustainability. The ESSP is formed by four international global environmental change research programmes (Fig. 1.4):

- **DIVERSITAS** – an integrated programme of biodiversity science
- **IHDP** – International Human Dimensions Programme on Global Environmental Change

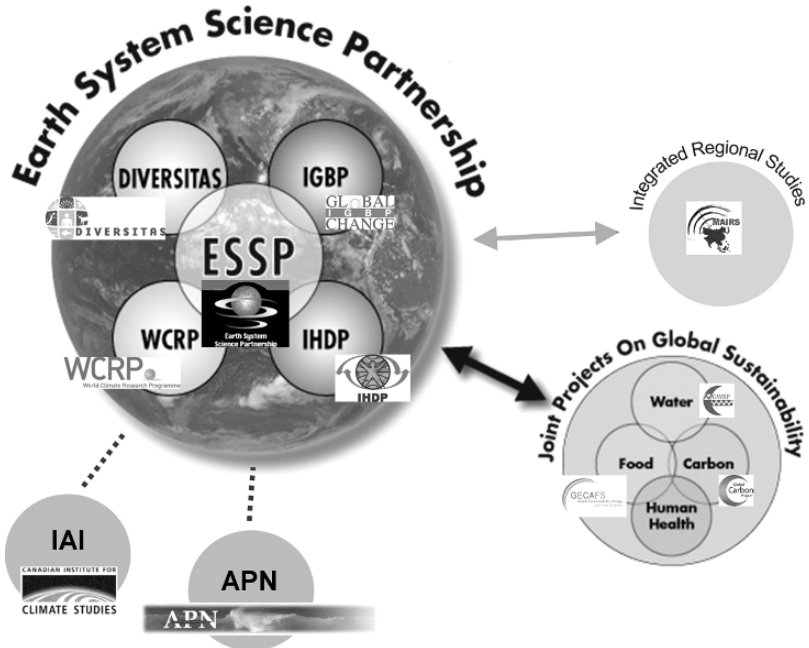


Fig. 1.4 Representation of the Earth System Science Partnership structure (Adapted from the ESSP web site). For acronyms see Table 1.1

- **IGBP** – International Geosphere-Biosphere Programme
- **WCRP** – World Climate Research Programme

The main activities of the ESSP are joint projects focused on global environmental changes regarding four topics that are decisive for human well-being: energy and carbon cycle (**GCP**, Global Carbon Project), food security (**GECAFS**, Global Environmental Change and Food Systems), water resources (**GWSP**, Global Water System Project) and human health (**GEC&HH**, Global Environmental Change and Human Health). The ESSP is also carrying out several integrated regional studies in support of sustainable development at the local level as the Monsoon Asia Integrated Study (**MAIRS**). ESSP partners collaborate closely with the Inter-American Institute for Global Change Research (**IAI**) and the Asia-Pacific Network for Global Change Research (**APN**).

1.5.1 Diversitas

The mission of **DIVERSITAS** is to encourage an integrative study of biodiversity, connecting biological, ecological and social disciplines in order to enhance a scientific knowledge for the conservation and sustainable use of biodiversity. To achieve this goal, **DIVERSITAS** is developing the following core projects (Fig. 1.5):

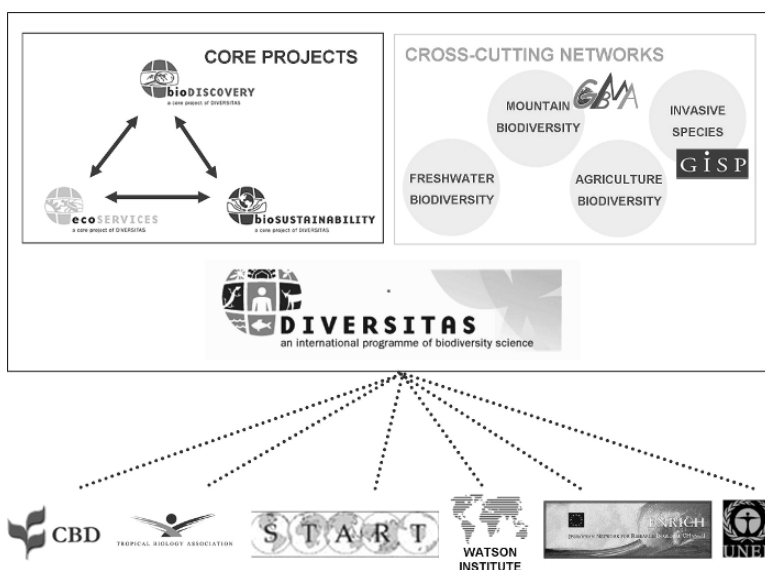


Fig. 1.5 Representation of DIVERSITAS structure. For acronyms see Table 1.1

bioDISCOVERY to assess current biodiversity and predict changes in the future, **ecoSERVICES** to assess human responses to changes in ecosystems services due to changes in biodiversity and **bioSUSTAINABILITY**, to guide policy that support sustainable use of biodiversity.

DIVERSITAS has also created four cross-cutting networks to investigate in particular topics: mountain biodiversity (**GMBA**, Global Mountain Biodiversity Assessment), freshwater biodiversity (**freshwaterBIODIVERSITY**), agriculture & biodiversity (**agroBIODIVERSITY**) and invasive species (**GISP**, Global Invasive Species Programme). In addition, DIVERSITAS participates actively in related activities, establishing strong relationships with: the United Nations Convention on Biological Diversity (**CBD**), the System for Analysis, Research and Training (**START**), the European Network for Research Global Change (**ENRICH**), the Tropical Biology Association (**TBA**), the United National Environment Programme (**UNEP**) and the Watson Institute for International Studies.

1.5.2 The International Human Dimensions Programme on Global Environmental Change (IHDP)

The mission of the International Human Dimensions Programme on Global Environmental Change (**IHDP**) is to encourage and to coordinate research on the human dimensions of global environmental change. IHDP is currently developing six core projects (Fig. 1.6):

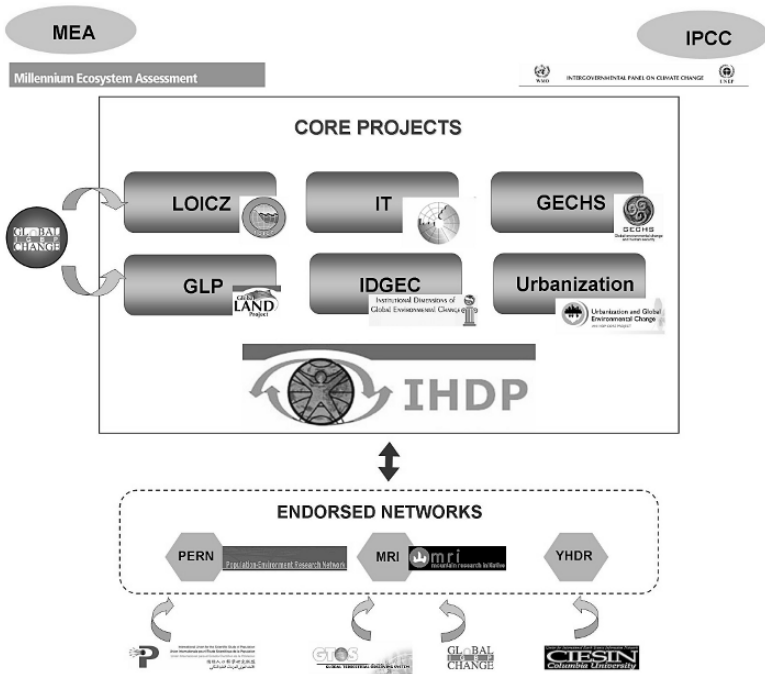


Fig. 1.6 Representation of the International Human Dimensions Programme structure. For acronyms see Table 1.1

- **GECHS**, Global Environmental Change and Human Security – Evaluating the relationship between both concepts.
- **IDGEC**, Institutional Dimensions of Global Environmental Change – Assessing the role of social institutions in producing and solving environmental problems.
- **IT**, Industrial Transformation – Exploring new ways to cover human needs using resources in a sustainable manner.
- **LOICZ**, Land-Ocean Interactions in the Coastal Zone – Studying human use of coastal systems.
- **Urbanization and Global Environmental Change** – Evaluating the interactions between global environmental change and urban processes.
- **GLP**, Global Land Project – Studying the effects of human activities on land in terrestrial and aquatic systems.

In addition, IHDP is collaborating in other scientific activities and networks: the Population Environment Research Network (**PERN**), aiming to encourage on-line exchange among social and natural scientists worldwide, the Mountain Research Initiative (**MRI**), investigating global change in mountain regions, and the Young Human Dimensions Researchers (**YHDR**), seeking to make easier the work of young researchers in the area of human dimensions of global change. The results of IHDP research contribute to international synthesis processes as the

Millennium Ecosystem Assessment (MEA) and the Intergovernmental Panel on Climate Change (IPCC).

1.5.3 The International Geosphere-Biosphere Programme (IGBP)

The mission of the International Geosphere-Biosphere Programme (IGBP) is to study the interactions between physical, biological and chemical processes of the Earth System and the changes that they are suffering due to human impacts. This research is developed by a set of core projects focused on the main compartments of the Earth system (land, ocean, and atmosphere), the points of contacts between them and the integration of Earth system information by means of palaeo-environmental studies and modelling. These projects are (Fig. 1.7):

- **AIMES**, Analysis, Integration and Modelling of the Earth System – Analysing the human impacts in the global biogeochemical cycles.
- **GLOBEC**, Global Ocean Ecosystem Dynamics – Studying the effects of global change on marine populations.

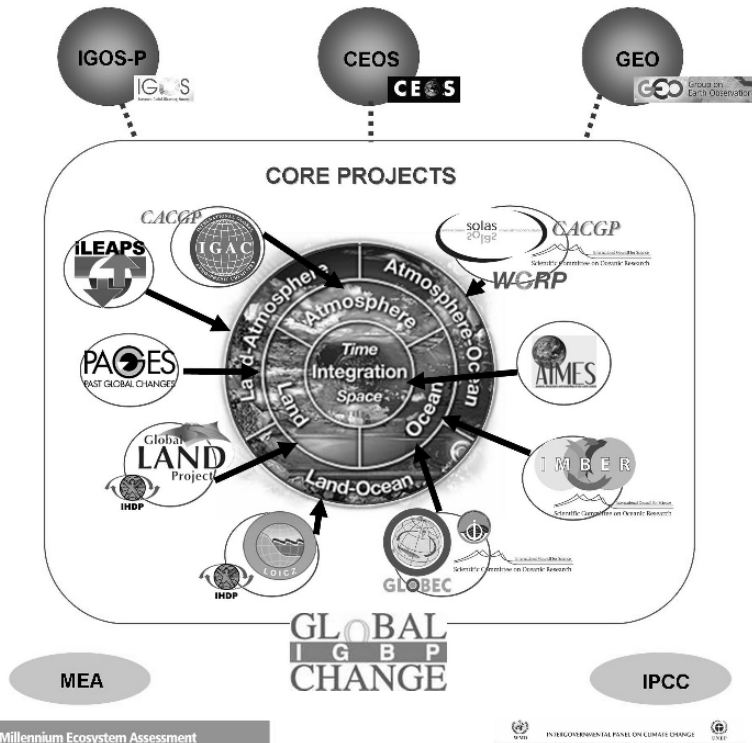


Fig. 1.7 Representation of the International Geosphere-Biosphere Programme structure (Adapted from the IGBP web site). For acronyms see Table 1.1

- **GLP**, Global Land Project – Co-sponsored with IHDP (see Sect. 5.2).
- **IGAC**, International Global Atmospheric Chemistry – Examining the role of atmospheric chemistry in the Earth System.
- **ILEAPS**, Integrated Land Ecosystem-Atmosphere Processes Study – Assessing the transport and the transformation of energy and matter through the land-atmosphere interface by the action of physical, chemical and biological processes.
- **IMBER**, Integrated Marine Biogeochemistry and Ecosystem Research – Studying and predicting ocean responses to global change.
- **LOICZ**, Land-Ocean Interactions in Coastal Zone – Co-sponsor with IHDP (see Sect. 1.5.2).
- **PAGES**, Past Global Changes – Studying the Earth’s environment in the past in order to make predictions for the future.
- **SOLAS**, Surface Ocean-Lower Atmosphere Study – Analysing the main biogeochemical-physical interactions between the atmosphere and the ocean and the effects of global change on this system.

IGBP is also linked to the global observations community (participating in IGOS, GEO and CEOS), collaborates with other international organizations (the Scientific Committee for Oceanic Research (**SCOR**), the Commission on Atmospheric Chemistry and Global Pollution (**CACGP**) and the Intergovernmental Oceanographic Commission (**IOC**) and contributes to global assessments as the Millennium Ecosystem Assessment (**MEA**) and the Intergovernmental Panel on Climate Change (**IPCC**).

1.5.4 The World Climate Research Programme (WCRP)

The mission of the World Climate Research Programme (**WCRP**) is to study climate variability and climate change. To achieve this mission, WCRP is developing the following core projects (Fig. 1.8):

- **GEWEX**, Global Energy and Water Cycle Experiment – Observing and modelling the global hydrological cycle.
- **CLIVAR**, Climate Variability and Predictability – Observing, simulating and predicting the Earth’s climate system.
- **SPARC**, Stratospheric Processes And their Role in Climate – Assessing the interaction between chemical, radioactive and dynamical processes in the stratosphere.
- **CLIC**, Climate and Cryosphere – Evaluating the effects of climatic variability and change on the cryosphere.
- **SOLAS**, Surface Ocean-Lower Atmosphere Study – Co-sponsor with IGBP (see Sect. 1.5.3).

WCRP is also participating in GEO, works closely with GCOS and GOOS and contributes to the efforts of the Intergovernmental Panel on Climate Change (**IPCC**), the United Nations Framework Convention on Climate Change (**UNFCCC**) and the Millennium Ecosystem Assessment (**MEA**).

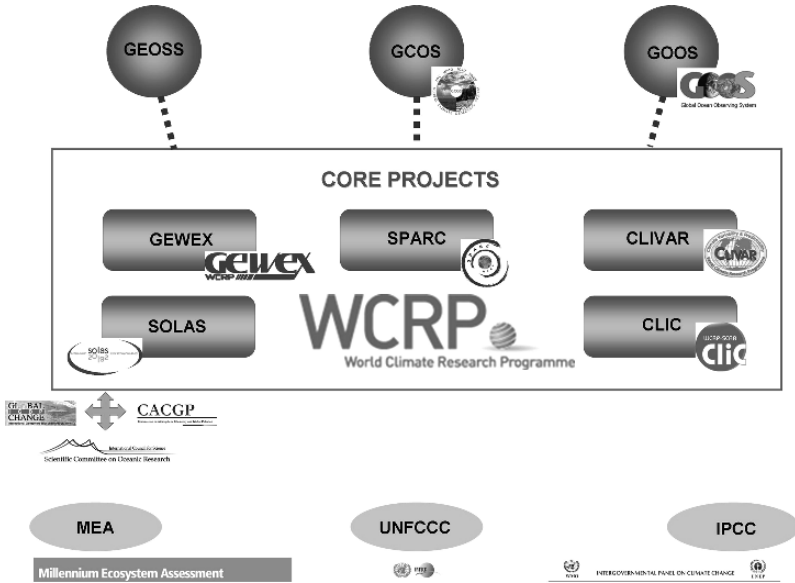


Fig. 1.8 Representation of the World Climate Research Programme structure. For acronyms see Table 1.1

1.6 Monitoring Networks and Databases

1.6.1 The International Cooperative Programmes (ICP)

In the framework of the Convention on Long-range Transboundary Air Pollution the Working Group on Effects was established in order to develop international cooperation in the research on air pollutant effects. Its six International Cooperative Programmes (ICPs), based on long-term monitoring, identify the most endangered areas: ICP Forests, ICP Waters, ICP Materials, ICP Vegetation, ICP Integrated Monitoring and ICP Modelling and Mapping. There are currently 51 countries involved in the Convention as Parties.

1.6.2 Long-Term Ecological Research Networks: *ILTER and Others*

The International Long Term Ecological Research (**ILTER**) is a “network of networks” engaged in long-term, site-based ecological and socioeconomic research

aiming to obtain a good knowledge of ecosystem functioning. ILTER was created in 1993 following the successful previous example of the Long Term Ecological Research Network (**US-LTER**) in United States. The US-LTER programme was established in 1980 with a small set of sites, number that has increased to 26 over the years covering an extended variety of ecosystems.

Since the foundation of ILTER, long-term ecological research initiatives have spread quickly. This is due to the recognition of the importance of long-term research in order to understand complex environmental issues such as global change. Up to now, thirty-two formal national LTER networks have become ILTER members and many other countries are working on it (Fig. 1.9). This is the case of some European countries like Spain, for instance, that is making efforts to consolidate the Spanish LTER Network, **REDOTE**. At European level, the network of excellence **ALTER-net** promotes the integration among all the actors involved in biodiversity research, monitoring and policy in order to develop a European LTER Network.

Focused on Africa, **ROSELT** Network is providing long-term ecological data in order to improve the knowledge of the processes, causes and effects of desertification in the circum-Saharan area.

1.6.3 Fluxnet

FLUXNET is a “network of regional networks” of micrometeorological tower sites that record the exchanges of water vapour, carbon dioxide and energy between

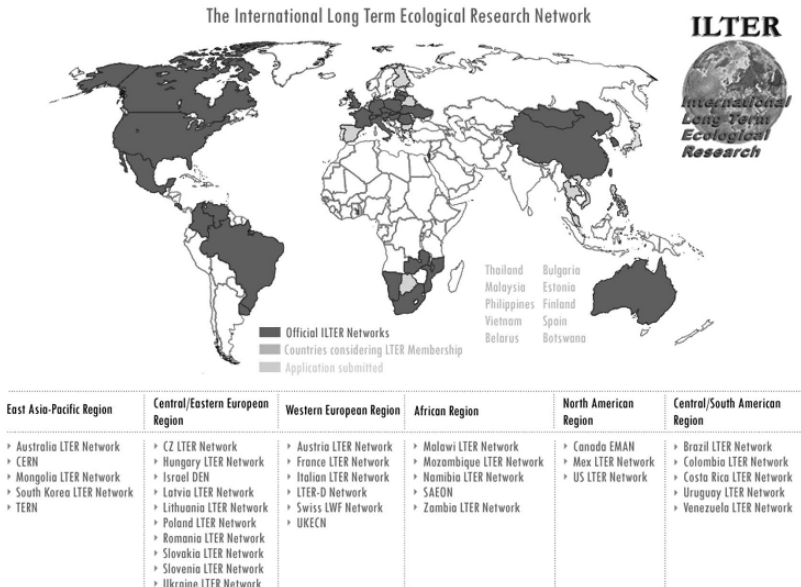


Fig. 1.9 Official members of the International Long Term Ecological Research Network and countries that are considering joining it. Source: ILTER

terrestrial ecosystems and atmosphere using eddy covariance methods. Currently, FLUXNET includes over 400 tower sites operating in continuous. Data related to the vegetation, hydrology, soil and meteorological characteristics at the tower sites is also collected. FLUXNET is supported by ILEAPS (See Sect. 1.5.3)

1.6.4 The Biosphere Reserve Integrated Monitoring (BRIM)

The Biosphere Reserve Integrated Monitoring (**BRIM**) is an initiative launched in 1991 in order to monitor abiotic, biotic and socio-economic parameters in the world network of Biosphere Reserves providing integrated data. Biosphere Reserves are sites recognized by UNESCO for supporting sustainable development, conservation and research. Currently, 507 sites from 102 countries worldwide are included within the World Network sharing experience and information. BRIM, whose aim is to build on existing initiatives, is collaborating with other international programmes and long-term initiatives, as GTOS and ILTER.

1.6.5 Databases

It is clear that global change is an issue that requires collaboration and cooperation among researchers worldwide beyond national boundaries. Data sharing becomes crucial to facilitate synthesis processes and significant advance in scientific knowledge. Currently, there is an extraordinary development of new tools and protocols in order to make easier data store and management. These tools, in combination with the use of Internet, have permitted a very simple and rapid access to the information and a wide spread of scientific results with a remarkable example in the gene bank, where DNA sequences are shared. A variety of scientific organizations have already made available their databases including useful data for the study of global environmental changes. These are some examples:

- The U.S. Long Term Ecological Research Network (**US-LTER**, www.lternet.edu) provides long-term data series related to climate, biodiversity, nutrients, fauna, vegetation, substrate, hydrology and ecophysiology from different ecosystems in the United States.
- The Global Biodiversity Information Facility (**GBIF**, www.gbif.org) has created a database comprising global biodiversity information.
- The NOAA National Geophysical Data Center (**NGDC**, <http://www.ngdc.noaa.gov/>) provides long-term geophysical data, as well as earth observations from space.
- The USGS Center for LIDAR Information Coordination and Knowledge (**CLICK**, <http://lidar.cr.usgs.gov/index.php>) facilitates access to data of LIDAR remote sensing.

1.7 Conclusions

As shown throughout this text, there is currently a large number of scientific programmes, monitoring networks and international organisations involved in global change research. The existence of so many initiatives is itself a proof of the importance of global change and reveals the general concern over the new situation that the Earth system is facing today. The population growth and the increasing impact of human activities over the last century have produced dramatic changes in the functioning of ecosystems whose consequences in the future are still complex to evaluate. Due to the global dimension of these environmental changes, it is required to develop strategies at a global level, to encourage international collaboration and to promote communication among the society, the scientific community and the policy makers. Following this principle, the Kyoto Protocol constitutes a historical milestone in cooperation and commitment at global level. This is the first international agreement aiming to reduce greenhouse-gas emissions responsible of climate change and even though it seems insufficient to reverse the negative influence of human activities on Earth climate, its international dimension is unprecedented. The Protocol was signed in 1997 but it did not enter into force until the 16th February 2005 without the support of one of the most strategic countries, the United States. Those that have signed the Kyoto Protocol are already adopting appropriate measures to reduce the emissions. But even though all these actions are highly valuable, they are not enough. There is still much research to do to prevent climate change and to mitigate the effects of global change, since many of these effects are still poorly understood. Delaying the making of decisions is a big risk for the sustainability of our planet and the survival of future generations. But such decisions can not be made without a global long term and multidisciplinary vision at which all the initiatives described here are aimed.

Acknowledgments This chapter has been possible thanks to the discussions within REDOTE, GLOBIMED and CEICAG Networks funded by the Spanish Ministry of Education and Science. It has benefited by the insightful comments of Gerardo Benito, Regino Zamora, Sergi Sabater and Teresa Sebastiá. We would also like to acknowledge the support and help from our colleagues at the Centro de Ciencias Medioambientales (CSIC), especially from Silvia Matesanz.

References

- Arrhenius S (1896) On the influence of carbonic acid in the air upon the temperature of the ground. The London, Edinburgh, and Dublin Philosophical Magazine and Journal of Science vol 41 pp 237–276
- Ciais P, Reichstein M, Viovy N, Granier A, Ogee J, Allard V, Aubinet M, Buchmann N, Bernhofer C, Carrara A, Chevallier F, De Noblet N, Friend AD, Friendlingstein P, Grünwald T, Heinesch B, Keronen P, Knohl A, Krinner G, Lonstau D, Manca G, Matteucci G, Miglietta F, Ourcival JM, Papale D, Pilegaard K, Rambal S, Seufert G, Soussana JF, Sanz MJ, Schulze EP, Vesala T and Valentini R (2005) Europe-wide reduction in primary productivity caused by the heat and drought in 2003. *Nature* vol 437 pp 529–533

- Elias S (2003) Millennial and century climate changes in the Colorado Alpine. In: Greenland D, Goodin DG and Smith RC (eds) *Climate variability and ecosystem response at Long-Term Ecological Research sites*. Oxford University Press pp 370–383
- Ehrlich PR and Wilson EO (1991) *Biodiversity studies: Science and policy*. Science vol 253 pp 758–762
- Foley JA, DeFries R, Asner GP, Bardford C, Bonana G, Carpenter SR, Chapin FS, Coe MT, Daily GC, Gibb HK, Helkowski JH, Holloway T, Howard EA, Kucharik CJ, Monfreda C, Patz JA, Prentice IC, Ramankutty N and Snyder PK (2005) Global consequences of land use. Science vol 306 pp 570–574
- Foster DR, Knight DH and Franklin JF (1998) Landscape patterns and legacies resulting from large, infrequent forest disturbances. *Ecosystems* vol 1 pp 497–510
- Gage SH (2003) Climate variability in the North Central region: Characterizing drought severity patterns. In: Greenland D, Goodin DG and Smith RC (eds) *Climate variability and ecosystem response at Long-Term Ecological Research sites*. Oxford University Press pp 56–73
- Goodin DG, Fay PA, and McHugh MJ (2003) Climate variability in Tallgrass Prairie at multiple timescales: Konza Prairie Biological Station. In: Greenland D, Goodin DG and Smith RC (eds) *Climate variability and ecosystem response at Long-Term Ecological Research sites*. Oxford University Press pp 411–423
- Greenland D (2003) An LTER Network overview and introduction to El Niño-Southern Oscillation (ENSO) Climatic signal and response. In: Greenland D, Goodin DG and Smith RC (eds) *Climate variability and ecosystem response at Long-Term Ecological Research sites*. Oxford University Press pp 102–116
- Greenland D, Goodin DG and Smith RC (2003) An introduction to climate variability and ecosystem response. In: Greenland D, Goodin DG and Smith RC (eds) *Climate variability and ecosystem response at Long-Term Ecological Research sites*. Oxford University Press pp 3–19
- Greenland D, Goodin DG, Smith RC and Swanson FJ (2003) Climate variability and ecosystem response – Synthesis. In: Greenland D, Goodin DG and Smith RC (eds) *Climate variability and ecosystem response at Long-Term Ecological Research sites*. Oxford University Press pp 425–449
- Hansen J, Nazarenko L, Ruedy R, Sato M, Willis J, Del Genio A, Koch D, Lacis A, Lo K, Menon S, Novakov T, Perlwitz J, Russell G, Schmidt GA and Tausnev N (2005) Earth's energy imbalance: Confirmation and implications. Science vol 308 pp 1431–1435
- Harries JE, Brindley HE, Sagoo PJ and Bantges RJ (2001) Increases in greenhouse forcing inferred from the outgoing longwave radiation spectra of the Earth in 1970 and 1997. *Nature* vol 410 pp 355–357
- IPCC, 2001: *Climate Change 2001: Synthesis report*. A Contribution of Working Groups I, II and III to the Third Assessment Report of the Intergovernmental Panel on Climate Change [Watson, R.T. and the Core Writing Team (eds.)]. Cambridge University Press, Cambridge, United Kingdom and New York, NY, USA, 398 pp
- Levitus S, Antonov JI, Boyer TP and Stephens C (2000) Warming of the world ocean. Science vol 287 pp 2225–2229
- Mackenzie FT, Ver LM, Lerman A (2002) Century-scale Nitrogen and Phosphorus Controls of the Carbon Cycle. *Chemical Geology* vol 190 pp 163–178
- McHugh MJ and Goodin DG (2003) Interdecadal-Scale variability: An assessment of LTER climate data. In: Greenland D, Goodin DG and Smith RC (eds) *Climate variability and ecosystem response at Long-Term Ecological Research sites*. Oxford University Press pp 213–225
- Millennium Ecosystem Assessment, (2005) *Ecosystems and human well-being: Synthesis*. Island Press, Washington, DC.
- O'Neill BC, Mackellar FL and Lutz W (2001) *Population and climate change*. Cambridge University Press, USA
- Parmesan C, Root TL and Willing MR (2000) Impacts of extreme weather and climate on terrestrial biota. *Bulletin of the American Meteorological Society* vol 81 pp 433–450

- Postel SL, Daily GC and Erlich PR (1996) Human appropriation of renewable freshwater. *Science* vol 271 pp 785–788
- Reid WVC and Miller KR (1989) The scientific basis for the conservation of biodiversity. World Resources Institute, Washington DC
- Richards JF (1991) Land transformation. In: Turner BL, Clark WC, Kates RW, Richards JF, Matthews JT, and Meyers WT (Eds). *The Earth as transformed by human action: Global and regional changes in Biosphere over the last 300 years*. Cambridge University Press, New York, pp 163–178
- Rojstaczer S, Sterling SM and Moore NJ (2001) Human appropriation of photosynthesis products. *Science* vol 294 pp 2549–2552
- Roughgarden J, Running SW and Matson PA (1991) What does remote sensing do for ecology? *Ecology* vol 72 pp 1918–1922
- Sanderson EW, Malanding J, Levy MA, Redford KH, Wannebo AV and Woolmer G (2002) The human footprint and the last of the wild. *Bioscience* vol 52 No 10 pp 891–904
- Schlesinger WH (2006) Global change ecology. *Trends in ecology and evolution* vol 21 pp 348–351
- Secretariat of the Convention on Biological Diversity (2006) *Global Biodiversity Outlook 2*. Montreal, 81 + vii pages
- Vitousek PM (1992) Global Environmental Change: An Introduction. *Annual Review of Ecology and Systematics* vol 23 pp 1–14
- Wessman CA (1992) Spatial scales and global change: Bridging the gaps from plots to GCM grids cells. *Annual Review of Ecology and Systematics* vol 23 pp 175–200

Chapter 2

NASA Earth Observation Satellite Missions for Global Change Research

Emilio Chuvieco and Chris Justice

Abstract This chapter reviews the main missions of NASA and, secondarily, other US agencies, providing global observation of the Earth's environment, with special emphasis on Landsat and the Earth Observing System (EOS) missions. An analysis of the main policies towards long-term data archival and accessibility, and an assessment of the immediate future is also addressed.

2.1 NASA Earth Observing Agenda

In the National Aeronautics and Space Act of 1958 it was stated that the activities of the administration should include the expansion of human knowledge of the Earth and of phenomena in the atmosphere and space. As part of the U.S. National Space Policy of 1996, the National Aeronautics and Space Administration (NASA) was charged with conducting a program of research to advance scientific knowledge of the Earth through space-based observation and development and deployment of enabling technologies. NASA currently undertakes a wide range of activities related to the study of global change. As a space agency, one of its primary functions is the design, construction and launch of artificial satellites and space vehicles. However, NASA also supports a considerable body of research which utilizes data from its earth observation satellites and provides the archive and distribution of these data. In addition NASA provides funding to develop applications of societal benefit using the satellite data, education and outreach. NASA also undertakes cooperation with other agencies of the US government, as well as other space agencies and international organizations.

Following the main objectives of this book, our review of NASA activities will be focused on those aspects related to global change research. Most satellite missions are global by nature, since most satellites provide a world-wide observation. However, in this chapter we will restrict to those missions that have relevance to global change researchers and decision makers. When studying global change special emphasis is given to those observations which are being formed into consistent long-term data records.

Before moving into the analysis of main NASA EOS missions, a brief comment on the general strategy of NASA in relation to global change research will be addressed.

The current NASA Earth Science program has evolved from its Mission to Planet Earth and Global Habitability in the 1980's and 1990's, to its Earth Science Enterprise, which is currently part of the latest administrator's initiative on space exploration, scientific discovery and aeronautics research. A recent NASA reference document (Parkinson et al. 2006), describes the current NASA mission: "to improve life here, to extend life to there, to find life beyond". Within this scheme, the agency has developed an Earth Science program that addresses critical issues related to improving our knowledge of the Earth system. Research focus areas identified by the program have a strong emphasis on climate change and its potential impacts, including climate variability and change, atmospheric composition, carbon cycle, ecosystems, land cover and land use change and biogeochemistry, water and energy cycles, weather and the Earth surface and interior.

The main component of NASA's contribution to these research issues is provided by the Earth Observing System (EOS) program, which was designed in the early 1980s, and received a strong impetus during the nineties. EOS was designed to provide a consensus list of critical variables defined by the EOS Investigators Working Group (IWG), based on scientific recommendations by national and international programs such as the Intergovernmental Panel on Climate Change (IPCC) and the Committee on the Environment and Natural Resources (CENR). The list of variables included those related to seven major areas: 1) Radiation, Clouds, Water Vapor, and Precipitation, 2) Oceans, 3) Greenhouse Gases, 4) Land-Surface Hydrology and Ecosystem Processes (including land cover change), 5)Glaciers, Sea Ice, and Ice Sheets, 6) Ozone and Stratospheric Chemistry, and 7) Volcanoes and Climate Effects of Aerosols (Fig. 2.1).



Fig. 2.1 Earth Systems Science at NASA

These seven science priorities have guided the selection of the instruments to incorporate in new missions, and are still the focus for future systems (Table 2.1). NASA has also provided funds for developing data products, currently termed Earth Science Data Records (ESDR's) based on satellite observations, to enable the use of the data in scientific research and decision making at different spatial scales. Currently, the EOS program includes multiple satellites and sensors, some of them as a result of international cooperation (Table 2.1). NASA's open data access policy and education efforts reinforce the international cooperation.

One aspect of the EOS concept missing from previous NASA programs is the comprehensive character of the mission, which coordinates data acquisitions across multiple platforms to allow benefits from data synergy. This approach has implied the creation of the morning and afternoon constellations, meaning a set of satellites that have the same orbit and acquire data almost simultaneously. The morning constellation crosses the Equator at 10.30 am and pm, and is composed of the Landsat 7, EO-1, Satellite for Scientific Applications (SAC-C, with Argentina), and EOS Terra. The afternoon constellation is composed of EOS Aqua and Aura, and PARASOL, and is soon to be followed by CALIPSO, Cloudsat and the Orbiting Carbon Observatory (OCO). These missions have equatorial crossings in the early afternoon, around 1:30 p.m. local time (and in the middle of the night, around 1:30 a.m.). Flying these satellites in formation facilitates the integration of their data for the study of albedo, surface temperature and processes, vegetation and land-surface cover, ocean characteristics, and cloud properties. Further, having the Moderate Resolution Imaging Spectroradiometer (MODIS) and Clouds and Earth Radiant Energy System (CERES) instruments on both the Terra and Aqua satellites provides scientists an opportunity to examine aspects of the diurnal cycle of the many parameters being measured by these instruments (Parkinson et al. 2006).

Another important aspect of the integrated use of different satellite sensors is the growing emphasis on calibration and validation of the raw data and the derived products. A great economic and human effort investment has been made to assure that EOS observations are properly calibrated, hence physical units can be used across different sensors to help up-scaling of observations. The calibration process includes laboratory measurements, in-flight calibration devices, and vicarious methods, based on ground reference panels and the Moon. Some of these are performed before launch (development and verification of algorithms and characterization of uncertainties resulting from parameterizations and their algorithmic implementation) and some others after launch of the instruments. These include refinement of algorithms and uncertainty estimates based on near-direct comparisons with correlative measurements and selected controlled analyses or application implementations (King et al. 2003).

EOS standard products are derived from raw data in a consistent and well-documented way. The technical documentation is available online, and includes a full description of the algorithms used. These documents are named ATBD's (Algorithm Theoretical Basis Documents) and are developed by the principal investigator responsible for each product in coordination with the EOS Senior Project Scientist.

The ATBDs are peer-reviewed before their approval, and include a technical background, science rationale, algorithm theoretical description, sources of

Table 2.1 NASA Earth Science Satellite Program, 1991–2010 (after Parkinson et al., 2006)

Launch	Satellite	Mission Objectives
1991	UARS	Measure upper atmospheric characteristics to examine stratospheric and mesospheric chemistry and dynamic processes.
1991–2000	NASA Shuttle Missions	Measure atmospheric ozone (SSBUV), atmospheric and solar dynamics (ATLAS), atmospheric aerosols (LITE), and surface height (SLA), through a series of Shuttle-based experiments. Shuttle Radar Topography Mission (SRTM), including X-SAR, SIR-C, and GPS instruments, was launched February, 000 (joint with Germany and Italy).
1991	Meteor-3/TOMS	Monitor and map atmospheric ozone (joint with Russia).
1992	TOPEX/Poseidon	Monitor changes in sea-level height to study ocean circulation (joint with France).
1996	Earth Probe/TOMS	Monitor and map atmospheric ozone. Together with TOMS aboard Nimbus-7 (launched 1978) and Meteor-3 (launched 1991), the Earth Probe TOMS provides a data set of daily ozone for over two decades.
1997	Orbview-2/SeaWiFS	Monitor ocean productivity (an ocean-color data purchase).
1997	TRMM	Measure precipitation, clouds, lightning, and radiation processes over tropical regions (joint with Japan). Data from CERES instruments on Terra, Aqua, and TRMM extend the long-term radiation-budget record that began with the three-satellite configurations of ERBS (launched 1984), NOAA-9, and NOAA-10, each carrying the Earth Radiation Budget Experiment (ERBE) instrument.
1999	Landsat 7	Monitor the land surface through high-spatial-resolution visible and infrared measurements (joint with USGS).
1999	QuikSCAT	Measure ocean surface wind vectors, with the SeaWinds instrument.
1999	Terra	Collect global data on the state of the atmosphere, land, and oceans, and their interactions with solar radiation and with one another (includes Canadian and Japanese instruments). See TRMM entry for the radiation-budget measurements with the CERES instruments on Terra, Aqua, and TRMM.
1999	ACRIMSAT	Monitor total solar irradiance.
2000	CHAMP	1) Map Earth's gravity field and its temporal variations; 2) map Earth's global magnetic field and its temporal variations; 3) perform atmospheric/ionospheric sounding (cooperative with Germany).
2000	EO-1	Collect data to allow paired scene comparisons between EO-1 Advanced Land Imager (ALI) and Landsat 7 Enhanced Thematic Mapper Plus (ETM+).
2000	SAC-C	Perform various environmental, magnetic, navigation, space radiation, and other experiments. (Cooperative mission with Argentina, with contributions from Brazil, Denmark, France, and Italy).
2001	Jason	Monitor ocean height to study ocean circulation (joint with France).

(continued)

Table 2.1 (continued)

Launch	Satellite	Mission Objectives
2001	Meteor-3M/ SAGE III	Retrieve global profiles of atmospheric aerosols, ozone, water vapor, other trace gases, temperature and pressure in the mesosphere, stratosphere, and troposphere (joint with Russia).
2002	GRACE	Measure Earth’s gravity field and its variations with time (joint with Germany).
2002	Aqua	Monitor atmospheric, land, ocean, and ice variables for improved understanding of the Earth’s water cycle and improved understanding of the intricacies of the climate system (includes Brazilian and Japanese instruments). See TRMM entry for the radiation-budget measurements with the CERES instruments on Terra, Aqua, and TRMM
2002	ADEOS II (Midori II – Japan)	Monitor ozone, aerosols, atmospheric temperature, winds, water vapor, SST, energy budget, clouds, snow and ice, ocean currents, ocean color/biology, from visible-to-thermal-infrared radiance/reflectance, microwave imaging, and scatterometry (includes French and U.S. instruments).
2002	ICESat	Measure elements of ice-sheet mass balance, cloud-top and land- surface topography, and vertical profiles of aerosol and cloud properties.
2002	SORCE	Measure the total and spectral solar irradiance incident at the top of Earth’s atmosphere.
2004	Aura	Measure atmospheric chemical composition; tropospheric/stratospheric exchange of energy and chemicals; chemistry-climate interactions; air quality (includes joint Netherlands/Finland and joint U.K./U.S instruments).
2006	CALIPSO	Measure the vertical distribution of clouds and aerosols (joint with France).
2006	CloudSat	Measure cloud characteristics, to increase the understanding of the role of optically thick clouds in Earth’s radiation budget (joint with Canada).

uncertainty and errors, calibration and validation protocols, and practical considerations. They are available at: eosps0.gsfc.nasa.gov/eos_homepage/for_scientists/atbd/index.php.

Product validation is an additional critical task that has been soundly addressed in the EOS program. The responsibility for product validation lies primarily with the product Principle Investigator (P.I.). In addition independent validation teams have been established for different variables and ecosystems (Morisette et al. 2002). EOS instrument science teams are responsible for overseeing the instrument design and build, the on flight performance, algorithm development and product validation, and specific activities are carried out for each instrument (<http://eosps0.gsfc.nasa.gov/validation/>), including airborne and field campaigns. Examples of these campaigns include the SAFARI2000 (Southern African Regional Science Initiative – Dry Season Campaign), the SMEX (Soil Moisture Experiment 2002 and 2003), and the AMSR-E Antarctic Sea Ice (AASI).

2.2 A Review of NASA EO Missions

2.2.1 *Beginnings*

Since the beginning of aerial navigation, the new perspective providing by vertical surveillance attracted both civilian and military users, although the latter have led the technological developments since the beginning. Earth Observation from airborne cameras was initiated in the 19th Century and used extensively during the World Wars I and II, and later on during the so-called Cold War. The greater distances covered by radar systems, prepared the ground for satellite-borne observation sensors. After the incident of the U-2 in 1960, the U.S. Government emphasized the importance of developing a reliable satellite surveillance system, which had in fact been initiated in 1959 with the launching of the first CORONA Keyhole (KH)1 military satellite.

On the other hand, the manned space missions developed during the sixties for the Moon race initiated, almost incidentally, the observation of earth resources from space photography, which was the seed for planning specific missions for this purpose. These developments were in parallel to the activities of the first meteorological satellites, the Television and Infrared Observational Satellites (TIROS-1) launched in April 1960, which soon began to show the interest of global observation of atmospheric conditions and circulation patterns, and provided early warning of serious natural catastrophes.

2.2.1.1 Manned Missions (Apollo – Skylab – Space Shuttle)

During the Mercury, Gemini and Apollo programs, several experiments were planned to acquire photography, to help better understand geological features and remote areas that had previously been rarely observed. These photographs provided the impetus for the creation of space programs oriented towards the study of our planet, from which current EOS is indebted (Fig. 2.2).

The Skylab space laboratory launched in 1973 included a full set of experiments oriented towards Earth Observation. This part of the mission was named EREP (Earth Resources Experiment Package), and included diverse sensors: a multi-spectral scanner, two micro-wave sensors and two photographic cameras (the multi-spectral camera S 190A, with six bands, and the high resolution Earth Terrain Camera (NASA 1977)). Photographs from these systems were used for various studies, although they were mainly oriented toward land cover, agriculture and geological mapping (Hart 1975; NASA 1977).

The continuation of manned EO initiatives was possible through different missions of the Space Shuttle. In the early eighties, the Space Shuttle included several high-resolution cameras. During 1983, around 1000 photographs were acquired by the metric camera RMK 20/23, in a cooperative mission with the ESA, including both panchromatic and color infrared films, which were proven useful for mapping applications using standard photographic restitution procedures (Konecny 1986).

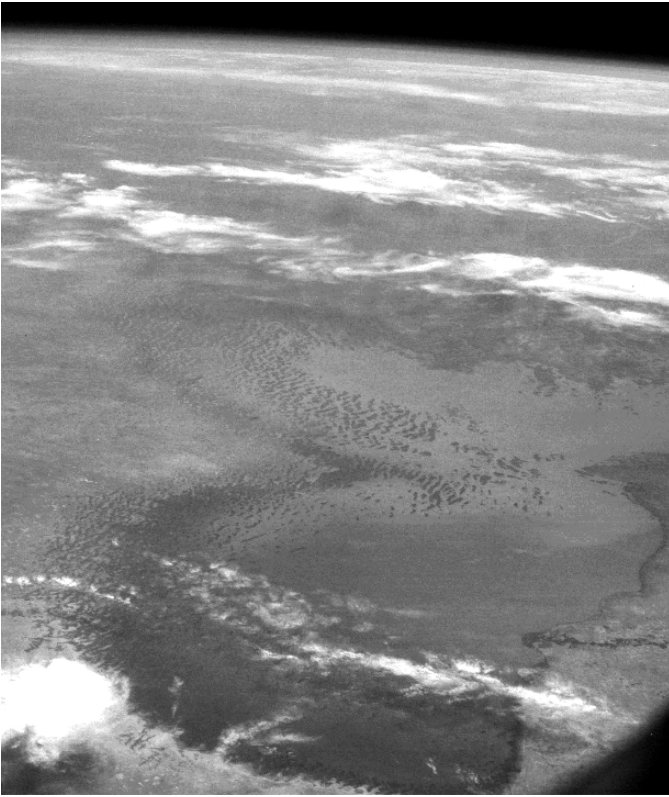


Fig. 2.2 Image of Lake Chad, Africa, acquired in October 1968 by Apollo 7 crew. Image courtesy of Earth Sciences and Image Analysis Laboratory, NASA Johnson Space Center

During those years another sophisticated camera was included on board the Space Shuttle in several missions. It was named Large Format Camera, since it covered twice the territory (23×46 cm) of an ordinary aerial photography film. It was used for basic cartography, as well as thematic interpretation (Francis and Jones 1984; Lulla 1993). Other cameras on board the Space Shuttle have been the Hasselblad 70 mm, Aerotechnika and more recently, the Electronic Sill Camera, a digital camera with up to 2048×2048 pixels (Lulla 1993). Most of those photographs, as well as those from declassified military systems and some Russian satellites can be accessed through the Global Land Information System (GLIS), the image portal of the U.S. Geological Survey web server, or through the NASA Gateway of Astronaut Photography of Earth (<http://eol.jsc.nasa.gov/>). These photographs provide a sporadic historical record to monitor environmental change (Lulla and Dessinov 2000).

The Space Shuttle also incorporated some RADAR missions, to test new technologies in microwave Earth observation. These missions were the Shuttle Imaging Radar (SIR) A, B and C, on flight in 1981, 1984 and 1994, respectively. The first two were L band RADAR, with a spatial resolution of 25 to 40 m, and HH polarization,

and a wide observation angle: 47° in SIR-A and 15 to 60° in SIR-B. SIR-C included three bands (L, C and X), at different polarization, various observation angles (from 20 to 55°), with a spatial resolution of 25 to 30 m and digital recording.

2.2.1.2 Exploratory Missions: HCMM – Seasat

Some of the technologies included on the Space Shuttle were previously tested in exploratory missions. This is the case of the synthetic aperture RADAR technologies, which were tested with the Seasat mission. This satellite was only active for a few months in 1978, but it was a milestone in the use of active microwave data for Earth observation. The Seasat included synthetic aperture radar working with L-Band and HH polarization, at an incidence angle between 20 and 26° . The spatial resolution was 25 m. The data were recorded in film. The system also included a microwave altimeter with high precision to measure the Ocean geoid. Seasat data were mainly used for oceanographic applications, although some studies were conducted for geological and land cover mapping (Elachi 1982).

The Heat Capacity Mapping Mission (HCMM) was also relatively short, from 1978 to 1980. It was oriented towards demonstration of potential uses of thermal sensors for geological, snow cover and plant applications. The system had a circular sun-synchronous orbit which allowed the spacecraft to sense surface temperatures near the maximum and minimum of the diurnal cycle. Day/night coverage over a given area between the latitudes of 85 deg N and 85 deg S occurred at intervals ranging from 12 to 36 h (once every 16 days). The resolution of the sensor was approximately 500 m for the visible band and 600 m for the thermal band, both at nadir, with a field of view of 716 km (Short and Stuart 1982).

2.2.2 Landsat Program

The success of the first space photographs and the routine use of aerial survey photography made it possible to conceive of a mission exclusively oriented towards the observation of natural resources. This mission initially named the Earth Resources Technology Satellite (ERTS) was launched on 23rd July 1972. After the launch of the second satellite, in 1975, the program was renamed Landsat. Without doubt, the Landsat program has been the most important for civilian Earth Observation, providing a continuous coverage of our planet for the last 35 years, at medium spatial resolution. The critical impact of this series of satellites and the immense variety of world-wide users explains the great concern about the continuity of this program, which was seriously impacted by the loss of Landsat-6, and the subsequent technical failure of scan line corrector on Landsat-7 in late 2003, and the extremely slow response to replacing this broken instrument. An update on the technical characteristics of the program can be found at: <http://landsat.gsfc.nasa.gov/>.

2.2.2.1 Orbital Characteristics

The first three Landsat satellites had a Sun-synchronous polar orbit, at 917 km, with a revisiting period of 18 days and a 10.30 a.m. Equatorial crossing time. The third and fourth Landsat satellite modified their instrument configuration and orbital characteristics. The orbital height was decreased to 705 km, the orbital period was reduced and the revisiting observation was improved to 16 days in temperate latitudes. Overpass time remained similar to the previous Landsats, crossing the Equator around 10.10 am. The next two satellites of the mission, Landsat-6 and 7, changed again the appearance (Fig. 2.3), although they maintained the orbital characteristics of their two predecessors. Landsat-6 was lost shortly after the launch in 1993, while the Landsat-7 was launched 1999 and still is working although with a serious technical problem.

2.2.2.2 Sensors

The first three Landsat included digital multi-spectral scanners (MSS) and three video cameras (RBV, Return Beam Vidicon), the first two and just one, at higher resolution, for Landsat-3. The cameras did not work properly in the first two satellites; hence the MSS was really the most useful sensor of the mission until the launch of Landsat-4. The MSS had an 11.56° field of view, able to observe an area of 185×185 km at 57×79 m nominal resolution. It covered four bands of the spectrum (green, red, and two in the near infrared, numbered as 4, 5, 6, and 7, respectively). Designed to imitate true and false color infrared photography, Landsat-3 included an updated version of the MSS with a thermal band. Data were digitally acquired and recorded on board or transmitted in real time to a set of acquisition antennas. Bands 4 to 6 were coded in seven bits (between 0 and 127) and band 7 in six bits (0 and 63).

The launch of the Landsat-4 and 5 gave a boost to the program with a more sophisticated multispectral scanner sensor designed primarily for remote sensing of vegetation. It was named the Thematic Mapper (TM) and improved on the spatial, spectral resolution and radiometric resolution of the MSS, from 79 to 30 m, from 4 to 7 bands, and from 6 to 8 bits quantization. Landsat-7 included an improved version of the TM, named the ETM+, with similar characteristics to TM,

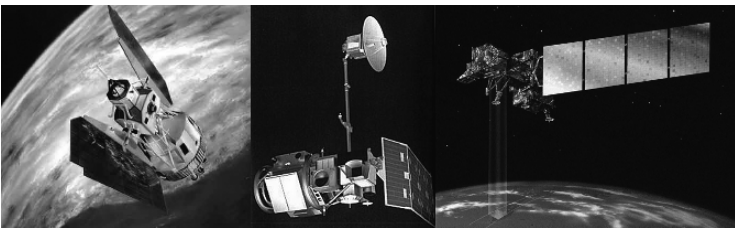


Fig. 2.3 Different Landsat spacecrafts, from left to right: Landsat-2, Landsat-5 and Landsat-7

but with an additional panchromatic band with a 15 m spatial resolution, and improved resolution of the thermal band to 60 m. New bands included two in the short-wave infrared (SWIR, 1.6 to 2.2 μm), which are very valuable for estimating water content of soils and plants, and improving atmospheric correction, as well as one in the thermal infrared. NASA through its Landsat Pathfinder program had demonstrated the necessity for repeat coverage and large volume wall to wall mapping using Landsat for global change research. An important step forward for Landsat 7 was the reduction in per-scene costs from the unaffordable commercial rates and the implementation of a long term acquisition plan to acquire seasonal coverage globally dramatically increasing the availability of data. (Arvidson et al. 2006).

Unfortunately, the ETM+ encountered a serious technical problem in May 2003 when the scan line corrector a hardware component of the instrument failed.

2.2.2.3 The Future of the Landsat Program

The broad variety of thematic and geographical users of Landsat explain the great interest raised concerning the continuation of this mission. In 1984, in a misguided effort to commercialize Landsat data, the Reagan Administration transferred the Landsat program to the private sector (O.T.A. 1984). A few months later, in 1985, a single company, EOSAT received the rights to sell products Landsat for a 10 year period, with the commitment of participating in the development of future sensors. As a result the price of data was increased considerably which severely limited science and applications use. On the other hand, the government maintained the physical control of the platform (through NOAA), and kept the commitment to cooperate in the development of Landsat-6 and 7. Further budgetary reductions brought into question this commitment, and by 1989, even the continuity the Landsat-4 and 5 was under discussion.

The numerous pressures of the scientific and professional community, the development of space programs by other countries (notably France with the SPOT system), the growing interest in global observation of environmental change based on the historical archive of MSS data, and the strategic contribution of Landsat imagery in the first Gulf War (1991), led to a greater commitment for the Landsat program by the Federal Government. In 1992, the Land Remote Sensing Policy Act was approved, which included a shift in the management of the Landsat mission, which was transferred back to the government, initially to the Department of Defense and the NASA, and subsequently to the Department of Interior by the U.S. Geological Survey, in collaboration with NASA and NOAA. This Act gave renewed impetus to Landsat-7, and increased emphasis on data continuity (Williamson 2001). The planning for a follow-on mission to Landsat 7 has been tortuous. A proposal by industry in response to a request from to build the follow-on instrument was rejected by NASA in due primarily to costs.

A proposal to include two Landsat instruments as part of the operational National Polar Orbiting Environmental Satellite Suite to be managed by NOAA was considered and rejected.

In December 2005 NASA was instructed by the Office of Science and Technology Policy to acquire a single Landsat Data Continuity Mission in the form of a free-flyer spacecraft with USGS taking responsibility for the mission operations. This latest request is currently in process, with an earliest projected launch date of 2011(<http://ldcm.nasa.gov/>). Although this plan gives some hope for a continuity mission, the approach is to build just one instrument, which exposes the program to risk, based on the experience of Landsat 6 and is small step to meeting the real observation needs from this class of instrument (Goward and Skole 2005).

The Landsat program has both benefited and suffered from not being an operational system. The research status of the program has enabled a progressive evolution and improvement of the instrumentation. The lack of operational commitment has meant that there is no replacement instrument is ready for launch when the current system fails, data continuity is therefore compromised, operational users are obliged to seek other non-U.S. data sources and new instruments have to be commissioned and built which takes at least 3 years.

As a result we now have a malfunctioning Landsat 7 since 2003, a single Landsat Data Continuity Mission planned for launch in 2011 and a widening data gap in Landsat data continuity.

The Landsat Mission concept was developed in the late 1960's and needs to be revisited. Although the spectral bands (visible to shortwave infrared) and the spatial resolution have been successively refined to meet the needs of the users, the frequency of overpass every 16 days remains far short of what is needed, particularly given cloud cover. For example for agricultural applications, coverage every 6 days is needed to capture changes in crop condition (URL: http://www.fao.org/gtos/igol/docs/meeting-reports/ag-IGOL-meeting-report_v10.pdf). The Indian Remote Sensing satellite advanced wide-field sensor (AWiFS) operating in three spectral bands in VNIR and one band in SWIR with 56-metre spatial resolution and a 750 km swath is capable of providing multiple acquisitions per month. The USDA is using data from this latter system to replace its use of Landsat data. With shrinking budgets for earth observation, an alternative approach for NASA could consider would be to launch a constellation of well-calibrated microsatellites with visible to shortwave infrared sensors providing a 6 day repeat coverage, following the example of the Disaster Management Constellation program (http://centaur.sstl.co.uk/datasheets/Mission_DMC.pdf).

2.2.3 Terra and Aqua

Terra is the flagship of the EOS program, and the first example of the new strategy adopted by NASA in the Earth Science program. Terra was successfully launched in December, 1999 and it includes a wide variety of sensors oriented towards the analysis of global processes. The platform is located in a near-polar, Sun-synchronous orbit, crossing the Equator around 10.30 am and pm. The orbital height is 705 km, with a period of 98.88 minutes and a repeat cycle of 16 days. The platform dimensions are

2.7 × 3.3 × 6.8 m and the total weight is 5,190 kg. It carries five sensors (MODIS, CERES, MISR, MOPITT and ASTER) designed for global observations of critical land, oceans and atmospheric variables (<http://terra.nasa.gov>).

Aqua was launched in May, 2002, and it has similar orbital characteristics to Terra, but with a lag period of six hours, and therefore crosses the Equator at 1.30 am and pm. The satellite is lighter than Terra, weighing 2,934 kg. It carries six sensors (AIRS, AMSR-E, CERES, HSB and MODIS), with an instrument configuration oriented towards ocean sensing (<http://aqua.nasa.gov>).

The main sensors of Terra and Aqua are described below.

2.2.3.1 MODIS

The Moderate-Resolution Imaging Spectroradiometer (MODIS) is a 36-band spectroradiometer measuring visible and infrared radiation, at different resolutions. The first two bands cover the red and near infrared and have 250 m pixel size. The next five have 500 m spatial resolution and cover several bands in the visible, near infrared and SWIR spectral bands. As with the 250 m bands these were selected primarily for land observations and mimic the Landsat Thematic Mapper bands. The other spectral channels have a 1 km resolution and include several in the visible, near infrared, middle infrared and thermal infrared for oceans and atmospheres studies and land thermal monitoring. The field of view covers 2300 km and provides daily world-wide observations. The MODIS is carried on both the Terra and Aqua missions, and therefore, four daily acquisitions (two daytime, two nighttime) are available for most of the Earth. MODIS was designed to provide accurate measurements of several critical variables. Approximately, 40 standard products are produced from the MODIS data (Table 2.2), and distributed through the Distributed Active Archive Center (DAACs: <http://daac.gsfc.nasa.gov>).

2.2.3.2 Other Instruments on the Terra – Aqua Spacecraft

The Clouds and the Earth's Radiant Energy System (CERES) is a radiometer that measures global radiation and cloud properties. It is carried on both the Terra and Aqua satellites, as well as in the TRMM mission. Two CERES instruments are on board of each platform, one cross-track scanning, measuring the earth radiation budget, and the other in azimuth scanning mode, computing angular radiance information. CERES has three bands measuring total radiance, short-wave radiance and thermal radiance. The spatial resolution is 20 km This sensor is expected to be included in the future NPOES polar satellites program.

The Advanced Spaceborne Thermal Emission and Reflection Radiometer (ASTER) is the only high-spatial sensor included on the Terra satellite. It was built by Japan who takes care of data production and shares distribution with the USGS. ASTER has 15 channels: four at 15 m pixel size, covering the green, red, and near infrared, six at 30 m resolution covering the SWIR, and other five in the thermal infrared. The two near infrared bands provide stereoscopic coverage,

Table 2.3 MODIS standard products (updated from Parkinson, 2006)

Product Name or Grouping	Processing Level	Coverage	Spatial/Temporal Characteristics
Level 1B Calibrated, Geolocated Radiances	1B	Global	0.25, 0.5, and 1 km/daily (daytime and nighttime)
Geolocation Data Set	1B	Global	1 km /daily (daytime and nighttime)
Aerosol Product	2	Global over oceans, nearly global over land	10 km/daily daytime
Total Precipitable Water	2	Global	Varies with retrieval technique; 1 km near-infrared/daylight only, and 5 km infrared/ day and night
Cloud Product	2	Global	1 or 5 km/once or twice per day (varies with parameter)
Atmospheric Profiles	2	Global, clear-sky	5 km/daily (daytime and nighttime)
Atmosphere Level 2 Joint Product (select subset)	2	Global	5 or 10 km/once or twice per day (varies with parameter)
Atmosphere Level 3 Joint Product	3	Global	1.0° latitude-longitude equal-angle grid/daily, 8-day, and monthly
Cloud Mask	2	Global	250 m and 1 km/daily
Surface Reflectance; atmospheric Correction Algorithm Products	2	Global land surface	500 m, 0.05°, and 0.25°/daily
Snow Cover	2, 3	Global, daytime	500 m and 0.05°/daily; 500 m and 0.05°/8-day; 0.05°/monthly
Land Surface Temperature (LST) and Emissivity	2, 3	Global land surface	1 km, 5 km/daily; 1 km/8-day
Land Cover/Land Cover Dynamics	3	Global, clear-sky only	1 km and 0.05°/yearly
Vegetation Indices	3	Global land surface	250 m, 500 m, 1 km/16-day; 1 km/monthly
BRDF/Albedo	3	Global land surface	1 km, 0.05°/16-day
Land Cover Change and Conversion	3, 4	Global, daytime	250 m, 500 m/96-day, yearly
Thermal Anomalies/Fire	2, 3	Global, daytime/ nighttime	Swath (nominally 1-km) (Level 2); 1 km/daily, 8-day (Level 3)
Leaf Area Index (LAI) and Fraction of Photosynthetically Active Radiation (FPAR)	4	Global	1 km/8-day
Net Photosynthesis and Net Primary Production	4	Global	1 km/8-day, yearly

(continued)

Table 2.2 (continued)

Product Name or Grouping	Processing Level	Coverage	Spatial/Temporal Characteristics
Normalized Water-Leaving Radiance (412, 443, 488, 531, 551, and 667 nm)	2, 3	Global ocean surface, clear-sky only	1 km/daily (Level 2); 4 km, 9 km/daily, 8-day, monthly, seasonal, yearly (Level 3)
Chlorophyll a Concentration	2, 3	Global ocean surface, clear-sky only	1 km/daily (Level 2); 4 km, 9 km/daily, 8-day, monthly, seasonal, yearly (Level 3)
Ocean Diffuse Attenuation Coefficient at 490 nm	2, 3	Global ocean surface, clear-sky only	1 km/daily (Level 2); 4 km, 9 km/daily, 8-day, monthly, seasonal, yearly (Level 3)
Sea Surface Temperature (11 μm , day and night; 4 μm , night)	2, 3	Global ocean surface, clear-sky only	1 km/daily (Level 2); 4 km, 9 km/daily, 8-day, monthly, yearly (Level 3)
Sea Ice Cover and Ice-Surface Temperature	2, 3	Global, daytime and nighttime over nonequatorial ocean	1 km, 0.05°/daily
Epsilon of Aerosol Correction at 748 and 869 nm	2, 3	Global ocean surface, clear-sky only	1 km/daily (Level 2); 4 km, 36 km, 1°/daily, 8-day, monthly, yearly (Level 3)
Aerosol Optical Thickness (869 nm)	2, 3	Global ocean surface, clear-sky only	1 km/daily (Level 2); 4 km, 9 km/daily, 8-day, monthly, seasonal, yearly (Level 3)
Ångstrom Coefficient (531–869 nm)	2, 3	Global ocean surface, clear-sky only	1 km/daily (Level 2); 4 km, 9 km/daily, 8-day, monthly, seasonal, yearly (Level 3)

and therefore they can be used to generate digital terrain models and to measure cloud properties. Since ASTER images are acquired simultaneously with the coarser resolution MODIS, they can be used for product validation (Csiszar et al. 2006). However, ASTER does not operate continuously, but is only acquired for selected scenes, and so its data coverage is less comprehensive than for example Landsat 7.

The Multi-Angle Imaging Spectroradiometer (MISR) is one of the first sensors providing a multiangular observation of the whole planet. It acquires images at 9 different angles (at nadir plus at 26.1, 45.6, 60 and 70.5 degrees, forward and backward) and in 4 spectral bands (blue, green, red and near infrared). This configuration facilitates the analysis of atmospheric optical thickness of the atmosphere (Fig. 2.4), cloud type and height, leaf area index and fractional absorbed photosynthetically active radiation. Each image covers 360 km at a variable spatial resolution, which depends on the observation angle, although the most common are 275, 550 and 1100 m. MISR flies on the Terra platform.

The Measurements of Pollution in The Troposphere (MOPITT) instrument was primarily designed to measure carbon monoxide and methane concentrations. The

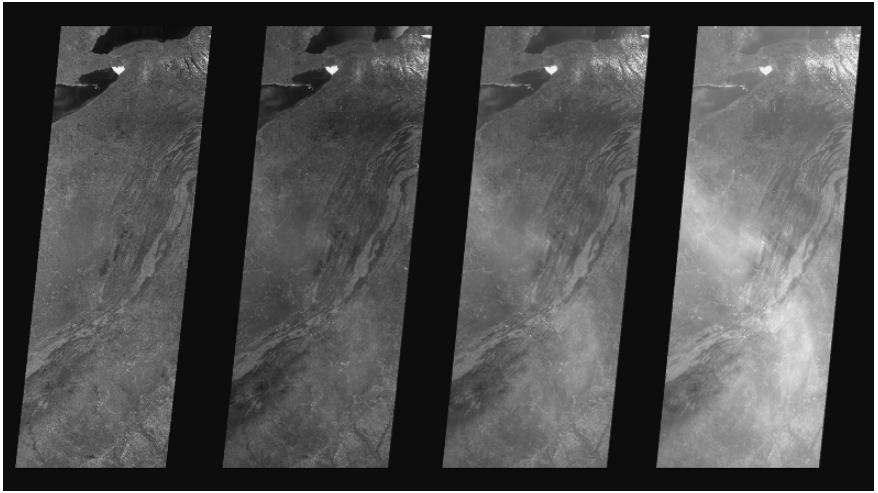


Fig. 2.4 MISR image of Eastern United States from nadir and several oblique angles (<http://visibleearth.nasa.gov/>)

sensor uses a correlation spectroscopy technique, which estimates the concentration of a gas by spectral selection of emitted or absorbed radiance, using a sample of the same gas as a filter. The sensor has a resolution of 22 km with a swath width of 640 km. It was included in the Terra platform, as part of a cooperation agreement with Canada.

The Atmospheric Infrared Sounder (AIRS) is a high spectral resolution grating spectrometer containing 2378 infrared channels (from 3.7 to 15.4 μm) for obtaining atmospheric temperature profiles. AIRS also has 4 visible/near-infrared channels (from 0.4 to 1 μm), for characterizing cloud and surface properties and obtaining higher spatial resolution than the infrared measurements. It is included on the Aqua platform.

The Advanced Microwave Scanning Radiometer (AMSR-E) is a Japanese instrument on board the Aqua platform. It includes a 12-channel microwave radiometer designed to monitor a broad range of hydrologic variables, including precipitation, cloud water, water vapor, sea surface winds, sea surface temperature, sea ice, snow, and soil moisture.

The Advanced Microwave Sounding Unit-A (AMSU-A) is a 15-channel microwave sounder designed to obtain temperature profiles in the upper atmosphere and to provide a cloud-filtering capability for the AIRS infrared measurements, for increased accuracy in troposphere temperature profiles. It is on board the Aqua satellite, as well as the latest in the NOAA Polar Orbiting Environmental (POES) satellite series (after NOAA-15).

The Humidity Sounder for Brazil (HSB), provided atmospheric water vapor profile measurements until February 2003 when it lost operation. It includes a 4-channel microwave sounder designed to obtain atmospheric humidity profiles under cloudy conditions and to detect heavy precipitation under clouds. It is included on the Aqua platform.

2.2.4 Other NASA Global Observation Missions

Aura is an international mission oriented to the study of atmosphere's chemistry and dynamics, including ozone observations, aerosols and trace gases. The mission was launched in 2004 in a sun-synchronous orbit, with equatorial crossing at 1.45 p.m. The satellite includes four instruments: the High Resolution Dynamics Limb Sounder (HIRDLs), the Microwave Limb Sounder (MLS), the Ozone Monitoring Instrument (OMI), and the Tropospheric Emission Spectrometer (TES). The OMI is the primary instrument, and continues the monitoring of stratospheric ozone trends that was initiated by the Nimbus program.

The Earth Radiation Budget Satellite (ERBS) is a mission oriented towards the analysis of solar radiation and sun-earth radiation interactions. It was launched from the Space Shuttle in 1984, and carried two instruments, the Earth Radiation Budget Experiment (ERBE), that measures radiation budgets, and the Stratospheric Aerosol and Gas Experiment (SAGE II), oriented towards the distribution of aerosol, ozone, water vapor, and nitrogen dioxide. ERBE continues the measurements, on board the NOAA satellites.

ICESat is an ice monitoring mission, launched in 2003. Its main novelty is the incorporation of the first space-borne LIDAR, primarily designed for ice sheet and sea ice altimetry products (Fig. 2.5) with secondary products being cloud/aerosol and land/vegetation data. The sensor is named Geoscience Laser Altimeter System (GLAS). GLAS is an advanced laser altimeter with very precise stellar orientation and GPS for accurate position determination. It includes two wavelengths (near infrared and green), with a footprint of 70 m and an across track separation of 170 m. Although, GLAS measurements are mainly oriented toward ice height estimations, they also have potential for retrieval of vegetation parameters, although the estimations are more robust in the absence of rough terrain (Harding and Carabajal 2005).

The QuikSCAT satellite was launched in 1999 to measure wind fields in the oceans. It orbits in a sun-synchronous trajectory at 803 km, crossing the Equator at 6 p.m. The satellite includes a 13.4 GHz Ku-band scatterometer named SeaWinds, measuring the backscattered signal from Earth over a continuous, 1800-km-wide swath centered on the subsatellite track at 25×35 km pixel size. SeaWinds data are very valuable for improving our knowledge of ocean currents and local effects of air mass movements (Chelton et al. 2004).

Finally, the Earth Observing Mission (EO-1: <http://eo1.gsfc.nasa.gov/>), which was aimed at developing and testing new instruments for future operational missions, that will have a significant increase in performance while also having reduced cost and mass. The mission was launched in 2000 and carries three innovative sensors: Hyperion, ALI and LEISA. Hyperion was the first civilian hyperspectral space-borne sensor. It acquires 220 spectral bands between 0.4 and $2.5 \mu\text{m}$ with 30 m resolution over narrow strip of 7.5×180 km. Despite its low signal to noise ratio, it has provided very useful information to test the potential of hyperspectral satellite data for forestry and geological applications (Goodenough et al. 2003; Roberts et al. 2003).

The EO-1 mission also includes a multispectral pushbroom scanner, the Advanced Land Imager (ALI), which was developed to test potential replacement

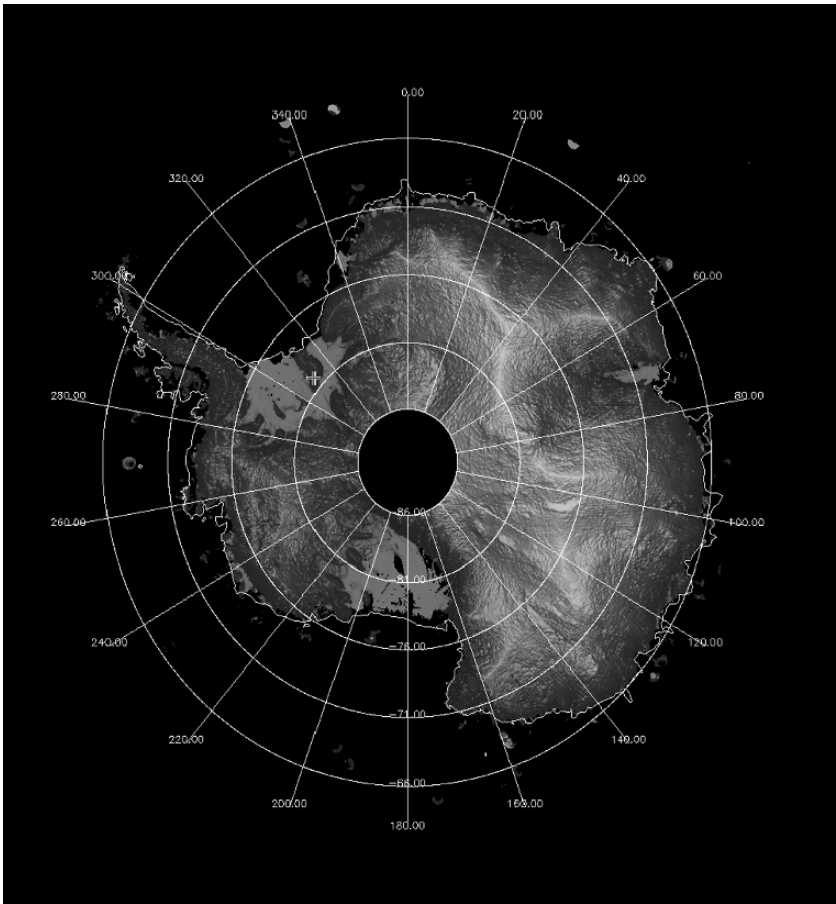


Fig. 2.5 ICESat elevation data over Antarctica (<http://icesat.gsfc.nasa.gov/>)

technology for the Landsat-ETM + sensor, since it provides similar spectral and spatial resolution, at a fraction of its costs. The ALI has 9 multispectral bands at 30 m resolution, plus one panchromatic band at 10 m. ALI was found to have a similar performance to ETM, with the exception of the absent thermal channel.

Finally, the EO-1 also incorporates an advanced atmospheric correction sensor, named Linear Etalon Imaging Spectral Array (LEISA), Atmospheric Corrector, which provides estimations of water vapor content for correction of the visible and near infrared channels.

2.3 NASA Data Access and Maintenance Policy

The EOS missions generate unprecedented amounts of daily data that need to be properly calibrated, processed, archived, documented and then made accessible for a wide range of scientists. Terra, Landsat and Aqua offer the highest volume of

average data rates, accounting for more than 35 Mbps between the three of them. The flow of data acquisition, processing and access is guided by the Earth Observing System Data and Information System (EOSDIS), at eight Distributed Active Archive Centers (DAACs) for different locations in the US and foreign sites (Table 2.3). Data capture and Level 0 processing is done commonly at EOSDIS facilities. Product generation is performed according to the guidelines submitted by the different Science teams. Data archive, management and distribution is generally done through the DAACs, using a common EOS Data Gateway (EDG). The EOS Clearing House (ECHO) will eventually replace the EDG, for more consistent searches and retrievals. Searches for different data products are facilitated through the Global Change Master Directory (GCMD, <http://gcmd.gsfc.nasa.gov/>), which provides metadata descriptions of Earth science data sets and services relevant to global change research. The GCMD holds more than 16,200 data set descriptions and 1,400 Earth science service descriptions, which consist of information on how to obtain the data or service and often include direct access to the data or services. The DAAC centers process, archive, document, and distribute data from NASA's past and current research satellites and field programs. Each center serves one or more specific Earth science disciplines (Table 2.3) and provides data products, data information, services, and tools unique to its particular science. In addition a

Table 2.3 Distribution data centers, disciplines, and contact information

Data Center	Discipline	Web page
Alaska Satellite Facility ASF Distributed Active Archive Center	Synthetic Aperture Radar (SAR), Sea Ice, Polar Processes and Geophysics	www.asf.alaska.edu
GSFC Earth Sciences Data and Information Services Center	Atmospheric Composition, Atmospheric Dynamics, Global Precipitation, Ocean Biology, Ocean Dynamics, and Solar Irradiance	daac.gsfc.nasa.gov
Global Hydrology Resource Center GHRC	Hydrologic Cycle, Severe Weather Interactions, Lightning, and Convection	ghrc.msfc.nasa.gov
Langley Research Center	Radiation Budget, Clouds, Aerosols, and Tropospheric Chemistry	eosweb.larc.nasa.gov
Land Processes	Land Processes	LPDAAC.usgs.gov
National Snow and Ice Data Center NSIDC	Snow and Ice, Cryosphere and Climate	nsidc.org
Oak Ridge National Laboratory	Biogeochemical Dynamics, Ecological Data for Studying Environmental processes	www.daac.ornl.gov
Physical Oceanography	Oceanic Processes and Air-Sea Interactions	podaac.jpl.nasa.gov
Socioeconomic Data and Applications Center SEDAC,	Population, Sustainability, Geospatial Data, and Multilateral Environmental Agreements, Natural Hazards, Poverty	sedac.ciesin.columbia.edu

number of science computing facilities are distributing non-standard products customized for different user communities such as the MODIS Rapid Response System (<http://rapidfire.sci.gsfc.nasa.gov/>), the Fire Information for Resource Management System (FIRMS) project (<http://maps.geog.umd.edu/firms/>) and the Global Land Cover Facility (GLCF) (<http://glcf.umiacs.umd.edu/index.shtml>)

NASA policy on data management and accessibility emphasizes the importance of providing timely and easy access to both calibrated data and derived geophysical data products. The main aspects of this policy can be summarized in three aspects: archival, accessibility and affordability. NASA promotes the archival and documentation of long-term data sets to support the Earth Science program. Considering the large volumes of data acquired by same sensors, this is a major effort that is absolutely essential for analyzing climatic impacts on Earth ecosystems and the atmosphere. In this regard, the generation and maintenance of the Pathfinder AVHRR Land Data (PAL: <http://daac.gsfc.nasa.gov/interdisc/readmes/pal ftp.shtml>) and, more recently, the Land Long Term Data Record (LTDR: <http://ltdr.nascom.nasa.gov/ltdr/ltdr.html>) should be properly acknowledged, since they offer one of the longest series available of satellite observations (mainly AVHRR images) in a consistent and comparable form, covering the whole planet.

A major characteristics of NASA's data policy is the openness of data search and retrieval. All NASA instruments (with the exception of Landsat-7) include a web service for free internet access to calibrated data and derived products. However, some restrictions may occur when international agreements so require, in case of sensors that are owned by another country (e.g. ASTER). Airborne and field validation data generated for validation studies are also generally accessible, as well as the documentation on the algorithms and source code used to generate the products (Parkinson et al. 2006). This policy greatly benefits the growth of EOS data users world-wide.

2.4 Interagency Collaboration in EO Program

In the last few years, a U.S. Interagency Working Group on Earth Observations (IWGEO) has been formed to develop a 10 year plan for implementing the U.S. components of the integrated Earth Observation System (<http://usgeo.gov/default.asp>). IWGEO is responsible for developing a U.S. National Plan for the Earth Observation System, in coordination with Academia and the Private Sector. The group includes representatives from 15 government agencies, from the Department of Health and Human Services, to Homeland Security, Agriculture, Commerce, Energy, Transportation and Interior, plus the Environmental Protection Agency, the U.S. Geological Survey, the National Science Foundation, Smithsonian Institution, U.S. Agency for International Development, Office of Science and Technology Policy, and Office of Management and Budget. Many of the initiatives of this coordination group are under the US Committee on Climate Change Science (CCSP) (<http://www.climate-science.gov/>).

As far as satellite missions are concerned, the main interagency cooperation has been between NASA and National Oceanic and Atmospheric Administration

(NOAA) in the context of weather and climate forecasting. NASA is responsible for the experimental satellite systems and NOAA for the operational systems. The main collaborative initiatives have been developed in the framework of the Geostationary and Polar-orbiting satellite systems, the former having been initiated in the early sixties. NASA's Goddard Space Flight Center (GSFC) is responsible for the construction, integration and launch of NOAA satellites, and operational control of each spacecraft is turned over to NOAA after the spacecraft is checked out on orbit.

The Geostationary Operational Environmental Satellite (GOES) mission is composed of two geostationary satellites working simultaneously, one located in the USA East coast and the other in the USA west coast. The former, GOES-12 is positioned at 75W longitude ant the Equator, while the latter, GOES-10 is positioned at 135 W longitude and the Equator. The main sensors on board are the Imager, which is a scanning instrument with five spectral channels and a spatial resolution from 1 km (visible) to 4 km (middle and thermal infrared) at the Equator, and the Sounder, which offers a profile of temperature and atmospheric humidity, as well as the distribution of ozone.

The polar meteorological satellites initially known as TIROS and ITOS were renamed NOAA after the launch of the sixth satellite, in 1979, which incorporated a new generation of sensors. The NOAA satellites were primarily designed for weather observation, but they have been extensively used for land and ocean applications as well. They are positioned at a Sun-synchronous orbit at a height from 833 to 870 km. Two satellites have worked simultaneously since 1979, providing early morning 8.30 am and late afternoon 14.30 pm coverage (Equatorial crossing), plus two night-time images.

The main sensor of the NOAA satellite series is named AVHRR (Advanced Very High Resolution Radiometer) (Cracknell 1997). It is multispectral scanning radiometer acquiring images at five spectral bands (red, near infrared, middle and thermal infrared). The visible and infrared bands do not have the benefit of on-board calibration and methods for vicarious calibration have had to be developed). The AVHRR field of view is $\pm 55.4^\circ$, which provides a spatial cover of 2300 km. The radiometric resolution is 10 bits and the spatial resolution at nadir is 1.1 km, but it is degraded to 2.4×6 km at the image margins because of the oblique angle. In addition to lower spatial resolution, the most oblique observations have greater atmospheric and observation artifacts, and therefore several authors recommend to avoid working with observation angles greater than $\pm 30^\circ$ (Goward et al. 1991).

AVHRR images can be processed in three different formats: LAC (Local Area Coverage), when data at full resolution (1.1 km) are recorded on board, HRPT (High Resolution Picture Transmission), when images are acquired in real time by ground receiving stations, and GAC (Global Area Coverage), when the 1 km resolution data are resampled on board at coarser spatial resolution (4×4 km). GAC data are used to compile a weekly product by NOAA named GVI (Global Vegetation Index), derived from the red and near infrared channels with 16 km pixel size (Kidwell 1990). NASA has maintained its own record of AVHRR data and a long time series of GAC data have been compiled for global scale studies (Fig. 2.6), named the Pathfinder AVHRR Land (PAL) data sets, following cooperation between NOAA and NASA. The dataset is composed of daily AVHRR

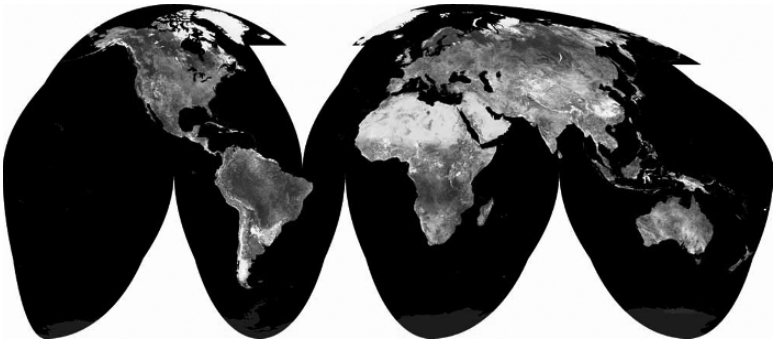


Fig. 2.6 World mosaic of AVHRR images used for global analysis of vegetation trends

data at 8 km equal area projection, and includes the original channels, plus NDVI and observation and illumination angles. These dataset cover the period from 1981 to the present, and is archived at the Goddard Distributed Active Archive Center (DAAC). The long term data record from multiple AVHRR instruments has created a number of challenges associated with instrument calibration and orbital drift. More recently an improved long term data record is being developed by NASA bridging between the AVHRR GAC data record and the MODIS data record (<http://ltdr.nascom.nasa.gov/ltdr/ltdr.html>). The AVHRR record initiated in 1981 will be extended into the future by inclusion of AVHRR's on the European METOP series of satellites for the morning overpass. The METOP series was launched in October 2006 (http://www.eumetsat.int/Home/Main/What_We_Do/Satellites/EUMETSAT_Polar_System/index.htm?l=en). The AVHRR has suffered from being an operational instrument, as necessary changes recognized decades ago, such as onboard calibration and global 1 km acquisition, have yet to be made.

Other sensors on board the NOAA satellite series are the High Resolution Infrared Radiation Sounder (HIRS/3 and HIRS/4), the Advanced Microwave Sounding Unit (AMSU-A and B), the Solar Backscatter Ultraviolet Spectral Radiometer (SBUV/2) and the Microwave Humidity Sounder (MHS). Some of them have been previously reviewed within the Terra or Aqua missions.

NASA also collaborates with the Department of Defense, through the Defense Meteorological Satellite Program (DMSP). The DMSP has been run by the Air Force Space and Missile Systems Center since 1976, and was primarily designed to obtain meteorological information (Diamond 2001). They have a similar orbital period to NOAA at 830 km, acquiring at least 2 images a day.

DMSP satellites include several sensors for cloud and atmospheric monitoring. The Operational Linescan System (OLS) includes two telescopes and a photomultiplier tube, which provides day and night images in two bands: visible to near infrared (0.5 to 0.9 μm) and thermal infrared (10.5 at 12.6 μm). The spatial resolution is 0.56 km at regional level, but the archive data sets contain imagery from low resolution (2.7 km). Nighttime visible data can be obtained because of the high-sensitivity of the photo-multiplier. Consequently, the sensor is able to obtain cloud

coverage from the moon reflection, as well as sources of light, which can be urban areas, oil wells, volcano eruptions or forest fires (Elvidge 2001). The Special Sensor Microwave Imager (SSM/I), was incorporated in the DMSP mission in 1987. It is a well calibrated microwave radiometer that provides sound information on several hydrological parameters (snow cover, frozen ground, sea ice, wind speed over the oceans and cloud liquid water).

Future developments of the polar weather observing satellites aims to include a more sophisticated sensor in the new generation of satellites, named National Polar-orbiting Operational Environmental Satellite System (NPOESS). The program is a cooperation effort of NASA, NOAA and Department of Defense. NPOESS is planned to become operational toward the end of this decade and will replace the present NOAA polar environmental satellites and the DoD polar meteorological satellites (http://www.ipc.noaa.gov/about_NPOESS.html). The NPOESS Preparatory Project (NPP), planned for launch in late 2009, is a joint NASA/ NPOESS Integrated Program Office (IPO) mission to extend key measurements in support of long-term monitoring of climate trends and of global biological productivity (Murphy 2006), <http://nppwww.gsfc.nasa.gov/science/>). It will extend the measurement series being initiated with EOS Terra and Aqua and provide risk reduction for NPOESS and a bridge for NASA's EOS missions. NPP will consist of four instruments: the Visible Infrared Imaging Spectroradiometer Suite (VIIRS), the Crosstrack Infrared Sounder (CRIS), the Advanced Technology Microwave Sounder (ATMS) and the Ozone Mapping Profiler Suite (OMPS) The VIIRS will replace the AVHRR and DMSP functionality and will extend the MODIS data (Murphy et al. 2001). The VIIRS will have 9 bands in the visible/near infrared, a day/night band, 8 bands in the middle infrared and 4 in the long wave infrared (Murphy et al. 2006). Currently there are plans to generate environmental data records (EDR's) from the VIIRS sensor to serve the operational user community.

The CRIS and the ATMS will collect atmospheric data to permit the calculation of daily temperature and moisture profiles. The CRIS will be an advance over the current HIRS instrument on the POES series, providing improved spatial resolution and an ability to measure temperature profiles with improved vertical resolution to an accuracy close to one degree Kelvin (http://www.ipc.noaa.gov/Technology/cris_summary.html).

The OMPS will measure total column and vertical profile ozone data, continuing the global daily data produced by the current ozone monitoring systems, the Solar Backscatter Ultraviolet radiometer (SBUV)/2 and Total Ozone Mapping Spectrometer (TOMS), but with higher resolution. The OMPS will consist of a nadir sensor and a limb profiler (http://www.ipc.noaa.gov/Technology/omps_summary.html).

2.5 The Future of United States EO Policy

The large increase of data provided by the NASA EOS era of instruments has fueled global change research. With the current refocusing of NASA priorities in response to the Bush Administration's goal of Mars exploration and limited

budget growth we are seeing a decrease in resources for Earth observation. A number of missions planned for the near-term have been cut or seriously delayed and instruments planned for climate observations have been recently removed from NPOESS due to cost overruns. The NPOESS approach of converging multiple polar observing systems into one national system, although appealing in principle is proving to be fraught with financial and technical problems. This comes at a time when there is an increasing demand for science-quality observations to study climate and global change. For the study of global change urgent attention needs to be given to continuing the long term records initiated for example by Landsat and the AVHRR, transitioning science quality measurements into the operational domain.

NASA's EO program has led the world since the 1960's, although recent trends counterbalance this supremacy, since other space agencies are increasingly active in satellite observation systems. A recent study of the National Academy of Sciences to advise NASA and NOAA on their imperatives for the next decade calls on the US government to renew its investment in EO and restore its leadership in Earth Science and Applications (National Research Council 2007). This study recommended 17 missions to be launched by NASA and NOAA, phased over the next decade and split between small, medium and large cost missions. These missions would provide "a firm foundation for Earth Science and the associated societal benefits in the year 2020 and beyond". The committee also recognized the need for flexibility in the program to leverage possible international activities, including sequencing missions, partnership initiatives, instrument combinations and launch capabilities. There is clearly an important role for the Committee on Earth Observation Satellites (CEOS) to play in the coordination of the various national EO programs into a truly integrated global observing system. The recent focus of CEOS on the Global Earth Observing System of Systems is a step in the right direction.

It is the authors' opinion that the pressing societal issues facing the global community related to climate and global change necessitates attention by the US Government and in turn a rebalancing of NASA program to strengthen Earth Observations.

References

- Arvidson, T., Goward, S., Gasch, J., & Williams, D. (2006). Landsat-7 long-term acquisition plan: Development and validation. *Photogrammetric Engineering and Remote Sensing*, 72, 1137–1146.
- Chelton, D. B., Schlax, M. G., Freilich, M. H., & Milliff, R. F. (2004). Satellite measurements reveal persistent small-scale features in ocean winds. *Science*, 303, 978–983.
- Cracknell, A. P. (1997). *The Advanced Very High Resolution Radiometer (AVHRR)*. London: Taylor & Francis.
- Csiszar, I. A., Morisette, J. T., & Giglio, L. (2006). Validation of active fire detection from moderate-resolution satellite sensors: The MODIS example in Northern Eurasia. *IEEE Transactions on Geoscience and Remote Sensing*, 44, 1757–1764.
- Diamond, H. (Ed.). (2001). *The United States detailed national report on systematic observations for climate*. Silver Spring: U.S. Department of Commerce, NOAA.

- Elachi, C. (1982). Radar images of the Earth from space. *Scientific American*, 247, 46–53.
- Elvidge, C. D. (2001). DMSP-OLS estimation of tropical forest area impacted by surface fires in Roraima, Brazil: 1995 versus 1998. *International Journal of Remote Sensing*, 22, 2661–2673.
- Francis, P., & Jones, P. (1984). *Images of Earth*. London: George Phillip and Son Ltd.
- Goodenough, D. G., Dyk, A., Niemann, K. O., Pearlman, J. S., Chen, H., & Han, T. et al. (2003). Processing Hyperion and ALI for forest classification. *IEEE Transactions on Geoscience and Remote Sensing*, 41, 1321–1331.
- Goward, S. N., Markham, B., Dye, D. G., Dulaney, W., & Yang, I. (1991). Normalized difference vegetation index measurements from the Advanced Very High Resolution Radiometer. *Remote Sensing of Environment*, 35, 257–277.
- Goward, S. N., & Skole, D. (2005). Landsat 2005: Time to Act. *Space News*, October 31.
- Harding, D. J., & Carabajal, C. C. (2005). ICESat waveform measurements of within-footprint topographic relief and vegetation vertical structure. *Geophysical Research Letters*, 32, L21S10, doi:10.1029/2005.GL023471, 4pgs.
- Hart, W. G. (1975). The use of Skylab data to study the early detection of insect infestations and density and distribution of host plants. In *NASA Earth Resources Survey Symposium* (pp. 203–220).
- Kidwell, K. B. (1990). *Global Vegetation Index. User's guide*. Washington, D.C.: NOAA/NESDIS/NCDC.
- King, M. D., Closs, J., Spangler, S., Greenstone, R., Wharton, S., & Myers, M. (Eds.). (2003). *EOS Data Products Handbook. Volume 1*. Washington, D. C.: National Aeronautics and Space Administration.
- Konecny, G. (1986). First results of the European Spacelab Photogrammetric Camera Mission. In K. H. Szekiela (Ed.), *Satellite remote sensing for resources development* (pp. 115–121). London: Graham and Trotman Ltd.
- Lulla, K. (1993). Space shuttle earth observations database for global urban applications. In K. N. Au (Ed.), *Cities of the world as seen from space* (pp. 15–19). Hong-Kong: Geocarto International.
- Lulla, K. P., & Dessinov, L. V. (Eds.). (2000). *Dynamic Earth Environments. Remote sensing observations from shuttle – Mir Missions*. New York: John Wiley and Sons.
- Morisette, J. T., Privette, J. L., & Justice, C. O. (2002). A framework for the validation of MODIS Land products. *Remote Sensing of Environment*, 83, 77–96.
- Murphy, R. E. (2006). The NPOESS Preparatory Project. In J. J. Qu, W. Gao, M. Kafatos, R. E. Murphy & V. V. Salomonson (Eds.), *Earth Science Satellite Remote Sensing. Vol. 1: Science and Instruments* (pp. 183–198). Beijing: Tsinghua University Press and Springer Verlag.
- Murphy, R. E., Ardanuy, P., DeLuccia, F. J., Clement, J. E., & Schueler, C. F. (2006). The visible infrared imaging radiometer suite. In J. J. Qu, W. Gao, M. Kafatos, R. E. Murphy & V. V. Salomonson (Eds.), *Earth Science Satellite Remote Sensing. Vol. 1: Science and Instruments* (pp. 33–49). Beijing: Tsinghua University Press and Springer Verlag.
- Murphy, R. E., Barnes, W. L., Lyapustin, A. I., Privette, J., Welsch, C., & De Luccia, F. et al. (2001). Using VIIRS to provide data continuity with MODIS. In *Proc. IEEE International Geoscience and Remote Sensing Symposium* (pp. vol 3: 1212–1214).
- NASA (1977). *Skylab Explores the Earth*. Washington: NASA, SP 380.
- National Research Council (2007). *Earth science and applications from space: National imperatives for the next decade and beyond*. Washington, DC: National Academy of Sciences Press.
- O. T. A. (1984). *Remote sensing and the private sector: Issues for discussion. A technical memorandum*. Washington, DC: U.S. Congress, Office of Technology Assessment, OTA-TM-ISC-20.
- Parkinson, C. L., Ward, A., & King, M. D. (Eds.) (2006). *Earth science reference handbook. A guide to NASA's Earth science program and earth observing satellite missions*. Washington, DC: National Aeronautics and Space Administration.
- Roberts, D. A., Gardner, M., Church, R., Ustin, S., Scheer, G., & Green, R. O. (2003). Evaluation of the potential of hyperion for fire danger assessment by comparison to the airborne visible/infrared imaging spectrometer. *IEEE Transactions on Geoscience and Remote Sensing*, 4, 1297–1310.

- Short, N. M., & Stuart, L. M. (1982). *The Heat Capacity Mapping Mission (HCMM) Anthology*. Washington DC: NASA Scientific and Technical Information Branch.
- Williamson, R. A. (2001). Remote sensing policy and the development of commercial remote sensing. In J. C. Baker, K. M. O'Connell & R. A. Williamson (Eds.), *Commercial observation satellites. At the leading edge of Global transparency* (pp. 37–52). Santa Monica: RAND – ASPRS.

Chapter 3

The Role of the European Space Agency in Global Change Observations


Olivier Arino

3.1 Introduction

In the last several decades, environmental issues that affect our planet have mobilised scientists, governments, financial institutions, citizen groups, private companies and environmental organisations in the entire world. The need for understanding of these problems has galvanised several scientific communities with the modellers, in particular, at the forefront. Most Earth Science models require input and control data, which, by their global nature, could only be provided through the observation of the Earth by remote sensing satellites. The European Space Agency has been developing Earth Observation satellites for more than 30 years for the meteorological community (e.g the METEOSAT satellite series) this has been expanded within the last 16 years toward the environment in general with the ERS-1, ERS-2 and ENVISAT satellites, (Fig. 3.1). Now following the positive demonstration that these environmental satellites are a fundamental data source for understanding and monitoring the environment, the European Space Agency together with the European Commission have agreed on the Global Monitoring for the Environment and Security programme. In this programme, after having actively participated in its definition, the European Space Agency is responsible for the development of the Space segment and the corresponding operational satellite series, Sentinel-1, Sentinel-2 and Sentinel-3 (Fig. 3.1). In the mean time the European Space Agency continues to investigate new technology capabilities through a series of Earth Explorer satellites each addressing challenging Earth systems questions (Fig. 3.2)

World governments have signed several multilateral environmental agreements (MEAs) pursuing solutions to alleviate environmental degradation worldwide. As an example, the United Nations Conference on Environment and Development (UNCED), also known as the “Earth Summit,” in Rio de Janeiro, Brazil in 1992, resulted in the definition of Agenda 21, a comprehensive plan of action to be implemented by organizations of the United Nations System, Governments, and Major Groups in every area in which human impacts on the environment, and the subsequent signature of multilateral environmental agreements such as the United Nations Convention to Combat Desertification (UNCCD), United Nations Convention on Biodiversity (UNCBD) and the United Nations Framework Convention on

Meteosat
 Since '78, 8 ESA developed Meteosat satellites have been launched



MSG-1
29.8.2002

MetOp
 Europe's first polar orbiting satellite for op. meteorology
 Launch: 2006



and now
GMES
Sentinel-1
Sentinel-2
Sentinel-3

ERS-1 1991
ERS-2 1995






Fig. 3.1 ESA developed satellite in 30 years from METEOSAT to GMES Sentinel series

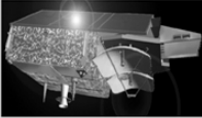
GOCE
 Earth gravity field and Geoid measurements
 Launch: 2007



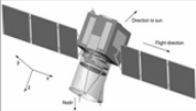
SMOS
 Soil moisture and ocean salinity measurements
 Launch: 2008



Cryosat-2
 Ice elevation and ice thickness measurements
 Launch: 2009



ADM-Aeolus
 Windspeed vectors measurements
 Launch: 2009



SWARM
 Earth magnetic field & Earth core dynamics meas.
 Launch: 2009+



EarthCARE
 Clouds, Aerosols & radiation measurements
 Launch: 2012+

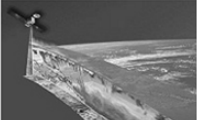


Fig. 3.2 ESA plans for Earth Explorer satellites

Climate Change (UNFCCC). The roadmap initiated in 1992 was continued at the World Summit on Sustainable Development (WSSD) held in Johannesburg, South Africa, in 2002. In fact, during the Johannesburg meeting, governments reinforced their commitment to sustainable development and its implementation at the local, regional, national, and international levels and recognised MEAs as useful instruments to achieve that objective.

The implementation of environmental conventions requires the collection, analysis and understanding of a huge amount of environmental information from local to global scales. This information serves environmentalists, to better understand the scientific background of the problems faced, policy makers, as a support for decision taking, environmental agencies, to put in place environmental plans and even the Convention Secretariats and related implementation bodies, to better assess the performance of the convention and apply enforcement procedures when necessary. In this context, EO technology can provide a significant contribution by:

- *Improving the scientific knowledge of the environmental problems addressed;*
- *Improving the basis for execution of National Action Plans (NAPs);*
- *Improving regulatory performance of MEAs;*
- *Broadening the political process;*
- *Contributing to create common databases and reporting procedures among different Conventions;*

Climate change is a global issue. It must be addressed with global models and global data are needed as input to these models. Earth Observation has a unique capacity to provide such global data sets in a continuous and consistent manner. However, Earth Observation also provides data on national and local scales, which can help in the implementation of the convention and protocol, and support the Parties in their reporting duties.

3.2 Global Observation from Satellites

The importance of systematic global observations for understanding climate change has been recognised by the UNFCCC since the beginning. Some of the variables essential for understanding and monitoring the climate system can be efficiently observed from space since this technology enables their systematic, global and homogeneous measurement (Global Climate Observing System (GCOS) Implementation Plan in support of the UNFCCC). The development and demonstration of pilot projects deriving some of the Essential Climate Variables as defined by the Committee on Earth Observation Satellites (CEOS) response to the GCOS implementation plan has been endorsed by the UNFCCC SBSTA during the 12th Conference of the Parties (COP-12).

Greenhouse gases and aerosols are the primary agents in forcing climate change; continuous observations that are spatially and temporally homogeneous are therefore required. Since 2002, measurements of ozone and greenhouse gases including

carbon dioxide (CO₂) (currently a research field) and methane (CH₄) exploiting satellite data have been demonstrated. Based on these observations the European Space Agency has developed several instruments (e.g. SCIAMACHY on board ENVISAT) that provide new capabilities for, for example, monitoring global methane concentration.

ESA has also initiated several global-scale projects in order to transform satellite data into meaningful parameters that provide insight into climate change issues. This “GLOB” family projects address several of the Essential Climate Variables described and listed in the CEOS Response to the GCOS Implementation Plan (Fig. 3.3).

The most relevant variables that can be measured from satellite over land are daily global albedo (fraction of sun light reflected back from the Earth), vegetation amount and state, fires and burnt areas, snow cover of both hemispheres, land cover, elevation maps of the ice sheet surfaces, glaciers evolution. Some of these variables are required as inputs to models designed to better understand the carbon cycle, others give an immediate view of climate change impact. Vegetation amount, fire location, timing and area affected, as well as additional information on the vegetation growth cycle (timing, duration, spatial and temporal variability) are being estimated globally within the GLOBCARBON project. Figure 3.4 is a monthly Leaf Area Index product at 1 km resolution as derived from VEGETATION and ATSR-2 satellite sensors combined. These products are used as input to Carbon Assimilation Models.

In common with vegetation, ocean algae absorb thousands of tonnes of carbon, forming one of the most important and long-lasting removal routes. By precisely measuring ocean colour, scientists can accurately estimate the concentrations of phytoplankton on a global scale. Coupling ocean colour measurements with atmospheric aerosol and trace gas measurements will also yield new insights into the chemical links between ocean and atmosphere. A long time-series of global ocean-colour information is to be provided by the GLOBCOLOUR project using amongst others the Envisat MERIS data (Fig. 3.5).

The large volume of data acquired from twenty years of satellite observations of sea surface temperature has given scientists a uniquely detailed view of the changing physical characteristics of the surface of the oceans, sampled at a rate impossible to achieve with only ship-based observations. The merging and combination of data measured independently by several different satellite systems into a set of data products that represent the best measure of sea surface temperature, presented in a form that can definitively show a global change. The observed trend in Sea Surface Temperature is a definitive sign of global warming and confirms that long time series of satellite measurement are required to address this issue at global scales, (Fig. 3.6).

Fire location has been globally analysed for more than a decade through the Along Track Scanning Radiometer (ATSR) World Fire Atlas (WFA) and these data are freely available from ESA. The WFA has been used to date by more than 900 scientific teams, most of them in the field of atmospheric modelling. Based on these observations fire activity, at least at night-time, seems not to have exhibited an increase within the last decade if the strong El Nino event of 1998 is excluded



Fig. 3.3 The GlobProject Series develop and demonstrate the processing of Essential Climate Variables from Satellite data

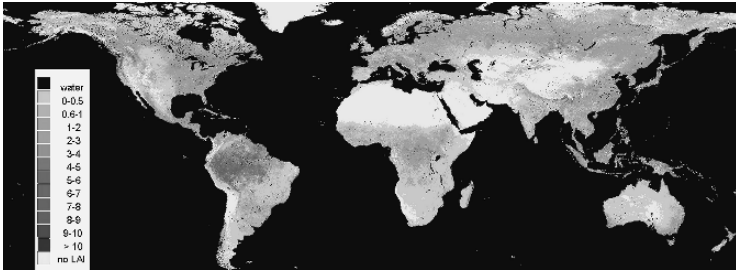


Fig. 3.4 The GLOBCARBON mean Leaf Area Index for August 1998, The GLOBCARBON Initiative: Global Biophysical Products For Global Terrestrial Carbon Studies, Stephen Plummer, Olivier Arino, Franck Ranera, Kevin Tansey, Jing Chen, Gerard Dedieu, Hugh Eva, Isidoro Piccolini, Geert Borstlap, Bart Beusen, Freddy Fierens, Walter Heyns, Roselyne Lacaze, Sebastien Garrigues, Tristan Quaife, Martin De Kauwe, Shaun Quegan, Michael Raupach, Peter Briggs, Ben Poulter, Alberte Bondeau, Peter Rayner, Martin Schultz, Nadine Gobron, Ian McCallum: Proceedings of the ESA ENVISAT Symposium, 23-27 April, Montreux, Switzerland

(Fig. 3.7). However, differentiation in the occurrence time and location is of essential value for trace gas emissions into the atmosphere and the WFA can be used to clearly identify regional variations over time.

The Polar Regions are especially sensitive to changes in climate, and models consistently predict future warming to be much more significant in these regions than elsewhere. However, the confirmation of model results is fraught with the difficulty

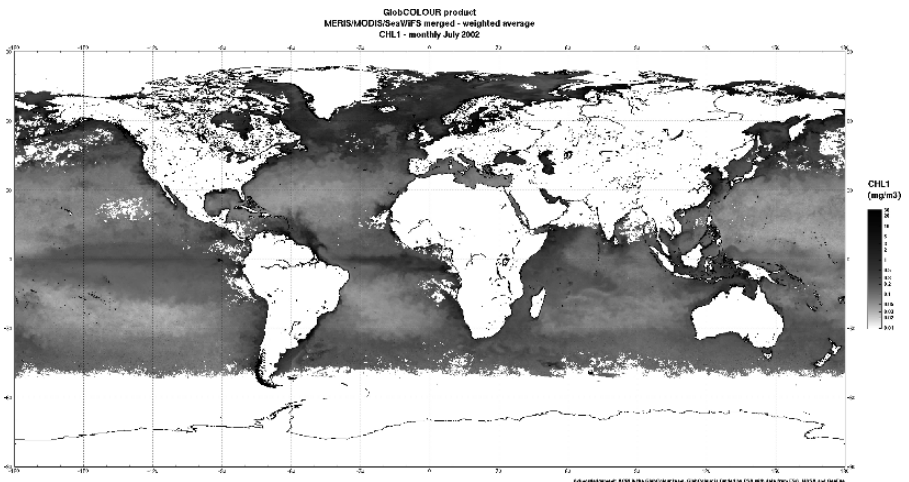


Fig. 3.5 The GlobColour Chlorophyll for July 2002, GlobColour: Developing a Merged Global Ocean Colour Data Set for Carbon-Cycle Research", Fanton d'Andon, Odile; Mangin, Antoine; Lavender, Samantha; Morel, André; Antoine, David; Durand, Dominique; Sorensen, Kai; Maritorea, Stephane; Fomferra, Norman; Neumann, Andreas; Demaria, Julien; Barrot, Gilbert; Pradhan, Yaswant; Lerebourg, Christophe; Quast, Ralf; Hoekedal, Jo; Pinnock, Simon Proceedings of the ESA ENVISAT Symposium, 23-27 Apr 2007, Montreux, Switzerland

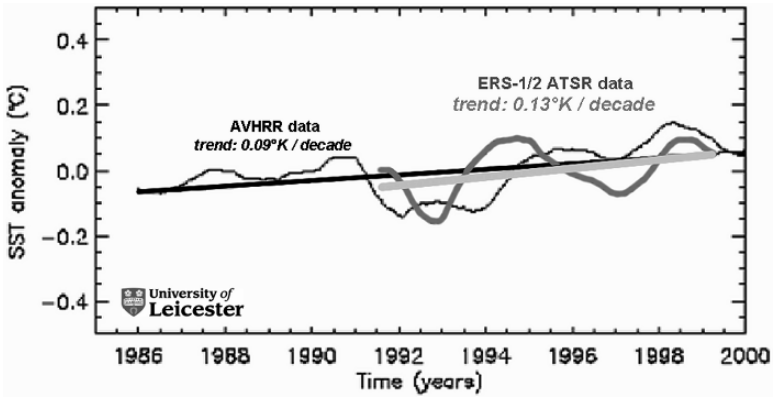


Fig. 3.6 Sea Surface temperature Trend over last two decades: S.P. Lawrence, D.T. Llewellyn-Jones and S.J. Smith, 2004. The measurement of climate change using data from the Along-track Scanning and Advanced Very-High Resolution Radiometers, Journal of Geophysical Research

of obtaining consistent or spatially comprehensive observations. The capacity of radar instruments to see through clouds means relevant variables can be observed from satellite. For example, the Antarctic continent and the surrounding sea ice extension can only be seen with radar, Fig. 3.8 shows a monthly mosaic collected from the ENVISAT radar imagery. Such mosaics can be updated every month and provide a regular snap shot of the southern continent.

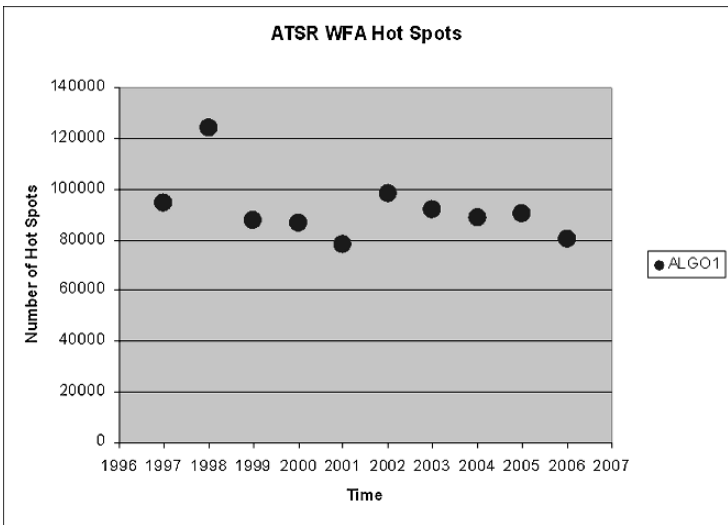


Fig. 3.7 The ATSR World Fire Atlas trend over last decade: the ATSR Wold Fire Atlas and its more than thousand Users, O. Arino, S. Casadio and S. Plummer, proceedings of the ENVISAT symposium, Montreux, 2007, <http://dup.esrin.esa.it/ionia/wfa/>

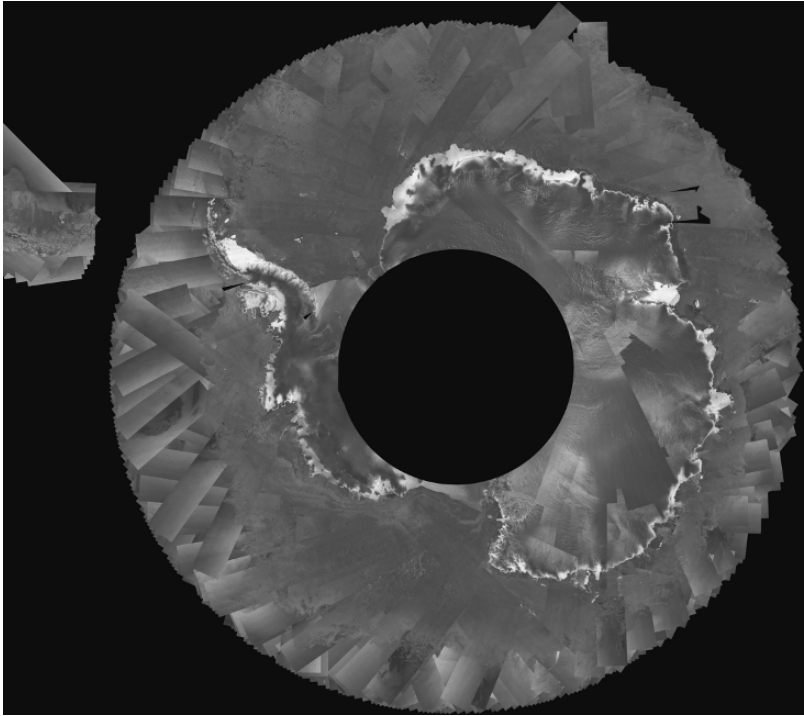


Fig. 3.8 The Antarctic Mosaic from ENVISAT ASAR Global Monitoring mode is processed and made public every week

3.3 Local and Regional Observations from Satellite: Land Use and Forestry

Human activities related to land use and forestry have a significant impact upon net emissions of carbon. The measurement and control of such activities is a primary function of the Kyoto Protocol, which obliges the Annex 1 (industrialised signatories to the Protocol) countries to report on these activities during the first commitment period and establish a baseline for 1990.

ESA started working with the UNFCCC secretariat in 2001 in order to support the Parties to the Kyoto Protocol in producing, using a combination of satellite images, ground measurements and other data, the required maps and statistics. To date more than a hundred million hectares have been mapped, and another hundred million will be mapped by the Kyoto Inventory and Forest Monitoring projects by 2008. All of Switzerland and Netherlands have been mapped for three different years, while the methodology has been applied over large parts of Italy, Germany, Spain, France, Greece, Denmark and Poland. The changes in land use and forestry during the periods between these years were also mapped. Standards and best working practices have been established, and all maps were verified using aerial photos, forest inventory data and other field measurements, and their utility assessed by

the ministry or agency in charge of the Kyoto Protocol reporting of each country. These ministries and agencies have also been actively involved in specifying the map characteristics and providing supporting ground data.

ESA is also working with non-Annex 1 countries to support their national communications under the UNFCCC. Capacity building is a strong component in such an exercise, depending on each country's resources. The issue of avoidance of tropical deforestation is a critical issue for reducing net emissions of carbon and will be a post-Kyoto Protocol reporting matter that ESA will address in the future through the Forest Monitoring project. Satellite images can be used both to establish a historical deforestation baseline and to monitor continuously deforestation and forest degradation. Pilot cases to assist in policy formulation for this issue are currently being developed.

Forest projects under the Kyoto Protocol's Clean Development Mechanism (CDM) can also be supported by satellite observations in order to identify optimal sites, establish baseline scenarios, monitor leakage effects and verify the plantation evolution. ESA is working in Uganda and Paraguay to demonstrate the usefulness of such services.

3.4 Conclusion

The next generation of EO satellites will provide novel and advanced capabilities to monitor the environment worldwide on a regular basis. The success of such new capabilities will depend on the capacity of the different actors involved in the space sector (i.e., space agencies, value-added companies, research institutions) to develop user-driven cost-effective operational applications.

ESA EO programmes will continue working in this direction, providing support to governments, scientists, international agencies, private companies and NGOs pursuing the goals and targets of environmental conventions. To this end, ESA maintains a continuous consultation process with the international user community through the organisation of thematic workshops (e.g., GlobWetland Symposium in October 2006) and the active participation at the COPs of the different conventions.

Acknowledgments To Diego Fernandez, Marc Paganini, Simon Pinnock, Stephen Plummer, Frank Martin Seifert, and Espen Volden from ESA and to VITO, ACRI, University of Leicester for providing material.

Chapter 4

Ozone in the Atmosphere

Monitoring Ozone Depth through Satellite Data

Abel Calle and Jose Luis Casanova

4.1 Introduction

Ozone is one of the most contradictory gases in the atmosphere: in spite of the fact that the content of this gas in the upper atmospheric layers is less than 12 ppm (parts per million), life would not be possible without it. And yet, close to biological systems is one of the most toxic gases produced by contamination. The noticeable alterations that are taking place affecting the distribution of this gas in the atmosphere and the environmental problem these changes imply is what is making of ozone a current point of interest which is being treated from different perspectives and methodologies.

Historically speaking, ozone was discovered in 1839 by Schönbein, a German chemist who detected it by its characteristically intense smell. This property is precisely the origin of its name, taken from the Greek “ozein” meaning “to smell”. Its chemical composition is formed by the combination of three oxygen atoms in a molecule and is represented as O_3 .

The stratospheric ozone, the layer of this gas situated in the stratosphere, is between 15 and 35 km of height, the maximum concentration being at 22 km. Although this band may seem too wide, under the temperature and pressure conditions of the Earth’s surface the ozone layer would be less than 3 mm wide, which shows how fragile this protective layer can be and how little concentrated it is: out of each ten million air molecules, two million correspond to breathable oxygen and just three of them are ozone molecules. Yet, this shield absorbs and filters out the ultraviolet radiation situated between the wavelengths of 0.2 and 0.3 μm , a region in the solar spectrum known as Hartley band. These are the nearest radiations to the visible spectrum and they have already gone through several filters situated in the upper layers of the atmosphere in charge of eliminating highly energetic radiations (ultraviolet, X radiation, gamma rays, etc). That’s why the ozone layer is the last resource to avoid an exposure which is incompatible with most earth biological systems. From a global perspective, the effects of the non-filtered solar radiation on both land and ocean’s micro organisms could seriously put the survival of the biosphere at risk.

In 1930, the British Sydney Chapman presented the theory from which the photochemical processes of ozone in the stratosphere can be explained. Simplifying, this theory says that the molecular oxygen dissociates as a result of highly

energetic ultraviolet radiation. The free released atoms have great affinity to react with other oxygen molecules with the help of other constituents, thus forming an ozone molecule. The newly formed ozone is destroyed in turn absorbing the ultraviolet radiation in Hartley band. As can be seen, the balance between formation and destruction reactions is very fragile and delicate.

Having seen its protective role, it is somehow paradoxical that the ozone situated in the lowest layers, called tropospheric ozone, can be an important secondary pollutant formed by the photo dissociation of nitrogen oxides (NO and NO₂) and volatile organic compounds that reach maximum values in the central hours of the day causing serious breathing and eye problems.

The discovery made a few years ago of the damage caused to the ozone distribution in some parts of the planet has been widely spread by the media causing an environmental alarm that still continues. As with other scientific episodes in the history of Science, the discovery of the damage to the ozone layer was surrounded by confusion and scientific inequalities. In September 1984, the University of Salonica organised the International Congress of Ozone. There, an unknown, young, Japanese scientist, Sigeru Chubachi, made a presentation in poster format warning about the very low measurements of ozone content detected in the Antarctic research station of the Japanese base of Syowa during the last two years in which he had been working there. As was expected, no one paid much attention to him and his results went unnoticed. Later, in May 1985, *Nature*, the most relevant scientific journal, published an article signed by Farman, Gardiner and Shanklin, where they warned about the important loss of ozone that was taking place in the Antarctic, which came to confirm certain hypothesis by Molina and Rowland on the possible destruction of the ozone layer caused by certain man-made chemicals. The latter, together with Crutzen, received the Nobel Prize in Chemistry in 1995.

In any case, satellites played a very important role in this episode. From October 1978, the American satellite Nimbus-7 was operative with three different sensors dedicated to the analysis of atmospheric ozone and related constituents: SAM II (Stratospheric Aerosol Measurement II), SBUV (Solar Backscatter Ultraviolet) and the most important one, TOMS (Total Ozone Monitoring System). The obvious question was: if the ozone layer had been measured through satellite since 1978, why wasn't the damage to it discovered until 1985? The shameful reason is that all the data obtained on the Antarctic during the months affected by minimum value measurements had been discarded by the data-quality control, which had a minimum value threshold below which data were considered to be wrong. Later on, after the alarm, all data were recovered by the GSFC (Goddard Space Flight Center) of NASA turning the sensor TOMS into the best instrument for the analysis and monitoring of this atmospheric catastrophe. TOMS can take up to 250,000 measurements of the planet a day.

The phenomenon known as the ozone layer hole makes reference to the sharp reduction in the values of total ozone content that takes place over practically all the Antarctic during the months of October and November mainly. There are many and very different causes which are still being analysed quantitatively with chemical models that involve more than 200 different reactions with various types of gases. With respect to the man-originated causes, the most harmful substances are the compounds called chlorofluorocarbons, or CFCs, which are released into the

atmosphere. These substances have been part of numberless industrial and household systems such as refrigeration circuits, air conditioning and propellants in *sprays*. At surface level, these molecules are very stable, but when they go into the stratosphere swept away by winds, they are destroyed by the energetic ultraviolet radiation and Chlorine atoms are released. From here, two consecutive reactions occur: the Chlorine destroys the Ozone in order to form Chlorine oxide, which breaks down again leaving Chlorine ready to destroy more ozone molecules. This cycle is repeated thousands of times. It's been calculated that up to 10,000 ozone molecules can be destroyed by a single atom of Chlorine in this process. The reason why this effect is more enhanced in the Antarctic has to do with dynamic causes that involve the existence of a strong cyclonic vortex in the south pole during the winter that causes the isolation of these substances and, consequently, the lack of mixing and ozone supplies from other latitudes.

In any case, there are many different mechanisms responsible for the destruction of ozone. Other causes related with the sources of nitrogen oxides in the stratosphere are being currently researched as well as the emissions from supersonic aeroplanes, the existence of polar stratospheric clouds that act as aerosol deposits inside the vortex, etc.

Political measures have been taken by the international community in order to protect the ozone layer. The most important agreement was the Montreal Protocol in 1987, which established the progressive reduction of certain substances until their total eradication. The declaration of Helsinki in 1989, the London Accord in 1990 and the Copenhagen Accord in 1992 came next. Important steps have been taken towards the eradication of this waste. However, taking into account that even in the case of their total disappearance more than 50 years would be needed for the atmosphere to regenerate, more drastic and immediate measures should be taken.

The measurement of ozone content is carried out through different techniques. The most important ground instrument is Dobson's spectrophotometer (the measurement unit took its name after Dobson). It measures the different absorption of two very close wavelengths, but only one of them is affected by the absorption of ozone. However, this tool does not provide information on the vertical distribution of this gas throughout the atmosphere. For this purpose, sounding are made with balloons which are capable of exploring the stratosphere sweeping away more than a ton of recyclable instruments. However, since this is still a very costly system, techniques based on the use of laser are being considered, such as LIDAR, which obtains both the vertical structure and its evolution.

Regarding satellites, since 1978 sensor TOMS, originally on board Nimbus-7 and later on satellites like the Russian Meteor-3 or the Japanese Adeos, has been the one mostly used for analyses on a large scale completing measurement series. The NOAA series satellites also include a sensor called HIRS with an infrared band centred in an ozone absorption peak at 9.6 μm . This band has been included in the current MODIS sensor and in the European geostationary MSG. GOME sensor of the European satellite ERS has been very important in the continuation of data series and, at this moment, we should mention the relevance of the European satellite ENVISAT, which carries GOMOS (Global Ozone Monitoring by Occultation of Stars) among other sensors. GOMOS is able to generate stratospheric ozone profiles with a high accuracy above 15 km from the measurement of a stellar spectrum when it is visualised from the space through the earth's atmosphere.

It is our hope that these current measurement systems and the most accurate ones that are still to come help us warn in time about the changes that are taking place and that political measures are taken in turn to palliate their effects.

4.2 Aspects Related with the Dynamic of Ozone

In spite of the importance that the atmospheric ozone has in the absorption of ultraviolet radiation, the total quantity of ozone in the atmosphere is very small (approximately two parts per million in weight) and it is not equally distributed throughout the atmosphere. Ozone is considered to be a very toxic pollutant when formed in the low stratosphere, but it is also known to be essential for the protection of biological systems when found in upper atmospheric layers.

The atmosphere is far from being a homogenous layer of chemical constituents. The distribution of elements and their behaviour is determined by the existence of several layers which differ more or less according to some physical magnitudes such as temperature, molecular mass or certain radioelectric properties. The most typical subdivision considering its vertical structure is the one suggested in 1960 by the International Union of Geodesy and Geophysics (IUGG), which established four differentiated layers characterised by a concrete variation of the temperature according to height.

These four layers are known as Troposphere, Stratosphere, Mesosphere and Thermosphere. The first two layers comprise approximately the first 60 km from the Earth's surface and they are directly involved in the existence and dynamic of atmospheric ozone. There is an interrelation between ozone destruction and other processes that take part in the climate change and global warming such as the greenhouse effect. The greenhouse effect, caused by a sharp increase in CO₂ and methane content in the atmosphere, is having important consequences in the deterioration of the environment. However, there are other substances, such as nitrous oxide and the chlorofluorocarbons compounds above mentioned, that also contribute to the global warming of the troposphere as they absorb the infrared radiation. There is a direct relation between the greenhouse effect and the problem of the decrease in ozone content. What is more, there is a reciprocal worsening of their effects. The link between both phenomena is the tropospheric ozone. The reduction of stratospheric ozone causes a larger flow of ultraviolet radiation in the troposphere and, consequently, an increase in the tropospheric ozone. Since ozone absorbs infrared radiation, it contributes to keep heat in the troposphere. The decrease of ozone and the global warming strengthen reciprocally their effects over the stratosphere and troposphere temperatures.

The stratosphere extends above the tropopause up to 50 km of height where a zone called stratopause starts. Its main characteristic is the presence of the ozone layer, name given to the zone where the practical totality of atmospheric ozone concentrates and that other classification criterion of atmospheric layers call ozonosphere. The ozone concentrated here absorbs a large quantity of the ultraviolet radiation that reaches this level. This effect is responsible for the increase of tem-

perature with height. In this way, the temperature value in the stratopause may reach 0°C. This is the main thermal characteristic of the stratosphere. The low air density above the tropopause and the increase of temperature with height causes the inexistence of vertical heat transportation in this zone, due to thermal stability. Only the dynamic action of some air whirls causes small vertical movements. This thermal structure, which is substantially different from the one in the troposphere, in which the strata are practically stable, is what gives this layer the name of stratosphere. However, horizontal movements and currents are extremely important in the stratosphere. The maximum temperature is reached in the summer pole due to the heat accumulated during six months of continuous radiation. The minimum temperature occurs in the winter pole, after the continuous cooling off that takes place during the six months corresponding to the polar night in which the ultraviolet radiation has not been absorbed by ozone. This causes a continuous current of winds in the direction of the winter pole that sweeps away substances found over the Equator and tropical regions towards higher latitudes. This is very important since the main stratospheric zones where the creation of ozone takes place are precisely the Equator and tropical regions due to higher solar radiation. The direction of these current changes with the seasonal changes in the poles.

The diagram in Fig. 4.1 summarizes the dynamic of ozone in the stratosphere. It shows the average ozone density measured by SBUV sensor on board Nimbus-7 (Solar Backscatter Ultraviolet Instrument) according to latitude and altitude. The orange and red colours show high-levels of ozone whereas blue and purple represent low levels. The measurements are taken in Dobson Units per kilometer. SBUV

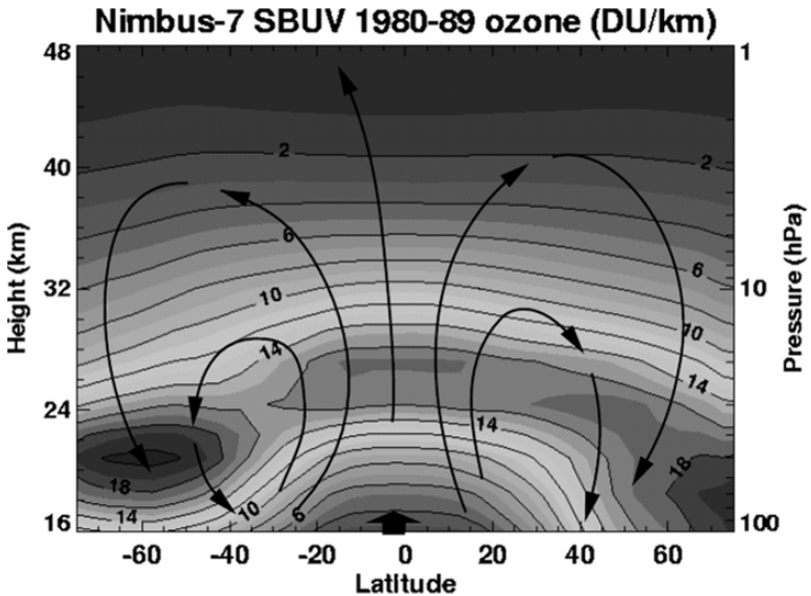


Fig. 4.1 Dynamic of ozone in the stratosphere. Data obtained from SBUV sensor on board of Nimbus-7 spacecraft. (Credits: NASA. *Studying Earth’s Environment From Space*. October 2006.)

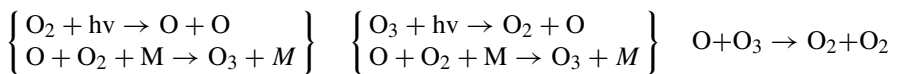
measures the number of ozone molecules in the layers and TOMS the total number of molecules from the surface to the outer space. SBUV data are from the period 1980–1989. The black arrows indicate the stratospheric circulation known as Brewer-Dobson circulation, which is responsible for the ozone distribution observed from the Equator to the pole. This distribution fluctuates according to season and hemisphere.

Contrary to what happens in the troposphere, the steep inclination of the sun rays over the poles enhances the thermal effects described since the absorption of the radiation by the ozone molecules is what causes these effects. The more inclined the solar rays are, the more probability of absorption.

Nowadays we know that there are many different mechanisms related to the dynamic of ozone, many of which are not still known in depth. Chemical processes produced by both natural and artificial substances on the one hand, and meteorological factors on the other mix together determining the annual and interannual distribution of ozone in the atmosphere.

4.2.1 Chapman's Theory

The first theory that explained the existence of the ozone layer was presented by S. Chapman in 1930 in a scientific essay entitled "A theory of upper-atmosphere ozone. Mem. Roy. Meteorol. Soc". This theory is summarised in just a few chemical reactions that take place in the stratosphere, where there is molecular oxygen that photodissociates with solar radiation giving place to atomic oxygen. Later, the oxygen combines again with molecular oxygen giving place to ozone molecules. The dissociation process is produced by ultraviolet radiation of wavelength less than 240 nm. Later, ultraviolet radiation of wavelength in the interval [240–320 nm] dissociates the ozone molecule releasing atomic and molecular oxygen. All this can be summarised as follows:



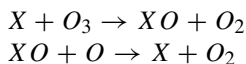
The concentration of ozone is a balance of formation and destruction reactions known as Chapman's reactions. There are many other catalytic reactions that include hydrogen, nitrogen, bromine and chlorine oxides. In the upper atmosphere, there is a high presence of molecular oxygen; in the lower layers, air is more dense, there is an increase in the absorption of UV radiation and the peak of ozone presence is found at around 20 km. The layer at this level is known as "Chapman's layer". This could be said to be the natural balance process. However, as has been observed since 1960, the levels of ozone destruction expected by Chapman's theory do not justify the sharp drop detected in the measures carried out.

4.2.2 Other Reactions of O₃ Destruction

Other chemical reactions in the stratosphere may also be the cause of the destruction of ozone and, contrary to the former ones, they do not have a completely natural origin. They are more related with the emission of pollutant substances that involve other chemical components:

- Hydrogen radicals (O, OH and HO₂) found in the atmosphere resulting from water vapour and methane dissociation.
- Nitrogen oxides (NO and NO₂) resulting from the oxidation of Nitrous Oxide (N₂O).
- Chlorine and Bromine compounds originated from the photochemical dissociation of chlorofluorocarbons compounds or CFCs.

These compounds, which are inert in the troposphere, get active in the stratosphere creating Nitrogen, Hydrogen, Chlorine and Bromine compounds that react in ozone destruction processes as catalysts. That is, they take part in chain reactions which finally result in the dissociation of the ozone molecule but keep their original state so that they can start another catalytic reaction again. These reactions can be represented as:

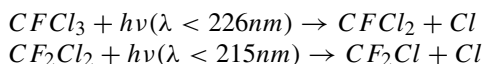


Molecule X (which could be H, OH, NO, Cl or Br) is the catalyst. The fact that the catalyst remains intact after the cycle of ozone destruction is completed, is very significant since it means that the same reaction can be re-started thousands of times until they are inactive. As has been said before, OH, NO, Cl and Br compounds may be originated both by natural atmospheric causes and by artificial causes that are the result of pollution.

The OH radical is created through the reaction between water (H₂O) and the excited form of oxygen O (¹D), which has an average life of less than a microsecond. In this way, two OH radicals are created. However, this process is rare due to the shortage of water in these levels of the atmosphere. It is more important the creation of the NO compound responsible for the destruction of 70% of ozone through natural causes in a catalytic way. This compound is formed similarly to the OH, but with N₂O instead of water, giving place to two NO molecules. With regard to Chlorine, this can be formed both in the Troposphere and in the Stratosphere. In the first case, from photodissociation of the Chlorine molecule (Cl₂) through radiation with a wavelength between 300 nm and 483 nm; in the Stratosphere, from photodissociation of ClH in the wavelength range of less than 220 nm, releasing a hydrogen atom. These processes are not very frequent since both Cl₂ and ClH are very active substances which get destroyed soon after their creation.

With regard to the artificial origin of these substances, OH comes mainly from water vapour emitted by jet planes, which most frequently fly at an altitude between

9 and 12 km, and from methane oxidation. Jet planes also release most of the artificially-originated NO. However, only a small part of it that is not eliminated by rain, reaches the ground as nitric acid bringing up the problem of acid rain. The artificial origin of Chlorine comes from photodissociation through ultraviolet radiation of *halocarbide compounds*. Halocarbides are compounds formed by the union of atoms from halogen elements (Chlorine and Fluorine mainly) with some Carbon atoms. Two of these halocarbides, freon 11 (CFCl₃) and freon 12 (CF₂Cl₂), are specially interesting for their high potential of ozone destruction due to the Chlorine they release. Next the reactions to produce Chlorine are shown:



4.2.3 Polar Stratospheric Clouds

Polar Stratospheric clouds are an important factor to describe the dynamic of ozone in the atmosphere. They are situated between 10 and 25 km of height and are especially present in the Antarctic since they appear with the low temperatures reached in winter in the stratosphere – in their surface there is a temperature of around 190°K-. These meteorological phenomena play an important role in ozone destruction processes due to the chemical reactions that take place in their surface. There, chemical compounds that are inactive for ozone turn into active elements that wait for spring rays of sunlight to come and initiate processes of ozone destruction.

Polar stratospheric clouds are formed mainly when a strong flow of tropospheric wind blows from the sea to the continent. These conditions are frequent in the Antarctic around the month of September when speeds of 110 km/hour are reached. The orography favours upward movements. Since the temperature in the low stratosphere in this time of the year reaches values close to 190°K it is always very close to saturation conditions. Thus, small adiabatic cooling caused by upward movements give place to water vapour saturation and, consequently, to the creation of stratospheric clouds (Fig. 4.2 included in the attached CD-ROM).

The two types of polar stratospheric clouds, more commonly known as PSCs, are mainly characterised by the size of their particles. PSCs type I are composed by very small particles of hydrated nitric acid (HNO₃- H₂O), with a size of 1 μm. They appear when temperatures reach 170°C. PSCs types II are formed by ice crystals with an approximate size of 10 μm and they contain H₂O and HNO₃. Due to the large size of their particles, they fall for effect of the gravity with velocities of 1 km/day.

The episodes of minimum Ozone content are often accompanied by the presence of PSCs. That's why their relation with the formation of the Ozone hole in the Antarctic was established in order to analyse the chemical compounds involved in the processes. As far as PSCs refers, the destruction of Ozone takes place mainly in two steps:

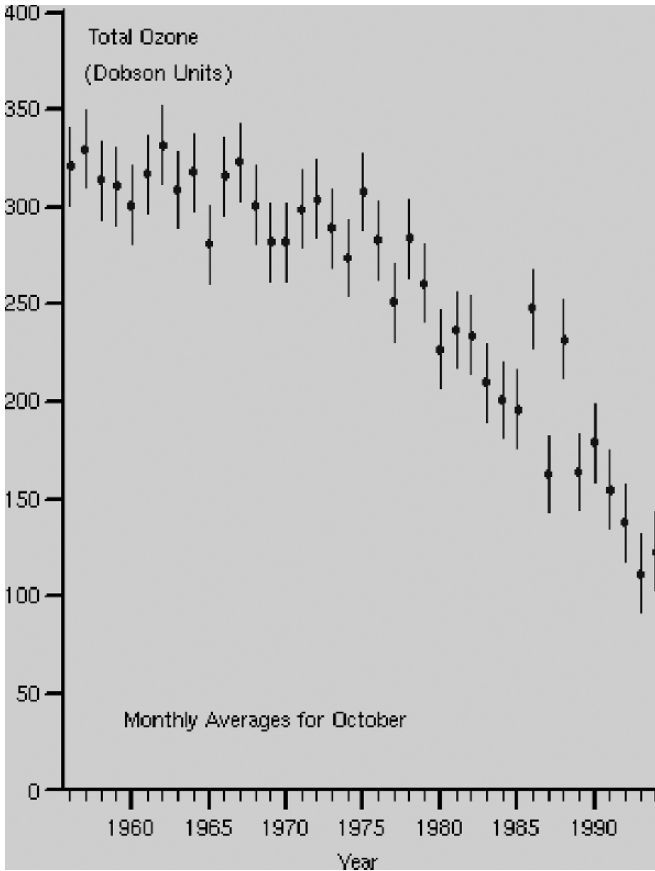
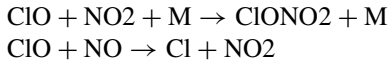
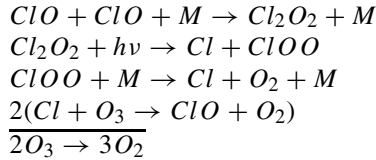


Fig. 4.2 Measurements of ozone depth in the Halley Bay station. (with permission Dr. Glenn Carver, Univ. of Cambridge, 2006, see references)

1. On the one hand, PSCs type I (formed by $\text{HNO}_3\text{-H}_2\text{O}$) that originate during the polar night have a tendency to reduce the supply of NO_x preventing the formation of reserve inert Chlorine compounds such as ClONO_2 . Large, medium-long-life ice particles of PSCs type II have a tendency to fall towards lower levels before fusion or sublimation is completed. In this way, the atmosphere tends to dehydrate in all the altitude range between the formation and the point where minimum values of water mixture are reached. Chemical reactions are also very likely to happen on the surface of these particles. According to laboratory measures, the reaction $\text{HCl} + \text{ClONO}_2 \rightarrow \text{Cl}_2 + \text{HNO}_3$ takes place on ice particles and could be very effective in the release of active Chlorine radicals at polar stratospheric temperatures. This happens during the polar night so that at the end of August most of the total stratospheric Chlorine is found as free Chlorine radicals.
2. With the arrival of sunlight caused by the desnitration of the vortex, the content of NO_x is very low and the reactions:



cannot be completed with other ClO reactions. Thus, the main cycle of ozone destruction is caused by the cycle of reactions:



The processes described have a great importance if we take into account the coordinated effect between Polar Stratospheric Clouds and the action of the polar vortex. Inside these clouds, vertical movements that act as “air filtering sheets” help increase desnitrification.

4.2.4 Polar Vortex

This dynamic characteristic of the atmosphere originates from the general circulation of winds that takes place in the Stratosphere covering the polar areas and it is caused by thermal changes in the atmosphere and Coriolis force. During the polar summer, the sun’s ultraviolet radiation is absorbed by the stratospheric ozone layer, which raises the temperature and causes the entry of East winds. When winter comes and with it the absence of solar radiation during the polar night, the air in the stratospheric layers cools off causing the drop of large masses of air towards lower levels. In this way, air starts spinning producing great-intensity winds that reach their maximum speed in spring. This vortex isolates completely the masses of air situated over the poles so that they can’t mix with air coming from middle latitudes.

However, there are two main differences between the two Earth poles that influence strongly in the formation of the polar vortex, making the south one be the most prominent of the two. In the first place, the Antarctic polar vortex is more stable than the Arctic one, since it is surrounded by a larger quantity of water instead of continental land as is the case of the Arctic. This factor helps winds spin better without encountering any obstacle that may destroy the vortex. In fact, the vortex is destroyed sometimes during the winter in the North Pole letting air from other latitudes in.

The cooling off of the air that gives origin to the vortex is more pronounced in the Antarctic due to astronomical causes. In the Antarctic winter, two effects take place: on the one hand, the inclination of the earth’s axis leaves the polar zone shaded (something normal in the winter season); on the other hand, winter is stronger due

to the fact that the Earth, with its slightly excentric orbit, is farthest away from the Sun, that is, it is at “aphelion”.

4.2.5 *The Ozone Hole*

Since it was first discovered, a lot has been said about the origin and causes of the so low levels of ozone reached in the Antarctic during the months of October. Although climatological effects must be analysed in the long term, which is not possible with the measurements available, artificial causes have taken on special significance after verifying that this sharp drop in the levels of ozone has not been progressive: observations from the scientific stations in the Antarctic have confirmed the alarming fall since 1975.

The discovery was first made by the Japanese scientist Sigeru Chubachi, who carried out measurements campaigns in the Japanese Antarctic base of Syowa (69°S, 39°E) during 1982–1983, base in which there had been a Dobson spectrophotometer since 1966. However, the international scientific community did not become aware of the real problem until Farman and his collaborators from the British Antarctic Survey alerted in 1985 to the very serious size the phenomenon had reached. The values found by Nimbus-7 spacecraft (the only one covering the pole with capacity to measure the ozone levels at that moment) were so low that the quality control processes had considered them to be wrong. The phenomenon of the ozone hole is the drop in ozone content that takes place during the austral spring over the Antarctic continent during a short period of time, with minimum values being reached at the end of October. After that, original values are recovered.

The situation has worsened since 1977 and in 1985 the destruction reached 50% of the concentration considered to be normal in those latitudes. These low quantities, inferior to 150 Dobson Units have also been reported in subsequent years. During the ozone hole of the Antarctic, values in the ozone layer not only are the values registered unusual, they also reveal the practical inexistence of the ozone layer in those latitudes. Images of this phenomenon have been taken from the data-base that the Goddard Space Flight Center of NASA has made available to users. It comes from TOMS data registered by Nimbus-7, whose characteristics will be described later.

There are three processes that may cause the destruction of ozone at a height of 20 or 30 km:

1. The direct spilling of these pollutant agents.
2. A permanent variation of the ultraviolet solar flow.
3. The transportation of gaseous chemical substances from the surface to the stratosphere.

This third cause was not believed to be possible since the tropopause where the change of thermal gradient takes place, was considered as a “lid” level that could not be crossed by gaseous masses coming from the troposphere. However, the exchange of large gaseous masses takes place in the intertropical convergent zone where there

are strong upward movements associated to cumulonimbus. There is another exchange zone of gaseous masses at 40° latitude during the summer, zone and time in which the tropopause is well defined. Therefore, the study of this phenomenon implies, first and above all, the study of the chemical compounds and reactions to which they give place. Certain atmospheric phenomena that enhance and facilitate the development of these reactions will be later described.

The scientific station Halley Bay was installed in the Antarctic in 1956 (Latitude 76 South, Longitude 26 West) by the British Antarctic Survey. Since then, regular measurements have been carried out with a Dobson spectrometer for the analysis of the evolution of the total ozone content. Figure 4.2 shows the total ozone content established in this station. Each point represents the average total ozone for the month of October. As can be seen, there is a strong discontinuity from 1975. In 1994, the total ozone in October was lower than half of the value obtained in the previous 20 years.

4.3 Measurement of Ozone from the Outer Space

Since there is knowledge of the damage to the ozone layer, the measurement and quantification of the total ozone content is a requirement in the design of all present spatial missions aimed at the observation of the environment. However, even before being aware of this problem, several spatial missions had already included some type of sensor for ozone monitoring, as was the case of TOMS. Next, we will describe the main methodologies used in this sense as well as their most relevant results.

4.3.1 TOMS Sensor

The spatial platform Nimbus-7 was launched by NASA from the base of the United States Air Force in Vandenberg (California) on 24 October 1978 and it worked satisfactorily until 6 May 1993 in a polar heliosynchronous orbit at 955 km of height. As a curiosity, the energy maintenance system didn't have enough power for all sensors, so the satellite had to work in cycles of performance: from 8% for SAM-II sensor (Stratospheric Aerosol Measurement) to 100% for the THIR radiometer (Temperature Humidity Infrared Radiometer) depending on the demands of the project. The Nimbus-7 mission was to carry out several experiments in the fields of Contamination, Oceanography and Meteorology as well as to calibrate data in other experiments carried out from ground stations. The most important sensor for our concern here was the Dispersed Ultraviolet Solar Radiation Spectrometer and the measurer of the total ozone depth: SBUV/TOMS.

TOMS sensor (Total Ozone Mapping Spectrometer) has provided the most relevant measurements in the spatial observation of this gas. This sensor has been installed on board the four spatial platforms that have taken measurements of this

atmospheric element: Nimbus-7, Meteor-3, Adeos and the Earth Probe TOMS. TOMS supplies daily, high-resolution maps of total Ozone by measuring the direct solar irradiance and the radiance dispersed through the Earth's atmosphere in six wavelength bands selected from the ultraviolet spectrum. In order to obtain the measure of ozone, a model of radiative transference is applied so as to obtain the dispersed radiance as a function of the ozone quantity, the geographic latitude, the sensor's "viewing" geometry and the surface's reflectivity conditions. The ozone is finally calculated from the correlations between the radiances measured by the sensor and the radiances calculated theoretically through the model for the same conditions. Thus, the Ozone value that satisfies the equation between the radiances measured and the radiances calculated is obtained. (McPeters et al., 1998).

The retro-dispersed radiance at a concrete wavelength will depend mainly on the profile of the total ozone quantity from the upper limit of the atmosphere to the surface since in the main wavelengths used by TOMS sensor, the absorption by other atmospheric components is negligible. At wavelengths more than 310 nm, the dispersed radiance is mainly solar radiation that after crossing the stratosphere is reflected by tropospheric components (aerosols, clouds, etc) that act like a dense reflection layer, and also by the Earth's surface. The practical totality of atmospheric ozone is found in the stratosphere and this stratospheric ozone has the effect of attenuating the radiation twice on its way from the sun to the satellite's sensor: it attenuates the radiation going towards the troposphere and the corresponding component that is reflected towards the satellite's sensor. The processes of reflection and dispersion are not isotropic so that directional effects derived from the sensor's viewing angles and the sun's position will have to be taken into account.

In order to eliminate the dependence on the wavelength in reflection processes, an algorithm has been used to make a model of the reflection surface through two reflection surfaces independently: the Earth's surface and the clouds, with a pressure of reflection level of 1.0 atm and 0.4 atm respectively. The contribution of each of these levels to the total reflectivity is obtained by comparing the radiances measured with calculated values for earth and cloud surfaces respectively. In this way, the retro-dispersed radiance that appears from the upper limit of the atmosphere and is captured by TOMS sensor, represented as I_m , can be expressed as the sum of the intensity of the atmospheric scattering I_a and the surface's reflection I_s :

$$I_m(\lambda, \theta, \theta_0, \Omega, P_0, R) = I_a(\lambda, \theta, \theta_0, \phi, \Omega, P_0, R) + I_s(\lambda, \theta, \theta_0, \phi, \Omega, P_0, R)$$

where the dependence terms are:

λ = wavelength in the ultraviolet spectrum.

θ = satellite's cenital angle from the Earth.

θ_0 = Sun's cenital angle.

ϕ = Azimuth angle.

Ω = Total quantity of ozone column.

P_0 = Pressure of the level of the reflection surface.

R = Effective reflectivity of the reflection surface.

The reflection term of the reflection surface can be expressed as:

$$I_s(\lambda, \theta, \theta_0, \Omega, P_0, R) = \frac{R \bullet I_d(\lambda, \theta, \theta_0, \Omega, P_0) \bullet f(\lambda, \theta, \Omega, P_0)}{1 - R \bullet S_b(\lambda, \Omega, P_0)}$$

with the terms:

S_b = Fraction of the radiation reflected from the surface, which has been reflected by the atmosphere towards the surface.

I_d = Total quantity of direct and diffused radiation that reaches the surface.

f = Fraction of radiation reflected towards the satellite in the θ direction.

As can be deduced, the denominator in the expression above is counting multiple reactions between the Earth and the Atmosphere. Special attention must be paid to the fact that the term S_b , radiation towards the surface, does not depend on the sun's cenital angle. On the other hand, the radiation that goes through a region where absorption and dispersion processes are taken place, is subject to *Bouger-Lambert law*, according to which the resulting radiation I_λ relates with the incidental radiation F_λ through the optical depth of the atmosphere τ for that wavelength through the expression:

$$I_\lambda = F_\lambda \bullet \exp(-\tau)$$

The optical depth τ_λ , depends in turn on the extinction coefficient of the gas that produces the attenuation and on the the optical mass (the relation between the optical depth in any direction and the vertical) In other words, the optical depth depends on the number of absorbents n in the whole column analysed and on these absorbents' efficiency α (that is, τ is proportional to $n \cdot \alpha$). In this way, the number of absorbents, that is, the total quantity of ozone should be proportional to number N , calculated as:

$$N = -100 \bullet \log_{10} \left(\frac{I}{F} \right)$$

where the factor 100 is introduced to work in an appropriate numerical range.

Therefore, the calculation model intends to obtain the values of N (N -values) from the radiative transference model for different quantities of ozone, different viewing conditions of sensor, surface properties, etc, and from these data, it tries to find the quantity of ozone that satisfies the N -values taken by TOMS sensor. This is done in two steps: An initial calculation of the ozone value is calculated from the difference between two N -values calculated in two wavelengths: one in which there is great absorption by the ozone and another one where there is no influence. Other N -values are calculated using the initial estimation as the ozone value. Since, generally speaking, there won't be a coincidence between the values calculated by the model and the values measured by the sensor, "remainders" will be established through the difference: $N_{\text{measured}} - N_{\text{calculated}}$. These "remainders" for triplets of selected wavelengths will allow us to correct the initial estimated value of ozone.

These triplets are formed by the two wavelengths previously described, apart from the 380 nm one on which the ozone has no influence. The spectral distance

between the pair of wavelengths is much shorter than the distance between this pair and the third component of the triplet (380 nm), so that the latter is used to establish the *line of base*. This is an iterative process so that the result of a triplet represents the new initial value estimated when applying the method on another triplet.

TOMS is the instrument dedicated to the observation of ozone from which longer temporal series have been obtained. Figure 4.3 shows the average ozone distribution in the atmosphere at different latitudes and different times of the year from TOMS data in the period 1979–1992. This figure shows a large quantity of synthesized information on the atmospheric and planetary distribution of total ozone depth.

Although for historical reasons, NIMBUS-7 spacecraft has been mentioned first at the beginning of this section, it must be pointed out that this sensor has been working on several other platforms. On NIMBUS-7 from October 1978, when it discovered the ozone hole providing the most unfortunate anecdote in data-processing, since all the series of ozone values taken on the Antarctic with values inferior to a concrete threshold were discarded by the quality control system. Later, TOMS sensor was installed on METEOR-3 spacecraft where it was operative from August 1991 until December 1994. The anecdote here is that this was the first and last instrument built in the USA that was installed on a satellite from the old Soviet Union at the end of the cold war.

Then, TOMS sensor was installed on the Japanese satellite ADEOS in order to continue the series of previous satellites. However, it was only active between July 1996 and July 1997, when it was replaced by EP-TOMS.

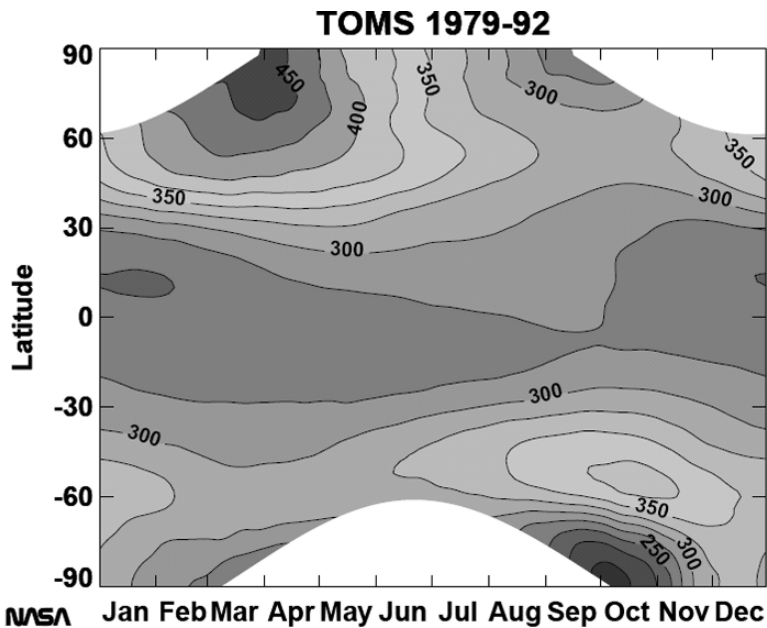


Fig. 4.3 Results of ozone depth for period: 1979–1992, from TOMS sensor. Units are Dobson units. (Credits: NASA. *Studying Earth’s Environment From Space*. October 2006)

Nowadays, the only instruments by NASA dedicated to the temporal monitoring of ozone are TOMS sensor on board the Earth Probe TOMS, from 1997, and the Ozone Monitoring Instrument (OMI) on board the satellite Aura, launched in July 2004 and that still continues on the Terra and Aqua series. Figure 4.4 shows the

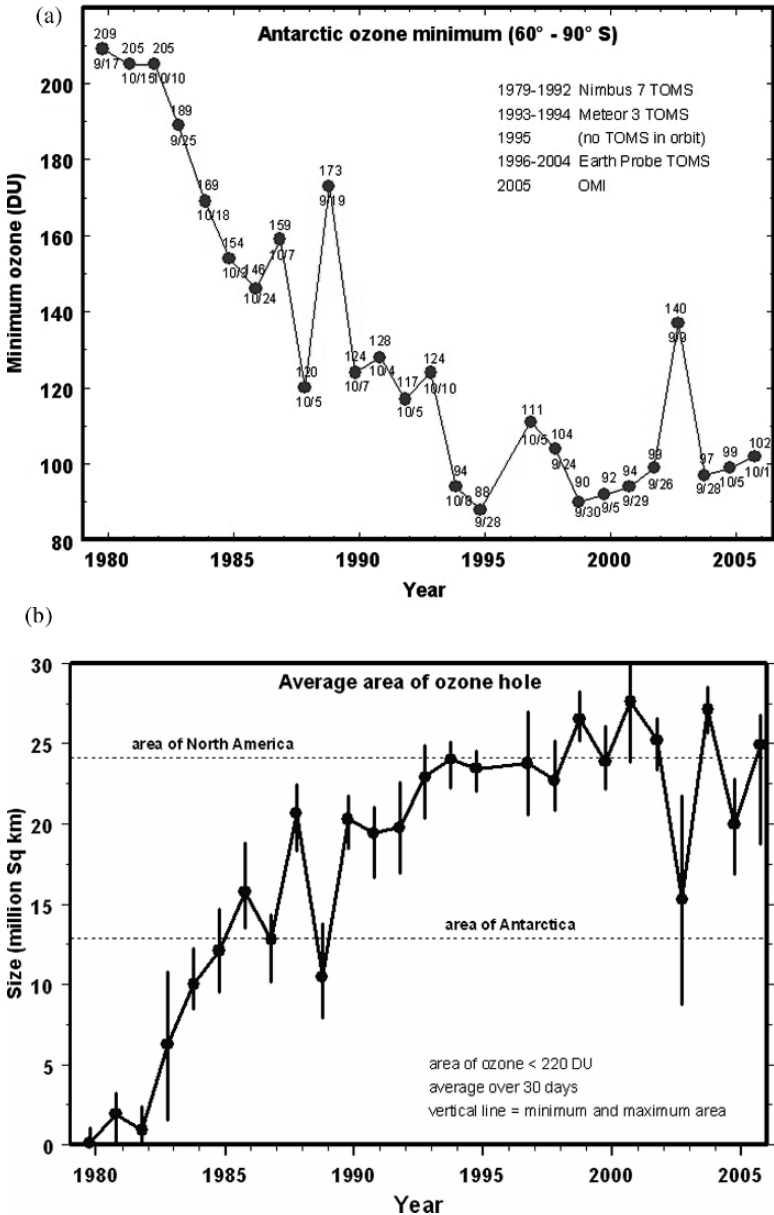


Fig. 4.4 Part a) Antarctic ozone minimum by means of TOMS. Part b) Average area of ozone hole by means of TOMS. (Credits from Ozone Processing Team. NASA/GSFC)

antartic ozone hole observed by TOMS sensor, showing minimum values and average area covered by hole.

4.3.2 GOME Sensor

GOME sensor (Global Ozone Monitoring Experiment) was the first European instrument in charge of monitoring the total ozone depth from the outer space. It is installed on board the ERS-2 (European Remote Sensing) satellite launched by the European Space Agency in April 1995 in heliosynchronous orbit. Data from ERS-2 are received in four stations around the world.

GOME is a spectrometer that measures the solar radiation reflected towards the space by the Earth's surface and by all atmospheric constituents. This instrument also measures the solar spectrum directly, without disturbances, so as to establish the reflectance of Earth+Atmosphere together. GOME measurement spectral range goes from the ultraviolet, 240 nm, to the near-infrared, 790 nm, with a spectral resolution of [0.2–0.4 nm]. This measurement range is used to establish other atmospheric constituents. In the concrete case of the vertical distribution of ozone, the range between 260 and 350 nm is used and ozone is established through a transportation model in the atmosphere and the chemical reactions involving ozone.

The physical fundament used by this sensor is the measurement of the atmosphere and the Earth's reflectance through the viewing in the nadir. If we limit ourselves to the spectral ranges where there is absorption by the ozone, this reflectance can be expressed through:

$$\rho(\lambda, \theta_0, \theta, \varphi - \varphi_0) = \frac{\pi I}{F_0(\lambda)} = P(\lambda) e^{-\sigma_{O_3}(\lambda) N_s}$$

where ρ is the reflectance I is the radiance coming from the Earth, λ the wavelength, θ is the viewing cenital angle, θ_0 the solar cenital angle, $(\varphi - \varphi_0)$ the sun-satellite relative azimuth angle, $F_0(\lambda)$ the extraterrestrial solar irradiance per atmosphere area unit, $\sigma_{O_3}(\lambda)$ the efficient section of ozone absorption, N_s the density of the ozone column and $P(\lambda)$ a polynomial that carries out a high-pass filtering. This equation is, in fact, Lambert-Beer law for reflectance. Numerical instruments using radiative transference models have proved that this equation is an approximation that calculates with accuracy the content of ozone for wavelengths above 320 nm.

Figure 4.5, is taken from PROMOTE and TEMIS projects, shows the temporal evolution of the ozone hole for period of August-December, explained in Dobson units and millions square kilometres. These results are been estimated by using GOME sensor.

Figure 4.7 in the attached CD-ROM, shows and graphic evolution of ozone hole by using GOME and SCIAMACHY European sensors on board ENVISAT. These data are been processed at German laboratory DLR.

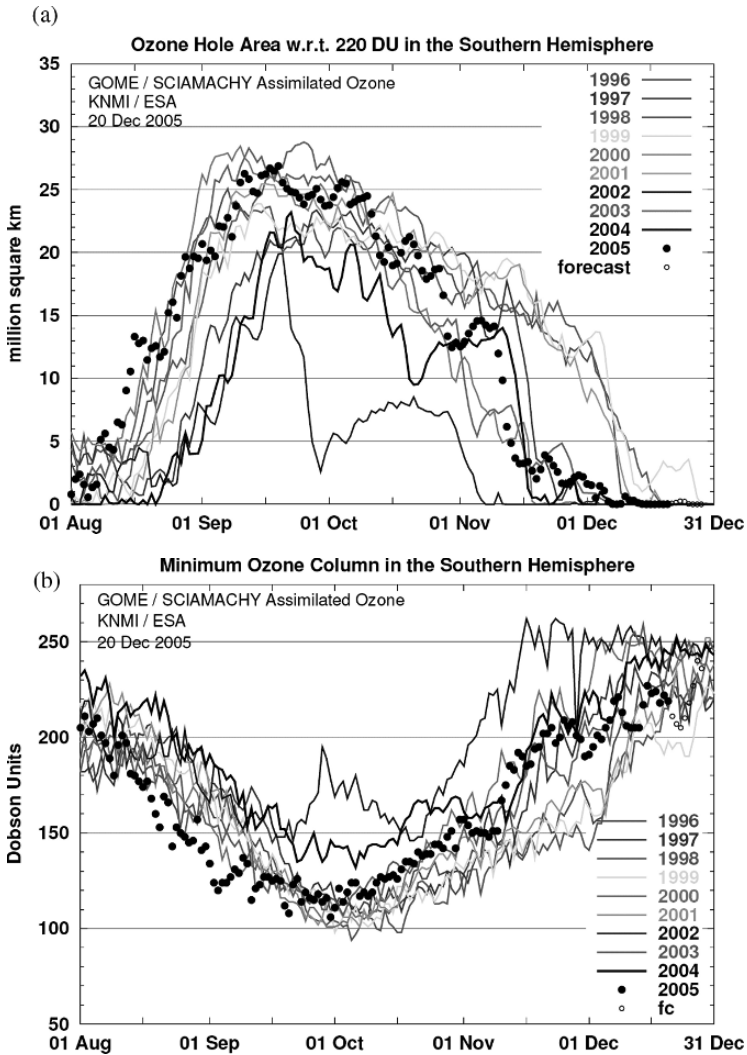


Fig. 4.5 Part a) The depth of the ozone hole is the lowest ozone column value in Dobson Units for latitudes below 30° south. Part b) The size of the ozone hole is the area on the globe in million square km of ozone column values below 220 DU. (credits: PROMOTE and TEMIS projects, with permission)

4.3.3 GOMOS Sensor

The ENVISAT satellite was launched by the European Space Agency in March 2002. This was a satellite of more than 8000 kg, breaking the tendency of Earth observation satellites, equipped with a large number of sensors aimed at the monitoring of the environment. Three of these sensors are especially relevant in the detection of atmospheric components: GOMOS, SCIAMACHY and MIPAS. GOMOS stands

for Global Ozone Monitoring by Occultation of Stars and it measures ozone and green-house-effect gases in the ultraviolet spectrum, visible and infrared, between 15 and 20 km of height. Figure 4.6 shows the Principle of measurement of GOMOS. This sensor is installed in the side of the satellite facing the Earth observing the occultation of programmed, successive stars and it is orientated in the opposite direction of the velocity vector. It must be pointed out that GOMOS is the first spatial instrument dedicated to the study of the Earth’s atmosphere that uses the Occultation-of-star technique.

The principle of measurement of GOMOS follows several steps: when a star from its database is above the horizon (considering by horizon a height of 120 km), its spectrum is analysed considering that it is not influenced by any atmospheric component. Later, the occultation of this star as it dives into the atmosphere is observed. The spectrum of any programmed star, $F(\lambda, z)$, is modified by the influence of all atmospheric constituents integrated in the line of sight from the star to the satellite according to Beer-Lambert law. If only ozone absorption is considered, the spectrum captured by the sensor is:

$$F(\lambda, z) = F_0(\lambda) e^{-\sigma_\lambda N(z)}$$

where λ is the wavelength and z the altitude of the line of sight above the horizon, which is calculated through the knowledge of the satellite’s position and the direction of the star; $N(z)$ is the quantity of ozone expressed in molecules/ cm^2 along the line of sight and σ the efficient section of ozone absorption. The quantity of ozone integrated along the line of sight is obtained by comparing the original and absorbed spectrums according to:

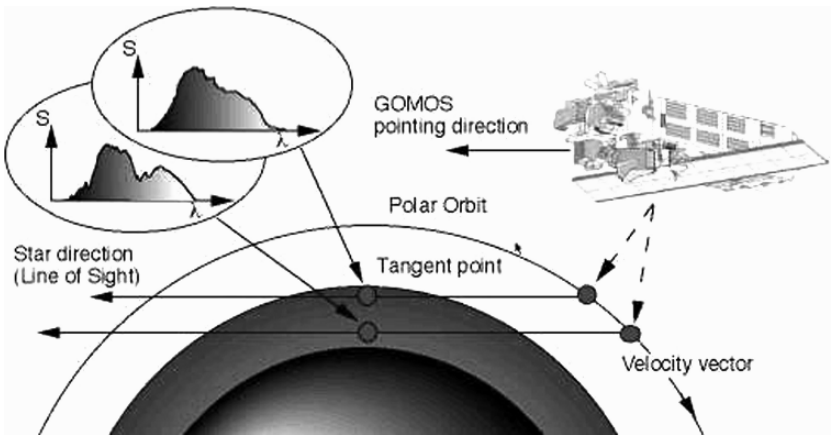


Fig. 4.6 Principle of measurement of GOMOS: Comparison of stellar spectrum before and after atmospheric influence. (GOMOS Product Handbook, ©ESA / Denmann Productions, Envisat satellite, artist’s impression)

Erythemal Action Spectrum

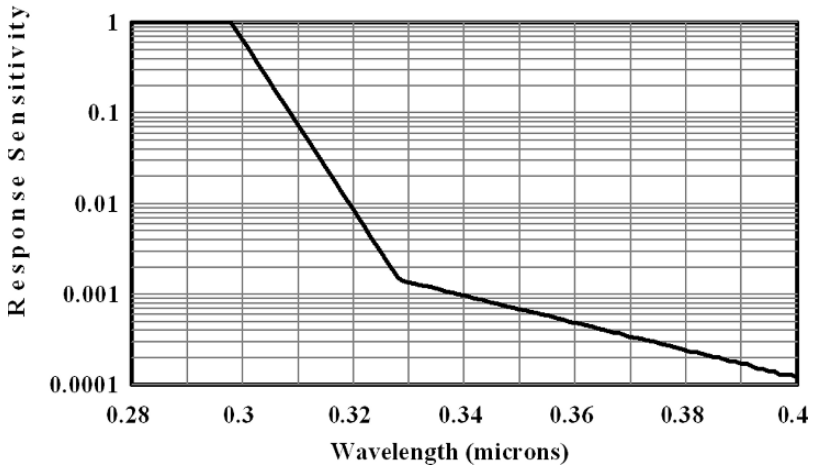


Fig. 4.7 Logarithmic graph of the erythemal action coefficient (McKinlay and Diffey, 1987)

$$N(z) = -\frac{1}{\sigma_\lambda} \log \left(\frac{F(\lambda, z)}{F_0(\lambda)} \right)$$

For each stellar occultation, a series of lines captured at different altitudes z are processed. The vertical distribution of ozone depth in molecules/ cm^3 can be established from these series. It is taken the approximation that the atmosphere is a symmetric sphere, which is called “onion layers” technique. The vertical resolution of measures corresponds to 1.7 km, since GOMOS carries out this process at intervals of 0.5 seconds. On the other hand, generally speaking, the accuracy of the measurements depends on the temperature and brightness of the star analysed. Above 30 km, Chappius band is used, where there is very little dependence. Below 30 km, however, the accuracy decreases as higher-magnitude stars (less bright) are used. The most accurate results are obtained at an altitude of around 60 km, with errors of around 0.5% for magnitude 0 and 3% for magnitude-2 stars.

In spite of the apparent simplicity of this method, many corrections must be introduced since the refraction effects of light through the atmosphere cause the deviation of rays depending on the atmosphere’s depth gradient, the crossing of rays from different stars seen at different levels and the chromatic refraction.

The advantage of this procedure is that the absolute measurement of ozone depth is carried out in a short interval of time, which guarantees that the procedure is auto calibrated and valid for long-functioning periods throughout the satellite’s life, without being affected by the damage time may cause on the sensor’s sensitivity. On the other hand, this measurement procedure differs from TOMS and SBUV

in that the latter measure the retro-dispersed ultraviolet radiation providing measurements on the total ozone depth instead of vertical profiles, as is the case of GOMOS.

Studies of tropospheric ozone by using satellite sensors is a very interesting topic that starts to provide results working in an indirect way, the product TOR (Tropospheric Ozone Residual) that consist in the estimation of tropospheric ozone by means of a difference between the total ozone, estimated by TOMS, and the stratospheric ozone estimated by SBUV (Solar Backscatter Ultraviolet).

4.3.4 Tropospheric Ozone

Today, tropospheric ozone can be estimated directly from space by means of sensor TES (Tropospheric Emission Spectrometer). The primary objective of TES is to make global, three-dimensional measurements of ozone and other chemical species involved in its formation and destruction. TES is a high-resolution imaging infrared Fourier-transform spectrometer that operates in both nadir and limb-sounding modes. TES global survey standard products include profile measurements of ozone, water vapor, carbon monoxide, methane, nitrogen dioxide, and nitric acid for 16 orbits every other day. TES Special Observations are research measurements of targeted locations or regional transects which are used to observe specific phenomena or to support local or aircraft validation campaigns (Atmospheric Science Data Center, 2006).

TES is instrument on board of satellite EOS-Aura, which is the EOS chemistry mission which aims to answer three important questions: is the ozone layer recovering, is air quality getting worse, and is the Earth's climate changing? Aura will continue the long term series of atmospheric chemistry measurements made by earlier missions. The Aura spacecraft operates in sun-synchronous polar orbit. The satellite carries four instruments: TES, OMI (Ozone Monitoring Instrument), MLS (Microwave Limb Sounder) and HIRDLS (High Resolution Dynamics Limb Sounder)

4.4 The Erythemal Irradiance

The biological effects caused by exposure to solar radiation comprise the whole spectrum. However, the solar ultraviolet spectrum conveys more risks due to the negative effects it has on most living organisms (Hoppe et al., 1996). Doses over the ones considered to be normal may cause severe damage to vegetation systems due to the alteration of their chlorophyllic functions. The most important effects are the reduction of harvests and the deterioration of sea phytoplankton.

Regarding animals, damages affect different organs, specially eye pathologies and deterioration of the immunologic system. In the case of human beings, there are also many skin dysfunctions, the most serious one being the cancerous melanoma. An overexposure to this type of radiation also causes serious alterations in the genetic ADN.

These human alterations depend mainly on individual characteristics so that any study on the risk of exposure will be incomplete if these factors are not taken into account. That's why it is necessary to introduce a radiation index for each individual that comprises the physical conditions of radiation and the biological type he/she belongs to. This is called phototype. There are 5 general phototypes for individuals, from African black to the albino type.

4.4.1 *Classification of Ultraviolet Radiation*

The biological effects of radiation in the ultraviolet spectrum interval depend strongly on the radiation wavelength. In 1932, the *Comite Internationale de Lumière* presented a division of the ultraviolet spectrum according to wavelength. Thus, three different regions are distinguished: A, B and C, according to the different biological effects they have.

- Region A of the spectrum, called UV-A radiation. It is the nearest ultraviolet spectral region to the visible spectrum and it comprises the wavelength interval $\lambda = 400 \text{ nm}$ to $\lambda = 320 \text{ nm}$. Although it is the least absorbed by the atmosphere, it is not too dangerous. Its is responsible for making skin darker and suntan.
- Region B of the spectrum, called UV-B radiation. It is the intermediate region of the ultraviolet spectrum, between $\lambda = 320 \text{ nm}$ to $\lambda = 280 \text{ nm}$. This radiation keeps a delicate equilibrium on the biological effects considered as normal. Small rises in the dose received may cause important damage to skin and eyes since it is not absorbed strongly by the atmosphere. Their effects are in the limit of the biologically permitted. It often causes sunburns and that's why it is also called sun burning radiation.
- Region C of the spectrum, called UV-C radiation. It is a very energetic radiation with very intense negative effects such as skin cancer and important eye diseases. It extends over the spectrum zone of $\lambda = 280 \text{ nm}$ to $\lambda = 200 \text{ nm}$. That's why it is called far-distant radiation or germicide radiation. This radiation is almost totally absorbed by the atmosphere.

4.4.2 *Curve of Erythematic Radiation*

UV-B type radiation, which causes the so called burning effect or erythematic effect, is the most interesting one from the point of view of prevention . The maximum

erythematic effect is found from 0.280 μm and it decreases as the wavelength increases. In order to quantify the total erythematic power of the radiation, a new magnitude has been defined corresponding to the total radiation pondered by a factor $\varepsilon(\lambda)$ called erythematic action coefficient, so that:

$$E_{eritem} = \int E(\lambda) \cdot \varepsilon(\lambda) d\lambda$$

E_{eritem} is the erythematic irradiance and $E(\lambda)$ the solar spectral irradiance at a wavelength λ at surface level. The dependence of the erythematic action coefficient on the wavelength has been studied and the curve in Fig. 4.7 (based on Mckinlay and Diffey, 1987) has been suggested to quantify the erythematic effect of radiation. This curve is at logarithmic scale so that the variation intervals can be distinguished clearly.

The erythematic action curve is a curve of biological effects. That's why the magnitude represented does not have physical units. The value of 300 nm has been taken as the effective unit value since this is the zone where the ultraviolet radiation registers the maximum erythematic power. From this curve, we can deduce that the integral in the calculation of the erythematic irradiance E_{eritem} , spread throughout the spectrum, has a value different from zero between 280 nm and 400 nm since for $\lambda > 400$ nm the erythematic power $\varepsilon(\lambda)$ is zero and for $\lambda < 280$ nm the solar radiation is almost totally attenuated by the atmosphere. As can be seen in the graph, an irradiance of I Watts/m² at a wavelength of 290 or 300 nm has an erythematic power equivalent to $I \cdot 10^4$ Watts/m² for wavelengths corresponding to the end of the erythemal action spectrum (≈ 400 nm).

The relation existing between the reduction in the concentration of total ozone and the consequent increase in the erythematic irradiance can be seen in Fig. 4.8: with ozone concentration, the erythematic irradiance increases potentially with negative exponential.

4.4.3 Minimum Exposure Erythematic Dose (MED)

The information supplied by the erythematic radiation described above is not enough to establish its harmful effects on individuals since it is an instantaneous radiation magnitude with power units per surface unit. Taking into account that the effects caused by solar radiation become apparent after exposure to the sun and have, as it is logical, an accumulative effect, it is necessary to relate erythematic irradiance to exposure time, thus finding units of energy per units of surface. For this purpose, the MED (Minimum Erythematic Dose) is defined as the minimum irradiance necessary to cause skin reddening after a concrete time of exposure to radiation, in spite of the fact that low-pigmented skin reddens earlier than a darker complexion. That is, it depends on the skin phototype of each person. An individual with a white-slightly-pigmented complexion is taken as the reference unit. The minimum erythematic dose has been found experimentally for these individuals with the following value: $1 \text{ MED} = 21 \text{ mJ/cm}^2 = 210 \text{ J/m}^2$.

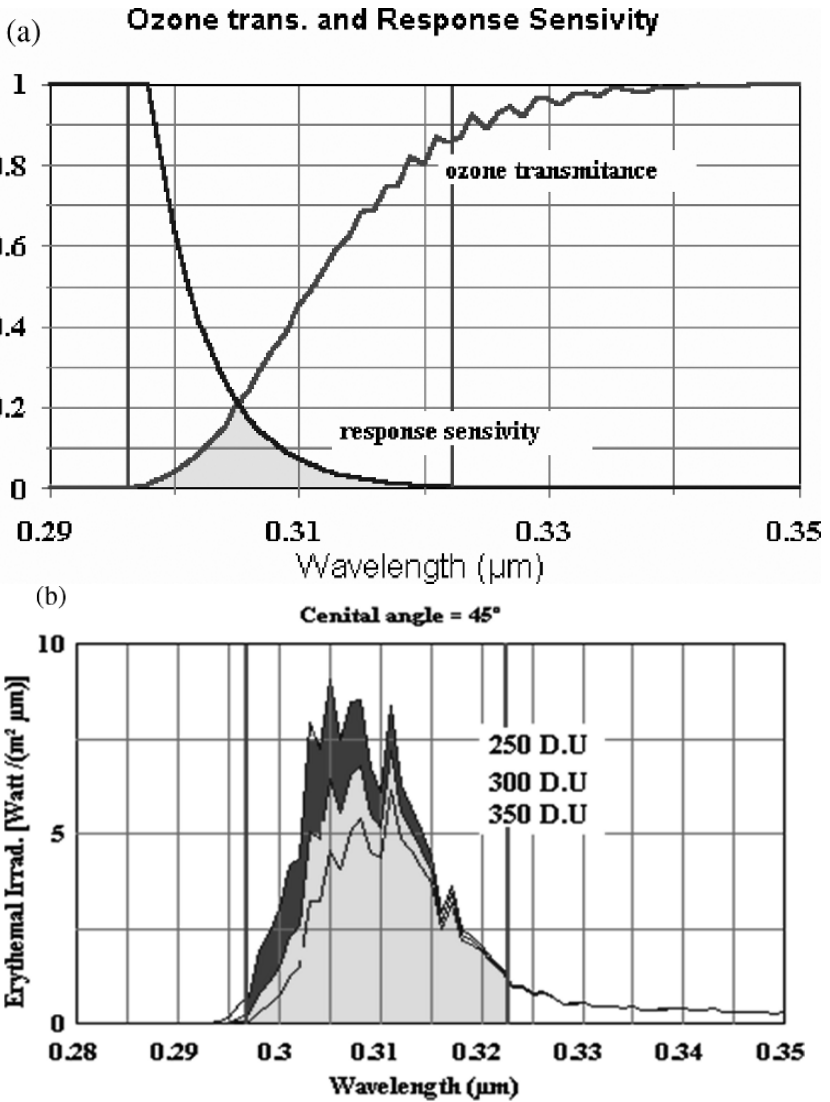


Fig. 4.8 a) Ozone transmittance and erythemal action. b) Spectral erythemal irradiance for different total ozone thickness values (Credits: Calle, et al, 2000)

4.4.4 Erythemal Irradiance Maps

Erythemal Irradiance Maps for clear skies are obtained from the interpolation of ozone values in the area of interest and applying solar radiance models. Figure 11 in the attached CD-ROM, shows characteristic summer values in Spain with a month of separation between May and August. Figure 12 in the attached CD-ROM, shows



Fig. 4.9 Radiometer BIOMETER 501 installed at CIBA. Dpt. Applied Physics University of Valladolid (Credits: Calle 1997). Its spectral response to UV radiation is the proposed by McKinley and Diffey

the erythemal spectral exposure expressed in Kj/m^2 for the month of July at a global level.

The validation of erythemal irradiance models is carried out through experimental data obtained from radiometers like the one in Fig. 4.9.

References

- Atmospheric Science Data Center (2006). URL: <http://eosweb.larc.nasa.gov/>
- Calle, A. (1997 December). Study of ozone depth and erythemal irradiance by means of NOAA images. Doctoral Thesis at University of Valladolid, Spain.
- Calle, A., Pérez, A.M. Casanova, J.L. (2000). Calculation and analysis of erythemal irradiance using experimental data and TOMS ozone data. Remote Sensing in the 21st Century. Proceedings of EARSeL Symposium. Ed. Balkema, Rotterdam, Brookfield, 2000.
- Carver, G. (2006). NCAS-Climate, ACMSU, Centre for atmospheric science, University of Cambridge. URL: <http://www.atm.ch.cam.ac.uk/tour/>

- GOMOS Product Handbook (2004). European space agency- Envisat GOMOS Product Handbook, Issue 1.2, September 2004.
- Hoppe, P., Rabe, G., Praml, G., Lindner, J., Jacobi, G., & Fruhmann, G. (1996). Are there risk groups in respect to acute effects of environmental ozone? Proceedings of 14th International Congress of Biometeorology. 1–8 September 1996, Ljubljana, Slovenia, Vol. 3, pp 40–49.
- McKinlay, A. F., & Diffey B. L. (1987). A reference action spectrum for ultra-violet induced erythema in human skin. In W. F. Passchier & B. F. M. Bosnjakovich, (Eds.), *Human exposure to ultraviolet radiation: risks and regulations* (pp. 83–87). Excerpta Medica International Congress Series No.744.
- McPeters, R.D., Bhartia, P.K., Krueger, A.J., Herman, J.R., Wellemeyer, C.G., & Seftor, C.J. et al. (1998). Earth Probe Total Mapping Spectrometer (TOMS). Data Products user's guide. NASA Technical publication 1998–206895.
- NASA. (2006 October). Studying Earth's Environment From Space. URL: <http://www.ccpo.odu.edu/SEES/index.html>

Chapter 5

Remote Sensing of Land-Cover and Land-Use Dynamics

Philippe Mayaux, Hugh Eva, Andreas Brink, Frédéric Achard and Alan Belward

Abstract Land is changing at a rate never achieved before. This evolution needs to be documented by robust and repeatable figures. Earth Observation tools play a key-role in the production of regular estimates of the landscape changes. In this chapter, we discuss the utility of Remote Sensing data for producing information on land-cover and on land-cover/land-use changes. Basic guidelines in terms of legend, data acquisition, classification techniques and validation are explained. For illustrating global land-cover projects, the recent Global Land Cover 2000 project is described.

Two main land-cover change phenomena are exposed in the text: tropical deforestation (at pan-tropical level and for the Congo Basin) and agricultural expansion in Africa (continental level and for Senegal). In 1990 there were some 1,150 million hectares of tropical rain forest with an annual deforestation area for the humid tropics estimated at 5.8 million hectares. A further 2.3 million hectares per year of forest are detected as degraded – e.g. due to fragmentation, logging and / or fires. In the sub humid and dry tropics, annual deforestation for the tropical moist deciduous and the tropical dry forests comes respectively to 2.2 and 0.7 million hectares. Southeast Asia is the region where forests are under the highest pressure with an annual change rate of 0.8–0.9%, while changes are moderated in South America (0.4–0.5%) and in the Congo Basin (0.2–0.3%). For the agricultural expansion, the reported study shows that Africa has lost 16% of its forests and 5% of its woodlands and grasslands over the 1975 to 2000 period, equating to over 50,000 km² per year of natural vegetation. The majority of this has been converted to agricultural lands. West Africa has seen the most change.

5.1 Introduction

Most of the 6.5 billion human inhabitants of this planet spend most of their time on the land; what covers the land and how humans use it has a profound effect on the functioning of the Earth system and on ways in which this global system is changing. The nature of the land cover (bare soil, rock, different types and quantities of vegetation, water-bodies, snow, ice, man-made materials and any combination

of the above) influences the Earth's climate system by affecting water and energy exchanges with the atmosphere, and greenhouse gas and aerosol sources and sinks (Sellers et al. 1997). The nature of the land cover will also affect the services provided to humans – everything from the obvious such as determining sources of food, fiber, medicines and the like, to the less obvious recreational and cultural influences on our lives.

Climate models describe land surface processes in terms of albedo, roughness, aerosol emissions, evapotranspiration and carbon exchange (GCOS 2003). Progress is undoubtedly being made in making such measurements directly from Earth Observing systems, but in terms of operational long-term data production much still remains to be achieved (GCOS 2006). However, these terrestrial climate variables can be inferred from land cover type (e.g. Running et al. 1994). So on a global scale land cover can be said to play a big part in determining climate. It is also true that on a regional or local scale the distribution of land cover is determined by climate. Changes in land cover are thus among the factors forcing global climate change, yet changes in land cover can also be reliable indicators of such change.

Land cover is not static, though the time scale of change varies enormously. Plant growth and differentiation lead to continual changes in vegetated surfaces (biochemical and molecular level dynamics constantly change plant form, function and structure); fires, disease and wind throw among other “natural” phenomena can cause dramatic changes in the distributions of entire plant communities; deserts, snow and ice can be considered permanent land cover features, though even here changes are apparent – glaciers and snow fields are retreating, desert margins shifting. And of course the ways in which humans use the land too causes change; seasonal changes such as the transformation from bare soil to standing water to a standing crop and back to bare soil characteristic of rice production; and more fundamental changes such as the clearance of forest for grazing and crop land.

Land-cover and land-use dynamics are very much part of the climate change story, but their role does not stop here. There is no universally accepted definition of global change (for some it includes the processes of economic globalization, for others it is bound by changes in the global environment that alter the capacity of the Earth to sustain life), yet wherever one chooses to limit the definition, land-cover and land-use dynamics have a role in the process of global change. These dynamics affect climate, land, freshwater –and even marine-productivity. They affect the chemistry of the atmosphere surrounding us; they determine how and where we can construct dwellings, communication, transport and energy networks and have profound influences on the biological diversity of our planet.

Global change science needs accurate, reliable and consistent documentation of land cover and land-use dynamics to improve our understanding of the way in which the different elements of the system actually function, ways in which they interact and to reduce uncertainty in any forecasts of change. The policy domain too needs such information. Internationally agreed multilateral environmental agreements, such as the Rio Conventions (United Nations Convention on Climate Change, UN Convention to Combat Desertification and Convention on Biological Diversity) to a greater or lesser extent contain mandatory reporting obligations concerning land

cover and cover change which in turn condition new policy decisions associated with these conventions.

Policy concerning sustainable development too calls for land cover and land-use monitoring. Land resources have high economic value, but this won't last if they are over exploited or poorly managed. Aid programmes want to know past land cover/use conditions, current status and likely future situations for the development of policies and operational strategies and to direct the utilization of resources; the long-term goal being sustainable management of land resources as part of the fight to eradicate poverty in developing regions of the world.

Notwithstanding the growing need for global information on our planet's land resources global monitoring programmes are still rare. By 1972 the US Earth Resources Technology Satellite (subsequently renamed Landsat) was in operation; however the data have yet to be used to create thematic maps showing the land cover of our planet treating all parts of the world equally, and representing actual land cover over a fixed, contiguous period of time. The first such map only became available in the 1990s and was based on much coarser resolution data from meteorological satellites (Belward et al. 1999; Loveland et al. 1999).

This process has continued: efforts have been done by the space agencies for making available large datasets providing the baseline material for a better land-cover characterisation; scientists are developing dedicated techniques for refining the measurements; policy-makers start to include such diagnostics in their decisions. This paper describes recent activities in global land cover/land-use mapping and monitoring. For each chapter (mapping and monitoring), the main methodological issues are addressed in a first time; key examples and trends are then detailed, while the future scientific and technological evolutions are finally outlined.

5.2 Land-Cover and Land-Use Mapping

With the advent of Earth Observing satellites, the task of faithfully characterizing the state of the Earth's land cover for large areas has become a real possibility. Up until recent times, land cover maps were necessarily restricted to local coverage, affected by aerial and field survey, or to gross generalizations, both spatially and thematically. Beginning in the early 1970's, satellite remote sensing techniques have been successfully applied to the mapping of local, national, continental and even of global land cover. Today, it is quite surprising to find that our knowledge of the real distribution of global land cover was until quite recently, poor.

The utility of land cover maps for natural resources management and planning from local to national scales is evident. At the global scale reliable land cover characterization is an important input into Global Circulation Models, enabling us to improve our understanding of the way in which the biosphere functions and to model future climate scenarios.

5.2.1 Data & Methods

The remote sensing data used for land cover mapping depend on the scale and extent of the task. For local (larger mapping scales of less than 1:1M) fine spatial resolution data (30 m pixel size) such as Landsat Thematic Mapper (TM) have been used.

Larger area, smaller scale, maps have used low spatial resolution data (> 500 m mapping unit) available from the NOAA AVHRR, SPOT VGT and Aqua/Terra MODIS instrument. While the former, finer spatial scale data, give better spatial information, the latter due to their high repeat cycle (often daily) give better temporal information, important when mapping seasonal features. More recently, the availability of global collections of fine spatial data sets combined with improvements in data storage and processing have opened up the use of this finer spatial resolution data for national and regional mapping.

5.2.1.1 Legend

The legend employed for any specific land-cover mapping is a compromise between the user requirements of the map and the intrinsic properties of the data source. The spatial resolution, satellite revisit time and spectral properties of the sensor all determine what is, and what is not, possible to map. Generally, the larger the area to be covered, the lower the spatial and thematic richness of the map. Recent global land cover maps, GLC 2000 and IGBP DISCover, are able to faithfully report around 20 classes at the global level. In case of the GLC2000 project, the global legend was expanded to more than 50 classes at the continental level (Eva et al. 2004; Mayaux et al. 2004) using the same input data as the global map.

A useful tool for the a-priori conception and definition of the legend and the inter-comparison of existing classification systems is the Land Cover Classification System (LCCS) developed by the Food and Agriculture Organization of the United Nations and the United Nations Environment Programme (Di Gregorio & Jansen 2000). LCCS describes land cover according to a hierarchical series of classifiers and attributes that separate vegetated or non-vegetated surfaces, terrestrial or aquatic/flooded, cultivated and managed, natural and semi-natural, life-form, cover, height, spatial distribution, leaf type and phenology.

5.2.1.2 Classification Techniques

Techniques for turning remote sensing images into categorical maps have also become more sophisticated. Originally, satellite remote sensing data were used in a similar way to aerial photographs, with black and white prints being photo-interpreted. The technique, when combined with good ground knowledge and other supporting material has been used successfully to provide both national (Boulvert 1986) and continental vegetation maps (White 1983). These techniques however fail to take advantage of the spatial fidelity and the full spectral richness of the data.

Digital image processing techniques can be used to statistically examine the data and create clusters using the spectral properties of the individual pixel elements, and with a time series, their temporal compartment. The clusters can either be trained, using ground data, or statistically dictated. When the clusters are trained (supervised classification) a ground truth data set needs to be provided so as to “train” the classifier. In the case of unsupervised training, the thematic class of each of the resulting clusters needs to be identified and given appropriate label. This approach is often used for large area maps as it requires little *a priori* knowledge and as suitable training data is difficult to apply for extended areas (i.e. for a supervised maximum likelihood classifier), as demonstrated by e.g. D’Souza et al. 1995. While fully exploiting the spectral properties of the data, this “pixel based” approach does not use the contextual information of the data – something the human eye makes extensive use of in photo-interpretation. In recent years this aspect of image processing has become more sophisticated and the use of “image segmentation” has become more commonly employed as part of the classification process.

5.2.1.3 Validation

The validation of land cover products cover small areas is usually achieved by the use of ground data – comparing the map fidelity with the ground data and reporting errors of omission and commission. However, for larger areas this data collection can be problematic, both the extent of the area concerned, the diverse ecosystems and to the lack of homogeneous national legends and, not least, the potential financial costs of such exercises. Therefore in practice, ground data are often replaced by satellite data of finer spatial resolution than that of the map (Strahler et al. 2006).

To validate the DISCover global map, the IGBP project aimed at selecting 415 1 km points across the globe for expert interpretation and comparison with the IGBP class (Scepan 1999). The assessment was carried out on 25 points randomly distributed across the globe for each class. While such a validation exercise gives a measure of reliability at the global level it does not preclude local mapping errors that can be avoided with a careful expert review of the preliminary product. Under the GLC 2000 project a two-stage process was carried out (Mayaux et al. 2006). The first stage was a quality control step, to eliminate macroscopic errors in the spatial delimitation of classes and of class labels. The second stage consisted of a statistical examination of the classes mapped at the global level. A stratified random sample of sites weighted by continent was selected, with 26 sites per land cover class. The sample sites consisted of Landsat TM scenes, interpreted by local experts. For a complete review of validation of global land-cover maps, see Strahler et al. (2006).

5.2.2 Global Products

The data collection of NOAA-AVHRR 1 km carried out under the aegis of the IGBP gave scientists for the first time access to a complete global dataset from a single

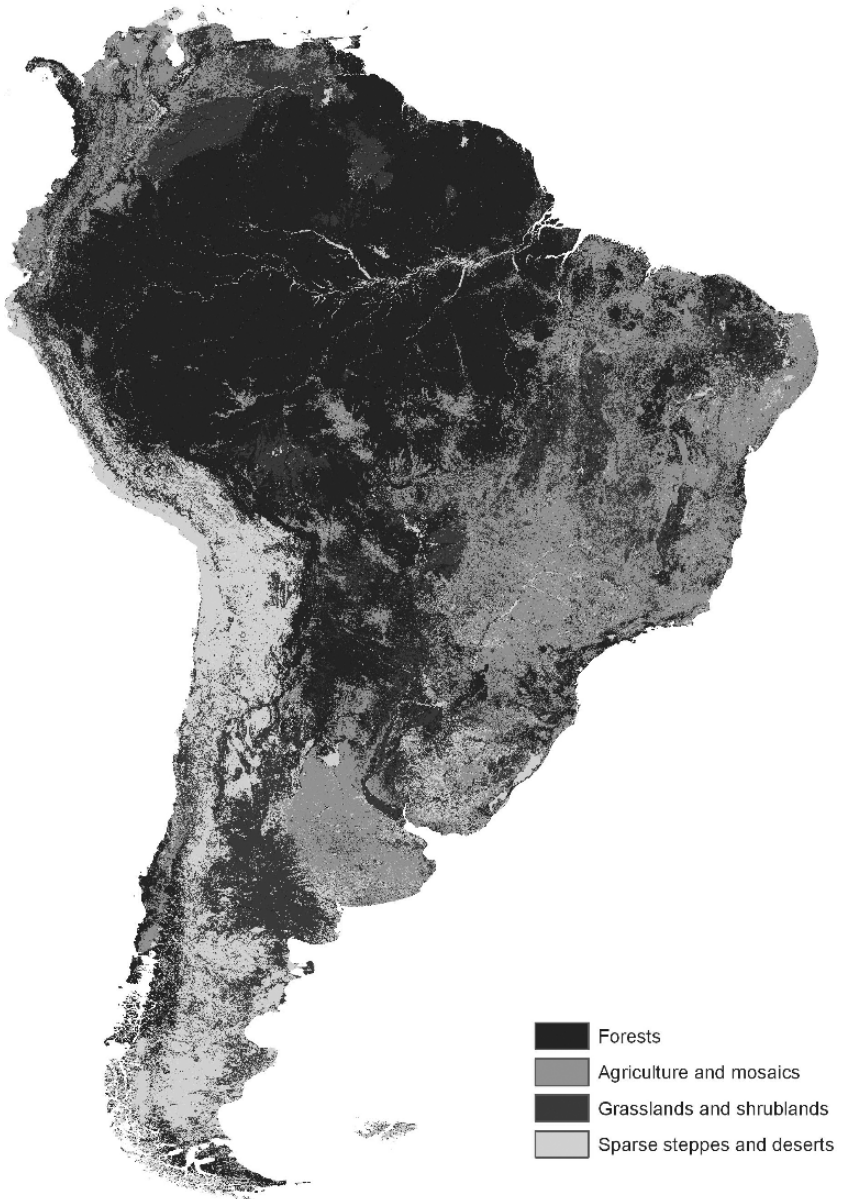


Fig. 5.1 GLC2000 land-cover map of South America derived from SPOT VGT data

source of satellite data appropriate for land cover mapping and land cover parameter characterisation (Loveland & Belward 1998). The data were used to produce the first global land cover map “DISCover” at 1 km spatial resolution from satellite data, with some 20 thematic classes. Since then new data sources, improved availability and access to data have allowed new products, both of land cover and land cover

parameters to be generated. Notable among these are the GLC2000 (Fig. 5.1) from SPOT VGT, which produced not only a global land cover map (Bartholomé and Belward 2005), but also several continental maps with more detailed local legends (Bartalev et al. 2003; Eva et al. 2004; Mayaux et al. 2004; Stibig et al. 2007). The medium resolution MODIS sensor (250–500 m resolution) has also been the source of a global land cover classification (Friedl et al. 2002).

5.2.3 Regional Products

When moving to land cover maps appropriate to national applications finer spatial resolution data have been employed. Both the AfriCover (11 countries in Africa) and Corine (EU) initiatives, producing national maps for a series of countries with a common legend, have used the finer spatial properties of the Landsat Thematic Mapper. Similarly the UK's Land Cover Map 2000 (LCM2000). These maps require finer spatial resolutions so as to meet the user requirements for use by government departments, national and regional agencies for environmental management and protection, land planning or watershed management. Specifically the UK assessment has been found useful for mapping animal disease distribution, bird and habitat relationships and forestry research (Fuller et al. 2002).

5.2.4 Prospects for Future Land-Cover Mapping

New prospects for global forest and land cover mapping emerge from recent developments of satellite sensors that acquire satellite imagery at “medium” spatial resolution (180–300 m). Whilst, still maintaining a global or regional view of the Earth's surface, the improved spatial detail of such images raises the prospect of better addressing land cover information needs at global and regional, but also at sub-regional and national levels. Indeed such data could establish the link between global and local observations. The first global land cover mapping approaches, such as the mapping of percentage tree cover (Hansen et al. 2003), highlight the advantages provided by the new sensors. A study on vegetation mapping in northern India has demonstrated the suitability of the new satellite imagery for mapping even complex land cover patterns at sub-regional scales (Roy & Joshi 2002).

In order to provide the scientific community with more precise information on the spatial distribution of habitat types, the European Space Agency, in collaboration with an international network of partners including JRC, FAO, UNEP, IGBP, GOCF and EEA, is now starting the production of a global land cover map for the year 2005 at 300 m spatial resolution using MERIS fine resolution mode data acquired between December 2004 and June 2006, as the main source (Arino et al. 2007). This new land cover product updates and complements other existing comparable global products, such as the GLC-2000. The thematic legend of the final product is compatible with the FAO-UNEP Land Cover Classification System (LCCS). The

map is being developed in such a way that any further update of the global land cover map will be at a recurrent cost to run the developed system.

5.3 Land-Cover & Land-Use Dynamics

Land-cover and land-use changes (LUCC) occur globally in a large variety of situations from the ecological and human point of view. This broad spectrum will have an impact on the Earth Observation data and techniques used for identifying the processes and measuring their magnitude. We will first examine the variation factors to take into account and review the technical parameters that are important to define for a reliable monitoring system. Then we will detail two major land-cover change processes and provide remote sensing-based estimates of tropical deforestation and agricultural expansion.

5.3.1 Factors of Variation

5.3.1.1 Nature of the Changes

Land cover and land use changes include the conversion from one land-cover class to another and the small changes within one class without changing its classification. (Coppin et al. 2004). The intensification of agriculture, the densification of urban settlements or the forest exploitation are good examples of continuous changes that do not modify the category of the main land-cover. However, as some basic attributes are modified, it can have a major impact for global change studies.

5.3.1.2 Temporal Permanence of the Change

Land-cover changes can affect the landscape for a few days (floods), some weeks (vegetation fires), one year (biomass density in the Sahelian belt), a few years (forest clear-cut) or for a longer period (urbanisation). In cases of temporary changes, the ecosystem resiliency allows for going back to a situation close to the initial one.

5.3.1.3 Direction of the Change

Changes are substantial and predominantly reduce the natural ecosystems at the benefit of human-driven landscapes (agriculture, cities...). However, the main tendency can hide spatial or temporal variations. For example, between 1975 and 2000, the overall pattern in Africa was the expansion of agriculture areas, including the creation of large irrigated perimeters, although in Angola existing installations were

abandoned and converted to natural vegetation since the civil war did exclude the maintenance of any agricultural activity.

5.3.1.4 Intensity of the Change

The amplitude of LUCC can largely fluctuate from one region to another. Tropical humid deforestation is massive in some continents (Southeast Asia) and very limited in others (Central Africa). Even at the national scale, neighbour countries can have very different deforestation figures (FAO 2005). The urbanisation rates are also depending on socio-economic drivers that make some cities more attractive than others even at a local scale.

5.3.1.5 Spatial Distribution of the Change

LUCC is not a uniformly distributed phenomenon. Main LUCC processes are located in small areas at the middle of large ecosystems. Moreover, for the same intensity and direction, land-cover changes can be differently distributed in space. Principal deforestation spatial patterns include massive, diffuse, linear, insular shapes (Jeanjean & Achard 1997). In the same way, the increase of croplands either create a few big agricultural areas, or provoke the appearance of small fields in natural vegetation.

5.3.2 Methodological Issues

Some technical parameters of the measurements can be adjusted for optimising the LUCC measurements and taking into account the above-mentioned heterogeneity.

5.3.2.1 Spatial Resolution

The scale of the phenomenon largely indicates the appropriate spatial resolution of the data to be used. The transition from a forest to a non-forest is detectable at medium resolution (300–500 m, but accurately measurable at fine spatial resolution (30–50 m). At very high resolution, the changes measured by remote sensing correspond to small openings in the canopy that do not correspond to deforestation situations, in the same way that the electron microscope is appropriate for observing organelles, but not entire cells. Diffuse continuous changes, like the reduction of ecosystem productivity, is better analysed with broad satellite data that spatially integrate large areas subject to these changes.

5.3.2.2 Temporal Resolution

The LUC analysis must be conducted in a temporal window tailored to the temporal behaviour of the event. Ephemeral changes such as fires or floods, can only be detected with very frequent data, daily or better. Seasonal shifts from one year to the average need to analyse the whole profile of some biophysical parameters, reconstructed from time series of daily images along the season. Drastic changes (clear cut, urbanisation) do not happen in short times and are efficiently estimated only with long enough time intervals.

5.3.2.3 Statistical Design

As previously said, high spatial resolution data are required in order to guarantee the accuracy of measures in detailed land-cover changes. However, it is rarely feasible to complete a wall-to-wall assessment with such data for cost and efficiency reasons, and many studies will rely on statistical sampling similar to classical forest inventories, with an acceptable precision (Czaplewski 2002). In this case, the spatial pattern of the dynamic phenomenon must orient the statistical design to a certain sampling density and to a certain size of the units. Continuous diffuse events can be accurately measured with a few large sampling units (e.g. Landsat full scenes), while a large number of small sampling units will be considered for assessing clustered events with a high spatial auto-correlation.

5.3.2.4 Classification Techniques

Different classification/interpretation techniques are used in change detection, from the purely visual interpretation, the development of indices, the calculation of change vectors (Lambin et Strahler 1994), unclassified clustering and the object-oriented classification. Each method has its own advantages and limitations and should be evaluated in front of the specificities of each study. For a complete review of change detection techniques, see Coppin et al. (2004).

5.3.2.5 Validation

Compared to the land-cover validation, the LUC validation asks for including the time dimension in the accuracy assessment. Indeed, errors can affect the change process, with the classical omission/commission errors. But even an overall agreement on the change (or not change) can hide dramatic errors on the labelling of the class. The dimension of the matrix increases the complexity of the sampling strategy. For getting round this problem, the land-cover change maps can be simplified to binary features (e.g. forest/non forest) with eventually an intermediate class, as shown on Fig. 5.2.

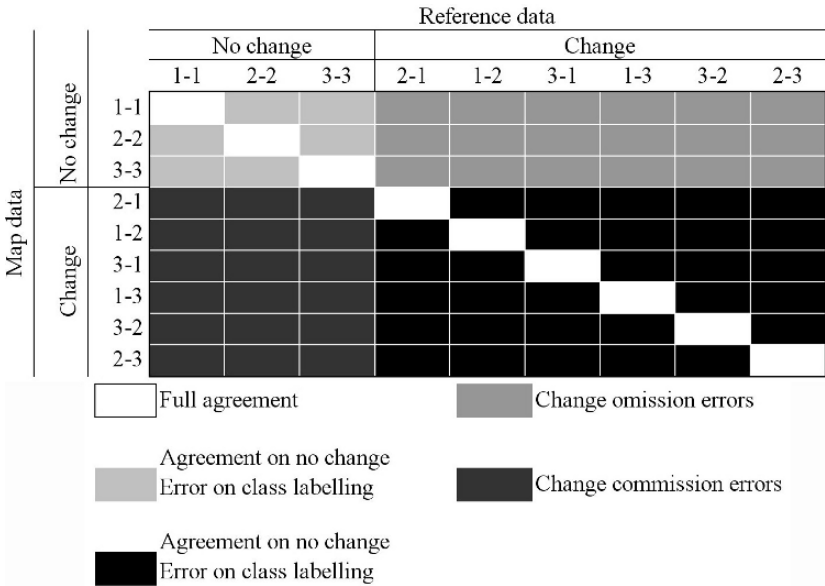


Fig. 5.2 Change detection confusion/error matrix for time 1 and time 2 maps each consisting of 3 land cover classes (adapted from Strahler et al., 2006)

5.3.3 Tropical Forests

Tropical deforestation is of prime interest since it threatens the terrestrial biomes with highest biodiversity rates. Local forest change dynamics, detected over very large extents, are necessary to derive regional and national figures for multilateral environmental agreements and sustainable forest management.

5.3.3.1 Global Level

While many developed countries have built up detailed national forest inventories, global scale assessments of tropical forest distribution and how it is changing have received attention from the scientific community only since the early 1990s, and current programmes still vary in terms of methods and results. Our understanding of the magnitude and the location of deforestation is imprecise due to the geographically concentrated pattern of the phenomenon, which reduces the efficiency of the sampling techniques.

We explore these issues using results from two recently completed programmes (FAO Forest Resources Assessment 2000 and JRC TREES II), both exploiting the global imaging capabilities of Earth observing satellites.

The Global Forest Resources Assessment (FRA, FAO 2001, 2005) is based primarily on available information provided by national authorities. Classifications and methodologies used in the forest inventories often differ from country to country, as

they are adapted to national objectives and to the local ecological context. Consequently, the Forest Resources Assessment programme has implemented, since FRA 1990, independent remote sensing surveys of forest cover changes to complement the national data. The main technical steps are: (i) two-stage stratified random sampling using the geographical region and the forest cover derived from vegetation maps, (ii) analysis by local teams using interdependent interpretation of multi-date Landsat scenes from three points in time (around 1980, 1990 and 2000), (iii) area estimates based on dot-grid counting applied to the visual interpretations with a grid-size of 2 km (iv) estimates of state and change at the regional, ecological and pan-tropical levels.

The primary objectives of the TREES II (Achard et al. 2002, Mayaux et al. 2005) were to use a new remote sensing-based approach to produce relevant information, more accurate than that currently available, on the state of humid tropical forest ecosystems, and to analyse this information in terms of deforestation and forest degradation trends. This involved six main technical steps: (i) the wall-to-wall mapping of tropical forests at coarse resolution, (ii) the identification of “deforestation hot spot areas” using knowledge from regional experts, (iii) the implementation of a stratified systematic sampling scheme with 100 sample sites covering 6.5% of the humid tropical domain, (iv) the assessment of change at each site, based on multi-date Landsat (around 1990 and 1997) interpreted by local partners using a common approach, (v) the statistical estimation of forest and land cover transitions at continental level.

We summarize the main technical parameters of the two projects in Table 5.1.

The results from these independent studies show a high degree of conformity and provide a good understanding of trends at the pan-tropical level. The continental FRA 2000 statistics aggregate all the tropical forest types (rain forest, moist deciduous forest and dry forest), while the deforestation figures by forest type are only

Table 5.1 Technical specifications of the FAO FRA-2000 and JRC TREES-II sampling and interpretation strategies

	FRA 2000 (RS)	TREES II
Domain	Dry and humid tropics	Humid tropics
Dates	1980, 1990, 2000	1992, 1997
Sampling strategy	two-stage stratified random sampling based on regions and forest cover	three-stage stratified random sampling based on regions, deforestation hot spots and forest cover
Sampling frame n / N	Landsat reference system 117 / 1203	Hexagonal tessellation (equal-area) 104 / 740
Imagery	Landsat full scenes	Landsat (full and quarter scenes according to the landscape complexity)
Interpretation	Visual interdependent interpretation	Visual interdependent interpretation
Legend	2 levels: 9 fixed classes + 12 options	Hierarchical scheme (life form, cover, water regime...)
Digital files	Grid 2 × 2 km	Full interpretation
Aggregation	stratum, continent, global	continent, global

available at the global scale. This precludes any direct comparison with the TREES results at the continental level, since TREES covers only the humid tropics. At pan-tropical scale, the annual deforestation area for the humid tropics is estimated by the two studies at 4.9 and 5.7 million ha respectively, an area approximately twice the size of Belgium. A further 2.3 million ha per year of humid forests are detected as degraded by fragmentation, logging, or fires. In the sub humid and dry tropics, annual deforestation for the tropical moist deciduous and the tropical dry forests comes to 2.2 and 0.7 million ha respectively.

The three continents reveal considerable differences in change rates measured by the FRA and TREES projects. In relative terms, Southeast Asia has the highest annual rate of deforestation while Africa is losing its forests at about half this rate. Latin America shows the lowest relative deforestation rate but at 2.5×10^6 ha yr⁻¹; in absolute terms this is almost the same as that estimated for Southeast Asia. Forest degradation shows a similar overall pattern. It is most prominent in Southeast Asia, intermediate in Africa, and lowest in Latin America. It is worth mentioning that these estimates represent only those elements of degradation which can be identified from satellite imagery, and do not include processes such as selective removal of trees. Reforestation is most evident in Southeast Asia, where it arises mainly from the transition of former mosaics and woodland to forest. It is less widespread in Latin America and is limited in Africa.

The FRA 2010 will take lessons from the previous exercises and will be operated in coordination with JRC, NASA and local partners. The survey will be extended to all lands (not just the pan-tropical zone), and will be based on a much higher number of smaller samples (about 10,000), covering 1% of total land area, sampled systematically. A 10 km × 10 km sample will be located at each intersection of the one-degree lines of latitude and longitude that overlies land. These dimensions were chosen to allow spatially explicit monitoring at a scale relevant to land management. Time series of high or very-high resolution remote-sensing data will be attached to

Table 5.2 Humid tropical forest cover estimates for the TREES-II project, the FRA-2000 programme and the AVHRR time series analysis

	Latin America (10 ⁶ ha)	Africa (10 ⁶ ha)	Southeast Asia (10 ⁶ ha)	Global (10 ⁶ ha)
TREES (1990–1997)				
Forest cover in 1997	653	193	270	1,116
Net annual deforested area	2.2 ± 1.2	0.7 ± 0.3	2.0 ± 0.8	4.9 ± 1.3
Annual regrowth area	0.28 ± 0.22	0.14 ± 0.11	0.53 ± 0.25	1.0 ± 0.32
Annual degraded area	0.83 ± 0.67	0.39 ± 0.19	1.1 ± 0.44	2.3 ± 0.71
Mean deforestation rate	0.33%	0.36%	0.71%	0.43%
FRA 2000 Remote Sensing Survey ² (1990–2000)				
Forest cover in 2000 ¹	780	519	272	1571
Net annual deforested area	4.2 ± 1.1	2.1 ± 0.4	2.3 ± 0.6	8.6 ± 1.3
Mean deforestation rate	0.51%	0.34%	0.79%	0.52%

Note 1: The estimates refer to the f3 definition in the FRA RS. The forest f3 include the following classes: closed forest, open forest, long fallow and one third of the fragmented forest.

Note 2: Only the national statistics of the countries covering the TREES domain were included in the current table.

each sampling location through a quality-controlled, standardized and decentralized process. This approach should deliver regionally accurate estimates of forest cover change, as well as national estimates for those countries where sampling intensity is sufficient.

5.3.3.2 A Regional Case: The Congo Basin

Current deforestation estimates in Central Africa were derived either from coarse to medium resolution imagery or from wall-to-wall coverage of limited area. Whereas the first approach cannot grasp small forest changes widely spread across a landscape, the operational costs limit the mapping extent in the second approach. This research developed and implemented a new cost-effective approach to derive area estimates of land cover change by combining a systematic regional sampling scheme based on high spatial resolution imagery with object-based unsupervised classification techniques (Duveiller et al. 2007). This is the first attempt to use the new sampling design developed by FAO for FRA 2010 over large areas.

Forest cover change measurements were accounting for the spatial characteristics of change processes in Central Africa:

- Zones of deforestation are relatively small, and their measurement requires data at an appropriately fine spatial scale.
- Forest massifs are extensive but deforestation is not uniformly distributed in time and in space. Change is a distinctly non-random process.
- Large regions, mainly in coastal zones, are under quasi-permanent cloud cover.
- The measurement time scale needs to be adapted to the forest cover change processes and to their spatial distribution.

Methods

The survey of the Central African tropical forest consists of 571 sample sites of 10×10 km separated by 0.5° intervals and regularly distributed over the forest domain in the Congo River basin. This represents a sampling density of 3.3%. A Landsat TM image extract and a Landsat ETM+ image extract, acquired respectively in the years 1990 (± 2 years) and 2000 (± 2 years), are available at every sample site.

The 571 image pairs were screened by a first visual inspection whose main objective is to identify the sample sites where change has occurred between the two dates and eliminate sites with poor radiometric quality or large cloud coverage. Out of the initial 571 sample sites of the survey, 390 image pairs were fully processed. The visual screening identified 165 sites where forest cover changes occur between 1990 and 2000.

The processing chain can be decomposed into three steps. First, multi-date objects segmentation is obtained for every pair of extracts. In this step, groups of adjacent pixels that show a similar land cover change trajectories between the 2 dates are delineated into objects. In a second step, the objects of every single-date extract are

classified by unsupervised procedures. Finally, visual interpretation is conducted to label the classes and edit possible classification errors. The time required to interpret each extract is significantly reduced since a whole group of objects, considered as similar by the automatic classification, is treated simultaneously. Ten land cover classes are used from dense forest, degraded forest, long fallow & secondary forest, forest-agriculture mosaic, agriculture & short fallow, bare soil & urban area, non forest vegetation, forest-savannah mosaic, water bodies and no data. A validation was conducted based on an independent interpretation of 20% of the population.

Results

The annual gross deforestation rate for Central Africa’s tropical forest is estimated at 0.21% per year. The spatial distribution of this process (Fig. 5.3) as shown by this study reflects, with more detail, the deforestation hot spots identified in 1998 by the TREES project (Achard et al. 1998). Deforestation is clearly accentuated along the Congo River, especially in the region between the river and the northern frontier of the forest. Deforestation generally seems to be more important on the periphery of forest.

A first remark concerning the survey is that over 30% of the initial sample units had to be discarded because they were not usable. Important cloud coverage on either extract is the main cause for this problem. A high proportion of unusable sample

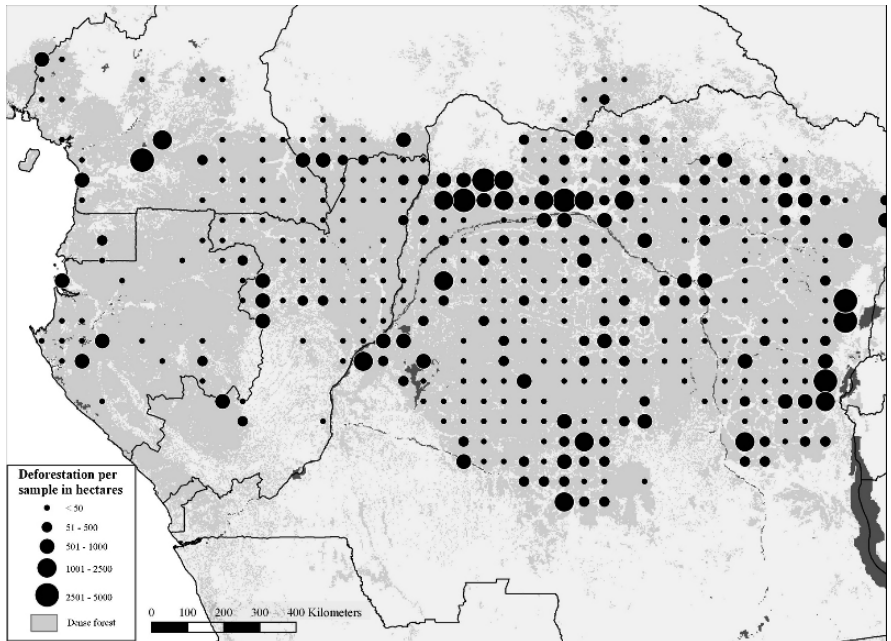


Fig. 5.3 Spatial distribution of deforestation in the Congo Basin. The circle size is proportional to the forest lost in the sampling unit (total area = 10,000 ha)

Table 5.3 Basin wide and national figures for annual deforestation and degradation rates between 1990 and 2000. The confidence interval and the number (n) of processed samples are mentioned for every country

Country	Samples	Gross deforestation	Gross reforestation	Net deforestation	Net Degradation
Cameroon	32	0.20% ± 0.26%	0.06% ± 0.06%	0.14%	0.02%
Congo-Brazzaville	54	0.07% ± 0.04%	0.05% ± 0.06%	0.02%	0.01%-
Gabon	21	0.12% ± 0.11%	0.03% ± 0.03%	0.09%	0.07%
Eq. Guinea	2	0.31% ± 0.41%	0.69% ± 0.91%	–	–0.47%
C.A. Republic	14	0.12% ± 0.10%	0.06% ± 0.08%	0.06%	0.02%
D.R.Congo	267	0.25% ± 0.06%	0.05% ± 0.01%	0.20%	0.12%
Central Africa	390	0.21% ± 0.05%	0.05% ± 0.01%	0.16%	0.09%

sites are found on coastal countries (Gabon, Equatorial Guinea and Cameroon) which render their nation-wise estimates less reliable. Equatorial Guinea is a drastic example where national figures are based on a single site which happened to undergo more reforestation than deforestation. The national figures can only be considered as robust for Congo, Central African Republic and Democratic Republic of Congo where the processed samples are well distributed over the forest domain (Table 5.3).

5.3.4 Croplands

The continuous population growth provokes an augmentation of food demand that is largely leading to agricultural expansion to the detriment of natural ecosystems.

5.3.4.1 Agricultural Expansion in Africa: Estimates at Continental Scale

The African continent is characterized by a vast variety of landscapes which include many biologically rich and unique eco-regions, such as the tropical forests, montane forests, savannah and grasslands and coral reef fringed islands. But in the last 25 years Africa's land cover has experienced unprecedented rates of changes. The historical abundances of natural resources, has been subjected to a series of major disturbances, both "natural" and man-made; drought, civil disturbances, large population increases and the impacts of "globalization." Each of these has had implications for land-use requirements, with subsequent impacts on natural vegetation cover, biodiversity, socio-economic stability and food security. The modification of the vegetation cover, with a predominant clearing of natural vegetation, may have a long-term impact on sustainable food production, freshwater- and forest resources, the climate and last but not least human welfare (Foley *et al.* 2005).

The following study aimed at assessing main land cover changes in sub-Saharan Africa over the 1975 to 2000 period by using the capabilities of Earth observing satellites.

Methods

The analysis is based on the mapping capacity of high spatial resolution Earth observing satellites which have been operating since the early 1970s. While these types of data are appropriate for the mapping task they have a restricted coverage both in time and in space. To cover the full sub-Saharan region a huge number of scenes would be required, with important cost implications, both in image acquisition and processing. A standard technique adopted in land cover inventories, is therefore to use a sampling strategy across the target area. Based on the White/UNESCO vegetation map of Africa, which aggregates similar land cover types in so called “eco-regions,” a stratified random sample of 57 study sites was selected from a hexagonal based grid across sub-Saharan Africa (Fig. 5.4). For each of these sites, remotely sensed satellite images from 1975 and 2000 were acquired. The historical satellite images came from Landsat Multi-Spectral Scanner (MSS), with a spatial resolution of 80 m and the recent satellite images from the Landsat TM and ETM, which have a finer spatial definition of 30 m. Furthermore, in order to improve the variance of the estimates and to reduce errors which occur in full scene classification, in each of the 57 sites nine sub-scenes of 20 by 20 km were extracted and used to assess the land cover. Finally, 511 sub-scenes we analyzed covering about 1% of sub-Saharan Africa (Brink et al. 2007).

The sub-scenes were independently classified using an unsupervised classification algorithm and then visually interpreted into four main land cover classes (forests, non-forest vegetation, agriculture and barren) along with water and “no data” (clouds/missing area). The *forest* class includes closed evergreen, semi-evergreen and dry deciduous forests with at least 40% of coverage. Deciduous open

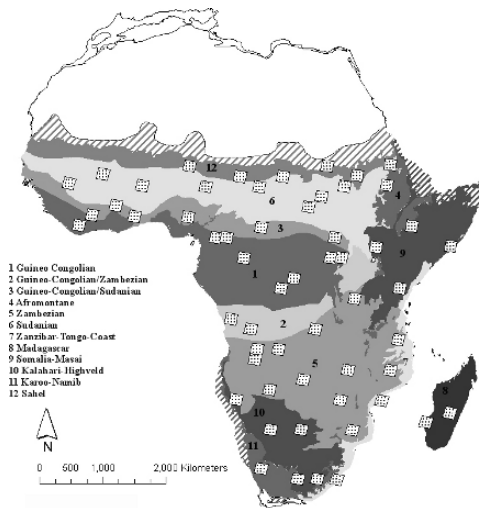


Fig. 5.4 Eco-region stratification and sample sites. Eco-regions as described in White’s (1983) Vegetation map of Africa. The striped areas represent the permanent deserts which were not included in the study

forests, shrub and grass savannahs and shrub lands are in the *non-forest vegetation* class. The *agriculture* class relates to the agricultural domain including irrigated and rain-fed croplands, smallholdings and plantations. In certain circumstances, man-made pastures will be classified under this heading, which occurs predominantly in the Sahel and Sudanian regions, where arid shrub lands have been cleared for grazing. Natural pastures (in fact a land-use term) will be classified under *non-forest vegetation*. The class *barren* includes very sparse grasslands (or pseudo-steppe), bare soil and rocks. While the class *water* was included in the interpretation it is not reported in the assessment as a special sampling scheme would be required to assess their current area extent.

For each sub-scene and each reference year the proportions of land cover were calculated for every class and the changes between the two dates assessed. The results were then extrapolated by direct expansion to the different strata and to the whole of sub-Saharan Africa.

Results

In the year 2000 sub-Saharan Africa was covered by slightly more than 17% of agriculture, almost 20% of forests, 60% of non-forest vegetation like wood- and shrub lands and savannas, over 2% of barren land, excluding the permanent deserts, and less than 1% of water (Eva et al. 2006, Mayaux et al. 2004) (Table 5.4). Extrapolating these total figures over White's (1983) vegetation map of Africa shows the Sudanian region to contain the most agriculture (29%), the Zambezian region the highest proportion of non-forest vegetation (25%), and the majority of the forests within the Guineo-Congolian region (66%). On the other hand the variations in land cover within region reveals that six of the twelve regions have important proportions of agricultural domains (*i.e.* > 20%) the Afromontane region (32%), the Zanzibar-Tongo Coastal region (30%) the Sahel (29%) the Sudanian (26%) Madagascar (24%) and Guinea-Congolia/Zambezia (23%). The Guineo-Congolian zone is dominated (82%) by the Congo basin forest while in the other regions, non-forest natural vegetation dominates (Eva et al. 2006).

Looking back in time and analysing the dynamics from 1975 to 2000 shows that sub-Sahara's land cover has undergone major changes. The most impressive change over the 25 year period has been an increase of 57% in agricultural areas over the whole sub-Saharan Africa. The area covered by agriculture increased from 215 10⁶ ha in 1975 to 338 10⁶ ha in 2000, which gives an annual rate of 2.3% (Table 5.5). At the same time forest and non-forest natural vegetation have decreased by 16% and 5% respectively, which equals 5.2 10⁶ ha (52,000 km²) of natural vegetation lost per year. In total this means that sub-Saharan Africa has lost some 130 10⁶ ha of natural vegetation (forests and non-forests) over the last 25 years. Evaluating these results on the eco-region level shows that the agricultural expansion at the expense of natural vegetation is a general trend in most eco-regions. Only in the Guinea-Congolian/Zambebian region, and more specifically in Angola, some agricultural land abandonment was observed, probably due to civil disturbance. The major changes occur in the Sudanian region, which accounts for over one quarter

Table 5.4 Sub-Saharan land cover for the year 2000 disaggregated by eco-regions (water not reported but is included in the total)

	Agriculture	Forest	Non Forest vegetation	Barren	Total
	(000 ha)	(000 ha)	(000 ha)	(000 ha)	(000 ha)
GUINEO- CONGOLIAN	36,973	243,293	14,221	45	295,489
GUINEA- CONGOLIA/ZAMBEZIA	987	17,638	60,687	–	79,454
GUINEA- CONGOLIA/SUDANIA	28,932	26,354	65,151	49	124,899
AFROMONTANE	26,751	865	54,156	488	82,403
ZAMBEZIAN	49,734	43,691	300,391	3,110	399,787
SUDANIAN	97,823	18,523	251,138	2,601	370,956
ZANZIBAR-TONGO- COAST	16,254	2,387	34,454	–	53,337
MADAGASCAR	14,610	8,752	34,244	1,975	60,325
SOMALIA-MASAI	18,666	5,138	125,213	26,432	175,626
KAROO-NAMIB	280	–	37,263	11,805	49,425
KALAHARI- HIGHVELD	7,938	–	119,489	2,435	130,131
SAHEL	39,599	800	92,188	516	134,393
TOTAL	338,548	367,441	1,188,594	49,456	1,956,226
PERCENT	17.3	18.8	60.8	2.5	100.0
GLC 2000	330,300	363,800	1,211,000	48,300	
DIFFERENCE FROM GLC 2000	2.5	1.0	–1.9	2.4	

(26%) of the total increase in agriculture land, and as a consequence has the largest proportion loss of natural vegetation (36% of the total). Other regions with major losses in natural non-forest vegetation are the Somalia-Masai (19%) and Sahel (29%) eco-regions. The forest domain has the highest proportional losses of land cover. Despite the Guineo-Congolian region which has the highest proportion of forests, but also the least changes on forest cover, all other regions have lost between 20% and over 60% of their forests. The data on changes in “barren” areas only relate to the non-arid zones since permanent deserts were excluded from the study. Nevertheless, significant increases in barren areas are seen in the Sudanian (70,000 ha),

Table 5.5 Land cover changes in Sub-Saharan Africa between 1975 and 2000

	Agriculture	Forest	NF veg.	Barren
	(000 ha)	(000 ha)	(000 ha)	(000 ha)
Land cover 1975	215,274	438,917	1,247,980	42,912
Land cover 2000	338,687	367,592	1,189,085	49,477
Total change	123,413	–71,325	–58,894	6,565
Total (%) change	57	–16	–5	15
Average annual change	4,937	–2,853	–2,356	263
Average annual (%) change	2.3	–0.7	–0.2	0.6

Karoo-Namib (25,000 ha), and Somalia-Masai (154,000 ha) regions, which account for over 80% of the changes (Eva et al. 2006).

5.3.4.2 A National Case: Land-Cover Changes in Senegal

This section illustrates a good example at the national level. All results come from a remarkable study by Tappan et al. (2004). Like many countries in sub-Saharan Africa, Senegal is experiencing significant changes at many levels—climatic, environmental, agricultural, demographic, political, and socio-economic. The decline in rainfall during the last 200 years in the West Africa Sahel has been the most substantial and sustained in the world, and only during the 20th century Senegal experienced four main droughts. The population has increased tenfold since 1900, but agriculture production has grown only moderately in the last decades. The combination of these coupled environment and human factors has led to unprecedented pressure on Senegal's limited land resources.

The objective of the study (Tappan et al. 2004) was to estimate land use and land cover changes over Senegal using readily available time-series satellite imagery covering three periods in time (1965, 1985, and 2000), and practical sampling and change analysis techniques.

Methodology

To assess the land use and land cover changes in Senegal three types of images with three different dates were selected: Corona satellite photographs from 1965 (2 m spatial resolution), Landsat (TM) images from 1984 and 1985, and Landsat ETM+ images from 1999 and 2000. In addition to the satellite images extensive fieldwork during early 1980s and mid-to-late 1990s were carried out. The sampling strategy was based on a random sample of 10 km by 10 km samples stratified by eco-region. The eco-regions were defined through the integration of various components of the natural and socio-economic landscapes. 13 eco-regions were defined covering the whole of Senegal. A total of 93 samples were analysed, resulting to 4.6 percent of the total land area.

The image analysis was based on visual interpretation. After delineation and classification, the area of each class was measured by randomly placing a fine dot grid over the sample. Dot counts were summed for each class, converted to a percentage of the sample area and summarized by eco-region and by period.

Results

The results of the 35 years time series analysis show moderate change in the land use and land cover when aggregated at country level. Agricultural expansion has been the main source of change, increasing from 17% in 1965 to 19.8% in 1985 and 21.4% in 2000. The outcome show also that the rate of expansion slowed down

during the last period. Cropland expanded at a rate of $27,715 \text{ ha year}^{-1}$ from 1965 to 1985 and $20,573 \text{ ha year}^{-1}$ from 1985 to 2000. Agriculture is expanding at cost of Senegal's forests and savannas. In 35 years about half of the countries dense forest (canopy cover $>80\%$) has been lost, decreasing from 4.4% to 2.6%. More moderate changes occurred in the savanna class which declined from 73.7 to 69.6% during the analyzed time frame. Concerning increases are seen in Senegal's bare and degraded soils which grew from 0.7 to 1.7%. The expansion of a "badland" type landscape has become quite apparent in several eco-regions.

Although statistically significant, these figures are different when compared to FAO figures (FAO 2001). Tappan et al. estimated an annual deforestation rate of $333 \text{ km}^2 \text{ year}^{-1}$ compared to a higher rate of $520 \text{ km}^2 \text{ year}^{-1}$ assessed by FAO. Also Stephenne and Lambin (2001), who applied a dynamic simulation model to assess land cover changes over nearly the same time period, obtained much higher change rates compared to Tappan's et al. study.

At eco-region level some areas are undergoing major transformations, while others remain fairly stable. Generally, the agriculture regions are located in the western part of the country whereas vast pasture areas are situated towards the dryer eastern part of Senegal. The "Peanut Basin," or "West central agricultural eco-region" (Fig 5.5), has been the most fundamentally altered by centuries of human activity, experiencing a nearly complete transformation of its landscapes. Today, continuous cultivation under scattered trees has replaced all remaining of the natural vegetation. Similar patterns and pressure on the natural vegetation were observed in the other western eco-regions like the "Saloum agricultural region," the "Casamance" and the "agriculture expansion region" (Fig. 5.5). The traditional sylvo-pastoral regions in the eastern part of Senegal show a strong trend of rain-fed agriculture encroachment in the "northern and southern sandy pastoral eco-regions" and in the "eastern transition region" whereas the unfertile "ferruginous pastoral eco-region" is affected by severe land degradation processes due to overstocking and overgrazing.

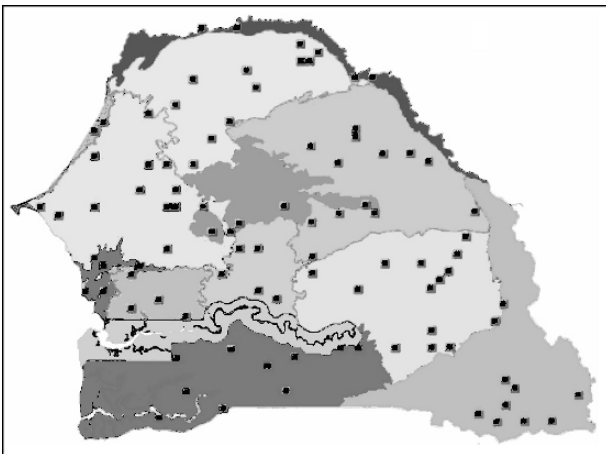


Fig. 5.5 Eco-regions of Senegal and the sampling frame (adapted from Tappan et al. 2004)

Furthermore, the typical wood and shrub savannah of these areas has been heavily degraded due to charcoal production. The “shield eco-region” in the far East of the country is located at great distance from Senegal’s population centres and has very limited agricultural potential. Furthermore, a large part of this region falls under the protection of the Niokolo-Koba National Park. Consequently, the results from the land use and land cover trends analysis show a relatively stable situation with very little pressure on the natural vegetation.

The availability of a 35 years high resolution satellite images time series allowed monitoring and quantifying long-term changes in Senegal’s natural resources. Results aggregated at national level showed moderate changes, with a modest decrease in savannas and expansion of croplands. However, at eco-region level, some areas were experiencing rapid changes, whereas in other relative stability were observed.

5.4 Conclusions and Perspectives

New imaging capacities and new processing technologies are continuously improving the understanding and characterisation of our Earth surface. Higher frequency of data acquisition, combined with a finer spatial resolution gives access to the scientific community to data archives never compiled before. On the other hand processing technologies, like object-oriented methods, drastically improve our capacity of extracting reliable and sound information on the physical parameters of the Earth surface. However, the ground validation of remotely-sensed information is often insufficient to produce accurate and well-accepted figures. Although it can be observed globally from space, land cover change occurs at a very local scale and requires good ecological and socio-economic knowledge to correctly interpret the reflectance registered by the satellite.

The land-use change is more problematic, especially in natural ecosystems that could be multi usages. The inclusion of socio-economic parameters in the analysis can help to derive general patterns, but a local knowledge is once again needed for providing information relevant for decision-makers. The involvement of local partners from the conception to the validation of long-term monitoring systems is essential. It augments the reliability of the interpretations, ensures relevance to the local context, provides important elements of capacity-building, and crucially, also leads to greater acceptance of the final estimates by local communities.

With remote sensing technology, one can produce independent and up to date estimates of both land cover and cover change. However, national, international and academic institutions have had difficulties delivering accurate information in a way that is useful and relevant for policy formulation, implementation and follow-up. One prominent reason has been the inability of the agencies concerned to establish a commonly accepted, independent, cost-effective and long-term mechanism to deliver remote sensing data to users. Such a framework is still needed. International organisations like GEO (Group on Earth Observations), GTOS (Global Terrestrial Observing System), GOFC-GOLD (Global Observation of Forest Cover – Global Observation of Land-cover Dynamics) or the European GMES (Global Monitoring

of Environment and Security) must play a major role in the coordination of individual initiatives for setting up real long-term monitoring systems at a moment where the planet suffers from drastic changes. This is an extraordinary challenge, but the scientific community is ready to accept it.

References

- Achard F., Eva H., Glinni A., Mayaux P., Richards T., & Stibig H.J., (1998). *Identification of deforestation hot spot areas in the humid tropics*, TREES Publications Series B, N°4, European Commission, Luxembourg, EUR 18079, 102.
- Achard, F., Eva, H., Stibig, H. J., Mayaux, P., Gallego, J., Richards, T., & Malingreau, J. P., (2002). Determination of deforestation rates of the world's humid tropical forests, *Science* 297, 999–1002.
- Arino O., Leroy, M. F., Ranera, D. Gross, P. Bicheron, F., & Niño, C. et al. (2007). GLOBCOVER: A Global Land Cover Service, ENVISAT Symposium, Montreux Switzerland 23–27 April 2007.
- Bartalev, S., Belward, A. S., Ershov, D., & Isaev, A. S. (2003). A New SPOT4-VEGETATION Derived Land Cover Map of Northern Eurasia. Intern. *Journal of Remote Sensing*, 24, 1977–1982.
- Bartholomé, E., & Belward, A. S. (2005 May). GLC2000: A new approach to global land cover mapping from earth observation data. *International Journal of Remote Sensing*, 26(9), 1959–1977.
- Belward, A. S., Estes, J. E., & Kline, K. D. (1999). The IGBP-DIS global 1 km land cover data set DISCover: A project overview. *Photogrammetric Engineering and Remote Sensing*, 65, 1013–1020.
- Boulvert, Y. (1986). Carte phytogéographique de la République Centrafricaine à 1:1,000,000, Notice Explicative No104, Editions de l'ORSTOM, Paris.
- Brink, A., & Eva, H. D. (2007). Monitoring 25 years of land cover change dynamics in Africa: A sample based remote sensing approach. *Journal of Land Use Science – in preparation*.
- Coppin, P., Jonckheere, I., Nackaerts, K., Muys, B., & Lambin, E. (2004). Digital change detection methods in ecosystem monitoring: A review. *Int. J. Remote Sens.* 25(9), 1565–1596.
- Czaplewski, R. L., (2002). Can a sample of Landsat sensor scenes reliably estimate the global extent of tropical deforestation? *Int. J. Remote Sensing*, 24, 1409–1412, 2003.
- D'Souza, G., Malingreau, J. P., & Eva, H. D. (1995). Tropical forest cover of South and Central America as derived from analyses of NOAA-AVHRR data. TREES Publications Series B3, EUR 16274 EN, Luxembourg, European Commission, 52 p.
- Di Gregorio, A., & Jansen, L. (2000). *Land cover classification system, classification concepts and user manual*, Food and Agriculture Organisation of the United Nations:Rome.
- Duveiller, G., Defourny, P., Desclée, B., & Mayaux, P., (2007). Deforestation in Central Africa: Estimates at regional, national and landscape levels by advanced processing of systematically-distributed Landsat extracts, Remote Sensing of Environment, in press.
- Eva, H. D., Belward, A. S., De Miranda, E. E., Di Bella, C. M., Gond, V., & Huber, O. S. et al. (2004). A land cover map of South America. *Global Change Biology*, 10, 1–14.
- Eva, H. D., Brink, A., & Simonetti, D. (2006). Monitoring Land Cover Dynamics in sub-Saharan Africa. /EUR 22498. Office for Official Publications of the European Communities, Luxembourg.
- FAO, (2001). Global Forest Resources Assessment 2000 Main report, FAO Forestry paper 140, 479 pp., Food and Agriculture Organization of the UN, Rome.
- Foley, J. A., Defries, R., Asner, G. P., et al. (2005). Global consequences of land use changes. *Science*, 309, 570–574
- Friedl, M. A., McIver, D. K. Hodges, J. C. F., Zhang, X. Y., Muchoney, D., & Strahler, A. H. et al. (2002). Global land cover mapping from MODIS: Algorithms and early results. *Remote Sensing of Environment*, 83(1–2), 287–302.

- Fuller, R. M., Smith, G. M., Sanderson, J. M., Hill, R. A., & Thomson A. G. (2002). The UK Land Cover Map 2000: Construction of a parcel-based vector map from satellite images. *Cartographic Journal*, 39, 15–25.
- GCOS, (2003). The second report on the adequacy of the global observing systems for climate in support of the UNFCCC, April 2003, GCOS-82, WMO Technical Document 1143 (WMO; Geneva), 74 pp.
- GCOS, (2006). Systematic observation requirements for satellite-based products for climate; Supplemental details to the satellite-based component of the "Implementation Plan for the Global Observing System for Climate in Support of the UNFCCC (GCOS-92)," WMO/TD No.1338, (WMO Geneva), 103 pp.
- Hansen, M., DeFries, R., Townshend, J.R.G., Dimiceli, C., Carroll, M., & Sohlberg, R. (2003 September). Global percent tree cover at a spatial resolution of 500 meters: First results of the MODIS Vegetation continuous fields algorithm, *Earth Interactions*, 7, 1–15.
- Jeanjean H., & Achard, F. (1997). A new approach for tropical forest area monitoring using multiple resolution data. *Int. J. Remote Sensing*, 18, 2455–2461.
- Lambin E. F., & Strahler A., (1994). Multitemporal change-vector analysis: A tool to detect and categorise land-cover change processes using high temporal resolution satellite data. *Remote Sensing of Environment*, 48, 231–244.
- Loveland, T. R., & Belward, A. S. (1998). The International Geosphere Biosphere Programme Data and Information System Global Land Cover Data Set (DISCover): *Acta Astronautica*, 41(4–10), 681–689.
- Loveland, T. R., Zhu, Z., Ohlen, D. O., Brown, J. F., Reed, B. C., & Yang, L., (1999). An analysis of the IGBP Global Land-Cover Characterization Process. *Photogrammetric Engineering and Remote Sensing*, 65, 1021–1032.
- Mayaux P., Bartholomé, E., Fritz, S. & Belward, A. (2004). A new land-cover map of Africa for the year 2000, *Journal of Biogeography*, 31, 1–17.
- Mayaux, P., Holmgren, P., Achard, F., Eva, H., Stibig, H-J., & Branthomme, A. (2005). Tropical forest cover change in the 1990s and options for future monitoring. *Philosophical Transactions of the Royal Society B.*, 360, 373–384.
- Mayaux, P., Strahler, A., Eva, H., Herold, M., Shefali, A., & Naumov, S. et al. (2006). Validation of the Global Land Cover 2000 Map IEEE-Transactions on Geoscience and Remote Sensing 44 (7), 1728–1739, doi 10.1109/TGRS.2006.864370.
- Roy, P. S., & Joshi, P. K., (2002). Forest cover assessment in north-east India – The potential of temporal wide swath satellite sensor data (IRS-1C WiFS). *Int. Journ. of Remote Sensing* 23(22), 4881–4896.
- Running, S. W., Loveland, T. R., & Pierce, L. L., (1994). A vegetation classification logic based on remote sensing for use in global scale biogeochemical models, *Ambio*, 23, 77–81.
- Sellers, P. J., Dickinson, R. E., Randall, D. A., Betts, A. K., Hall, F. G., & Berry, J. A. et al. (1997). Modelling the exchanges of energy, water, and carbon between continents and the atmosphere. *Science*, 275, 502–509.
- Stephene, N., & Lambin, E. (2001). Backward land-cover change projections for the Sudano-Sahelian countries of Africa with a dynamic simulation model of land-use change (SALU). In: Matsuno, T., & Kida, H. (Eds.), Present and future of modeling global environmental change: Toward integrated modeling (pp. 255–270). Terrapub, Tokyo.
- Stibig, H-J., Belward, A. S., Roy, P. S., Rosalina-Wasrin, U., Agrawal, S., & Joshi, P. K. et al. (2007). A land cover map for South and Southeast Asia derived from SPOT-4 VEGETATION data, *Journal of Biogeography* 34, 625–637.
- Strahler, A. S., Boschetti, L., Foody, G. M., Friedl, M. A., Hansen, M. C., & Herold, M., et al. (2006). Global land cover validation: Recommendations for evaluation and accuracy assessment of global land cover maps, *Luxembourg: Office for Official Publication of the European Communities, EUR 22156 EN*, 2006, 48 p.
- Tappan, G., Sall, M., Wood, E., & Cushing, M., (2004 March 23). Ecoregions and land-cover trends in Senegal. *Journal of Arid Environments* 59(3), 427–462.
- White, F (1983). *The vegetation of Africa: A Descriptive Memoir to accompany the UNESCO/AEFTAT/UNSO Vegetation Map of Africa*. Paris, UNESCO.

Chapter 6

Satellite Observation of Biomass Burning

Implications in Global Change Research

Emilio Chuvieco

Abstract Biomass burning, which involves wildland fires as well as agricultural and grassland burnings, plays a critical role in the environmental equilibrium of our planet, since it is a major driving force in land cover transformations and contributes significantly to greenhouse gas emissions. Several satellite missions provide critical information required to better understand the temporal and spatial distribution of biomass burning. Satellite images provide objective and comprehensive information on global patterns of fire occurrence, as well as data on factors affecting fire ignition and propagation. Recent improvements in spatial, temporal, and spectral resolution of satellite remote sensing systems reduce past uncertainties – systems can now be used to obtain a more precise evaluation of burned areas and post-fire effects on soils and plants. Greater efforts are required to operationally use Earth Observation data in fire prevention and early warning. Longer time series data are required to acquire a better understanding of fire regimes, and their mutual relationships with global warming.

6.1 The Role of Fire in Global Change Analysis

Fire is a natural process driving landscape transformation for many terrestrial ecosystems, which are adapted in one way or another to recurrent burning. Fire has positive and negative effects on soil, water, vegetation and the atmosphere, the review of which are outside the scope of this text. Figure 6.1 presents a general scheme on which aspects of biomass burning might be considered at global-scale, by identifying the uses of fire by human beings, the effects of fire on environment and society, and the main factors driving global fire activity.

Fire results in the transformation of dead or senescent vegetation into its mineral components, providing a short-term pulse of key nutrients that facilitate vegetation regrowth. Intentional setting of fire is a common practice in savanna areas of Africa or South America, where millions of hectares are burned annually to remove unpalatable grasses and to promote the growth of fresh grass for grazing (Van Wilgen 1997). In forested areas, fire aids in stand thinning, the clearing of understory vegetation, and promotes vertical stratification of the forest canopy. As a result of these

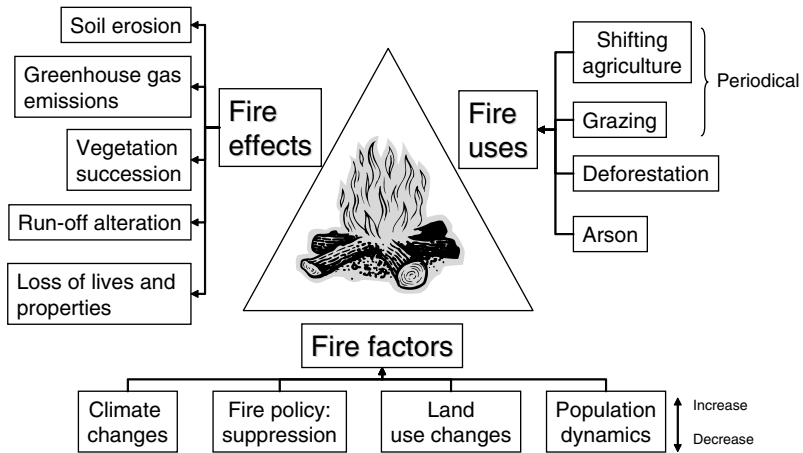


Fig. 6.1 Framework for analysis of biomass burning at global scale

positive feedbacks, natural fire regimes provide a common framework for species succession (Johnson and Miyanishi 2001; Omi 2005).

However, fire has also been used historically as a clearing tool for land use transformation, removing trees from forested areas for agricultural or grazing purposes. These transformations may be perennial or cyclical, depending on the type of agricultural practice in place. For most tropical countries, shifting cultivation has been the traditional form of farming (Spencer 1966). This regime is based on using fire to remove forest cover while fertilizing the land by providing N and other nutrients to mineral soils. After a few years, yields are reduced as a result of intense rainfall that results in leaching of nutrients from soils and soil erosion. As a result, farmers need to move to another forested area to start a new cycle, and from there on to another one, until they return to the original location in 30 to 40 years. In recent decades, these cycles have been shortened, as a result of a more intense land use, and therefore the crop production is increasingly degraded. Reduced agricultural yields, in turns, increases poverty and migration to urban regions.

The use of fire for permanent land cover change has been historically associated with movements of the agricultural frontier, as it was evident in the temperate forest of North America during the eighteenth and nineteenth centuries (Pyne 1995). Currently, the conversion of forested to agricultural or grazing areas is mainly occurring in tropical forests. Deforestation is one of the main factors to take into account in global carbon budgets, since they affect large areas (Houghton et al. 1985), and accounts for a significant proportion of total greenhouse emissions: 26% for carbon dioxide, 48% for methane and 33% for nitrous oxide has been estimated from deforestation processes (Houghton 2005). The relation between fire and deforestation, both complete clearing and selective logging, has been well documented (Cochrane et al. 1999; Skole and Tucker 1993; Souza et al. 2005).

For industrialized societies, the opposite trend has been observed, since land abandonment has occurred over the past century, as a result of changes in economic

policy and immigration to cities. As a result, in many areas, patterns of traditional human-ignited fire activities have been altered and long-established practices in rural areas (grazing, energy consumption from wood, etc) have also been discarded. These changes have resulted in a larger accumulation of fuels, which increase fire intensity and severity compared to natural conditions, altering landscape structure that was historically shaped by less severe fires (Vega-Garcia and Chuvieco 2006).

The effects of global warming on natural fire regimes have recently been observed lately, especially in boreal regions, where fire seasons tend to last longer and may be more severe (Kasischke and Turetsky 2006).

In summary, increased intensity during burning associated with deforestation in tropical regions and during natural fires in temperate and boreal forests, and increased fire occurrence in boreal forest as a result of climate change all emphasize the importance of improving our understanding of global biomass burning.

In spite of the importance of and interest in biomass burning, a significant amount of information is still required to better understand the spatial-temporal patterns of fire occurrence. In most regions, fire statistics are scarce and mainly focus on commercial forest plantations, leaving aside wildland, savanna and agricultural fires. Only few countries have maintained consistent statistics on fire occurrence, and even fewer generate a cartographic inventory of fire-affected areas. Consequently, only general information about the spatial-temporal distribution of fire is available, which prevents a better understanding of fire regimes and their relationship to human activities and global climatic changes.

6.2 Contributions of Earth Observation Data

Satellite remote sensing is an especially suitable tool for fire monitoring and research. The wide area coverage and high observation frequency provided by satellite-borne sensors, the potential rapid access to acquired data, as well as their collection of data using near and thermal IR data, make their data a very valuable resource for fire detection and mapping and management fire-prone areas.

From the first airborne sensor campaigns of the late sixties (Hirsch et al. 1971) until now, a great range of remotely sensed systems have been used for mapping and analysis of wildland fires. During the 1980s and 1990s, the primary sensors used for fire monitoring were the Thematic Mapper (TM) on board Landsat-4 and 5, and the Advanced Very High Resolution Radiometer (AVHRR) on board the NOAA satellites. The most extensive use of satellite data in this context was the detection of active fires and the mapping of burned areas. The former was based mainly on multiband thresholds and contextual techniques, while the latter was addressed by several techniques: statistical classification, logistic and multiple regressions, neural networks, decision trees, post-fire and multitemporal thresholding, etc., both using high and low spatial resolution sensors. Good summaries of satellite detection and mapping of fires can be found in several textbooks, such as Ahern et al. (2001) and Chuvieco (1999; 2003).

In recent years, new sensors have been added for analyzing global biomass burning, the most important being the Moderate-Resolution Imaging Spectroradiometer (MODIS) sensor on board the Terra and Aqua platforms. Other sensors have been used to derive operational burned area products, such as the VEGETATION, on board the French SPOT-4 and 5 satellites, and the Along Track Scanning Radiometer (ATSR-1 and 2) on board the European ERS satellites and the Advanced ATSR (AATSR) on the Envisat. Higher resolution sensors have been used to generate fire products as well, including the high resolution (1 to 4 m; Ikonos or Quickbird) to medium-high resolution sensors (20–60 m, such as ASTER, IRS-AWIFS or SPOT-HRV).

During the last decade, the range of applications for fire monitoring and management has significantly increased, making satellite remote sensing the main input data source for generating critical information on biomass burning, especially for global applications. A review of current developments will follow, preceded by a presentation of the spectral and temporal requirements for the analysis of global fire activity.

6.3 Physical Basis for Satellite Observation of Biomass Burning

The use of remotely sensed data in fire applications can be grouped into three categories, depending on whether the need for improved information is the determination of fire danger conditions (pre-fire), the detection of hot-spots (active fires), or the analysis of fire effects (post-fire) (Chuvieco and Martín 1994; Jain et al. 2004). These three information needs have different spatial and temporal requirements depending on whether they are implemented by local, regional or national managers (Fig. 6.2). At local scale, the spatial resolution is most critical, while at national scale, frequent coverage is often the highest priority. For fire danger estimation, the main required for a regional manager is to detect changes in vegetation water content, one of the leading factors controlling fire ignition and propagation, while the local manager is mainly interested in fuel loads and horizontal and vertical

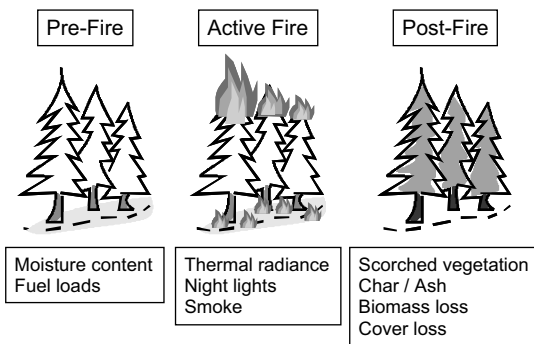


Fig. 6.2 Temporal stages in fire management and main physical variables that can be remotely observed

distribution of fire fuels. Active fire detection requires a high observation frequency (hourly), combined with a fine radiometric sensitivity to avoid false alarms. In contrast, post-fire assessment of burning impacts is not constrained by temporal resolution, since most burn severity evaluation can be carried out weeks or even months after the fire is over. In this case, the spectral and spatial resolution will be the main requirements.

The physical basis to remotely detect fire information varies according to the information required. When the requirement is to estimate fuel moisture content, the contrast between reflectance in the short-wave infrared (SWIR: 1–2.5 μm) and the near infrared (NIR: 0.7 to 1 μm) is most commonly used (Ceccato et al. 2001; Hunt et al. 1987; Sims and Gamon 2003)., although some authors have proposed the use of two narrow bands in the NIR (Peñuelas et al. 1997). Most spectral indices are sensitive to the amount of water per leaf area (named, equivalent water thickness, EWT), while fuel moisture content (FMC) is a measure of the amount of water per dry matter (DM). Therefore, an accurate estimation of FMC requires both the variations of water and DM contents (Danson and Bowyer 2004; Fourty and Baret 1997; Riaño et al. 2005). The use of thermal IR data to estimate water content has also been tested by several authors (Jackson et al. 1981; Vidal et al. 1994). The relations between water and temperature are governed by the rate of evapotranspiration (ET) from plants, which uses part of the incoming radiation to convert liquid to gaseous water (latent heat) as a mechanism of thermal regulation. Water stress implies a reduction in ET, and therefore an increase in surface temperature when compared to non-stressed plants (Moran et al. 1994).

For fuel loads and fuel type mapping, the main target variable is the vertical and horizontal arrangement of the vegetation components. This application has been pursued with different sensors, with the most accurate results obtained using sensors that measure heights, instead of reflectance, using mainly airborne sensors, such as the interferometric RADAR and LIDAR (Riaño et al. 2004).

Active fire detection is commonly based on the middle infrared (MIR) spectral region (3–5 μm), where following the Wien displacement law, the peak sensitivity to spectral radiance is at the temperature of a vegetation burning (500 to 1,000 K). The contrast between radiance in this region and the thermal infrared (TIR) band (10–12 microns) offers a straightforward discrimination of active fires over average Earth temperatures (300 K), providing the sensor has enough radiometric sensitivity and the fire is large enough relative to the sensor target pixel size. Active fires can also be discriminated by the light they display in nocturnal images, if the sensor offers high sensitivity to low radiances and that stable lights (cities, industries) can be properly discriminated from intermittent ones (fires, volcano eruptions). Detection of fires has been achieved through the analysis of smoke plumes, as well.

Finally, post-fire effects are discriminated by analyzed the changes in leaf color, leaf area index and soil substratum after the fire has been extinguished. The short-term signal is dominated by charcoal, ash, and scorched leaves, while the medium to long-term signal is associated with lost of vegetation abundance or changes in species composition (Pereira et al. 1999; Roy and Landmann 2005).

6.4 Satellite Information for Assessing Fire Risk

Following a terminology that is generally accepted in natural hazard literature, the term risk refers to the combination of the physical probability that an undesired event occurs and the degree of potential damages caused by that event (Jones 1992). Within this framework, the assessment of fire risk should consider both the likelihood that a fire affects a particular area (danger), as well as the values at stake within that area (vulnerability) (Allgöwer et al. 2003). The former should consider the probability that a fire ignites and propagates, while the latter should take into account socio-economic values (properties, recreation resources, wood value, etc.), as well as the potential environmental damage (vegetation degradation, soil erosion potential, lost of endemic species, landscape quality, etc.) that may result from a fire.

The role of remote sensing data in fire risk assessment can also be grouped into these two categories: (1) generation of critical variables for fire ignition or propagation (Chuvieco et al. 2003b); and (2) assessment of resource values at risk. Most studies using satellite data for fire risk assessment have focused on the former, especially in the estimation of fuel moisture content and distribution of fuel types. Little effort has yet been dedicated to estimate vulnerability, although in recent years some analysis have been conducted with high-resolution images and census data to assess the risk potentials in the urban wildland interface (Radeloff et al. 2005). Additionally, a global analysis of population distribution has been performed within the context of natural hazards prevention (Dobson et al. 2000), which may have potential for global analysis of human-caused wildland fires.

6.4.1 Fuel Type Mapping

Description of fuel properties is critical in all phases of fire management and fire research (Chuvieco et al. 2003c): prevention (for fire danger estimation); suppression (fire behaviour modelling), and fire effects assessment (trace gas emissions, vegetation recovery after fire). Since the combination of fuel properties of different vegetation species is almost infinite, the most relevant fuel properties are simplified by generating broad categories that are named fuel types. Depending on the specific information requirement, approaches for fuel type classification may be very different, since they will consider some fuel properties or others. The most well-known fuel classification systems were developed for fire behaviour modelling. In this context, fuel types can be defined as “an identifiable association of fuel elements of distinctive species, form, size, arrangement, and continuity that will exhibit characteristic fire behaviour under defined burning conditions” (Merrill and Alexander 1987). Commonly, a fuel type has a range of quantitative parameters associated to each category, such as average fuel load, density, compactness, distribution of fuel beds by size, etc.

Several fuel type classification schemes have been proposed, the best known being the U.S. Forest Service’s Northern Forest Fire Laboratory (NFFL) of Missoula

(Montana), which was developed within the Behave fire propagation model (Burgan and Rothermel 1984). This scheme was developed for surface fires propagation studies and has 13 fuel types, where the groups are based on the primary nature of the surface fuel: herbaceous, shrubs, and dead leaves, slash residues and basal accumulation material.

Other fuel type classification systems include the National Fire Danger Rating System (NFDRS) fuel type classification, which used 20 models and it was intended for general fire danger estimation (Deeming et al. 1978), and the Canadian Forest Fire Behaviour Prediction (FBP) System, with 16 fuel types (Hirsch 1996).

Mapping surface fuel types from remotely sensed data presents two main challenges. On one hand, in many cases surface fuels are hidden below a dense overstory canopy, and are therefore difficult to retrieve from satellite observations. The second problem is associated with estimating of fuel heights and biomass loads, which are required to differentiate several categories, since those parameters are critical in fire propagation.

In spite of these difficulties, researchers have carried out fuel type mapping from medium and high-resolution sensors, using primarily Landsat-TM and MSS data (Anderson et al. 1993; Fazakas et al. 1999; Riaño et al. 2002). The results show accuracies above 80% for some categories (grasses, dense forest, dense shrub), but failed for those that require height estimations for discrimination (models 4, 5 and 6 of the NFFL system, for instance) or those that were under the canopy layer (model 7 of NFFL). Recent studies have shown the potential improvements in fuel type mapping from very-high resolution data, when several categories of spatial aggregation are considered (Arroyo et al. 2006).

RADAR and LIDAR systems have been used to overcome limitations of passive optical systems for mapping fuel types. The retrieval of understory information has been attempted by several studies based on L band RADAR data (Hyypä et al. 2000; Ranson et al. 2001), but unfortunately L-band RADAR missions have been very brief, and therefore little experience is available from these data at global scales. On the other hand, active microwave data do not yet provide sufficiently accurate estimation of canopy height, with uncertainties greater than 5 m (Hyypä et al. 2000; Toutin and Amaral 2000), and therefore the discrimination of shrub fuel types becomes unfeasible. Additionally, microwave signal has shown to have limited sensitivity to high biomass levels (Kasischke et al. 1997).

Airborne LIDAR sensors have proven more successful in the estimation of those geometrical properties that are required for fuel type mapping (Morsdorf et al. 2004; Riaño et al. 2004; Riaño et al. 2003), such as crown base height or crown bulk density (Fig. 6.3). The main drawbacks of this technology are its high costs and highly localized coverage, since most high-resolution sensors are airborne and with narrow fields of view. Accuracy is generally good enough for retrieval of critical fuel parameters although in shrubs fuels, the estimations are more controversial. In a recent study by Riaño et al. (2007a), standard LIDAR processing did not provide enough accuracy for height estimations of shrub species, and it was necessary to rely on passive optical sensors to improve detection of base heights.

Consequently, it is not possible with current sensors to generate a global fuel type maps, since biomass loads and geometrical properties are difficult to retrieve

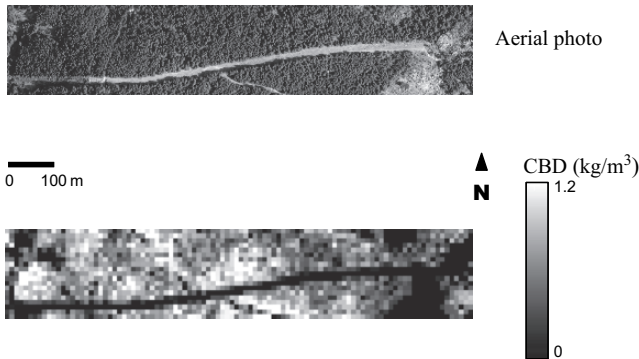


Fig. 6.3 Crown Bulk Density estimated from airborne LIDAR data in the Canencia Forest (north of Madrid). Data processed by D. Riaño (see Riaño et al., 2004)

from optical sensors. Unfortunately, the only orbiting LIDAR system, on board the Icesat satellite, was not designed for vegetation studies and it is not well suited for global retrieval or fuel properties. The coarse footprint (60–70 m) and the footprint cross track separation between orbits (up to 15 km) create severe difficulties for retrieval biomass loads, especially in rough terrain (Harding and Carabajal 2005; Lefsky et al. 2005). A global airborne LIDAR database is being put together (<http://www.lidarxchange.com/>) that could be used for calibration and validation of fuel classes estimates from optical sensors. At least for general fuel categories, optical sensor data can provide enough accuracy, integrated with other ancillary data or ecological modelling (Rollins et al. 2004), but additional effort is required to improve parameterization of those fuel classes. Meanwhile, the closest available products are vegetation or land cover maps, which provide global information on the spatial distribution of vegetation classes (Friedl et al. 2002; Price 2003; Zhu and Evans 1994), but do not offer quantitative information on their characteristics (biomass loads, heights, density, etc.), and therefore can only be used as a simple-generalized approach to fuel type mapping.

6.4.2 Mapping Temporal Patterns of Fuel Moisture

Fuel moisture content (FMC) is a critical variable for fire ignition and fire propagation studies, since the amount of water on plants is inversely associated to its flammability and fire rate of spread (Dimitrakopoulos and Papaioannou 2001; Nelson 2001). It also affects greenhouse emissions derived from fires, as a result of the impact of FMC on burning efficiency (Korontzi et al. 2004).

FMC has been traditionally based on field observations and meteorological fire danger indices. The former are more reliable and provide a direct measurement, but only offers estimation of local study areas. While meteorological indices provide a wider spatial perspective, they are only indirect estimations since they are based on atmospheric conditions (temperature, humidity, wind, etc.), which in turn affect

plant moisture, but in a different way depending on species physiology. For this reason, they are mainly oriented towards estimating FMC of dead fuels, which are more directly related to changes in atmospheric characteristics.

The spatial and temporal coverage provided by remote sensing systems offers a reasonable alternative for estimating FMC of live fuels at regular time intervals. Unlike meteorological indices, which depend on the specific conditions where the weather stations are located, remote sensing data are spatially comprehensive, covering the whole territory at various spatial resolutions, from few meters to few kilometers, depending on the sensor. Moreover, remote sensing data are based on physical characteristics related to vegetation condition (reflectance or temperature) at the time of imaging, whereas meteorological indices measure live FMC indirectly, through the analysis of atmospheric characteristics from which vegetation water status is estimated.

Several authors have shown the potentials of remote sensing data to estimate water content of plants, both using simulation models (Ceccato et al. 2001; Ceccato et al. 2003; Fourty and Baret 1997; Zarco-Tejada et al. 2003), and empirical approaches (Chuvieco et al. 2004b; Chuvieco et al. 2002b; Peters et al. 2002; Sims and Gamon 2003; Tian et al. 2001). FMC studies have used a wide variety of sensors, including laboratory spectroradiometric measurements, and medium and coarse resolution sensors. Laboratory studies provide important information for understating the effects of external factors, such as illumination angle, density and leaf area index (De Santis et al. 2006; Gillon et al. 2004).

Medium-resolution sensors have been used experimentally to test the sensitivity of spectral reflectance spatial-temporal variations in vegetation moisture, but they are not useful for operational estimation of FMC in fire danger applications because they lack enough temporal resolution. Successful estimation of FMC have been reported with Landsat-TM/ETM images, using empirical approaches on agricultural plots (Chen 2005; Holben et al. 1983; Thompson and Wehmanen 1979), as well as for natural vegetation, grasslands and shrublands, in fire danger estimation (Chuvieco et al. 2002b). RADAR C-band data have also been used for this purpose (Beaudoin et al. 1995; Couturier et al. 2001), but results are more uncertain since the texture components tend to veil the moisture variability of the backscatter signal (Bourgeau-Chavez et al. 1999; Leblon et al. 2002)

The estimation of FMC from satellite data in operational fire danger assessment can only be approached from coarse-spatial resolution sensors, which have the required revisiting frequency to account for short-term variations in plant moisture conditions. Until the launch of the MODIS sensor, the available high temporal resolution sensors did not provide sufficient spectral sensitivity for confident retrieval of FMC. Analyses based on AVHRR images relied in Normalized Difference Vegetation Index (NDVI) time series analysis. While the NDVI is a sound indicator of chlorophyll content and leaf area index, it does not provide a direct estimation of water content (Ceccato et al. 2003). Only when changes in moisture content affect directly the greenness of plants, the NDVI is suitable to monitor FMC, which mainly occurs with herbaceous species (Chuvieco et al. 2004a). For this reason, experiences of retrieving FMC from NDVI data in grasslands have been generally successful (Chladil and Nunez 1995; Chuvieco et al. 2002b; Hardy and Burgan 1999; Paltridge

and Barber 1988). However, the estimations are more erratic with shrub species (Alonso et al. 1996; Chuvieco et al. 2004a; Everitt and Nixon 1986). For this reason, the combined use of surface temperature and NDVI has also been recommended for FMC retrieval from AVHRR images (Chuvieco et al. 2003a; Chuvieco et al. 2004b; Moran et al. 1994), as well as the analysis of the differences between surface and air temperature, as a surrogate of evapotranspiration (Sandholt et al. 2002; Vidal et al. 1994).

The use of MODIS data for water estimation has been successfully tested in several biomes (Cheng et al. 2006; Dennison et al. 2005; Roberts et al. 2006; Stow et al. 2005; Yebra et al. 2007; Zarco-Tejada et al. 2003), providing a sound alternative for FMC retrieval. MODIS offers much higher spectral sensitivity than AVHRR for estimation of water content, since includes several spectral bands in the SWIR and NIR as well as the transition between the NIR and red bands, which has also proven susceptible to water content (Stow et al. 2005). With these foundations, NASA, under a project directed by Susan L. Ustin (www.cstars.ucdavis.edu), is studying the addition of a MODIS global vegetation canopy water content product.

SPOT-Vegetation images have also been used for water content estimation. While providing less spatial resolution than MODIS (1000 versus 500 m), for bands with similar spectral coverage, this sensor offers higher geometric and radiometric accuracy than AVHRR, and it includes a band in the SWIR. Initial results on the retrieval of FMC from SPOT Vegetation have been successful (Chuvieco et al. 2004a; Cocero et al. 2001).

6.5 Active Fires Products from Space Observations

Detection of active fires from space has been used extensively to analyze spatio-temporal patterns of fire occurrence (Dwyer et al. 2000), to account for emissions derived from fires (Randerson et al. 2005) and to relate deviations from fire regimes to major climatic events (van der Werf et al. 2004). Consequently, active fire detection is very relevant for global change studies.

At more local scales, identification of fire outbreaks is also required for fire managers for planning first attack, and subsequently for monitoring fire behavior. A typical target for a fire manager is to detect a new fire within less than 30 minutes after ignition occurs. Once the fire starts, and considering its dynamics, information on fire growth needs to be updated very frequently as well. Therefore, the use of satellite data for operational identification of new fire outbreaks or for fire monitoring requires a high observation frequency, which it is currently provided only by geostationary satellites (15 to 30 minutes revisiting time). The utility of these data for fire monitoring was first demonstrated for fires in South America (Prins and Menzel 1992), and then it has been used for routine retrieval of active fires since 1998 (Prins et al. 1998). However, the coarse resolution of these sensors precludes their use in operational fire detection, since the detectable burning area commonly exceeds the optimal threshold for fire initial attack. The improvements in spatial

and spectral resolution of second-generation of geostationary satellites may provide a semi-operational scenario in the next future (Calle et al. 2006).

Meanwhile, the use of medium to coarse spatial resolution sensors deployed on board polar orbiting platforms has provided the alternative for global analysis of active fires over the past 25 years. These sensors offer one or two images per day, which it is not enough frequency for early detection, but it does provide critical information on fire activity. Obviously, those fires starting after image acquisition will not be detected until the next image, or missed if they are extinguished prior to the acquisition of the next one. In addition, those fires under thick cloud coverage will not be detected, but at least a global view of spatio temporal patterns of fire occurrence can be obtained.

The AVHRR sensor has been the most widely used for active fire detection since 1979. Its use started at the beginning of the eighties, when the first studies for monitoring fire activities in tropical and boreal regions were published (Flannigan and Vonder Haar 1986; Matson et al. 1984). The proposal of a simple mixing method for detection of sub-pixel fire spots (Dozier 1981) was also widely used, with reasonable accuracies in densely vegetated areas. However, it should be pointed out that the AVHRR was not designed for active fire detection, and therefore the thermal sensitivity of its MIR channel (band 3, 3.55–3.93 μm) was not very suitable for this task, with a low saturation threshold at $\approx 47^\circ\text{C}$. This low threshold can eventually lead to confusion with other hot targets (exposed soils, for instance), or with highly reflective zones. Consequently, a simple threshold in this channel does not provide a sufficiently accurate discrimination of fires. Confusion with other surfaces is very common in semiarid areas, where forests are often mixed with croplands or bare soil (Martín et al. 1999). In areas with dense vegetation cover, surface temperatures tend to be cooler, and therefore the potential confusions with fires are lower. Nocturnal images can also reduce false alarms (Langaas 1992), but they increase the risk of biasing fire detection, since much biomass burning is conducted during the central hours of the day (Giglio et al. 2003b; Kennedy et al. 1994). Some other hot targets, such as certain industries and gas flares linked to oil extraction or energy production, may also saturate the MIR channel. Confusion with highly reflective surfaces such as clouds and cloud edges is also possible, since they can be very reflective and saturate the MIR channel. False alarms related with the saturation of the MIR channel may occur with lakes, reservoirs, rivers and other water bodies, as a result of specular reflection (Martín et al. 1999). This phenomenon, known as Sun glint, only occurs within a certain geometry of illumination and observation. In spite of these problems, since AVHRR was operationally operated and a long time series of images were available, it provided the input data for a number of global scale fire detection projects.

The first global effort to obtain a world wide active fire coverage was undertaken by the International Geosphere Biosphere Program (IGBP) Data and Information System (DIS) core project. The project was aimed to develop a Global Fire Product (GFP), from a consistent series of AVHRR images at full spatial resolution (1.1 km at nadir). Daily AVHRR data were collected for the period April 1992 to December 1993 by the IGBP-DIS 1 km AVHRR Global Land Project (Eidenshink and Faundeen 1994). Fires were identified using a multiband threshold and contextual

algorithm developed by Flasse and Ceccato (1996). A cloud-masking algorithm was also performed, based on the criteria proposed by Saunders and Kriebel (1988). Data processing was done at the Joint Research Centre (JRC) in 1996 and 1997 (Stroppiana et al. 2000b). This product was the basis of several global analysis of fire occurrence patterns, which identified those regions with more recurrent extensive fires, the main world fire regimes with the most active periods of the year, and the differences between latitude belts, especially between African and Central American fires (Dwyer et al. 2000).

Following this experience, the JRC undertook another global project to obtain global coverage of fire activities. The project was named "world fire web", and it was based on a common processing chain for a decentralized network of receiving stations that covered most of the Earth land surface (Pinnock and Grégoire 1999). The detection algorithm was also based on Flasse and Ceccato's work, and it was systematically applied to AVHRR afternoon images. Unfortunately, this project only lasted a few years (Grégoire et al. 2001)

Regional projects to detect active fires in AVHRR images were developed in South East Asia (Malingreau et al. 1985), Canada (Flannigan and Vonder Haar 1986; Li et al. 2000), the U.S.A. (Matson et al. 1987), Russia (Sukhinin et al. 2004), Africa (Kennedy et al. 1994; Langaas 1992), Brazil (França and Setzer 2001; Matson and Holben 1987; Setzer and Pereira 1991) and many other regions of the world.

During the last decade, the European Space Agency (ESA) proposed the use of the ATSR on board the ERS-1 and 2 to monitor active fires globally. The project was named World Fire Atlas and has been working since 1995 to the present (<http://dup.esrin.esa.int/ionia/wfa/index.asp>). After 2003, the project relies on data from the Advanced ATSR, on board the Envisat satellite. The discrimination of active fires is based on two single thresholds applied to the night images of the 3.7 μm channel: one at 312 K and the other, less conservative, at 308 K, which generate two different products (Piccolini and Arino 2000). These products are offered every 2 days at 1 km spatial resolution. The discrimination of active fires from ATSR should be less noisy than with day time AVHRR images, since it avoids solar contamination, and it is claimed to have less bidirectional reflectance problems. However, the product is potentially less complete than AVHRR detections, since fires lasting a diurnal cycle are not detected.

Another sensor that has been used for active fire detection is the Visible and Infrared Scanner (VIRS) on board the Tropical Rainfall Measuring Mission (TRMM). The satellite was launched in 1997 into a circular orbit inclined at 35° at 350 km initially, and 402.5 km after 2001. Being an Equatorial orbit, the sensor acquires information at different times of the day, which provides a better understanding of fire regimes, at the cost of non observing areas above or below 38 degrees. The VIRS has five bands covering the visible, NIR, MIR and TIR regions of the spectrum. Channel 3 has a similar spectral resolution as AVHRR, with a nominal spatial resolution of 2.1 km Its saturation threshold is also similar to AVHRR: 321.2 K. The algorithm to detect active fires in VIRS images was similar to the one applied to MODIS and AVHRR images, with multiple band thresholds and contextual criteria (Giglio et al. 2003b). Using this algorithm, monthly series of active fire products have been generated since 1998 to present, using a 0.5° resolution cell. This information has

been used for estimations of biomass burning emissions associated to El Niño events (Randerson et al. 2005).

The development of the Earth Observing System (EOS) missions during the nineties was built upon the experiences of working sensors, and therefore new systems were developed to solve or mitigate identified problems of previous missions. MODIS characteristics are a clear example of this progress, since the sensor was explicitly design to improve retrieval reliability of several key variables (Justice et al. 2002b). Specifically for detecting the active fires, MODIS includes two MIR bands, one with high thermal sensitivity (up to 500 K) and the other with a lower one (saturation at 331 K), as well as high-sensitivity TIR bands (saturation at 400 K). These improvements reduce the potential of false alarms found in AVHRR data analysis, while preserving temporal resolution. The algorithm for fire identification is based on thresholds over the MIR channel and on the difference between the MIR and TIR channels. Additionally, contextual rules (deviation from background signal) are applied for candidate pixels (Justice et al. 2002a). Improvements were made in a second revision of the algorithm (Giglio et al. 2003a). The validation efforts conducted have found a good relationship with fires detected in higher resolution images, although problems still remain with the presence of dense smoke and understory fires (Csaszar et al. 2006; Morisette et al. 2005).

Global processing with this algorithm produces several active fire products: daytime, nighttime and daily fire product (MOD14G, D and A1, respectively), 8 day summary fire product at full resolution and 8 day summary at coarse-spatial resolution for global climate modelling (<http://modis-fire.umd.edu/>). The products are generated from data obtained from both Terra and Aqua satellites, providing two complete, daily coverages of the world. A quick summary of fire outbreaks is offered daily by the rapid response system (<http://rapidfire.sci.gsfc.nasa.gov/>). Additionally, 10 day composites of detected fires are available by the same system, and monthly and year summaries within the Web Fire Mapper of the University of Maryland (<http://maps.geog.umd.edu/firms/default.asp>; Fig. 6.4). These active fire products have been the basis for a large number of analysis associated to global gas emissions (Randerson et al. 2006; Venkataraman et al. 2006), analysis of fire regimes (Csaszar et al. 2005; Giglio et al. 2006a), studies on factors associated with fire occurrence (Mollicone et al. 2006), and relations of fire with tropical deforestation (Morton et al. 2006).

Global analysis of fire activity has also been generated from the Operational Linescan System (OLS) on board the DMSP (Defense Meteorological Satellite Program). In this case, the fires are detected from the visible part of the spectrum (light instead of heat, as other reviewed sensors) during night acquisitions (Elvidge 2001; Fuller and Fulk 2000). At local scales, airborne detection and monitoring of fires has also been carried out (Ambrosia and Brass 1988), using MIR and TIR sensor systems. More recently the use of unmanned systems have also been successfully tested (Ambrosia et al. 2003).

New sensors are being planned to more readily fulfill the specific needs of operational fire detection and fire growth monitoring. The most innovative projects in this regard are the BIRD program of the German DLR (Briess et al. 2001) and the Fuegosat promoted by the Spanish company Insa (Martínez et al. 2000).

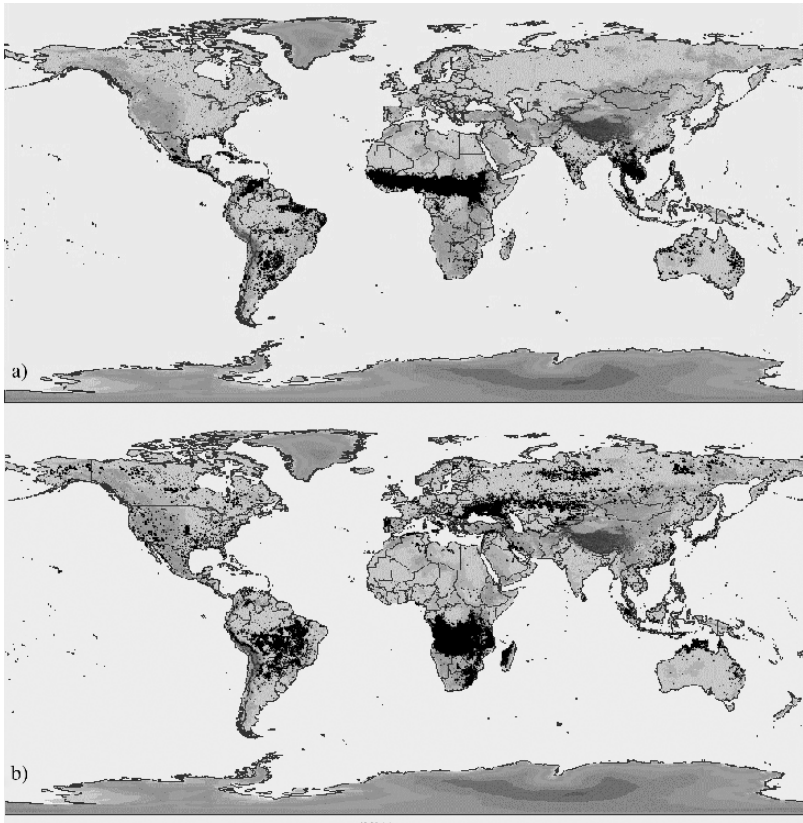


Fig. 6.4 Global fire spots detected by the MODIS sensor in 2005: January (a), July (b). Maps taken from the Fire Information for Resource Management Systems at U. Maryland (<http://maps.geog.umd.edu/firms/maps.asp>)

6.6 Analysis of Fire Effects

The assessment of fire effects accounts for the different impacts of fire on biophysical and socio-economic values. Most commonly, they refer to the analysis of post-fire changes in soil, water, vegetation and atmosphere in relation to pre-fire conditions.

In spite of the importance of detecting active fires, these products do not provide a complete evaluation of fire-affected areas, since several factors (fire length, temporal resolution of satellite overpass, cloud obscuration, etc.) may preclude the detection of an important number of fire events. Several attempts have been made to relate active fires to burned area (Giglio et al. 2006b), which emphasise the spatial differences between these two parameters.

Consequently, the evaluation of fire effects have mainly focused on mapping burned areas at different spatial and temporal resolutions. The discrimination of burn severity (levels of post-fire affects on vegetation communities) has received

less attention, although a growing interest in this topic is reflected in the scientific literature as discussed below. Finally, the effects of fire on water, soil, fauna and atmosphere have not been widely analyzed using satellite data, with the exception of the estimations of gas emissions derived from biomass burnings. These estimations are based on approximating the amount of biomass burned and the emission coefficients for each biomass type.

All these post-fire analysis tend to highlight the short-term effects of fire, but medium to long-term effects are also critical on understanding vegetation and landscape composition changes.

6.6.1 Burn Area Mapping

The most common use of remotely sensed data for burned land mapping has concentrated at local scales, using medium to high-resolution sensors, such as Landsat-TM/ETM+, SPOT-HRV, IRS-WIFS/AWIFS and SAC_C-MMMRS (Chuvieco and Congalton 1988; Chuvieco et al. 2002a; García-Haro et al. 2001; Garcia and Chuvieco, 2004; Jakubauskas et al. 1990; Koutsias et al. 1999; López García and Caselles 1991; Salvador et al. 2000; Siljeström and Moreno 1995; Vázquez et al. 2001). The accuracies for burned area mapping are regularly above 80% for discriminating the fire perimeter, especially when medium to large fires (>100 hectares) are considered.

Generation of global analyses of burn areas was initiated from AVHRR images during the nineties. Most commonly, burn scar areas were discriminated from a multitemporal comparison of NDVI or other spectral indices (Kasischke and French 1995; Martín and Chuvieco 1995; Pereira 1999), although some combination of thermal and optical channels was also used (Fraser et al. 2000; Roy et al. 1999). Extensive regions have been mapped from AVHRR temporal series, especially in the boreal forest, where burned land maps derived from this sensor are proving the effects of global warming on fire regimes (Sukhinin et al. 2004). Similarly to other fire applications, AVHRR data provided reasonable estimations when the spectral signal show enough contrast with the background, which in post-fire conditions happened for large burn scars (>1000 hectares), when the images were acquired close enough to fire extinction. AVHRR lacked radiometric and geometrical temporal consistency to provide more accurate results (Maggi and Stroppiana 2002).

Global burned scars products from full resolution AVHRR data have not been developed so far, but temporal series of burn scar maps have been created from the Pathfinder AVHRR Land (PAL) program (http://daac.gsfc.nasa.gov/interdisc/readmes/pal_ftp.shtml), which included a global archive AVHRR data at a degraded resolution (8×8 km) since 1982. The discrimination of burned areas using coarse resolution AVHRR was carried out using the algorithm developed by Barbosa et al (1999a). This product was used to show that burned area was significantly related to climatic fluctuations associated to El Niño events (Carmona-Moreno et al. 2005; Riaño et al. 2007b).

More recently, other sensors with greater sensitivity for mapping burned scars have been used to create global inventories of burned areas. In 2000, two world-wide projects were developed at 1 sq km spatial resolution. The first project, named GBA2000, was coordinated by the JRC, and based on SPOT-Vegetation data. Daily images were acquired, mosaicked and composited in 10 day periods using a variation of the minimum albedo rule (Sousa et al. 2003). Burn scar areas were discriminated using a set of global algorithms, developed by different expert groups. The final results are available online (http://www-tem.jrc.it/Disturbance_by_fire/products/burnt_areas/global2000/global2000.htm), and in the process of being validated (Tansey et al. 2004).

The second world-wide project was named GLOBSCAR and was an initiative of the European Space Agency. The project was based on daily ATSR-2 images, on board the ERS-2 satellite, acquired during 2004. Two algorithms to discriminate burned areas were proposed (named K1 and E1), based on different thresholds on the NIR and TIR spectral bands, the K1 algorithm (Piccolini and Arino 2000), and on red, NIR, TIR and several vegetation indices, the E1 algorithm (Simon et al. 2004). These two algorithms created two different burned area products, which are available online at <http://dup.esrin.esa.it/ionia/projects/summary24.asp>.

The spectral and spatial enhancements of the MODIS sensors over other global-scale instruments, such as AVHRR, Vegetation and ATSR, should facilitate the generation of global maps of burned areas from this sensor data. Several studies have already shown an improved discrimination of MODIS over other sensors in regional

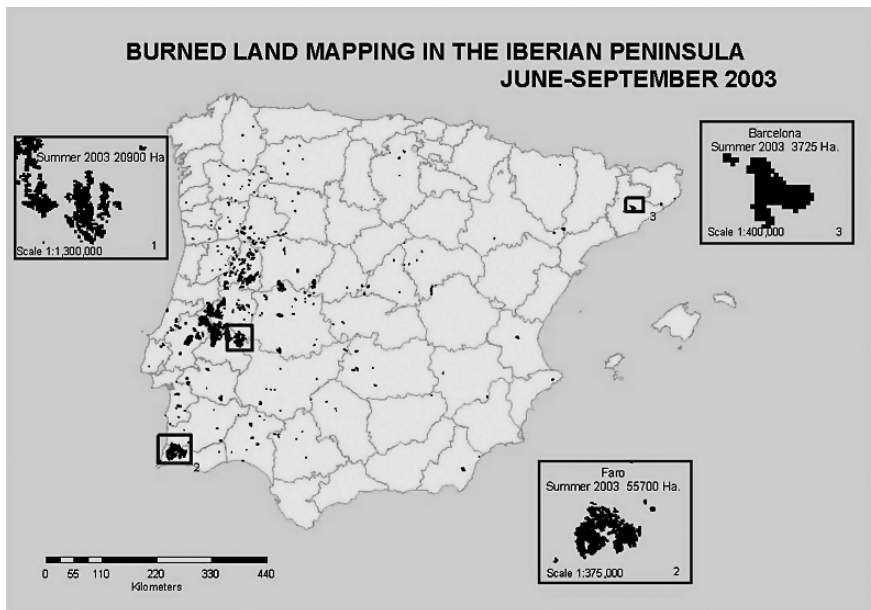


Fig. 6.5 Burn scar areas in the Iberian Peninsula from MODIS data. Images processed by Pilar Martin for the European Project Spread. Used with permission

studies (Chuvienco et al. 2005; Li et al. 2004; Martín et al. 2002; Sá et al. 2001): Figure 6.5. The next collection of MODIS land variables (which are to be released soon) will include a new standard product with global burned land areas at 500 m spatial resolution. The algorithm to generate this product is based on a multitemporal change detection approach that labels the pixels according to the differences found between modeled and actual reflectance, taking into account bidirectional reflectance corrections (Roy et al. 2005b; Roy et al. 2002).

Finally, other global-scale burn scar projects are being developed by the European Space Agency, using AATSR, VEGETATION, and the new MERIS hyperspectral sensor on board the Envisat satellite. The generic term for this undertaking is GLOBCARBON, and it involves the development fully calibrated estimates of several land products, such as Burnt Area Estimates (location, timing, area affected), leaf area index and active photosynthetic radiation, and vegetation growth cycle (timing, duration, spatial and temporal variability). The GLOBCARBON Burnt Area Estimate products (BAE) are global maps of monthly difference products representing the new burnt areas detected in the last month with a minimum confidence ratio index of 80% (<http://dup.esrin.esa.it/ionia/projects/summary43.asp>).

6.6.2 Determination of Burn Severity

While the discrimination of burned/unburned areas has been achieved with reasonable good results, even from low-resolution satellite data, burn severity estimation remains a challenge. Burn severity, defined as the amount of ecosystem transformation as a result of fire, has a significant effect on gas emission estimates derived from biomass burning, since it is related to the amount of biomass consumed by the fire (commonly named burned efficiency, which is currently one of the most uncertain components of global estimations of biomass burning emissions) (Chuvienco et al. 2004a). Additionally, it is closely linked to vegetation recovery after a fire (Pérez and Moreno 1998; Wheatherspoon and Skinner 1995). The longer and more intense a fire is, the more severe are the effects of the fire and the slower the vegetation recovers. Fire intensity and duration depend on fire behavior, which is controlled by different variables related to the fuel properties (load, moisture content, chemical properties), fire weather, and to the surrounding environment (slope, aspect, wind, rainfall, etc.).

The evaluation of burn severity can be undertaken using different approaches (Lentile et al. 2006). The methods are closely linked to the objectives of the evaluation which may include an assessment of vegetation recovery, soil erosion potential, or landscape fragmentation (Key and Benson 2002). Traditionally, burn severity assessment has been undertaken using field methods, mainly considering the changes in soil color and condition, depth of the affected organic layer, amount of scorched leaves or remaining branches (Key and Benson 2004; Moreno and Oechel 1989; Pérez and Moreno 1998). The cost of this approach, as well as the lack of spatial representation associated with field methods, have led to the use of remotely sensed images, since they provide relatively cheap and spatially comprehensive coverage of an area of interest.

Several authors have used remotely sensed data for discriminating burn severity levels using empirical approaches (Caetano et al. 1994; Cocks et al. 2005; Díaz-Delgado et al. 2001; Epting et al. 2005; Miller and Yool 2002; Parra and Chuvieco 2005; Rogan and Franklin 2001; van Wagendonk et al. 2004; White et al. 1996).

Most studies have been conducted with Landsat TM/ETM+ images, since they provide appropriate spectral and spatial resolution for burn severity discrimination at landscape level. However, post-fire reflectance is greatly affected by spatial and temporal variability of burn severity (Key 2005), as well as other environmental factors. Fully burned or undisturbed areas generally have a distinctive spectral reflectance, but most studies have found it problematic to discriminate intermediate severity values (Jakubauskas et al. 1990; Miller and Yool 2002; Minick and Shain 1981). Hyperspectral sensors, such as AVIRIS and Hyperion, may offer greater spectral sensitivity to these intermediate values of burn severity (Parra and Chuvieco 2005; van Wagendonk et al. 2004), but additional efforts are required to better understand the signal derived from different burning conditions, especially when several vertical strata need to be assessed. As a future research topic, building an improved severity index should incorporate improved knowledge of how fires of different severity displace the position of prefire vegetation in multispectral space (Roy et al. 2006).

To address this problem, reflectance simulation models may be used to simulate the spectral variation caused by different burn severities. The use of radiative transfer models (RTM) in fire effects assessment was first achieved within the framework of evaluating the potential of satellite data to discriminate understory fires in tropical regions (Pereira et al. 2004). Specifically for burn severity discrimination, Chuvieco et al (2006) have recently proposed the application of the Kuusk two-layer RTM for simulating different burn severity conditions in short-term and medium-term temporal scenarios. The main factors considered were the changes in soil substrate color (from soil to carbon), the changes in leaf properties (from wet to dry), and the changes in leaf area index (Fig. 6.6). The inversion of this model was successfully tested in the retrieval of burn severity for a large forest fire in Mediterranean conditions using Landsat-TM/ETM data (De Santis and Chuvieco 2007). The simulations could also be applicable to other sensors, but additional simulations need to be done to reduce errors for intermediate values of severity (Chuvieco et al. 2007).

All those studies on burn severity rely on medium to high spatial resolution images. Few experiences are available on the potential application of coarse resolution images to burn severity, and therefore the generation of global products for this goal would probably still require several years.

6.6.3 Use of Satellite Data for Emission Estimations

Several authors have proven that biomass burning is a significant source of carbon to the atmosphere (Andreae 1991), hence is an essential factor to consider when evaluating climate changes at the global level. Great inter-annual and intra-annual variability of biomass burning (Hoffa et al. 1999; van der Werf et al. 2006) requires that monitoring emissions is done at frequent temporal scale, and therefore remote

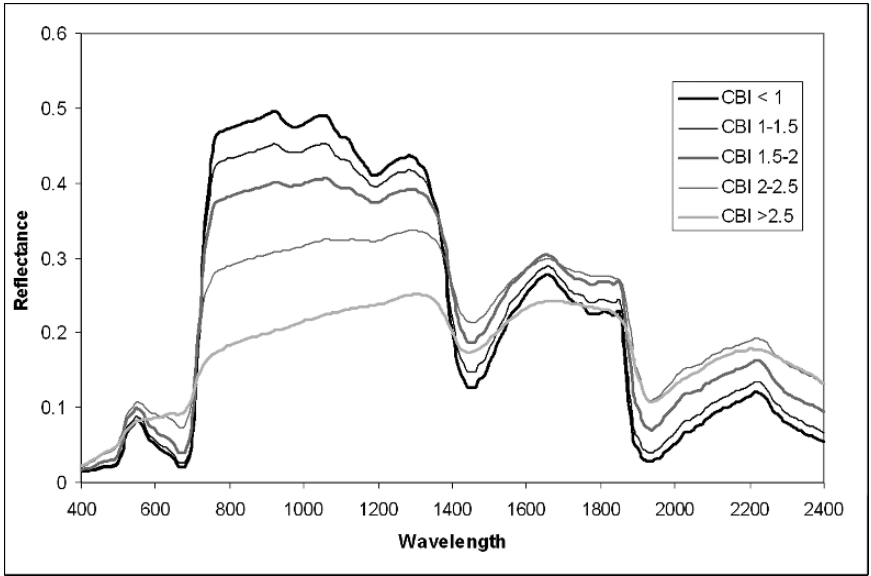


Fig. 6.6 Simulated reflectance for different burn severity values. CBI is a composite burn index, which ranges from 0 (none) to 3 (high) severity. From Chuvieco et al., 2006. Use of a radiative transfer model to simulate the postfire spectral response to burn severity, *Journal of Geophysical Research*, vol. 111, G04S09, doi:10.1029/2005JG000143. Copyright 2006 American Geophysical Union. Reproduced by permission of AGU

sensing of active fires and/or burned areas are a critical input to global fire emissions models (Palacios-Orueta et al. 2005).

Two main approaches for estimating biomass burning emissions have been proposed in the literature. The first one is based on direct measurements of trace gas released during a fire. This approach has been implemented from field measurements (Ferek et al. 1998; Hao et al. 1996), as well as from remote sensing analysis of smoke components (Ferrare et al. 1990; Kaufman et al. 1992; Randriambelo et al. 1998). Both, field and remote sensing gas emissions measurements require simultaneity with active fires, either experimental or actual ones. This is difficult due to operational difficulties to synchronize measurements campaigns with fire activity.

The second approach to estimate gas emissions derived from fire is based on accounting for the main factors associated to the emission process, mainly biomass loss and gas emission coefficients. The most widely used model was formulated by Seiler and Crutzen (1980):

$$M_{i,j,k} = BL_{i,j,m} \times BE_{i,j,m} \times BS_{i,j} \times E_k \times 10^{-15}$$

where, $M_{i,j,k}$ is the amount of gas k released for a specific area (with i,j coordinates) in Tg, $BL_{i,j,m}$ is the biomass load (dry matter) for the same area in $gr\ m^{-2}$ (assuming the area has a homogenous cover of fuel/vegetation type m); $BE_{i,j,m}$ is the burning efficiency (i.e. proportion of biomass consumed, 0–1) of fuel/vegetation type m ;

$BS_{i,j}$ is burned surface of the same area (m^2); and, E_k is the amount of trace gas k released per dry matter unit ($gr\ Kg^{-1}$ of biomass).

Remote sensing is an excellent source of information to derive some of those input parameters (Ahern et al. 2001; Barbosa et al. 1999b; Palacios-Orueta et al. 2005; Stroppiana et al. 2000a).

The most common use of satellite data in the estimation of biomass emissions have been the retrieval of burned areas, either from active fires or from actual burn scars. The former approach has been more extended, because of the greater availability of fire detection over burned land mapping. As previously commented active fire may not provide an accurate estimation of actual burned area and therefore the estimations from available active fire products may underestimate actual emissions (Giglio et al. 2006b; Liousse et al. 2004).

The second critical variable to estimate gas emissions is the assessment of biomass loads. This has been traditionally undertaken in remote sensing literature from indirect inferences of net productivity or vegetation density. However, there is always a great uncertainty in measuring biomass loads when vertical measurements are not available. As explained above, at present only LIDAR sensors provide a sound estimation on vertical distribution of vegetation, but this is confined to local scales until satellite borne LIDAR systems are launched. Surrogates of this information may be obtained through the analysis of multiseasonal trends of spectral vegetation indices, providing a base biomass load is available (Palacios-Orueta et al. 2004). Recent years efforts to estimate Net Primary Productivity of Vegetation may also help the estimation of biomass loads (Zheng et al. 2001).

Finally, the burning efficiency, that is the amount of biomass actually consumed by the fire, has been estimated from field measurements (Fearnside et al. 2001), and by analyzing pre-fire moisture content (Levine 2000), since the amount of water is inversely related to fire intensity and duration. Some studies have proposed the use of relative variation of NDVI (greenness indices), as a surrogate of fuel moisture content to estimate burning efficiency (Barbosa et al. 1999b). However, as said before, greenness indices only facilitate good estimations of water content for herbaceous vegetation, and therefore the method needs to be adapted to shrubs and forested areas (Chuvieco et al. 2004a).

In any case, satellite data have a great potential for estimating critical variables in fire emissions. The use of different spatial-resolution sensors may be used to up-scale field or local scale measurements to regional or global scenarios (Fig. 6.7), and therefore spatial heterogeneity of biomass loads and burning efficiency can be better considered. Additionally, the temporal frequency of remote sensing observations may greatly improve time-domain estimations of gas emissions (Palacios-Orueta et al. 2005).

6.7 Validation of Global Fire Products

The main challenge for using global products, either fire or any other critical variable, is obtaining a quantitative estimate of the accuracy of the results. When assessment is not properly done, the estimations derived from these products carry along

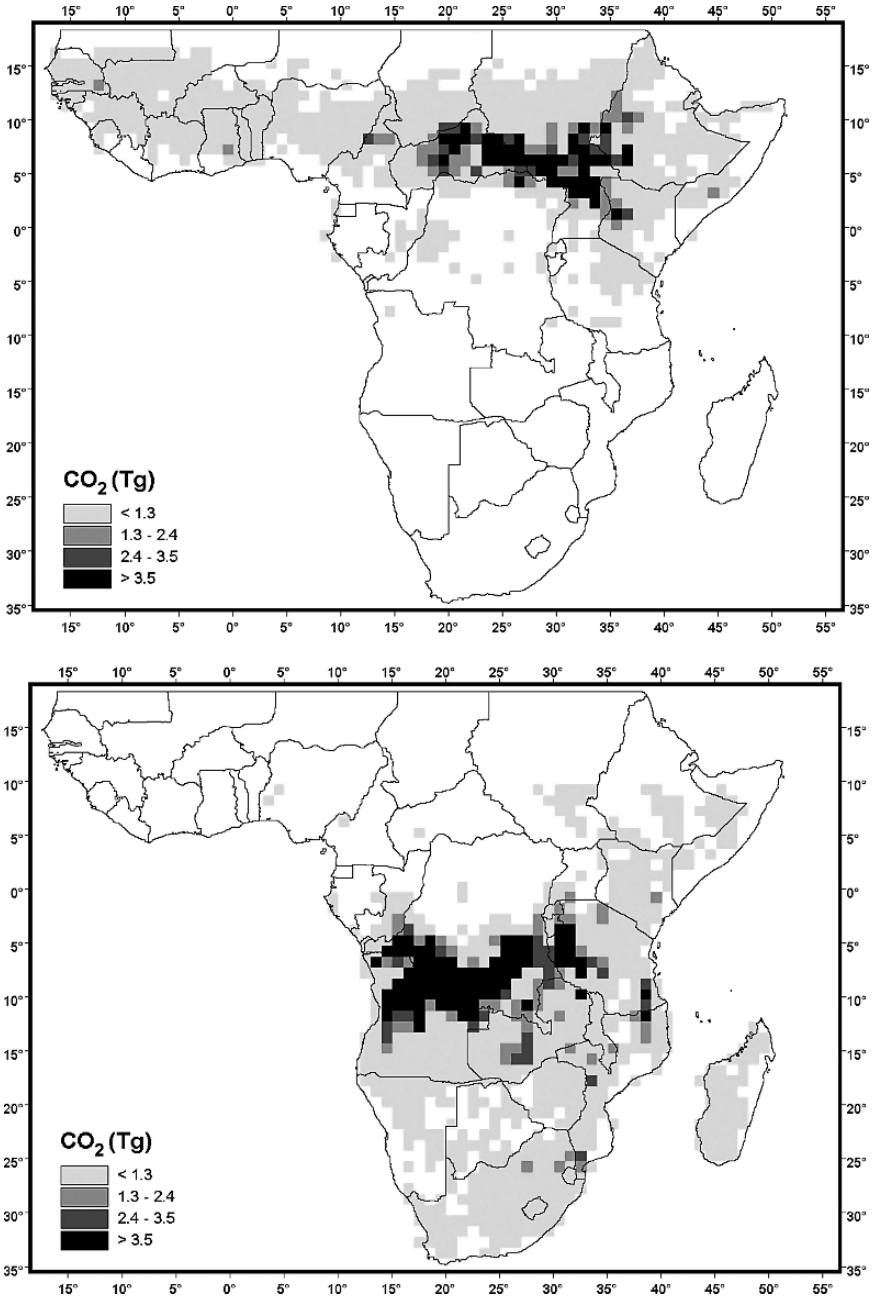


Fig. 6.7 Estimations of CO₂ emissions from African biomass burning. Upper, January, Lower, July. From Palacios-Orueta et al., 2004. Remote sensing and geographic information system methods for global spatiotemporal modelling of biomass burning emissions: Assessment in the African continent", *Journal of Geophysical Research*, 109, D14S07, doi:10.1029/2004JD004734. Copyright 2004 American Geophysical Union. Reproduced by permission of AGU

a great level of uncertainty, and cross-checking with other products do not reveal which is more accurate (Boschetti et al. 2004; Korontzi et al. 2004).

Validation efforts of world-wide coverage products are obviously very costly and time consuming, and there is always a practical limit on the potential of being spatially representative. Within the MODIS Land science team, researchers have been working on validation of MODIS standard products (Morissette et al. 2002). Other global scale projects, such as GBA2000 and Globscar included some assessment, with a rough estimation of accuracy. However, the discrepancies between these products are surprisingly high (Boschetti et al. 2004).

The most common strategy to validate coarse spatial resolution products uses higher spatial resolution images, acquired simultaneously with the coarser one, or at least close enough as to derive a similar estimation. A common example is the use of ASTER images to validate active fire detection from MODIS, since they are carried out in the same satellite (Csiszar et al. 2006). This is especially critical for active fire detection, since the comparison images need to be acquired almost simultaneously. However, the comparison between these two sensors is not trivial, since they have very different spatial resolutions (60×60 m, ASTER versus 1 sq km for MODIS), which makes complex to compute the proportions that actual burns of such diverse areas.

For burn scars assessment, the temporal issue is not as critical as in active fire assessment, since the burn scars have a longer permanence. Therefore, non-simultaneous images can be used, or even from different dates. For this goal, the use of Landsat-TM/ETM+, CBERS or SPOT-HRV data, have been the most common. Burn scars delineated with these high resolution images are then cross-tabulated with those extracted from coarse resolution images to obtain confusion matrices and to compute omission and commission errors. Considering the great differences in spatial resolution between the two sources, an alternative to cross-tabulation is to obtain a scatter graph of burned land proportions identified by the two sensor sources, using a defined grid size (5×5 km, for instance). The correlation between the two data sources provides a measure of consistency, and the regression parameters, an estimation of the quality of area estimations (Roy et al. 2005a).

Other authors have suggested a validation strategy based on comparing discriminated burn scars with active fires, at least to evaluate spatial agreements patterns (Roy et al. 2005b). Obviously, these two products refer to the same phenomenon but with a very different perspective, since active fires only register a particular momentum in fire behavior, while burn scars refer to a more stable signal and affect a different territory. However, their comparison would at least serve to address omission errors, providing the active fire detections are correct.

6.8 Current Challenges for Global Observation of Biomass Burning

As reviewed in this chapter, satellite Earth Observation offers a wide variety of critical information for prevention and assessment of biomass burning impacts. At global scale, the most extended products are those associated with active fire

detection, which have been developed for the last 25 years, mainly from AVHRR, but also from ATSR, MODIS and geostationary satellites. Within the last five years, a growing interest on deriving global burned land products have implied the availability of two covers (GBA2000 and Globscar) and the development on new ones that soon will be released (MODIS Burned Product, Globcarbon), then enhancing our capacity of monitoring changes in fire regimes and atmospheric emissions derived from biomass burning. Burn severity products should be added to the wishing list, but the current interest is focused on high spatial and spectral resolution sensors, and global products are not yet fully envisaged.

Finally, the use of satellite data for early warning is still far from completion. The estimation of moisture conditions would require a global system of meteorological observations at proper spatial resolutions and a more detail monitoring of subtle changes in surface reflectance and temperature as a result of plant drying. The former may be based on forecasted data using global climate models, the latter requires the development of water content maps, which will hopefully be included in the next generation of MODIS standard products. Vertical profile sensors, such as LIDAR or long-wave RADAR systems, providing a global survey of biomass loads are strongly required to improve fuel management operations that would eventually lead to less catastrophic fires, as well as to better monitor regeneration trends after fire and get better account for gas emissions.

Acknowledgments The author wishes to express his gratitude to Eric Kasischke, David Roy and David Riaño for their very valuable comments and corrections.

References

- Ahern, F. J., Goldammer, J. G., & Justice, C. O. (Eds.). (2001). *Global and regional vegetation fire monitoring from space: Planning a coordinated international effort*. The Hague, The Netherlands: SPB Academic Publishing.
- Allgöwer, B., Carlson, J. D., & van Wagendonk, J. W. (2003). Introduction to fire danger rating and remote sensing. Will remote sensing enhance wildland fire danger rating? In E. Chuvieco (Ed.), *Wildland fire danger estimation and mapping. The role of remote sensing data* (pp. 1–19). Singapore: World Scientific Publishing.
- Alonso, M., Camarasa, A., Chuvieco, E., Cocero, D., Kyun, I., Martín, M. P., & Salas, F. J. (1996). Estimating temporal dynamics of fuel moisture content of Mediterranean species from NOAA-AVHRR data. *EARSEL Advances in Remote Sensing*, 4, 9–24.
- Ambrosia, V. G., & Brass, J. A. (1988). Thermal analysis of wildfires and effects on global ecosystem cycling. *Geocarto International*, 1, 29–39.
- Ambrosia, V. G., Wegener, S. S., Sullivan, D. V., Buechel, S. W., Dunagan, S. E., & Brass, J. A. et al. (2003). Demonstrating UAV-Acquired real-time thermal data over fires. *Photogrammetric Engineering and Remote Sensing*, 69, 391–402.
- Anderson, G. L., Hanson, J. D., & Haas, R. J. (1993). Evaluating Landsat Thematic Mapper derived vegetation indices for estimating above-ground biomass on semiarid rangelands. *Remote Sensing of Environment*, 45, 165–175.
- Andreae, M. O. (1991). Biomass burning: Its history, use and distribution and its impacts on environmental quality and global climate. In J. S. Levine, (Ed.), *Global biomass burning : Atmospheric, climatic, and biospheric implications* (pp. 3–21). Cambridge, Mass: MIT Press.

- Arroyo, L. A., Healey, S. P., Cohen, W. B., Cocero, D., & Manzanera, J. A. (2006). Using object-oriented classification and high-resolution imagery to map fuel types in a Mediterranean region. *Journal of Geophysical Research-Biogeosciences*, *111*, doi:10.1029/2005JG000120.
- Barbosa, P. M., Grégoire, J. M., & Pereira, J. M. C. (1999a). An algorithm for extracting burned areas from time series of AVHRR GAC data applied at a continental scale. *Remote Sensing of Environment*, *69*, 253–263.
- Barbosa, P. M., Stroppiana, D., Gregoire, J. M., & Pereira, J. M. C. (1999b). An assessment of vegetation fire in Africa (1981–1991): Burned areas, burned biomass, and atmospheric emissions. *Global Biogeochemical Cycles*, *13*, 933–950.
- Beaudoin, A., Vidal, A., Desbois, N., & Deboux-Ros, C. (1995). Monitoring the water status of Mediterranean forests using ERS-1 to support fire risk prevention. In *International Geoscience and Remote Sensing Symposium, IGARSS '95. 'Quantitative Remote Sensing for Science and Applications'*, (pp. 963–966). Firenze, Italy.
- Boschetti, L., Eva, H. D., Brivio, P. A., & Gregoire, J. M. (2004). Lessons to be learned from the comparison of three satellite-derived biomass burning products. *Geophysical Research Letters*, *31*, L21501, doi:21510.21029/22004GL021229.
- Bourgeau-Chavez, L. L., Kasischke, E. S., & Rutherford, M. D. (1999). Evaluation of ERS SAR data for prediction of fire danger in a boreal region. *International Journal of Wildland Fire*, *9*, 183–194.
- Briess, K., Lorenz, E., Oertel, D., Skrbek, W., & Zhukov, B. (2001). *Fire recognition potential of the Bi-spectral Infrared Detection (BIRD) Satellite*. Berlin: Institute of Space Sensor Technology and Planetary Exploration, 2.
- Burgan, R. E., & Rothermel, R. C. (1984). *BEHAVE: Fire behavior prediction and fuel modeling system. Fuel subsystem*. Ogden, Utah: USDA Forest Service, GTR INT-167.
- Caetano, M. S., Mertes, L. A. K., & Pereira, J. M. C. (1994). Using spectral mixture analysis for fire severity mapping. *Proceedings of 2nd International Conference on Forest Fire Research* (pp. 667–677). Coimbra.
- Calle, A., Casanova, J. L., & Romo, A. (2006). Fire detection and monitoring using MSG Spinning Enhanced Visible and Infrared Imager (SEVIRI) data. *Journal of Geophysical Research – Biosciences*, *111*, doi:10.1029/2005JG000116.
- Carmona-Moreno, C., Belward, A., Malingreau, J. P., Hartley, A., Garcia-Alegre, M., & Antonovskiy, M., et al. (2005). Characterizing interannual variations in global fire calendar using data from Earth observing satellites. *Global Change Biology*, *11*, 1537–1555.
- Ceccato, P., Flasse, S., Tarantola, S., Jacquemoud, S., & Grégoire, J. M. (2001). Detecting vegetation leaf water content using reflectance in the optical domain. *Remote Sensing of Environment*, *77*, 22–33.
- Ceccato, P., Leblon, B., Chuvieco, E., Flasse, S., & Carlson, J. D. (2003). Estimation of live fuel moisture content. In E. Chuvieco (Ed.), *Wildland fire danger estimation and mapping. The role of remote sensing data* (pp. 63–90). Singapore: World Scientific Publishing.
- Chen, D. (2005). Vegetation water content estimation for corn and soybeans using spectral indices derived from MODIS near- and short-wave infrared bands. *Remote Sensing of Environment*, *98*, 225–236.
- Cheng, Y. B., Zarco-Tejada, P. J., Riaño, D., Rueda, C. A., & Ustin, S. (2006). Estimating vegetation water content with hyperspectral data for different canopy scenarios: Relationships between AVIRIS and MODIS indexes. *Remote Sensing of Environment*, *105*, 354–366.
- Chladil, M. A., & Nunez, M. (1995). Assessing grassland moisture and biomass in Tasmania. The application of remote sensing and empirical models for a cloudy environment. *International Journal of Wildland Fire*, *5*, 165–171.
- Chuvieco, E. (Ed.). (1999). *Remote sensing of large wildfires in the european mediterranean basin*. Berlin: Springer-Verlag.
- Chuvieco, E. (Ed.). (2003). *Wildland fire danger estimation and mapping. The role of remote sensing data*. Singapore: World Scientific Publishing.
- Chuvieco, E., Aguado, I., Cocero, D., & Riaño, D. (2003a). Design of an empirical index to estimate fuel moisture content from NOAA-AVHRR analysis in forest fire danger studies. *International Journal of Remote Sensing*, *24*, 1621–1637.

- Chuvieco, E., Allgöwer, B., & Salas, F. J. (2003b). Integration of physical and human factors in fire danger assessment. In E. Chuvieco (Ed.), *Wildland fire danger estimation and mapping. The role of remote sensing data* (pp. 197–218). Singapore: World Scientific Publishing.
- Chuvieco, E., Cocero, D., Aguado, I., Palacios-Orueta, A., & Prado, E. (2004a). Improving burning efficiency estimates through satellite assessment of fuel moisture content. *Journal of Geophysical Research – Atmospheres*, *109*, D14S07, doi:10.1029/2003JD003467, 1–8.
- Chuvieco, E., Cocero, D., Riaño, D., Martín, M. P., Martínez-Vega, J., de la Riva, J., & Pérez, F. (2004b). Combining NDVI and surface temperature for the estimation of live fuel moisture content in forest fire danger rating. *Remote Sensing of Environment*, *92*, 322–331.
- Chuvieco, E., & Congalton, R. G. (1988). Mapping and inventory of forest fires from digital processing of TM data. *Geocarto International*, *4*, 41–53.
- Chuvieco, E., De Santis, A., Riaño, D., & Halligan, K. (2007). Simulation approaches for burn severity estimation using remotely sensed images. *Journal of Fire Ecology*, in press.
- Chuvieco, E., & Martín, M. P. (1994). Global fire mapping and fire danger estimation using AVHRR images. *Photogrammetric Engineering and Remote Sensing*, *60*, 563–570.
- Chuvieco, E., Martín, M. P., & Palacios, A. (2002a). Assessment of different spectral indices in the red-near-infrared spectral domain for burned land discrimination. *International Journal of Remote Sensing*, *23*, 5103–5110.
- Chuvieco, E., Riaño, D., Aguado, I., & Cocero, D. (2002b). Estimation of fuel moisture content from multitemporal analysis of Landsat Thematic Mapper reflectance data: Applications in fire danger assessment. *International Journal of Remote Sensing*, *23*, 2145–2162.
- Chuvieco, E., Riaño, D., Danson, F. M., & Martín, M. P. (2006). Use of a radiative transfer model to simulate the post-fire spectral response to burn severity. *Journal of Geophysical Research – Biosciences*, *111*, doi:10.1029/2005JG000143.
- Chuvieco, E., Riaño, D., Van Wagtenok, J., & Morsdorf, F. (2003c). Fuel Loads and Fuel Type Mapping. In E. Chuvieco (Ed.), *Wildland fire danger estimation and mapping. The role of remote sensing data* (pp. 119–142). Singapore: World Scientific Publishing.
- Chuvieco, E., Ventura, G., Martín, M. P., & Gomez, I. (2005). Assessment of multitemporal compositing techniques of MODIS and AVHRR images for burned land mapping. *Remote Sensing of Environment*, *94*, 450–462.
- Cocero, D., Chuvieco, E., & Salas, J. (2001). El sensor SPOT-Vegetation, una nueva alternativa en la estimación de la humedad de la vegetación. In J. I. Rosell & J. A. Martínez-Casasnovas (Eds.), *Teledetección. Medioambiente y Cambio Global* (pp. 179–182). Lleida: Universitat de Lleida y Editorial Milenio.
- Cochrane, M. A., Alencar, A., Schulze, M. D., Souza, C. M., Nepstad, D. C., Lefebvre, P., & Davidson, E. A. (1999). Positive feedbacks in the fire dynamic of closed canopy tropical forests. *Science*, *284*, 1832–1835.
- Cocke, A. E., Fule, P. Z., & Crouse, J. E. (2005). Comparison of burn severity assessments using Differenced Normalized Burn Ratio and ground data. *International Journal of Wildland Fire*, *14*, 189–198.
- Couturier, S., Taylor, D., Siegert, F., Hoffmann, A., & Bao, M. Q. (2001). ERS SAR backscatter. A potential real-time indicator of the proneness of modified rainforests to fire. *Remote Sensing of Environment*, *46*, 410–417.
- Csiszar, I., Denis, L., Giglio, L., Justice, C. O., & Hewson, J. (2005). Global fire activity from two years of MODIS data. *International Journal of Wildland Fire*, *14*, 117–130.
- Csiszar, I. A., Morisette, J. T., & Giglio, L. (2006). Validation of active fire detection from moderate-resolution satellite sensors: The MODIS example in Northern Eurasia. *IEEE Transactions on Geoscience and Remote Sensing*, *44*, 1757–1764.
- Danson, F. M., & Bowyer, P. (2004). Estimating live fuel moisture content from remotely sensed reflectance. *Remote Sensing of Environment*, *92*, 309–321.
- De Santis, A., & Chuvieco, E. (2007). Burn severity estimation from remotely sensed data: Performance of simulation versus empirical models. *Remote Sensing of Environment*, doi:10.1016/j.rse.2006.1011.1022.

- De Santis, A., Vaughan, P., & Chuvieco, E. (2006). Foliage moisture content estimation from 1-D and 2-D spectroradiometry for fire danger assessment. *Journal of Geophysical Research – Biosciences*, *111*, doi:10.1029/2005JG000149.
- Deeming, J. E., Burgan, R. E., & Cohen, J. D. (1978). *The national fire-danger rating system – 1978*. Ogden, UT: USDA Forest Service, GTR INT-39.
- Dennison, P. E., Roberts Dar, A., Peterson, S. H., & Rechel, J. (2005). Use of normalized difference water index for monitoring live fuel moisture content. *International Journal of Remote Sensing*, *26*, 1035–1042.
- Díaz-Delgado, R., Pons, X., & Lloret, F. (2001). Fire severity effects on vegetation recovery after fire. The Bigues I Riells wildfire case study. In E. Chuvieco & M. P. Martín (Eds.), *Third International workshop on remote sensing and gis applications to forest fire management. New methods and sensors* (pp. 152–155). Paris: EARSeL.
- Dimitrakopoulos, A., & Papaioannou, K. K. (2001). Flammability assessment of Mediterranean forest fuels. *Fire Technology*, *37*, 143–152.
- Dobson, J. E., Bright, E. A., Coleman, P. R., Purfee, R. C., & Worley, B. A. (2000). Landsat: A global population database for estimating populations at risk. *Photogrammetric Engineering and Remote Sensing*, *66*, 849–857.
- Dozier, J. (1981). A method for satellite identification of surface temperature fields of subpixel resolution. *Remote Sensing of Environment*, *11*, 221.
- Dwyer, E., Pereira, J. M. C., Grégorie, J.-M., & DaCamara, C. C. (2000). Characterization of the spatio-temporal patterns of global fire activity using satellite imagery for the period April 1992 to March 1993. *Journal of Biogeography*, *27*, 57–69.
- Eidenshink, J. C., & Faundeen, J. L. (1994). The 1 km AVHRR Global Land Data Set – 1st Stages in implementation. *International Journal of Remote Sensing*, *15*, 3443–3462.
- Elvidge, C. D. (2001). DMSP-OLS estimation of tropical forest area impacted by surface fires in Roraima, Brazil: 1995 versus 1998. *International Journal of Remote Sensing*, *22*, 2661–2673.
- Epting, J., Verbyla, D. L., & Sorbel, B. (2005). Evaluation of remotely sensed indices for assessing burn severity in interior Alaska using Landsat TM and ETM+. *Remote Sensing of Environment*, *96*, 328–339.
- Everitt, J. H., & Nixon, P. R. (1986). Canopy Reflectance of two drought-stressed shrubs. *Photogrammetric Engineering and Remote Sensing*, *52*, 1189–1192.
- Fazakas, Z., Nilsson, M., & Olsson, H. (1999). Regional forest biomass and wood volume estimation using satellite data and ancillary data. *Agricultural and Forest Meteorology*, *98–99*, 417–425.
- Fearnside, P. M., Lima de Alencastro Graça, P. M., & Alves Rodriguez, F. J. (2001). Burning of Amazonian rainforests: Burning efficiency and charcoal formation in forest cleared for cattle pasture near Manaus, Brazil. *Forest Ecology and Management*, *146*, 115–128.
- Ferek, R. J., Reid, J. S., Hobbs, P. V., Blake, D. R., & Liousse, C. (1998). Emission factors of hydrocarbons, halocarbons, trace gases and particles from biomass burning in Brazil. *Journal of Geophysical Research-Atmosphere*, *103*, 32107–32118.
- Ferrare, R. A., Fraser, R. S., & Kaufman, Y. J. (1990). Satellite measurements of large-scale air pollution: Measurements of forest fire smoke. *Journal of Geophysical Research*, *95*, 9911–9925.
- Flannigan, M. D., & Vonder Haar, T. H. (1986). Forest fire monitoring using NOAA satellite AVHRR. *Canadian Journal of Forest Research*, *16*, 975–982.
- Flasse, S. P., & Ceccato, P. (1996). A contextual algorithm for AVHRR fire detection. *International Journal of Remote Sensing*, *17*, 419–424.
- Fourty, T., & Baret, F. (1997). Vegetation water and dry matter contents estimated from top-of-the-atmosphere reflectance data: A simulation study. *Remote Sensing of Environment*, *61*, 34–45.
- França, H., & Setzer, A. W. (2001). AVHRR analysis of a savanna site through a fire season in Brazil. *International Journal of Remote Sensing*, *22*, 2449–2461.
- Fraser, R. H., Li, Z., & Cihlar, J. (2000). Hotspot and NDVI Differencing Synergy (HANDS): A new technique for burned area mapping over boreal forest. *Remote Sensing of Environment*, *74*, 362–376.

- Friedl, M. A., McIver, D. K., Hodges, J. C. F., Zhang, X. Y., Muchoney, D., & Strahler, A. H., et al. (2002). Global land cover mapping from MODIS: Algorithms and early results. *Remote Sensing of Environment*, 83, 287–302.
- Fuller, D. O., & Fulk, M. (2000). Comparison of NOAA-AVHRR and DMSP-OLS for operational fire monitoring in Kalimantan, Indonesia. *International Journal of Remote Sensing*, 21, 181–187.
- García-Haro, F. J., Gilabert, M. A., & Meliá, J. (2001). Monitoring fire-affected areas using Thematic Mapper data. *International Journal of Remote Sensing*, 22, 533–549.
- Garcia, M., & Chuvieco, E. (2004). Assessment of the potential of SAC-C/MMRS imagery for mapping burned areas in Spain. *Remote Sensing of Environment*, 92, 414–423.
- Giglio, L., Csiszar, I., & Justice, C. O. (2006a). Global distribution and seasonality of active fires as observed with the Terra and Aqua Moderate Resolution Imaging Spectroradiometer (MODIS) sensors. *Journal of Geophysical Research-Biogeosciences*, 111, doi:10.1029/2005JG000142.
- Giglio, L., Descloitres, J., Justice, C. O., & Kauffman, J. B. (2003a). An enhanced contextual fire detection algorithm for MODIS. *Remote Sensing of Environment*, 87, 273–282.
- Giglio, L., Kendall, J. D., & Mack, R. (2003b). A multi-year active fire dataset for the tropics derived from the TRMM VIRS. *International Journal of Remote Sensing*, 24, 4505–4525.
- Giglio, L., van der Werf, G. R., Randerson, J. T., Collatz, G. J., & Kasibhatla, P. S. (2006b). Global estimation of burned area using MODIS active fire observations. *Atmospheric Chemistry and Physics*, 6, 957–974.
- Gillon, D., Dauriac, F., Deshayes, M., Vallette, J. C., & Moro, C. (2004). Estimation of foliage moisture content using near infrared reflectance spectroscopy. *Agricultural and Forest Meteorology*, 124, 51–62.
- Grégoire, J. M., Cahoon, D. R., Stroppiana, D., Li, Z., Pinnock, S., & Eva, H., et al. (2001). Forest fire monitoring and mapping for GOF: Current products and information networks based on NOAA-AVHRR, ERS-ATSR, and SPOT-VGT systems. In F. Ahern, J. Goldammer & C. O. Justice (Eds.), *Global and regional fire monitoring from space: Planning a coordinated international effort* (pp. 105–124). The Hague: SPB Academic.
- Hao, W. M., Ward, D. E., Olbu, G., & Baker, S. P. (1996). Emissions of CO₂, CO, and Hydrocarbons from fires in diverse african savanna ecosystems. *Journal Of Geophysical Research-Atmospheres*, 101, 23577–23584.
- Harding, D. J., & Carabajal, C. C. (2005). ICESat waveform measurements of within-footprint topographic relief and vegetation vertical structure. *Geophysical Research Letters*, 32, doi: 10.1029/2005GL023471, 023474
- Hardy, C. C., & Burgan, R. E. (1999). Evaluation of NDVI for monitoring live moisture in three vegetation types of the Western U.S. *Photogrammetric Engineering and Remote Sensing*, 65, 603–610.
- Hirsch, K. G. (1996). *Canadian Forest Fire Behavior Prediction (FBP) System : User's guide*. Edmonton, Canada: Northern Forestry Centre.
- Hirsch, S. N., Kruckeberg, R. F., & Madden, F. H. (1971). The bispectral forest detection system. In *7th Inter. Symp. on Remote Sensing of Environment* (pp. 2253–2259). Ann Arbor, MI.
- Hoffa, E. A., Ward, D. E., Hao, W. M., Susott, R. A., & Wakimoto, R. H. (1999). Seasonality of carbon emissions from biomass burning in a Zambian savanna. *Journal of Geophysical Research-Atmosphere*, 104, 13841–13853.
- Holben, B. N., Schutt, J. B., & McMurtrey, J. (1983). Leaf water stress detection utilizing thematic mapper bands 3, 4 and 5 in soybean plants. *International Journal of Remote Sensing*, 4, 289–297.
- Houghton, R. A. (2005). Tropical deforestation as a source of greenhouse gas emissions. In P. Moutinho & S. Schwartzman (Eds.), *Tropical deforestation and climate change* (pp. 13–21). Belem: Amazon Institute for Environmental Research.
- Houghton, R. A., Boone, R. D., Melillo, J. M., Palm, C. A., Woodwell, G. M., & Myers, N., et al. (1985). Net flux of carbon dioxide from tropical forests in 1980. *Nature*, 316, 617–620.
- Hunt, E. R., Rock, B. N., & Nobel, P. S. (1987). Measurement of leaf relative water content by infrared reflectance. *Remote Sensing of Environment*, 22, 429–435.

- Hyypä, J., Hyypä, H., Inkinen, M., Engdahl, M., Linko, S., & Zhu, Y. H. (2000). Accuracy comparison of various remote sensing data sources in the retrieval of forest stand attributes. *Forest Ecology and Management*, 128, 109–120.
- Jackson, R. D., Idso, S. B., Reginato, R. J., & Pinter, P. J. (1981). Canopy temperature as a crop water stress indicator. *Water Resources Research*, 17, 1133–1138.
- Jain, T. B., Pilliod, D., & Graham, R. T. (2004). Tongue-tied. Confused meanings for common fire terminology can lead to fuels mismanagement. A new framework is needed to clarify and communicate the concepts. *Wildfire*, 4, 22–26.
- Jakubauskas, M. E., Lulla, K. P., & Mausell, P. W. (1990). Assessment of vegetation change in a fire-altered forest landscape. *Photogrammetric Engineering and Remote Sensing*, 56, 371–377.
- Johnson, E. A., & Miyanishi, K. (2001). *Forest fires: Behavior and ecological effects*. San Diego, Calif.: Academic Press.
- Jones, D. A. (1992). *Nomenclature of hazard and risk assessment in the process industries*. Rugby, Warwickshire, UK: Institution of Chemical Engineers.
- Justice, C. O., Giglio, L., Korontzi, S., Owens, J., Morisette, J. T., & Roy, D., et al. (2002a). The MODIS fire products. *Remote Sensing of Environment*, 83, 244–262.
- Justice, C. O., Townshend, J. R. G., Vermote, E. F., Masuoka, E., Wolfe, R. E., & Saleous, N., et al. (2002b). An overview of MODIS Land data processing and product status. *Remote Sensing of Environment*, 83, 3–15.
- Kasischke, E., & French, N. H. (1995). Locating and estimating the areal extent of wildfires in Alaskan boreal forest using multiple-season AVHRR NDVI composite data. *Remote Sensing of Environment*, 51, 263–275.
- Kasischke, E. S., Melack, J. M., & Dobson, M. C. (1997). The use of imaging radars for ecological applications – A review. *Remote Sensing of Environment*, 59, 141–156.
- Kasischke, E. S., & Turetsky, M. R. (2006). Recent changes in the fire regime across the North American boreal region – Spatial and temporal patterns of burning across Canada and Alaska. *Geophysical Research Letters*, 33, 1–5.
- Kaufman, Y. J., Setzer, A., Ward, D., Tanre, D., Holben, B. N., Menzel, P., et al. (1992). Biomass burning airborne and spaceborne experiment in the Amazonas (Base-A). *Journal of Geophysical Research*, 97, 14581–14599.
- Kennedy, P. J., Belward, A. S., & Grégoire, J. M. (1994). An improved approach to fire monitoring in West Africa using AVHRR data. *International Journal of Remote Sensing*, 15, 2235–2255.
- Key, C. (2005). Remote Sensing sensitivity to fire severity and fire recovery. In J. Riva, F. Pérez-Cabello & E. Chuvieco (Eds.), *Proceedings of the 5th International Workshop on Remote Sensing and GIS applications to Forest Fire Management: Fire Effects Assessment* (pp. 29–39). Zaragoza: Universidad de Zaragoza, GOF-C-GOLD, EARSeL.
- Key, C., & Benson, N. (2002). Landscape Assessment, in Fire effects monitoring (FireMon) and inventory protocol: integration of standardized field data collection techniques and sampling design with remote sensing to assess fire effects. In *NPS-USGS National Burn Severity Mapping Project*.
- Key, C. H., & Benson, N. (2004). Ground Measure of Severity: The Composite Burn Index. FIRE-MON Landscape Assessment V4. <http://burnseverity.cr.usgs.gov/methodology.asp>
- Korontzi, S., Roy, D. P., Justice, C. O., & Ward, D. E. (2004). Modeling and sensitivity analysis of fire emissions in southern Africa during SAFARI 2000. *Remote Sensing of Environment*, 92, 255–275.
- Koutsias, N., Karteris, M., Fernández, A., Navarro, C., Jurado, J., Navarro, R., & Lobo, A. (1999). Burnt land mapping at local scale. In E. Chuvieco (Ed.), *Remote sensing of large wildfires in the european mediterranean basin* (pp. 123–138). Berlin: Springer-Verlag.
- Langaas, S. (1992). Temporal and spatial distribution of Savanna fires in Senegal and the Gambia, West Africa, 1989–1990, derived from multi-temporal AVHRR night images. *International Journal of Wildland Fire*, 2, 21–36.
- Leblon, B., Kasischke, E. S., Alexander, M. E., Doyle, M., & Abbott, M. (2002). Fire danger monitoring using ERS-1 SAR images in the case of northern boreal forests. *Natural Hazards*, 27, 231–255.

- Lefsky, M. A., Harding, D. J., Keller, M., Cohen, W. B., Carabajal, C. C., & Espirito-Santo, F. D. et al. (2005). Estimates of forest canopy height and aboveground biomass using ICESat. *Geophysical Research Letters*, 32, doi:10.1029/2005GL023971.
- Lentile, L. B., Holden, Z. A., Smith, A. M. S., Falkowski, M. J., Hudak, A. T., & Morgan, P. et al. (2006). Remote sensing techniques to assess active fire characteristics and post-fire effects. *International Journal of Wildland Fire*, 15, 319–345.
- Levine, J. S. (2000). Global biomass burning: A case study of the gaseous and particulate emissions released to the atmosphere during the 1997 Fires in Kalimantan and Sumatra, Indonesia. In J. L. Innes, M. Beniston & M. M. Verstraete (Eds.), *Biomass burning and its inter-relationships with the climate system* (pp. 15–31). Dordrecht – Boston – London: Kluwer Academic Publishers.
- Li, R. R., Kaufman, Y. J., Hao, W. M., Salmon, J. M., & Gao, B. C. (2004). A technique for detecting burn scars using MODIS Data. *IEEE Transactions on Geoscience and Remote Sensing*, 42, 1300–1308.
- Li, Z., Nadon, S., & Cihlar, J. (2000). Satellite-based detection of Canadian boreal forest fires: Development and application of the algorithm. *International Journal of Remote Sensing*, 21, 3057–3069.
- Liousse, C., Andreae, M. O., Artaxo, P., Barbosa, P., Cachier, H., & Grégoire, J. M. et al. (2004). Deriving global quantitative estimates for spatial and temporal distributions of biomass burning emissions. In C. Granier, P. Artaxo & C. E. Reeves (Eds.), *Emissions of atmospheric trace compounds* (pp. 77–120). Dordrecht: Kluwer Academic Publishers.
- López García, M. J., & Caselles, V. (1991). Mapping burns and natural reforestation using thematic mapper data. *Geocarto International*, 1, 31–37.
- Maggi, M., & Stroppiana, D. (2002). Advantages and drawbacks of NOAA–AVHRR and SPOT–VGT for burnt area mapping in a tropical savanna ecosystem. *Canadian Journal of Remote Sensing*, 28, 231–245.
- Malingreau, J. P., Stevens, G., & Fellows, L. (1985). Remote sensing of forest fires: Kalimantan and North Borneo in 1982–1983. *Ambio*, 14, 314–321.
- Martín, M. P., Ceccato, P., Flasse, S., & Downey, I. (1999). Fire detection and fire growth monitoring using satellite data. In E. Chuvieco (Ed.), *Remote sensing of large wildfires in the european mediterranean basin* (pp. 101–122). Berlin: Springer-Verlag.
- Martín, M. P., & Chuvieco, E. (1995). Mapping and evaluation of burned land from multi-temporal analysis of AVHRR NDVI images. *EARSeL Advances in Remote Sensing*, 4(3), 7–13.
- Martín, M. P., Díaz Delgado, R., Chuvieco, E., & Ventura, G. (2002). Burned land mapping using NOAA–AVHRR and TERRA–MODIS. In D. X. Viegas (Ed.), *IV International conference on forest fire research. 2002 Wildland fire safety summit* (p. 45). Luso, Coimbra, Portugal: Millpress.
- Martínez, S., Tourné, I., Gonzalo de Grado, J., & Casanova, J. L. (2000). Programa FUEGO: Detección y seguimiento de incendios desde el espacio. In *IX Simposio Latinoamericano de Percepción Remota*. Iguazú.
- Matson, M., & Holben, B. (1987). Satellite detection of tropical burning in Brazil. *International Journal of Remote Sensing*, 8, 509–516.
- Matson, M., Schneider, S. R., Aldridge, B., & Satchwell, B. (1984). *Fire detection using the NOAA-Series satellites*. Washington, DC: NOAA, NESDIS 7.
- Matson, M., Stephens, G., & Robinson, J. (1987). Fire detection using data from the NOAA–N satellites. *International Journal of Remote Sensing*, 8, 961–970.
- Merrill, D. F., & Alexander, M. E. (1987). *Glossary of forest fire management terms*. Ottawa: National Research Council of Canada, Committee for Forest Fire Management.
- Miller, H. J., & Yool, S. R. (2002). Mapping forest post-fire canopy consumption in several overstorey types using multi-temporal Landsat TM and ETM data. *Remote Sensing of Environment*, 82, 481–496.
- Minick, G. R., & Shain, W. A. (1981). Comparison of satellite imagery and conventional aerial photography in evaluating a large forest fire. In *Seventh International Symposium Machine Processing of Remotely Sensed Data* (pp. 544–546). West Lafayette.

- Mollicone, D., Eva, H. D., & Achard, F. (2006). Human role in Russian wild fires. *Nature*, *440*, 436–437.
- Moran, M. S., Clarke, T. R., Inoue, Y., & Vidal, A. (1994). Estimating crop water deficit using the relation between surface-air temperature and spectral vegetation index. *Remote Sensing of Environment*, *49*, 246–263.
- Moreno, J. M., & Oechel, W. C. (1989). A simple method for estimating fire intensity after a burn in California Chaparral. *Acta Ecologica (Ecologia plantarum)*, *10*, 57–68.
- Morisette, J. T., Giglio, L., Csiszar, I., & Justice, C. O. (2005). Validation of the MODIS active fire product over Southern Africa with ASTER data. *International Journal of Remote Sensing*, *26*, 4239–4264.
- Morisette, J. T., Privette, J. L., & Justice, C. O. (2002). A framework for the validation of MODIS Land products. *Remote Sensing of Environment*, *83*, 77–96.
- Morsdorf, F., Meier, E., Kotz, B., Itten, K. I., Dobbertin, M., & Allgower, B. (2004). LIDAR-based geometric reconstruction of boreal type forest stands at single tree level for forest and wildland fire management. *Remote Sensing of Environment*, *92*, 353–362.
- Morton, D., DeFries, R., Giglio, L., Schroeder, W., Csiszar, I., & Morisette, J. et al. (2006). Distinguishing between conversion and maintenance fires in the Amazon. In *Tenth LBA-ECO Science Team Meeting*. Brasilia, Brazil.
- Nelson, R. M. (2001). Water relations of forest fuels. In E. A. Johnson & K. Miyaniishi (Eds.), *Forest fires : Behavior and ecological effects* (pp. 79–149). San Diego, Calif.: Academic Press.
- Omi, P. N. (2005). *Forest fires : A reference handbook*. Santa Barbara, Calif.: ABC-CLIO.
- Palacios-Orueta, A., Chuvieco, E., Parra, A., & Carmona-Moreno, C. (2005). Biomass burning emissions: A review of models using remote-sensing data. *Environmental Monitoring and Assessment*, *104*, 189–209.
- Palacios-Orueta, A., Parra, A., Chuvieco, E., & Carmona, C. (2004). Remote sensing and geographic information system methods for global spatiotemporal modelling of biomass burning emissions: Assessment in the African continent. *Journal of Geophysical Research – Atmospheres*, *109*, 1–12.
- Paltridge, G. W., & Barber, J. (1988). Monitoring grassland dryness and fire potential in Australia with NOAA/AVHRR data. *Remote Sensing of Environment*, *25*, 381–394.
- Parra, A., & Chuvieco, E. (2005). Assessing burn severity using Hyperion data. In J. Riva, F. Pérez-Cabello & E. Chuvieco (Eds.), *Proceedings of the 5th International workshop on remote sensing and GIS applications to Forest Fire Management: Fire Effects Assessment* (pp. 239–244). Paris: Universidad de Zaragoza, GOF-C-GOLD, EARSeL.
- Peñuelas, J., Piñol, J., Ogaya, R., & Filella, I. (1997). Estimation of plant water concentration by the reflectance Water Index WI (R900/R970). *International Journal of Remote Sensing*, *18*, 2869–2875.
- Pereira, J. M. C. (1999). A comparative evaluation of NOAA/AVHRR Vegetation indexes for burned surface detection and mapping. *IEEE Transactions on Geoscience and Remote Sensing*, *37*, 217–226.
- Pereira, J. M. C., Mota, B., Privette, J. L., Caylor, K. K., Silva, J. M. N., Sa, A. C. L., & Ni-Meister, W. (2004). A simulation analysis of the detectability of understory burns in miombo woodlands. *Remote Sensing of Environment*, *93*, 296–310.
- Pereira, J. M. C., Sa, A. C. L., Sousa, A. M. O., Silva, J. M. N., Santos, T. N., & Carreiras, J. M. B. (1999). Spectral characterisation and discrimination of burnt areas. In E. Chuvieco (Ed.), *Remote sensing of large wildfires in the European mediterranean basin* (pp. 123–138). Berlin: Springer-Verlag.
- Pérez, B., & Moreno, J. (1998). Methods for quantifying fire severity in shrubland-fires. *Plant Ecology*, *139*, 91–101.
- Peters, A. J., Walter-Shea, E. A., Ji, L., Viña, A., Hayes, M., & Svodoba, M. D. (2002). Drought monitoring with NDVI-based standardized vegetation index. *Photogrammetric Engineering and Remote Sensing*, *62*, 71–75.
- Piccolini, I., & Arino, O. (2000). Towards a global burned surface world Atlas. *Earth Observation Quarterly*, *65*, 14–18.

- Pinnock, S., & Grégoire, J. M. (Eds.). (1999). *World fire web: A global fire observation system*. Luxembourg: Publications of the European Communities.
- Price, J. C. (2003). Comparing MODIS and ETM+ data for regional and global land classification. *Remote Sensing of Environment*, *86*, 491–499.
- Prins, E. M., Feltz, J. M., Menzel, W. P., & Ward, D. E. (1998). An overview of GOES-8 diurnal fire and smoke results for SCAR-B and 1995 fire season in South America. *Journal of Geophysical Research*, *103*, 31821–31836.
- Prins, E. M., & Menzel, W. P. (1992). Geostationary satellite detection of biomass burning in South America. *International Journal of Remote Sensing*, *13*, 2783–2799.
- Pyne, S. J. (1995). *World fire. The culture of fire on earth*. Seattle and London: University of Washington Press.
- Radeloff, V. C., Hammer, R. B., Stewart, S. I., Fried, J. S., Holcomb, S. S., & McKeefry, J. F. (2005). The wildland-urban interface in the United States. *Ecological Applications*, *15*, 799–805.
- Randerson, J. T., Liu, H., Flanner, M. G., Chambers, S. D., Jin, Y., & Hess, P. G. et al. (2006). The impact of boreal forest fire on climate warming. *Science*, *314*, 1130–1132.
- Randerson, J. T., van der Werf, G. R., Collatz, G. J., Giglio, L., Still, C. J., & Kasibhatla, P. et al. (2005). Fire emissions from C 3 and C 4 vegetation and their influence on interannual variability of atmospheric CO₂ and D13 CO₂. *Global Biogeochemical Cycles*, *19*, doi:10.1029/2004GB002366.
- Randriambelo, T., Baldy, S., & Bessafi, M. (1998). An improved detection and characterization of active fires and smoke plumes in south-eastern Africa and Madagascar. *International Journal of Remote Sensing*, *19*, 2623–2638.
- Ranson, K. J., Sun, G., Kharuk, V. I., & Kovacs, K. (2001). Characterization of forests in Western Sayani Mountains, Siberia from SIR-C SAR data. *Remote Sensing of Environment*, *75*, 188–200.
- Riaño, D., Chuvieco, E., Condés, S., González-Matesanz, J., & Ustin, S. L. (2004). Generation of crown bulk density for *Pinus sylvestris* L. from lidar. *Remote Sensing of Environment*, *92*, 345–352.
- Riaño, D., Chuvieco, E., Salas, J., Palacios-Orueta, A., & Bastarrica, A. (2002). Generation of fuel type maps from Landsat TM images and ancillary data in Mediterranean ecosystems. *Canadian Journal of Forest Research*, *32*, 1301–1315.
- Riaño, D., Chuvieco, E., Ustin, S. L., Salas, J., Rodríguez-Pérez, J. R., & Ribeiro, L. M. et al. (2007a). Estimation of shrub height for fuel type mapping combining airborne LiDAR and simultaneous color infrared ortho image. *International Journal of Wildland Fire*, *16*, 341–348.
- Riaño, D., Meier, E., Allgöwer, B., Chuvieco, E., & Ustin, S. L. (2003). Modeling airborne laser scanning data for the spatial generation of critical forest parameters in fire behavior modeling. *Remote Sensing of Environment*, *86*, 177–186.
- Riaño, D., Ruiz, J. A. M., Isidoro, D., Ustin, S. L., & Riaño, D. (2007b). Global spatial patterns and temporal trends of burned area between 1981 and 2000 using NOAA-NASA Pathfinder. *Global Change Biology*, *13*, 40–50, doi: 10.1111/j.1365-2486.2006.01268.
- Riaño, D., Vaughan, P., Chuvieco, E., Zarco-Tejada, P., & Ustin, S. L. (2005). Estimation of fuel moisture content by inversion of radiative transfer models to simulate equivalent water thickness and dry matter content: Analysis at leaf and canopy level. *IEEE Transactions on Geoscience and Remote Sensing*, *43*, 819–826.
- Roberts, D. A., Peterson, S., Dennison, P. E., Sweeney, S., & Rechel, J. (2006). Evaluation of Airborne Visible/Infrared Imaging Spectrometer (AVIRIS) and Moderate Resolution Imaging Spectrometer (MODIS) measures of live fuel moisture and fuel condition in a shrubland ecosystem in southern California. *Journal of Geophysical Research*, *111*, G04S02, doi:10.1029/2005JG000113.
- Rogan, J., & Franklin, J. (2001). Mapping wildfire burn severity in Southern California Forests and shrublands using enhanced Thematic Mapper imagery. *Geocarto International*, *16*, 89–99.
- Rollins, M. G., Keane, R. E., & Parsons, R. A. (2004). Mapping fuels and fire regimes using remote sensing, ecosystem simulation, and gradient modeling. *Ecological Applications*, *14*, 75–95.

- Roy, D., Frost, P., Justice, C., Landmann, T., Roux, J., & Gumbo, K. et al. (2005a). The Southern Africa Fire Network (SAFNet) regional burned area product validation protocol. *International Journal of Remote Sensing*, 26, 4265–4292.
- Roy, D., Jin, Y., Lewis, P., & Justice, C. (2005b). Prototyping a global algorithm for systematic fire-affected area mapping using MODIS time series data. *Remote Sensing of Environment*, 97, 137–162.
- Roy, D., & Landmann, T. (2005). Characterizing the surface heterogeneity of fire effects using multi-temporal reflective wavelength data. *International Journal of Remote Sensing*, 26, 4197–4218.
- Roy, D., Lewis, P. E., & Justice, C. O. (2002). Burned area mapping using multi-temporal moderate spatial resolution data—a bi-directional reflectance model-based expectation approach. *Remote Sensing of Environment*, 83, 263–286.
- Roy, D. P., Boschetti, L., & Trigg, S. N. (2006). Remote sensing of fire severity: Assessing the performance of the normalized burn ratio. *IEEE Transactions on Geoscience and Remote Sensing*, 3, 112–116.
- Roy, D. P., Giglio, L., Kendall, J. D., & Justice, C. O. (1999). Multi-temporal active-fire based burn scar detection algorithm. *International Journal of Remote Sensing*, 20, 1031–1038.
- Sá, A. C. L., Silva, J. M. N., Pereira, J. M. C., & Vasconcelos, M. J. (2001). Burned area detection in the Miombo of Northern Mozambique using MODIS and Landsat Data. In E. Chuvieco & M. P. Martín (Eds.), *Third international workshop on remote sensing and GIS applications to Forest Fire Management. New methods and sensors* (pp. 156–160). Paris: EARSeL.
- Salvador, R., Valeriano, J., Pons, X., & Díaz-Delgado, R. (2000). A semi-automatic methodology to detect fire scars in shrubs and evergreen forests with Landsat MSS time series. *International Journal of Remote Sensing*, 21, 655–671.
- Sandholt, I., Rasmussen, K., & Andersen, J. (2002). A simple interpretation of the surface temperature/vegetation index space for assessment of surface moisture status. *Remote Sensing of Environment*, 79, 213–224.
- Saunders, R. W., & Kriebel, K. T. (1988). An improved method for detecting clear sky and cloudy radiances from AVHRR data. *International Journal of Remote Sensing*, 9, 123–150.
- Seiler, W., & Crutzen, P. J. (1980). Estimates of gross and net fluxes of carbon between the biosphere and the atmosphere from biomass burning. *Climatic Change*, 2, 207–247.
- Setzer, A. W., & Pereira, M. C. (1991). Operational detection of fires in Brazil with NOAA-AVHRR. In *Twenty-fourth. International Symp. on Remote Sensing of Environment* (pp. 469–482). Rio de Janeiro.
- Siljeström, P., & Moreno, A. (1995). Monitoring burnt areas by principal components analysis of multi-temporal TM data. *International Journal of Remote Sensing*, 16, 1577–1587.
- Simon, M., Plummer, S., Fierens, F., Hoelzemann, J. J., & Arino, O. (2004). Burnt area detection at global scale using ATSR-2: The GLOBSCAR products and their qualification. *Journal of Geophysical Research – Atmospheres*, 109, D14S02, doi:10.1029/2002JD003622, 1–16.
- Sims, D. A., & Gamon, J. A. (2003). Estimation of vegetation water content and photosynthetic tissue area from spectral reflectance: A comparison of indices based on liquid water and chlorophyll absorption features. *Remote Sensing of Environment*, 84, 526–537.
- Skole, D., & Tucker, C. (1993). Tropical deforestation and habitat fragmentation in the Amazon. Satellite data from 1978 to 1988. *Science*, 260, 1905–1910.
- Sousa, A. M. O., Pereira, J. M. C., & Silva, J. M. N. (2003). Evaluating the performance of multitemporal image compositing algorithms for burned area analysis. *International Journal of Remote Sensing*, 24, 1219–1236.
- Souza, C. M., Roberts, D. A., & Cochrane, M. A. (2005). Combining spectral and spatial information to map canopy damage from selective logging and forest fires. *Remote Sensing of Environment*, 98, 329–343.
- Spencer, J. E. (1966). *Shifting cultivation in Southeastern Asia*. Berkeley: University of California Press.
- Stow, D., Nipadkar, M., & Kaiser, J. (2005). MODIS-derived visible atmospherically resistant index for monitoring chaparral moisture content. *International Journal of Remote Sensing*, 26, 3867–3873.

- Stroppiana, D., Brivio, P. A., & Grégoire, J.-M. (2000a). Modelling the impact of vegetation fires, detected from NOAA-AVHRR data, on tropospheric chemistry in Tropical Africa. In J. L. Innes, M. Beniston & M. M. Verstraete (Eds.), *Biomass burning and its inter-relationships with the climate system* (pp. 193–213). Dordrecht, Boston, London: Kluwer Academic Publishers.
- Stroppiana, D., Pinnock, S., & Gregoire, J. M. (2000b). The global fire product: Daily fire occurrence from April 1992 to December 1993 derived from NOAA AVHRR data. *International Journal of Remote Sensing*, *21*, 1279–1288.
- Sukhinin, A. I., French, N. H. F., Kasischke, E. S., Hewson, J. H., Soja, A. J., & Csaszar, I. A. et al. (2004). AVHRR-based mapping of fires in Russia: New products for fire management and carbon cycle studies. *Remote Sensing of Environment*, *93*, 546–564.
- Tansey, K., Grégoire, J. M., Stroppiana, D., Sousa, A., Silva, J., & Pereira, J. M. et al. (2004). Vegetation burning in the year 2000: Global burned area estimates from SPOT VEGETATION data. *Journal of Geophysical Research – Atmospheres*, *109*, D14S03, doi:10.1029/2002JD003598, 2–22.
- Thompson, O. R., & Wehmanen, O. A. (1979). Using Landsat digital data to detect moisture stress. *Photogrammetric Engineering and Remote Sensing*, *45*, 201–207.
- Tian, Q., Tong, Q., Pu, R., Guo, X., & Zhao, C. (2001). Spectroscopic determination of wheat water status using 1650–1850 nm spectral absorption features. *International Journal of Remote Sensing*, *22*, 2329–2338.
- Toutin, T., & Amaral, S. (2000). Stereo RADARSAT data for canopy height in Brazilian forests. *Canadian Journal of Remote Sensing*, *26*, 189–199.
- van der Werf, G. R., Randerson, J. T., Collatz, G. J., Giglio, L., Kasibhatla, P. S., & Arellano, A. F. et al. (2004). Continental Scale-partitioning of fire emissions during the 1997 to 2001 El Niño/La Niña period. *Science*, *303*, 73–76.
- van der Werf, G. R., Randerson, J. T., Giglio, L., Collatz, G. J., Kasibhatla, P. S., & Arellano, A. F. (2006). Interannual variability in global biomass burning emissions from 1997 to 2004. *Atmospheric Chemistry and Physics*, *6*, 3423–3441.
- van Wagendonk, J. W., Root, R. R., & Key, C. H. (2004). Comparison of AVIRIS and Landsat ETM+ detection capabilities for burn severity. *Remote Sensing of Environment*, *92*, 397–408.
- Van Wilgen, B. W. (1997). *Fire in southern African savannas : Ecological and atmospheric perspectives*. Johannesburg, South Africa: Witwatersrand University Press Thorold's Africana Books [distributor].
- Vázquez, A., Cuevas, J. M., & González-Alonso, F. (2001). Comparison of the use of WiFS and LISS images to estimate the area burned in a large forest fire. *International Journal of Remote Sensing*, *22*, 901–907.
- Vega-García, C., & Chuvieco, E. (2006). Applying local measures of spatial heterogeneity to Landsat-TM images for predicting wildfire occurrence in Mediterranean landscapes. *Landscape Ecology*, *21*, 595–605.
- Venkataraman, C., Habib, G., Kadamba, D., Shrivastava, M., Leon, J. F., Crouzille, B., Boucher, O., & Streets, D. G. (2006). Emissions from open biomass burning in India: Integrating the inventory approach with high-resolution Moderate Resolution Imaging Spectroradiometer (MODIS) active-fire and land cover data. *Global Biogeochemical Cycles*, *20*. GB2013, doi: 2010.1029/2005GB002547
- Vidal, A., Pinglo, F., Durand, H., Devaux-Ros, C., & Maillet, A. (1994). Evaluation of a temporal fire risk index in Mediterranean forest from NOAA thermal IR. *Remote Sensing of Environment*, *49*, 296–303.
- Wheatherspoon, C. P., & Skinner, C. N. (1995). An assessment of factors associate with damage to tree crowns from the 1987 wildfires in Northern California. *Forest Science*, *41*, 430–451.
- White, J. D., Ryan, K. C., Key, C. C., & Running, S. W. (1996). Remote sensing of forest fire severity and vegetation recovery. *International Journal of Wildland Fire*, *6*, 125–136.
- Yebra, M., Chuvieco, E., & Riaño, D. (2007). Estimation of live Fuel Moisture Content from MODIS images for fire risk assessment. *Agricultural and Forest Meteorology*, in press.
- Zarco-Tejada, P. J., Rueda, C. A., & Ustin, S. L. (2003). Water content estimation in vegetation with MODIS reflectance data and model inversion methods. *Remote Sensing of Environment*, *85*, 109–124.

- Zheng, D. L., Prince, S. D., & Wright, R. (2001). *NPP Multi-Biome: Gridded estimates for selected regions worldwide, 1989–2001*. Available on-line [<http://www.daac.ornl.gov/>]. Oak Ridge, Tennessee, U.S.A: Oak Ridge National Laboratory. Distributed Active Archive Center.
- Zhu, Z., & Evans, D. L. (1994). U.S. forest types and predicted percent forest cover from AVHRR data. *Photogrammetric Engineering and Remote Sensing*, 60, 525–531.

Chapter 7

Satellites Oceans Observation in Relation to Global Change

Manuel Cantón-Garbín

Abstract In this chapter we emphasize the importance of the oceans in the control of the Earth climate due to its capacity to transfer and redistribute heat over all the planet and due to its greenhouse gases absorption capacity. Satellites are measuring from thirty years ago physical and biological parameters (temperature, productivity, sea level, global winds and waves) that inform us about the global variability of these parameters during the last decades. It is not possible to infer long term changes from this time scale, but the changes measured from the space are in good agreement with the predictions from other data sources and climate models. If we stop immediately our contaminating and emissions of greenhouses gases activities, the Earth could take about 1,000 years to return to its “normal” cycles. It is too late to follow by the way of the sustainable development, it’s time for a sustainable retreat (Lovelock 2007). An irreversible global change could be so close to trust that the international agreements save to the civilization from global change. So, its time for fast actions.

7.1 Climate Change and its Causes

More than four thousand million years ago, the earth separated from the Sun and started its existence in the Solar System. The Earth’s climate was born at the same time. From then on, the climate has always been changing on any time scale we may consider, but never with the speed that it has been changing during the last century (see CD for a detailed set of figs. and images).

Changes in the climate constitute shifts in meteorological conditions lasting a few years or longer. If these changes are produced at minor temporal scales (days to years), we speak about the variability of the climate instead of change (Burroughs 2001, Uriarte A 2003).

In parallel with temperature changes and the snow and ice cover of the earth, the sea level has been fluctuating from -120 m to $+70$ m from the actual level, supposing the completely frozen or melting of oceans, respectively.

Furthermore, the climate is a nonlinear phenomenon (small variations in the initial conditions of the climatic system can produce wide variations in the system response or output), strongly joined and chaotic. This means that the climate as a whole can be unpredictable.

The reasons for climate change are numerous and condition the periodicity of the cycles differently. The Sun's activity, which is not constant, the amount of interstellar dust, the tilt of our planet's axis, precession around it and the eccentricity of its orbit, the arrangement of the continents, which has changed over time, volcanic activity on the Earth, the types and levels of biological activity which affect the composition of the atmosphere, ocean currents, which distribute heat over the terrestrial surface and alterations in which can cause very sudden regional changes in temperature, cosmic rays (Delibes and Delibes de Castro 2005) and variations in the Earth's magnetic field, among others, are some of the most important natural factors that produce climate change (Gribbin 1986).

Natural climate variations can also occur in the absence of change in external forcing as a result of complex interactions between components of the climate system (Donnadieu et al. 2004, Dwyer G.S. 2000, Ohmoto et al. 2004), such as the coupling between atmosphere and the ocean. The El Niño-Southern Oscillation (ENSO) phenomenon is an example of such natural "internal" variability on interannual time scales that we will study in Sect. 7.5 (IPCC 2001).

7.2 Climate Measurement

One important question in this context is how we measure the parameters involved in climate studies, such as temperature, humidity, winds, currents, rainfall, and others. For over one hundred years, we have had instruments which in principle can measure all the relevant climate parameters.

But, what about information on the climate millenniums or millions of years ago? In this case we have to use indirect (proxy) observations and measurements.

One type of proxy measurement consists of examining tree rings. The width and composition of every ring grown in every season gives an idea of local meteorological conditions during that season.

Ice cores from Greenland and Antarctica are a source of great importance providing us with information about the climate conditions up to a few hundred thousand years ago. The accumulation and compression of snow formed ice. Cores taken from this ice give us information on the amount of snow that fell every year, and gas trapped in air bubbles tells us about the composition of the atmosphere, composition of dust in the atmosphere, etc. (Burroughs 2001, Houghton 2004, Mastin 2004).

Similarly, sediments deposited on the ocean floor tell us about the kind of phytoplankton and zooplankton that lived at different times, about their vital environmental requirements and also about mineral sediments from the surface of the ocean and from land (ESA 2005).

7.3 The Role of the Ocean in Climate

Like the atmosphere, the ocean plays a fundamental role in nature. The sea affects climate profoundly, acting as a storage and distribution system that releases solar

energy, and at the same time, is the major source of humidity in the atmosphere. Photosynthesis by phytoplankton is one of the main processes contributing to the generation of oxygen in the atmosphere.

However, due to the huge area oceans occupy and the difficulty in finding detailed information with a sufficient measurement density, it has not been possible to make an observation or effective prediction of its behaviour. The absence of sufficient data on wind and pressure on the oceans has made long-term weather predictions for the continents impossible. In order to make effective predictions for one or two weeks, it would be necessary to have observations on the ocean surface with the same density and periodicity as on land.

Of capital importance for climate prediction is the knowledge of the factors that affect it. The atmosphere, the oceans and the interactions between them, which produce an exchange of matter, energy and momentum, are of the greatest importance in this study.

The chemical composition of the atmosphere, in particular the concentration of greenhouse gases (water vapour, methane and carbon dioxide CO_2) is of major importance for temperature control because of their property of retaining part of incoming solar radiation. Due to its long life, CO_2 is the most important greenhouse gas, in spite of the low percentage of its concentration in the atmosphere (Burroughs 2001).

The oceans absorb a large amount of heat energy from the atmosphere and land and redistribute this energy from the equatorial and tropical regions to the poles through the marine currents. In the northern hemisphere this transport is mostly by the Atlantic and in the southern hemisphere, by the Pacific Ocean.

A large amount of CO_2 is also absorbed and stored in the deep layers and sediments of the oceans. In particular, the upper 3 m of the oceans absorb as much heat as the entire atmosphere. This means that the oceans as a whole absorb, store and return more energy than the atmosphere. In fact, the heat capacity of the oceans is 1,100 times (99.9%) that of the atmosphere.

The oceans also act as a thermal memory of the climate system, because the deep currents control long-term climate change (millenniums) and the surface currents do the same in the short term (years) (Schiermeier 2006).

7.3.1 Ocean Circulation

The winds are responsible for generating the great ocean surface currents. The general circulation regime in the atmosphere is produced by convection from variation in the temperature with latitude and the Coriolis force (Fig. 7.1).

In the lower atmosphere, pressure is low at the equator, and the air is heated and rises. At about 30°N and S air cools and descends, and atmospheric pressure on the Earth's surface is high. There is therefore a pressure gradient from the subtropical highs toward the equatorial lows and, as winds blow from areas of high pressure to areas of low pressure, equatorward winds result. The Coriolis force deflects winds and atmospheric and oceanic currents to the right and left in the northern and southern hemispheres forming the Trade Winds. The same is true of the Westerlies and

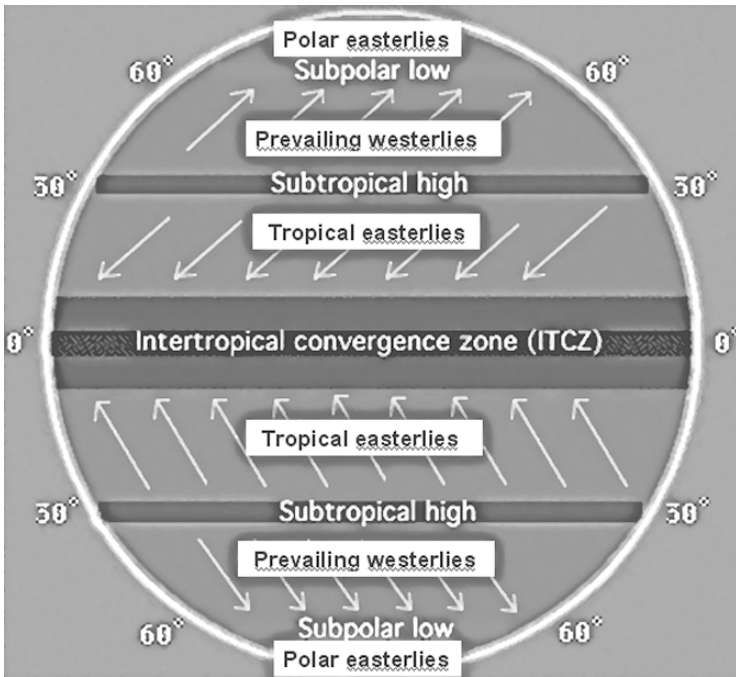


Fig. 7.1 General wind circulation (From WW2010 Project, Illinois Univ.)

Polar winds, producing the Hadley cells and general circulation. The net flow is heat transported from low to high latitudes (The Open University 1989).

When studying ocean circulation, it is advisable to do it in three parts: a) The mean circulation or general ocean circulation, caused by the prevailing winds in the surface layers of the ocean, b) circulation variable over time causing gyres and eddies that move with the general current. The energy associated with these gyres is generally rather more than that of the current itself and c) the deep **thermohaline circulation (THC)** produced by changes in temperature and salinity that cause the recently labeled **Ocean Conveyor Belt (OCB)**, with strong long-term repercussions on the climate.

7.3.1.1 Geostrophic Circulation

The equation of motion in oceanography enables us to study ocean dynamics. The forces that enter into this equation are gravity, the Coriolis force, pressure gradient force and friction. When friction is negligible, the force exerted by the pressure gradient is balanced by the Coriolis force (Fig. 7.2a), and the resulting flux under these conditions, perpendicular to both forces, is called geostrophic flux or regime. In this regime, the convergence of waters as a result of the anticyclonic winds in the NH, causes the sea surface to slope upwards towards the middle of the gyre. As a consequence, the water is affected by a horizontal pressure gradient force. Under

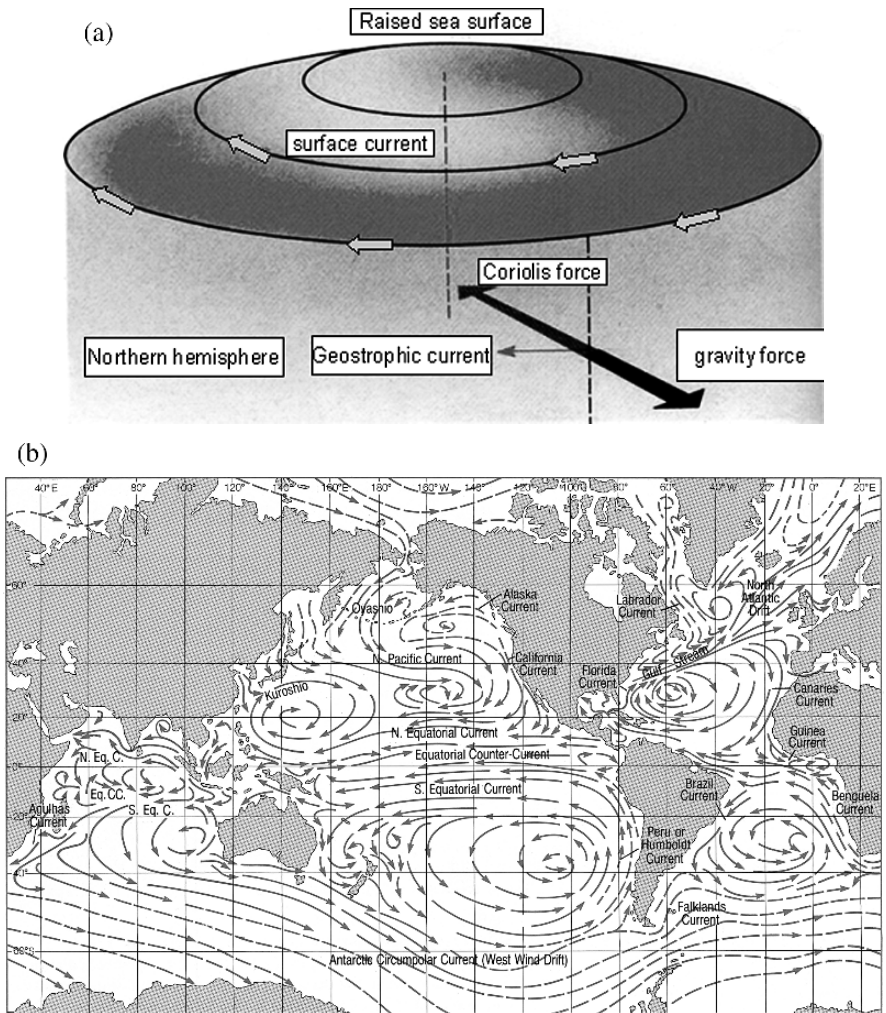


Fig. 7.2 a) Water slope and b) circulation under geostrophic regime (The Open University 1989)

steady conditions the horizontal pressure gradient force is balanced by the Coriolis force producing a clockwise gyre (NH) (Fig. 7.2b) and a slope that can be up to about 1 m in the intense western currents.

7.3.1.2 Ocean Eddies

Mesoscale eddies (Fig. 7.3), which have lengths of 30–200 km and last from weeks to a few months, represent the variability of ocean weather with regard to the average. They contain a significant proportion of the ocean’s energy and have been found

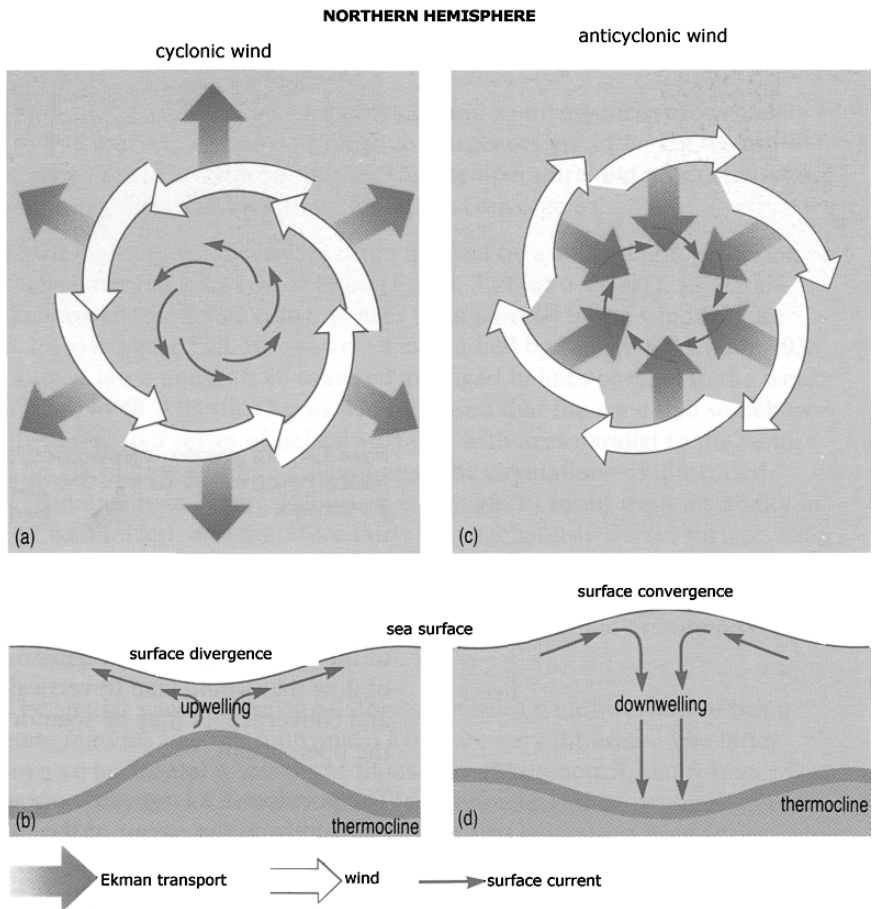


Fig. 7.3 Eddies produce variations in sea level at the sea surface (The Open University 1989)

everywhere in the oceans, the Gulf Stream (GS), in the Mediterranean (MEDDIES), in archipelagos (Canary and Hawaii Islands), and elsewhere (Parada et al 1998).

7.3.1.3 Thermohaline Circulation (THC), the Great Conveyor Belt (GCB) and the Abrupt Climate Change (ACC)

The Gulf Stream transports enormous amounts of heat from the Equator and the tropics to northern Europe and southern Greenland, where it meets the cold Labrador Stream (Fig. 7.4). Of particular importance for the climate is the effect of the warm Gulf Stream that reaches northern Europe and contributes to moderating the temperatures at these latitudes. In fact, the average temperature in northern Europe is about 6°C to 9°C higher than that at the same latitudes in North America.

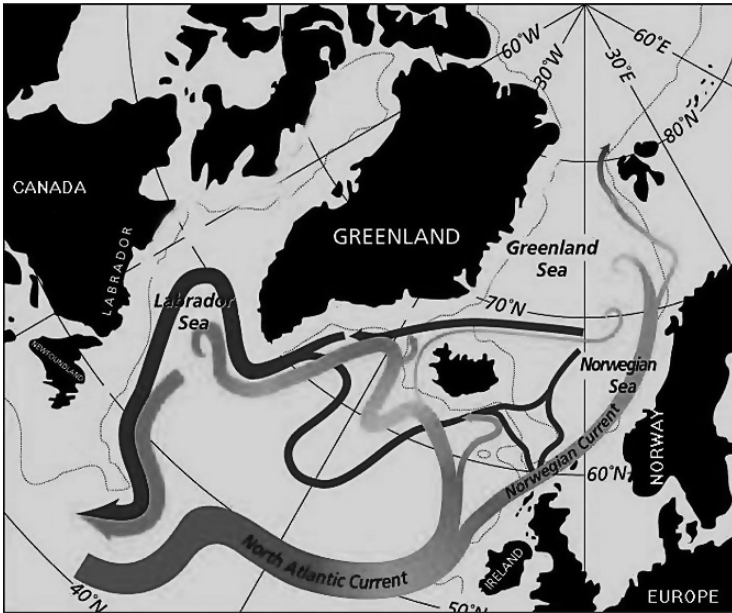


Fig. 7.4 The North Atlantic Current transports a large amount of heat from the tropics to northern Europe (From Calvin 1998)

When warm water from the **Gulf Stream (GS)** yields its heat to the atmosphere and cools, its density increases enough to sink and return southward thousands of meters deep, leaving space at these latitudes for new masses of warm surface water. This sinking does not occur in the Pacific because it is less saline than the Atlantic. Carbon dioxide is also transported during this circulation of cold and warm water. Cold water absorbs carbon dioxide from the atmosphere, and some of it sinks deep into the ocean. When deep water comes to the surface in the tropics, it is warmed, and the carbon dioxide is released back into the atmosphere.

Figure 7.5 shows how surface currents connect with deep currents to form the so called **Great Conveyor Belt (GCB)** (IPCC 2001).

It is known that the GCB has frequently become destabilized in the distant and recent past and could again become destabilized in the future with significant consequences to the climate (Stocker T.F. 1998). About 12,000 years ago, at the end of the last ice age, when the glaciers melted, there was a collapse in the THC from which Europe took 1000 years to recover.

The most vulnerable place where destabilization could begin is the area where water sinks in the North Atlantic. If, due to a global rise in temperatures, precipitation increased in northern Europe, or ice melts in Greenland were considerable, this increase in fresh water in that zone would slow down the arrival of warm water from the GS, which could cause this current to collapse. The effects would not take place on a global scale, but mainly in northern Europe, where the temperatures could drop around 8°C in Greenland, 6°C in continental coastal areas and about 2° in the interior (Osborn 2006). Depending on the time that the collapse or the

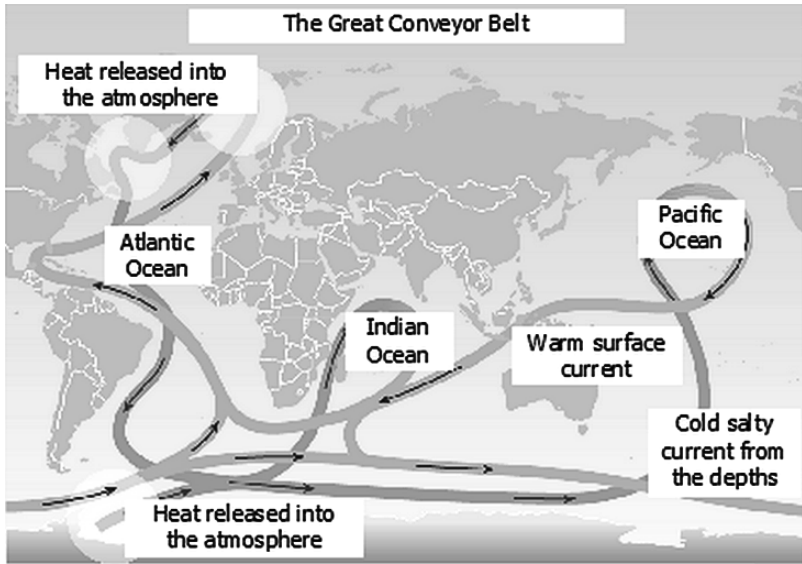


Fig. 7.5 Schematic illustration of the world's ocean circulation system, made up of the main North-South thermohaline circulation routes in each ocean basin which join in the Antarctic Circumpolar Current (From IPCC 2001)

significant decrease in the current took to appear (tens of years), this effect, known as **“abrupt climate change” (ACC)** could compensate in some zones the rise in temperatures due to global changing (Broecker 1997, Curry 2005, Bryden et al. 2005, Häkkinen and Rhines 2004, Rahmstorff 2002). The latest models from the Hadley Centre for Climate Prediction (UK), estimate that if the concentration of CO_2 were to increase very quickly by 2% a year until the concentration of CO_2 is stabilized at four times what it is now, the intensity of the GS would diminish by around 25%. Even so, the temperatures in the NW of Europe would still increase (Hadley 2006). As we are going to see in Sects. 7.4.2.3. and 7.4.2.1, the next salinity sensors and the altimeters can detect changes in the salinity and in the intensity of the GS, giving us information about the possibility of a collapse of the GS and about an ACC that could happen some tenths of years after the GS collapse.

Another additional effect would be the redistribution of chlorophyll in the North Atlantic. A study by (Schmittner 2005) reports the results of a model in which after the collapse of the THC, ocean productivity in the North Atlantic would take over 500 years to return to its original level.

An important study on the tendency of ocean warming by (Levitus et al. 2000) found that during the period from 1948 to 1998, the ocean temperature increased at least down to a depth of 3000 m, and that between 0 and 300 m, the temperature increased by 0.31°C . The most important increases have taken place in all of the oceans between 300 and 1000 m, and in the Atlantic, at over 1000 m.

7.4 The Role of Satellites in Measuring Climate Change

The range of oceanic parameters that can be measured from space is very wide, including ocean colour, surface temperature, sea surface height, and surface roughness on a variety of length scales from ripples to wave swells and larger. The application of satellite data in Oceanography are so diverse and are useful to the whole spectrum of biological, chemical and physical Oceanography (Robinson 1994).

But satellite measurements have some limitations. They have been making observations for only thirty years and are limited to direct measurement of the physical properties of the ocean surface, because electromagnetic radiation is strongly absorbed by water, although some topographic accidents below the surface ranging from tenths of meters to the seafloor can be detected indirectly. Satellite orbit characteristics also limit its time-sampling at a given location to discrete overpasses once or twice a day, or every several days.

However, there are at least three main reasons why Satellite Oceanography can make significant contributions:

a) It can provide a global, synoptic view of the oceans for study of basin-wide phenomena; b) it can make measurements that are either impossible or difficult by ordinary means and c) it can provide a low-frequency time series over long periods ranging from weeks to years, even at isolated oceanic locations (Cantón M 1991).

7.4.1 *Passive Versus Active Sensors*

Passive visible and infrared sensors measure the colour of the sea surface layer and the sea surface temperature (SST) respectively. Examples of active sensors are the Synthetic Aperture Radar (SAR), which measures the surface roughness of the sea surface, altimeters (ALT), which measure the surface roughness and height from a reference, and scatterometers, which measure the wind vector over the oceans. This year, the European Space Agency's (ESA) SMOS mission will add ocean salinity, another important ocean parameter, to the variables measured from space.

From these parameters measured directly by satellite, a wide range of indirect measurements can be found: Chlorophyll-a (Cla) concentration, ocean productivity, location of fisheries, waves on all scales, from ripples to long wavelengths and internal waves, intensity and direction of winds, topography of the seafloor, currents intensity and much more.

7.4.2 *Passive Sensors and Applications*

As mentioned above, sensors on satellites that operate in the visible, IR and microwave bands are used to study the ocean from space. Each band has advantages and disadvantages, each is used for studying different phenomena, and all of them

are being used with new generations of sensors and systems that are more and more sensitive and useful. In general, sensors operating in the visible and IR have the best spatial resolution, but they are limited in their observations by the presence of clouds and other atmospheric factors. Sensors operating in the microwave range have worst spatial resolution (except SAR), but their observations can penetrate clouds.

7.4.2.1 Ocean Observation from Visible Sensors

The human eye is able to observe in the visible (0.4 to 0.7 μm), but sensors on satellites that operate in this band can do it in much narrower bands, from 0.4 to 0.5 μm , (e.g., to measure only the blue colour). The **AVHRR** (Advanced Very High Resolution Radiometer) is used on Earth to calculate vegetation index using the IR and VIS channels. However, measurement of the concentration of Cl-a in the sea is much more complex than on Earth because of the low reemission levels of solar radiation scattered toward the sensor by these components. The solution for such measurements has been to design sensors with very narrow visible spectral bands only 20 nm wide, concentrating on the absorption and dispersion peaks of the Cl-a in phytoplankton.

The first sensor like this designed specifically for ocean observation was the Coastal Zone Color Scanner (**CZCS**), which operated on board NASA's experimental NIMBUS-7 mission from 1978 to 1986 and supplied tremendously valuable data. In 1996, two other sensors for measuring colour, the OCTS and the MOS, were launched. A better sensor than the CZCS, with an additional band at 670 nm for measuring Cl-a and primary sea productivity, called the **SeaWiFS** has been available since 1997. The **MERIS**, the first sensor for measuring ocean colour launched by the **European Space Agency (ESA)** in March 2002 on board the **ENVISAT** satellite, and the **MODIS** series, an improved SeaWiFS with even narrower spectral bands than the first, launched on board the NASA's TERRA and AQUA platforms in 2000 and 2002, respectively, are now operating.

Figure 7.6 is a Cl-a image taken on 25th September 1983 by the CZCS in the Canary Islands. Notice how Cl-a acts as a natural tracer in the ocean, marking oceanographic structures of interest in the zone, the upwelling off the African coast and the eddies produced as a result of interaction between the Canary Current and the islands in the archipelago. In this image, SW of Gran Canaria island (the central rounded island) a clear cyclonic cold eddy appears with high Cl-a concentration in the borders and low concentration in the centre due to the upwelled and the divergence of waters (see Fig. 7.3). The extension of this eddy is about the same as the Gran Canaria island, with 30 km of radius. Also, two giant filaments of Cl-a (some hundreds of Km) coming from the upwelling reach the archipelago contributing to the enrichment in the productivity of these waters (Hernandez A et al 1993, Aristegui J et al 1994, Aristegui J et al 1997, Barton E D et al 1998).

The primary production averages measured by the SeaWiFS from 1997 to 2002 and the average measured by the CZCS from 1979–1986, shows the difference between the two periods. Global primary production has diminished by over 6% since early 1980. 70% of this decrease has been in the high latitudes of the NH, and coincides with the increase observed in SST. In spite of everything, it is not possible



Fig. 7.6 Image of Chl-a concentration found in the Canary Islands with the CZCS sensor on 9/25/83

to conclude that this decrease represents a long-term tendency or is due to decadal variation of the ocean (Gregg et al. 2003).

7.4.2.2 Infrared Ocean Observations

The sensors that operate in the infrared measure the radiation in that band emitted by a body because it is at a certain temperature over 0°K . They are therefore independent of solar radiation, which makes possible, among other things, to obtain night-time images of the **sea surface temperature (SST)**.

Furthermore, it is the only case in which the geophysical parameter of interest, the SST, can be obtained almost directly from the radiation measured by the sensor due to the relationship by Planck's Law of Radiation between radiation measured in the IR and the brightness temperature of the sea surface.

The sensor which has contributed the most to date to the measurement of the SST has been the **AVHRR** in the NOAA (National Oceanography and Atmospheric Administration) satellite series, mostly because of its easy and recently free acquisition. This series of satellites went into service in 1979 and at the present time continues in operation.

One of the direct applications to the study of global change consists of calculating deviations from the average SST (Strong 1989). Although this temperature is only representative of the temperature to a few meters below the surface, depending on wind and waves, it provides a first impression of what is happening on an average around the entire ocean surface for periods of months to decades and what the tendency is.

Figure 7.7 show a night time IR 3.7 micron thermal ATSR (Along Track Scanning Radiometer) image taken from the **ESA ERS-1** satellite on 19 October 1991. The region extending from the Canary Islands to the coast of Western Sahara (512 km \times 512 Km) is shown in this night-time thermal image. The most dramatic

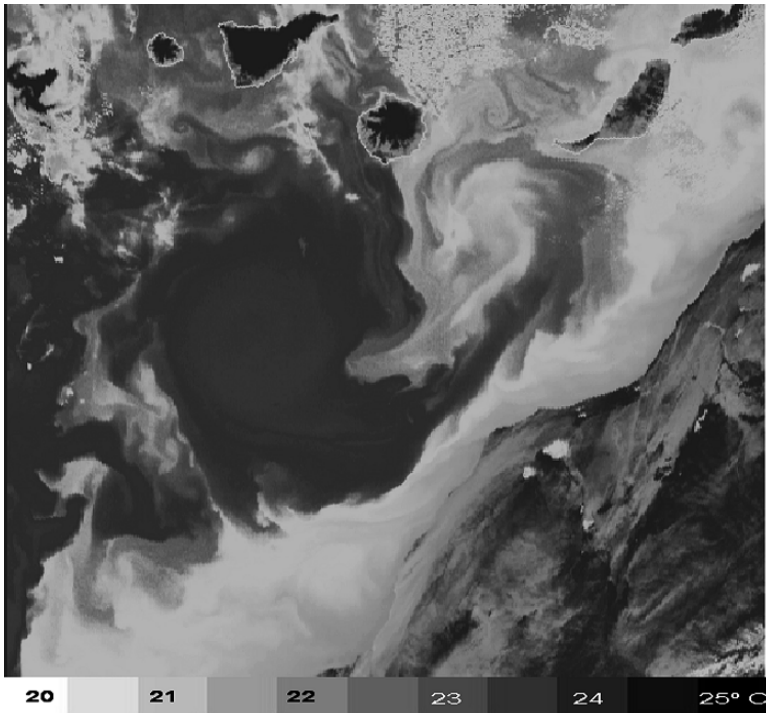


Fig. 7.7 ATSR night-time thermal IR image showing a giant anticyclonic eddy south of Gran Canaria (CCLRC, UK)

feature of this picture is the giant anticyclonic warm eddy structure in the Atlantic which is at a temperature of around 22°C , formed as a result of the turbulent mixing of the cold African coastal waters with the warmer central Atlantic water. This structure is around 200 km in diameter. Across the top of the image are several of the Canary Islands, from left, Gomera, Tenerife, Gran Canaria, Fuerteventura and Lanzarote. Although small, the islands exhibit large variations in altitude and therefore temperature, as can clearly be seen in the image, with the more-elevated central parts of each island appearing colder (darker) than the coastal areas (CCLRC 2003).

Figures 7.8a) and 7.8b) are maps of SST and Cl_a respectively for the region of the warm (light gray in SST) Gulf Stream taken from the USA AQUA-MODIS mission. Note the inverse correlation between SST and Cl_a and the meanders and gyres of the current when meet the cold (dark gray) Labrador current.

These set of images show the valuable information acquired for IR and VIS sensors, informing about phenomena that are difficult to observe and to sample from in situ measurements permitting to the scientists to study global and temporal phenomena related with the environment change.

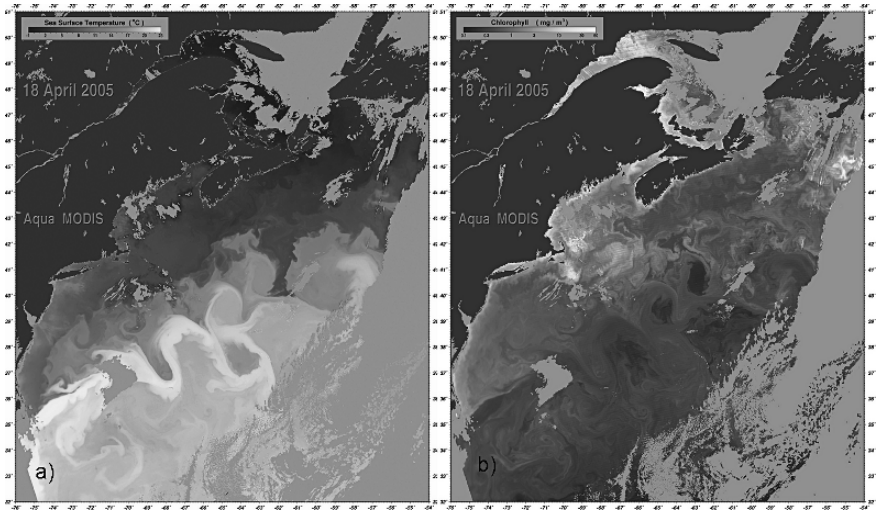


Fig. 7.8 a) SST and b) Cla in the Gulf stream measured by AQUA-MODIS (From NASA)

7.4.2.3 Passive Sensors in the Microwaves: Temperature and Salinity Measurement

It is possible to measure the SST from sensors that operate at microwave wavelengths. Instead of measuring the emitted radiation by the sea surface (SS) at IR, they measured the weak radiation emitted at microwaves but with coarser resolution than the IR sensors. On the contrary they have the advantage that at this long wavelengths there is no scatter of radiation by atmosphere permitting the measurement of SST at any time and with the presence of clouds. On 4 May 2002, NASA launched the Aqua satellite, the second of its Earth Observing System flagships. Since the mission's science operations began, Aqua's sensors have been returning spectacular views of our home planet. The Fig. 7.9 shows global sea surface temperature as measured on 1 June 2003, by NASDA's Advanced Microwave Scanning Radiometer for EOS (AMSR-E) aboard the satellite (NASA 2003).

The gray levels represent temperatures of the ocean's surface waters, ranging from a low of -2°C in the darkest areas to a high of 35°C in the brightest regions. Sea ice is shown as white and land is medium gray. Note the continuous coverage that AMSR-E provides around the world—because it makes its measurements through clouds, there are no gaps in the data. Notice the intense upwelling of relatively cold water in the eastern Pacific, along the equator. Strong easterly trade winds push these cold surface waters toward the west, resulting in a characteristic wave pattern called tropical instability waves.

This year the ESA is planning to launch a new sensor (SMOS) which up to now has not been operated from satellites. This passive microwave sensor, which works in the L band (1.4 GHz), measures soil moisture and sea surface salinity (SSS). If the results are satisfactory, a new parameter will be added to the four parameters directly measurable from space mentioned in Sect. 7.4.

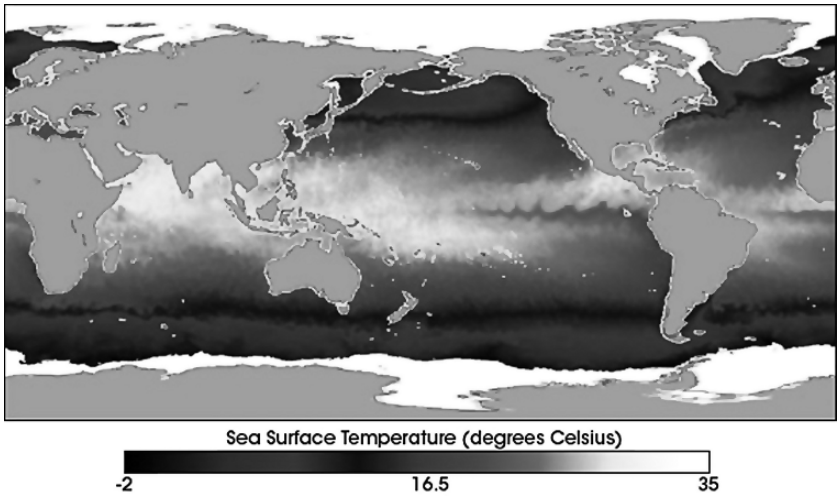


Fig. 7.9 SST from AQUA-AMSR-E for the 1 of June 2003 (From NASA)

The sensor applies the concept of aperture synthesis to measure the brightness-temperature of the sea surface with its Y-shaped antenna at different inclinations during different overpasses. This temperature weakly depends among other factors, on salinity. (at nadir 0.75 K per psu for an SST of 30°C, decreasing to 0.5 K per psu at 20°C, and 0.25 K per psu at 0°C), This instrument will require wind and SST measurements found with other instruments to find the salinity. Fig. 7.10 is a simulation of ocean salinity at global scale.

The SMOS is expected to be able to provide 10-day average salinity measurements with an accuracy of 0.1 psu in 200km swaths (ESA 2007).

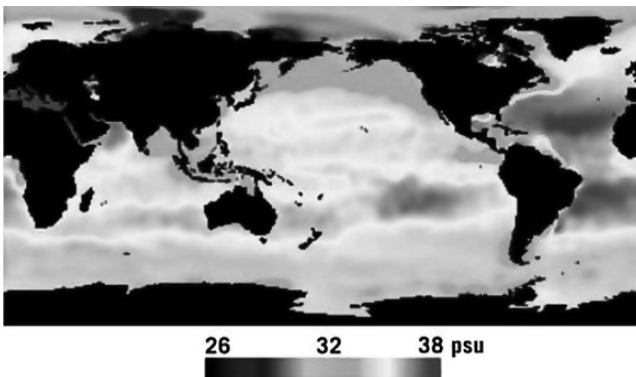


Fig. 7.10 Simulated seasonal (winter) sea-surface salinity map (From ESA)

7.4.3 Active Sensors: Synthetic Aperture Radar (SAR)

The SAR, in principle, is not as useful as other sensors for the study of global change due to its high spatial resolution, reduced spatial coverage and low temporal resolution. In spite of that, the SAR is one of the most versatile instruments available for studying the oceans. Like other active sensors working at microwave frequencies, data acquisition is not perturbed by clouds or light rain. From the measurement of the backscatter coefficient (σ), which is proportional to the power received at the sensor divided by the power of the pulse sent to the surface, this instrument enables wave measurement at the ocean surface in all wavelengths, from ripples and millimetric waves due to surface tension to long waves with their wave spectra. Indirect detection of internal waves, topographic accidents some tenths of a meter below the surface, oil slicks at the surface and a whole variety of phenomena that modify sea surface roughness is also possible.

The SAR sends an oblique radio wave toward the sea surface. This wave is backscattered toward the sensor, depending on other sea surface roughness factors. By the Doppler Effect, the image is the brightest where SS is the roughest and the darkest are the smoothest. In the Fig. 7.11, the Prestige oil spill can be seen clearly at Galicia (NW Spain) in November 2002, since the oil smoothes out the SS and impedes formation of waves that produce backscattering of the radio wave.

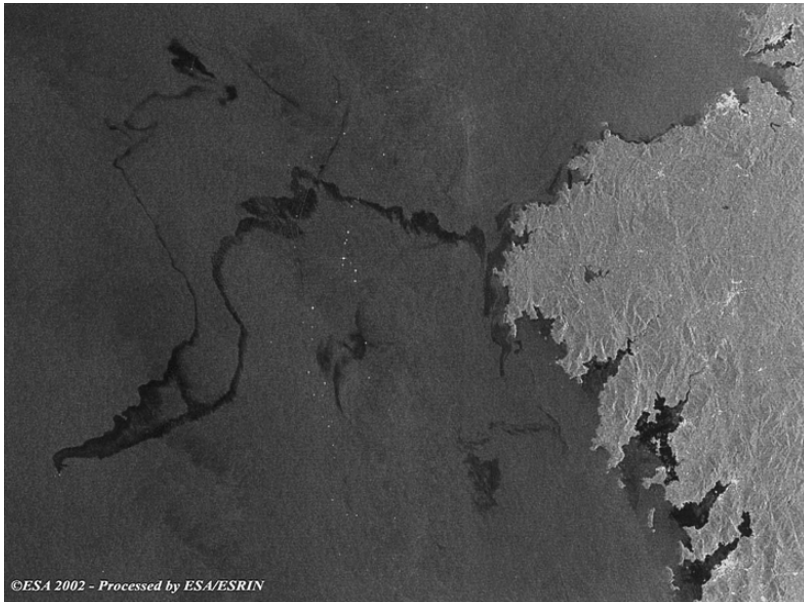


Fig. 7.11 ASAR ENVISAT 17-NOV-2002 (ESA)

7.4.3.1 Scatterometers

The wind is a fundamental variable for the study of the ocean surface. The wind drives waves, mesoscale upwellings and gyres, wakes and the great surface currents. The wind vector was measured for the first time by the NASA SEASAT satellite launched in 1978. In addition to a scatterometer for wind measurement, in this novel, short-lived mission (it only provided data for three months), the satellite also carried an altimeter and an SAR.

The scatterometer is a radar that emits oblique pulses toward the sea surface from several antennas at different angles. Wind intensity (U) is measured using the backscatter coefficient (σ), since for angles of incidence on the surface over 15° , there is an almost linear relationship between wind intensity and σ . This is logical because the greater the wind intensity, the greater the surface roughness and thus also σ . σ is also function of the relative wind direction (θ) with respect to the observation antenna. If there are two or more antennas observing the surface at different angles, the wind direction can be found from the intersect points of the $\sigma = \sigma(U, P, \theta, \phi)$ curves, where P is the radar polarization and ϕ is the angle of incidence of the pulses on the surface.

The European ERS-1 (1991–1999) and ERS-2 (1995–2003) satellites carried two scatterometers on board that worked in the C band (5.3 GHz) and had three antennas each. Although the ENVISAT satellite did not carry any scatterometers on board, the ESA plans to launch new scatterometers in future METOP meteorological satellites.

In 1999, the NASA launched the QuikSCAT to replace the NSCAT, a scatterometer with a parabolic dish antenna that emits pulses toward the sea in a circular

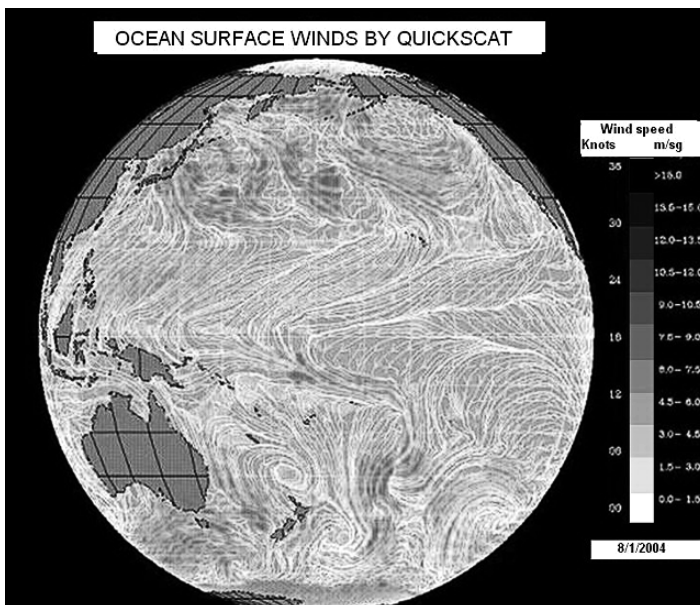


Fig. 7.12 Global winds for the 8/1/2004 computed from NSCAT (From NASA)

pattern, making it possible to observe σ in a single zone from many different angles while maintaining the angle of incidence.

Global measurement by this instrument in difficult-to-access zones such as the Pacific Ocean, are shown in Fig. 7.12, taken on 01 August 2004. The QuikSCAT measures wind intensity with a 2 ms^{-1} accuracy in the $3\text{--}20 \text{ ms}^{-1}$ range and 10% in the $20\text{--}30 \text{ ms}^{-1}$ range.

One interesting result it is the possibility to find from the scatterometer data the vorticity over the sea surface. The vorticity is defined as the rotational of the velocity field in a fluid, but in meteorology and oceanography is usual to call vorticity to the vertical component of the rotational. By substituting the drag coefficient in the equations of motion, it is possible to draw maps like the ones shown in Fig. 7.13 (Ramos A G et al 1997a) where dark gray represent positive vorticity (upwelling) and light gray negative vorticity (downwelling). Fig. 7.13 is a vorticity map around Madagascar. At the top right of this map there is a dark area that correspond to the eye of intense hurricane Odille (30-III to 17-IV 1994) (Ramos A G et al 1997b).

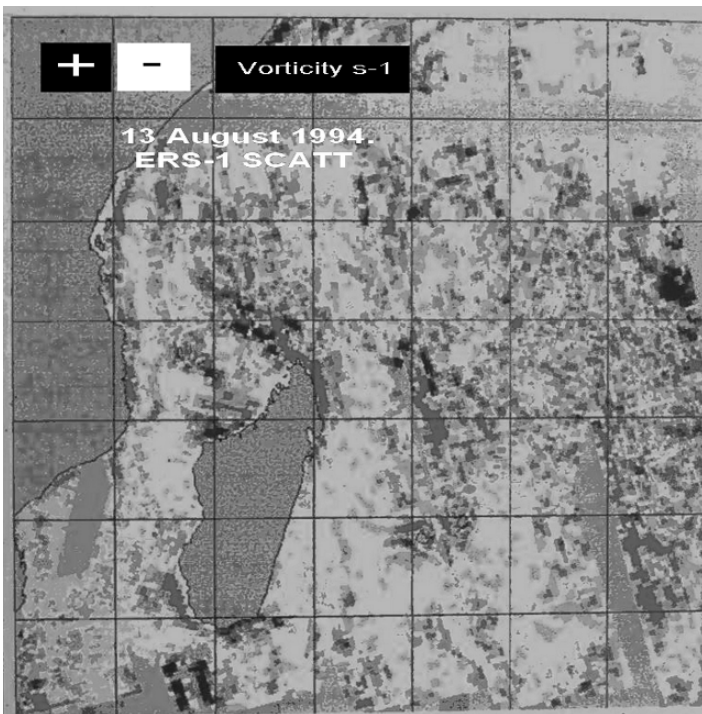


Fig. 7.13 Vorticity around Madagascar and cyclone Odile

7.4.3.2 The Altimeter

Ocean Surface Topography

Although the altimeter is conceptually very simple instrument, it provides the oceanographer with a wide variety of direct and indirect parameters. It is a radar that emits a perpendicular pulse toward the SS, and measures the time this pulse takes to go and return from an orbit of about 700 km with such extreme accuracy that the satellite-SS distance may be measured to within 2-cm (Fig. 7.14). Knowing the geoid (equipotential surface that coincides with the mean SS in absence of winds and currents, that can be measured by in situ gravimetric observations, by means of the effect produced by variations in the geoid relative to the ellipsoid, of -100 to +500 m over the calculated satellite orbit where orbits cross or by averaging different measurements of height over the same overpass), it is possible to determine the **topography of the SS (OST)**, that is, the geoid-SS distance.

The measurement of this height is of tremendous value in Oceanography, since as mentioned in Sect. 7.3.1.1. the OST, along with the geostrophic flux equations, makes it possible to find the speed with respect to the mean circulation of intense

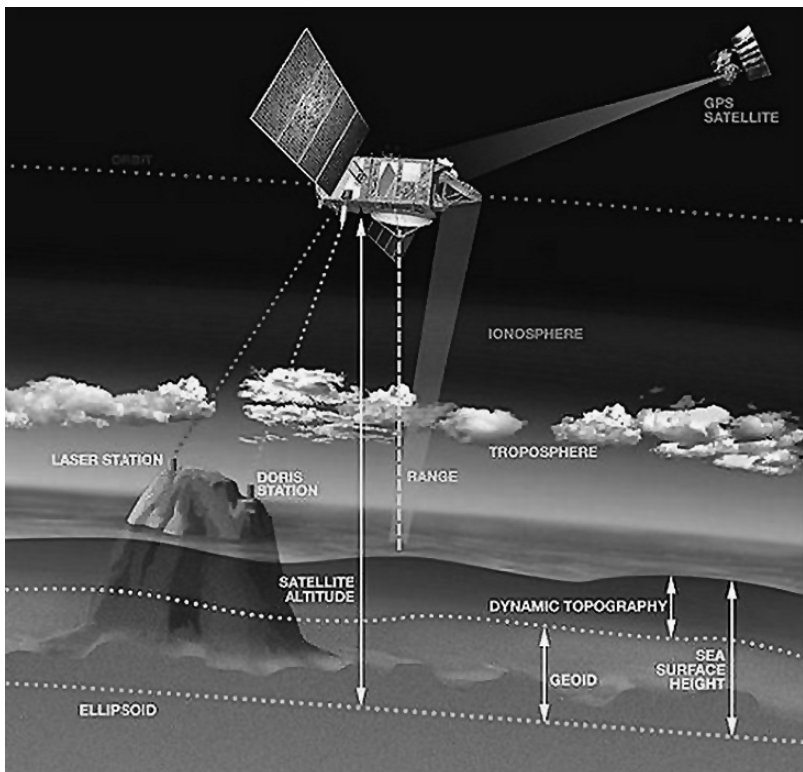


Fig. 7.14 Ocean surface topography measured by the altimeter radar (From AVISO)

geostrophic western boundary currents, horizontally confined in a 100 km-wide swath, in which there may be slopes of up to 1 m from one end to another, variation which is easily detectable by the altimeter. The eastern currents are considerably slower and have slopes of a few tens of cm, which are harder to detect, although they can also be detected by the altimeter. Similarly, mesoscale eddies can be found from the SS slope because of the 10-to-40 cm variations they produce in this slope.

From the Skylab in 1973, to the present TOPEX/POSEIDON (T/P), JASON and ENVISAT satellite RA-2, several altimeters on board satellites have observed the SS with spectacular results. If we show the variance in the OST instead of mapping current variability, we get what is called **eddy kinetic energy (EKE)**, which gives us information on the causes of variability in currents, meanders and eddies.

Figure 7.15a shows an EKE map inferred from the ERS-1 altimeter for the summer of 1992. During July 1992 in particular and generally during summers, the cold cyclonic and warm anticyclonic eddies activity is maximum in the Canary archipelago due to the big intensity of trade winds during this season (see Fig. 7.7). Figure 7.15b show a similar situation for the summer 1993 but obtained from T/P altimeter. These maps were compared with hydrographic measurements and Cla maps taken in the Canary region between 20.0–40.0° N and 19.0–9.0° W during 1992 and 1993. We observe very high correlation between in situ, EKE and SST maps.

ERS-1 data have shown mesoscale features around Canary Archipelago, mainly in winter (1993) and summer (1992–1993) behind the Gomera and Tenerife–Gran Canaria, respectively. In these cases the EKE showed maximum values, presumably associated with cyclonic and anticyclonic eddies detected by other authors on

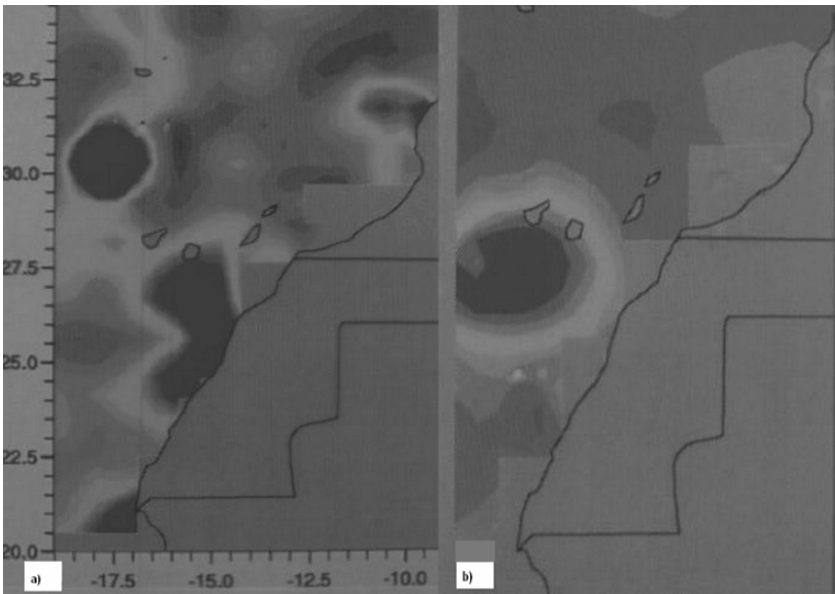


Fig. 7.15 a) EKE measured by ERS-1 altimeter. b) EKE measured by T/P

different occasions using different measurement techniques in the region. The EKE values vary from 0.035 to $0.040 \text{ m}^2 \text{ s}^{-2}$ in the summers of 1992 and 1993.

The comparison between the altimetric sea surface height and the hydrographic dynamic topography ($0/300$ dbars) revealed a high correlation between both measurements. It is possible that the negative sea level anomalies that have been obtained are associated with a cold filament from the African coastal upwelling (between Cape Yubi and Cape Bojador). This feature has been identified only in summer 1993 with altimeter data, even though filaments in Cape Ghir can be observed in spring when the wind intensity is usually increased in the zone.

Sea surface temperature images from summer 1992 and 1993 also show the features detected with altimetric data and in situ measurements. We have observed from the SST maps that the situation and the shape of the features are rather similar. This is the first time that ocean mesoscale features, such as eddies and filaments, have been studied in this region by means of altimeter data (Tejera et al a) 1997, Tejera et al b) 1997, Tejera et al 2002).

Figure 7.16 show an estimate of global ocean EKE obtained from five years of T/P altimeter data (from December 1992 to December 1997). The areas of major variability (Gulf Stream, Kuroshio current and Circumpolar Antarctic Current are showed in dark (IFM 2006). This type of maps makes it possible to study and predict short and long-term changes in surface currents.

Sea Level

When global temperatures rise, the sea does so also. The main factor affecting this rise is thermal expansion of the water in the sea as temperature rises. Other factors, in order of importance are melting of glaciers in Greenland and possible contributions in Antarctica, permafrost and variations in deposits of terrestrial water. Over the last century, the sea level rose from 1 to 2 mm/year, with water expansion from

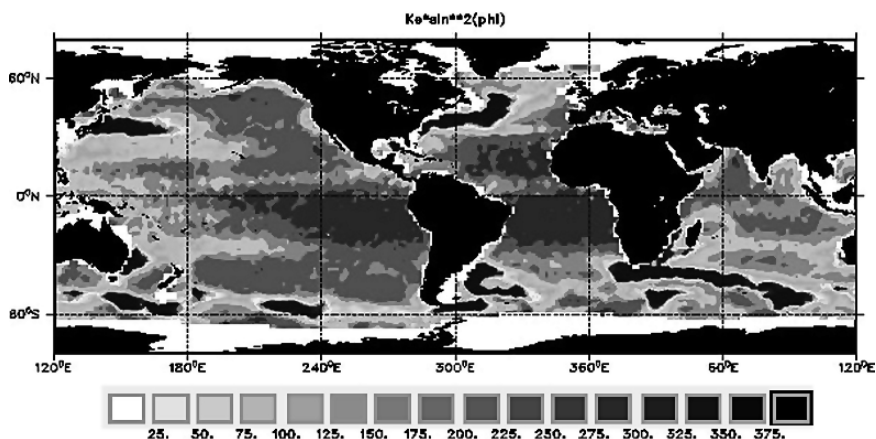


Fig. 7.16 EKE from 5 years of T/P data (XII-1992 to XII-1997) (From IFM 2006)

warming contributing 0.5 mm (Alley et al. 2005). By the end of the 21st century, the sea level is predicted to rise between 0.1 and 0.9 m depending on contributions in Greenland and the Antarctic. These two could raise the sea level about 70 m if they melted completely (Johannessen O et al 2005, Meehl G et al 2005, Velicogna I et al 2006).

The altimeter, the primary measure of which is the OST, can accurately estimate changes in sea level.

Figure 7.17 shows a map of the rate of mean sea level change (estimated simultaneously with annual and semi-annual variations) as a function of geographic location. The trends were calculated for the period from 1993 to 1998 (Cabanes et al. 2001). Notice how the rates have considerable spatial variation due to interannual variations in sea level, emphasizing the difficulty in determining the rate of sea level rise from short records of tide gauges lacking uniform global distribution.

The impact of a rise of only 1 m could be catastrophic for the world’s coastal zones and countries like Holland, Bangladesh or a large number of islands in the Pacific Ocean that are only a few meters above sea level.

Winds and Waves Measured by the Altimeter

The altimeter can also easily measure wind intensity and waves on the SS. Significant wave height $H^{1/3}$, defined as the average height of the highest one third of waves, is found by fitting a model curve to the slope in the rise of the pulse received by the sensor. Since the short pulses sent to the SS by the altimeter are

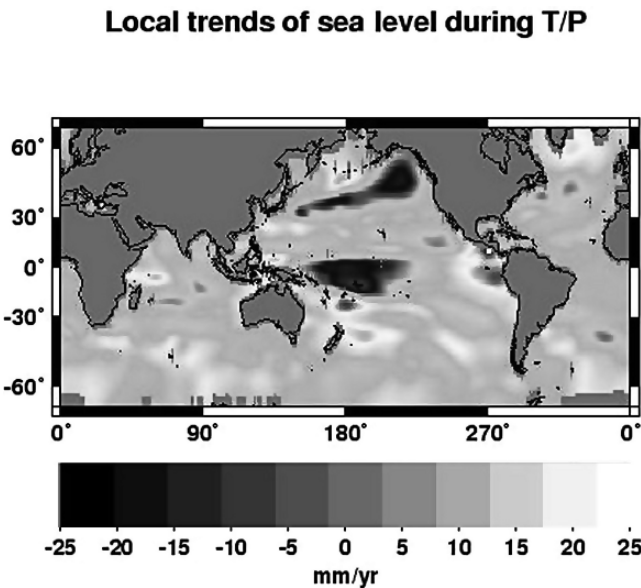


Fig. 7.17 Rate of mean sea level change from 1993 to 1998 (From Cabanes et al 2003)

lengthened due to the first reflection by the crests and afterward by the valleys between the waves, the higher the wave, the smaller the slope of the return pulse will be, assuming the pulse is shorter than the height of the waves. Therefore, short amplitude wave measurement accuracy depends on the length of the pulse transmitted.

Wind speed observations using the altimeter are based on measurement of σ from the Zenith. The higher the intensity of the wind, the more the radar signal is backscattered by the waves, the less energy is received by the sensor and therefore, the lower σ is.

Perhaps the most paradoxical application of Satellite Oceanography is the possibility of mapping seafloor topography. This is not due to radar penetrating the SS, but because seafloor elevations and depressions cause elevations and depressions, respectively, in the height of sea level, which persists after the small variations caused by the currents are averaged over time. Accidents in the seafloor on horizontal scales of 30 to 300 km cause changes in sea surface height of up to 30 m, compared to only 1 m in the large geostrophic currents. Surface height varies 2 to 3 m per km change in seafloor height.

7.5 “El Niño and La Niña”

As mentioned at the beginning, there are natural causes that have global or nearly global repercussion on the climate on interannual, decadal and longer time scales. Some of these phenomena are the North Atlantic Oscillation (NAO), the Arctic Oscillation (AO) and “El Niño” (**ENSO: El Niño Southern Oscillation**).

In Spanish El Niño means ‘the Christ Child’ – a name given to it by the Peruvian fishermen who hundreds of years ago noticed how sometimes their coastal waters grew unusually warm and fish grew scarce around Christmas time. They had no way of knowing they were naming a vast weather pattern whose effects strike much of the globe (ESA 2005).

ENSO events are perturbations of the ocean-atmosphere system that oscillate between three states of the climate, the “normal conditions”, La Niña and El Niño (Maslin 2004). El Niño is an irregular oscillation in tropical Pacific currents around the Equator. Usually, the wind blows in a westerly direction in this region (Fig. 7.18a). This pushes the warmer surface water into the western Pacific (which can be as much as a half-meter higher than surface levels in the east). In the eastern Pacific, colder water from below the ocean’s surface is pulled up from below to replace the water pushed west. So, the normal situation is warm water (about 30°C) in the west, cold (about 22°C) in the east.

In an El Niño, the winds pushing that water to the west get weaker. With thermal circulation some of the warm water piled up in the west is released and moves back east, and not as much cold water gets pulled up from below. This makes the water in the eastern Pacific warmer, an El Niño trademark (Fig. 7.18b) (ESA 2005).

El Niño doesn’t stop there. Warmer ocean waters weaken the winds, which in turn further warms the water, a cycle that makes El Niño even stronger.

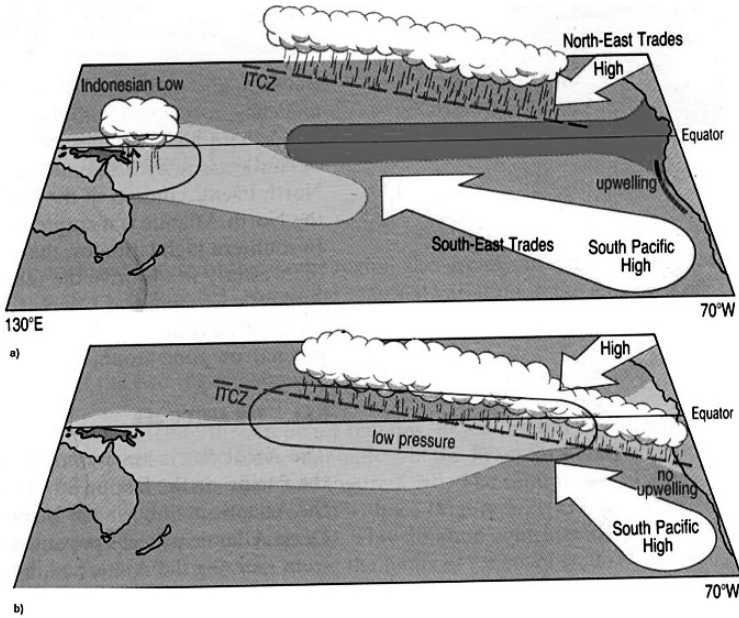


Fig. 7.18 Conditions in the Pacific during a) normal and b) El Niño years (The Open University 1989)

The best-known natural calamity characteristic of an El Niño event is probably the collapse of the anchoveta fishery off Peru, but its effects are considerably more wide-ranging than this, with consequences on climate patterns around the world. These can include vastly increased rainfall in South America, drought in Australia and fires across southeast Asia, dying coral reefs in India, severe winter storms in California, a heat wave in Canada and intense hurricanes ranging along the Pacific Ocean.

This phenomenon seems to occur every three to seven years. The El Niño of 1997–98 is estimated to have caused more than 30 000 million of US \$ of global property damage and an unknown toll in human lives.

La Niña is an equivalent cooling event during which the warm waters shift westwards to induce upwelling of cold water at the South América shores , reducing rainfall in the eastern equatorial Pacific but increasing it in the west (ESA 2005). La Niña is less frequent than El Niño, so they are asymmetric phenomenon. This asymmetry has yet to be explained from a theoretical point of view. In this sense, (McPhaden 1999) says, "...the strength of the 1997–1998 El Niño may be traceable to interactions of the ENSO cycle with some combination of global warming trends, the Pacific Decadal Oscillation , the seasonal cycle and the Madden-Julian Oscillation".

The ENSO may be observed perfectly from space, even before that it appears on the coasts of South America. The change in intensity and direction of the Trade Winds can be observed using scatterometers six months before Christmas, the changes in the SST by IR sensors such as the AATSR, the AVHRR or MODIS, the

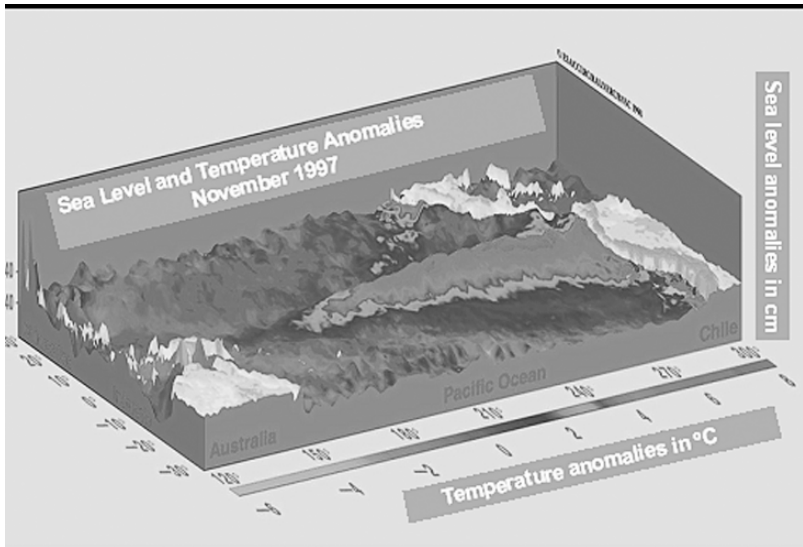


Fig. 7.19 Sea level and temperature anomalies for El Niño 1997 (From ESA)

changes in chlorophyll produced by the increase in the SST and the disappearance of the upwelling can be measured by sensors in the visible band such as the MERIS or the SeaWiFS and finally, the changes in the OST by altimeters such as the T/P, the ENVISAT RA-2 or the JASON (Fig. 7.19).

7.6 Conclusions

As we have seen, sensors installed onboard satellites provide us with a large and very diverse type of data for global observations. They are contributing for the last thirty years to the understanding of some complex phenomena that control our climate such as oceanic currents, coupled atmospheric-ocean phenomena, changes in oceans productivity and more. The use of satellite data together with the last generations of climate numerical models can be one of the most important keys to look in our future. But it is necessary a fast answer to stop the antropogenic global change. If we fail doing that, the earth will continue its travel through the universe, but without many passengers an board like many animal and vegetal species, including the human beings.

References

- Alley, R. B., Clark, P. U., Huybrechts, P., & Joughin, I. (2005). Ice-sheet and sea-level changes. *Science*, *310*, 456–460.
- Aristegui, J., Sangra, P., Hdez.-Leon, S., Cantón, M., Hdez-Guerra, A., & Kerling, J. (1994). Island-induced eddies in the Canary Islands. *Deep Sea Research*, *41*(10), 1509–1525.

- Aristegui, J., Tett, P., Hernandez-Guerra, A., Basterretxea, G., Montero, M.F., Wild, K., Sangra, P., Hernandez-Leon, S., Canton, M., Garcia-Braun, J. A., Pacheco, M., & Barton, E. D. (1997). The influence of island-generated eddies on chlorophyll distribution: a study of mesoscale variation around Gran Canaria. *Deep Sea Research I*, 44(1), 71–96.
- Barton, E. D., Aristegui, J., Tett, P., Cantón, M., García-Braun, J., Hernández León, S., Nykjaer, L., Almeida, C., Almunia, J., Ballesteros, S., Basterretxea, G., Escánez, J., García-Weill, L., Hernández-Guerra, A., López-Laatzén, A., Molina, R., Montero, M. F., Navarro-Pérez, E., Rodríguez, J. M., Van Lennig, K., Velez, H., Wild, K. (1998). The Transition Zone of the Canary Current Upwelling Region. *Progress in Oceanography*, 41, 455–504.
- Broecker, W. S. (1997). Thermoaline circulation, the Achilles heel of our climate system: Will man-made CO₂ upset the current balance? *Science* 278, 1582–1588.
- Bryden, H., Longworth, H., & Cunningham, S. (2005). Slowing of the atlantic meridional overturning circulation at 25° N. *Nature*, 438, 655–657.
- Burroughs, W. J. (2001). *Climate change: A multidisciplinary approach*. Cambridge University Press.
- Cabanes, C., Cazenave, A., & Le Provost, C. (2001). Sea level rise during past 40 years determined from satellite and in situ observations. *Science*, 294, 840–842.
- Calvin, W. H. (1998). The great climate flip-flop. <http://williamcalvin.com/>.
- Cantón Garbin, M., & Hernandez Guerra, A. (1991) La Teledetección de los océanos desde el espacio: Principios Físicos y Aplicaciones. *Rev. Española de Física*, 5(3), 8–14.
- CCLRC (2003). The ATSR Project. www.atsr.rl.ac.uk/images/sample/atsr-1/index.html.
- Curry, R. (2005). Dilution of the Northern North Atlantic ocean in recent decades. *Science*, 308, 1772–1774.
- Delibes, M., & Delibes de Castro, M. (Eds.). (2005). *La Tierra herida*. Destino, Spain.
- Donnadieu, Y., Godderis, Y., Ramstein, G., & Meert, J. (2004). A “snowball Earth” climate triggered by break up through changes in continental runoff. *Nature*, 428, 303–306.
- Dwyer, G. S. (2000). Unraveling the signals of global climate change. *Science*, 287, 246–247.
- ESA (2005). What causes El Niño?. www.esa.int/esaEO/.
- ESA (2007). ESA’s water mission: SMOS. www.esa.int/esaLP/.
- Gregg, W., Conkright, M., Ginoux, P., O’Reilly, J., & Casey, N. (2003) Ocean primary production and climate: Global decadal changes. *Geophysical Research. Letters*, 30(15), 1809–1812.
- Gribbin, J. (1986). *El Clima futuro*. Salvat. Spain.
- Hadley Centre, Meteorological Office, UK (2006). *Climate Change Science*. [www.metoffice.com/research/hadleycentre/pubs/brochures/B1. . . .](http://www.metoffice.com/research/hadleycentre/pubs/brochures/B1...)
- Häkkinen, S., & Rhines, P. (2004). Decline of subpolar north atlantic circulation during the 1990s. *Science*, 304, 555–559.
- Hernandez Guerra, A., Aristegui, J., Canton Garbin, M., & Nykjaer, L. (1993). Phytoplankton pigment patterns in the Canary Islands area as determined using Coastal Zone Colour Scanner Data. *Int. J. of Remote Sensing*, 14(7), 1431–1437.
- Houghton, J. T. (2004). *Global warming: the complete briefing*. Cambridge University Press.
- IFM (2006). Altimetry, ocean currents and the marine geoid. www.ifm.uni-hamburg.de/~wwwrs/altimetry.html.
- IPCC (2001). *The Scientific Basis*. Intergubernamental Panel for Climate Change.
- Johannessen, O. M., Khvorostovsky, K., Miles, M. W., & Bobylev, M. (2005). Recent ice-sheet growth in the interior of Greenland. *Science*, 310, 1013–1016.
- Levitus, S., Antonov, I., Boyer, T., & Stephens, C. (2000). Warming of the worlds oceans. *Science*, 287, 2225–2229.
- Lovelock K. J. (2007). *La venganza de la Tierra*. Planeta. Spain.
- Maslin, M. (2004). *Global warming: A very short introduction*. Oxford University Press.
- McPhaden, M. (1999). El Niño: The child prodigy of 1997–1998. *Nature*, 398, 559–562.
- Meehl, G. A., Washington, W., Arblaster, J., Hu, A., Buja, L., Strand, W., & Teng, H. (2005). *Science*, 307, 1769–1772.
- NASA (2003). www.earthobservatory.nasa.gov.
- NASA (2005). The physical ocean. <http://science.hq.nasa.gov/oceans/physical/index.html>

- Ohmoto, H., Watanabe, Y., & Kumazawa, K. (2004). Evidence from massive siderite beds for a CO₂-rich atmosphere 1.8 billion years ago. *Nature*, *429*, 395–399.
- Osborn, T., (2006). The thermoaline circulation. Climatic research Unit, UK. www.cru.uea.ac.uk/cru/info/thc.
- Parada Sanguino, M., Canton Garbin, M. (1998). Sea surface temperature variability in the Alboran sea from satellite data. *Int. Journal of Remote Sensing*, *19*(13), 2439–2450.
- Rahmstorff, S. (2002). Ocean circulation and climate during the past 120000 years. *Nature*, *419*, 207–214.
- Ramos, A. G., Pep, J., Williams, A., Petit, M., & Cantón, M. (1997a). Satellite derived scatterometer/ERS-1 sea surface wind stress curls in the oceans. ESA SP-414, 1391–1395.
- Ramos, A. G., Coca, J., Williams, A., & Cantón, M. (1997b). Satellite derived scatterometer ERS-1 sea surface wind vorticity in the Southwestern Indian Ocean. ESA Publications SP-405. The use and applications of ERS in Latin America, 235–239.
- Robinson, I., (1994). Satellite oceanography. John Wiley & Sons.
- Schiermeier, Q., (2006). Climate change: A sea change. *Nature*, *439*, 256–315.
- Schmittner, A., (2005). Decline of the marine ecosystem caused by a reduction in the Atlantic overturning circulation. *Nature*, *434*, 628–633.
- Stocker, T. F., (1998). The seesaw effect. *Science*, *282*, 61–62.
- Strong, A. E. (1989). Greater global warming revealed by satellite-derived sea-surface-temperature trends. *Nature*, *338*, 642–645.
- Tejera Cruz, A., Garcia Weil, L., Cantón-Garbín, M. (1997a). Study of mesoscale features and seasonal variability in the Canary Basin from GEOSAT, ERS-1 and TOPEX/POSEIDON altimeters data. ESA Publications SP-405. The use and applications of ERS in Latin America, pp. 211–218.
- Tejera Cruz, A., Garcia Weil, L., Cantón-Garbín, M. (1997b). Mesoscale variability in the Canary region from Altimetry. ESA Publications SP-414, pp. 1509–1515.
- Tejera, A., García-Weil, L., Heywood, K., & Cantón-Garbín, M., (2002). Observations of Oceanic Mesoscale Features and Variability in the Canary Islands area from ERS-1 Altimeter data, satellite infrared imagery and hydrographic measurements. *International Journal of Remote Sensing*, *23*(22), 4897–4916.
- The Open University (1989). Ocean Circulation. Pergamon Press.
- Velicogna, I., & Wahr, J., (2006). Measurements of time-variable gravity show mass loss in Antarctica. *Science*, *311*, 1754–1756.
- Uriarte, A. (2003). Historia del Clima. Servicio de Publicaciones del Gobierno Vasco. Spain.

Chapter 8

Observing Surface Waters for Global Change Applications

Richard G. Lawford

Abstract Water cycle observations play a major role in the detection, monitoring and prediction of global change. Furthermore, variations in the water cycle must be a central consideration when evaluating planning options to mitigate the impacts of climate variability and global change. Global change is used herein to describe the full range of impacts that humans have on the global water system. It is a continuing concern for society, since it plays a central role in the sustainability of the world's resource base and security issues. The continuing increase in the atmospheric concentration of greenhouse gases in the atmosphere is leading to changes in the Earth's climate including effects on the global water cycle (IPCC, 2001). Other human interactions in the Earth system are also causing significant changes in the water cycle (Hornberger et al., 2001). For example, the construction of dams and reservoirs and the drainage of wetlands over the last century have altered discharge patterns in many of the Earth's largest river basins.

This chapter describes the types of observational data needed to define baseline conditions against which future change can be compared. Integrated systems are needed to monitor change and its impacts. In this chapter these issues are addressed by considering the importance of surface waters and their sensitivity to change: by reviewing specific information requirements within each resource sector affected by change, and by exploring the potential of science and technology to provide new observational systems for monitoring surface waters and programs that address gaps in our current observational support for the resource sectors.

8.1 The Importance of Surface Inland Waters and their Sensitivity to Change

The availability of adequate and safe surface water supplies has been critical for the development of civilization and will continue to be for the foreseeable future. Civilization has not developed uniformly around the globe in part because precipitation and renewable surface waters are not evenly distributed. As a result some countries could be considered water-rich, while others are water-poor (Sullivan et al., 2003). These inequities have implications for national security, social and economic stability and environmental sustainability.

Nations such as Vietnam and Venezuela are located in wet areas while other countries like Algeria and Australia are predominately semi-arid. In some large nations, such as China, Canada and the United States, different parts of the country can have drought and flooding conditions simultaneously. Low levels of agricultural productivity caused by a lack of precipitation and irrigation water are deterrents to development in many arid and semi-arid regions. Despite sufficient water during average years in some developed countries, aggressive expansion has led to the commitment of resources to so many uses that the water available in dry years is less than the amount required to fulfill all the commitments. In the United States, different states have different laws to cope with these shortfalls. Some states allocate water to the most senior users in the basin first while other states prorate the water allocation according to the shortage that is being experienced (Fort, 2003). Either way, water shortages impose hardships on most communities.

Surface waters are also important for environmental health and services. Freshwater fish, water fowl and wetlands have requirements for water that are very critical although the needs are hard to quantify and difficult to incorporate into decision making processes rooted in economics. If society is to maintain its current level of ecosystem health and environmental services, these ecological demands for water must be satisfied.

There are a number of pressures on water resources, chief of which arise from the growth of the world's population (Vorosmarty et al., 2000; World Meteorological Organization (WMO), 1997). As cities grow and industrialization expands into new areas, the demands for water increase. Although the growth of water demand for irrigation for food production may slow over the coming decades, other demands such as water for biofuels is expected to increase. As people become concentrated in urban centers, the water supply systems that service these needs will continue to be burdened.

Human activities have other impacts on water resources. Humans are increasingly controlling runoff and surface water storage, although the consequences of their actions on the global water cycle are not well known. Environmental impact studies carried out for the construction of reservoirs, irrigation works and water diversions have shown that these developments have local impacts. However, systematic studies of the cumulative effects of these developments, especially in a global change context, remain in their infancy (Meybeck and Vorosmarty, 2004). As lands are given over to development, the natural drainage patterns of the landscape are disrupted. Land-use change (e.g., deforestation) also alters the evapotranspiration patterns and the supply of moisture from the surface to the atmosphere (Kabat et al., 2004; Henderson-Sellers et al., 1993). Some industries meet their needs for a steady supply of water by encouraging governments to build reservoirs that disrupt the natural flow patterns.

A better understanding of the global water cycle is needed to provide a basis for better predictions of the availability of water at local, regional and global scales. The global water cycle is responsible for the distribution of precipitation and, hence, the renewable water supply. The cycle consists of reservoirs and fluxes of moisture moving from one reservoir to another.

The climate has been changing in recent years. Global water cycle fluxes should be monitored to assess the intensification of the water cycle that is expected to occur as the climate changes. The rates of change are amplified by the global water cycle which is characterized by many non-linear processes. For example, a small change in precipitation can produce a larger percentage change in the runoff because the relationship between the two variables is non-linear and regionally unique.

Recent changes in the hydrological cycle have arisen because of the thermodynamic effects of climate change. In particular, the hydrologic cycle in areas where temperatures are increasing has been affected. Examples include changes in the seasonality of runoff in areas where temperatures are warming. As temperatures warm, thaw days during the winter become more frequent and the spring melt period begins earlier. As has been shown by Dettinger and Cayan (1995) for the western US this leads to earlier snow melt, runoff increases and shifts in runoff peaks and reductions in peak runoff amounts. Another water source affected by warmer temperatures is mountain glaciers. Recent reports (e.g., Barry, 2006) indicate that warmer temperatures during the past two decades have resulted in the melting of glaciers in all parts of the world. At higher latitudes, the runoff from the Arctic rivers in northern Russia has been increasing during the winter months in the period from 1940 to 2000, possibly reflecting greater rates of permafrost melt (Peterson et al., 2002).

Long-term records from meteorological and hydrographic monitoring stations are required to interpret potential climate trends and changes in variability. These data sets are needed to help resolve questions of importance to long-term infrastructure planning, such as, "if the water cycle is accelerating, what are the implications for flood frequencies?" In undertaking analyses to address these questions it must be recognized that the use of data for the detection of global changes imposes its own requirements for accuracy, precision and reliability.

Due to the great interest in weather and hydrologic phenomena, there are many records of key hydrometeorological variables. *In situ* data are widely available, although some issues of data processing are unresolved, such as the methods used for calculating the amounts of solid precipitation from gauge measurements and estimating the river flow under ice covers. Although the technologies for measuring stream flow are well-established, hydrographic observational capabilities are in decline in many countries (International Association of Hydrological Sciences (IAHS), 2001). Increasingly, satellites are being proposed as an alternate source of data for precipitation and hydrologic variables. Global measurements of surface and subsurface water and water quality from satellite systems are still at the experimental stage.

For climate prediction (e.g., seasonal to interannual) and monitoring, the availability of timely and high-quality precipitation information is critical. For example, the distribution of precipitation amounts over different time intervals is required for monitoring, for input into soil moisture models and for the initialization of forecast models. Accurate satellite estimates of precipitation are particularly suited for supporting climate prediction because ocean evaporation and sea surface temperature strongly influence the atmospheric circulation and, hence, the precipitation patterns. Koster et al. (2004) have shown that soil moisture also influences the predictability of precipitation over some land areas. This indicates that short-term climate

forecasts (monthly and seasonal) from models are also dependent on accurate soil moisture and precipitation estimates. In climate forecasts, small initialization errors can compound and grow into large biases. Reliable monitoring of precipitation and other surface energy and water fluxes can provide a basis for identifying and correcting the causes of these model biases. An operational integrated water cycle monitoring system that includes networks, satellite systems and data products for precipitation (e.g., Tropical Rainfall Measuring Mission (TRMM), Global Precipitation Mission (GPM), Global Energy and Water Cycle Experiment (GEWEX), Global Precipitation Climatology Project (GPCP)), as well as soil moisture (e.g., Soil Moisture Observing System), radiation balance for evapotranspiration (e.g., Clouds and the Earth's Radiant Energy System, High Resolution Infrared Radiation Sounder) and discharge/runoff (e.g., National Aeronautic and Space Administration (NASA) Surface Water Mission, together with four dimensional data assimilation (4DDA)), could provide a standardized record of climate variability.

8.2 Information Requirements of Different Sectors

While satellites provide a global perspective of water cycle information for decision making, frequently decision makers need data for specific locations or small watersheds. As described by Lawford et al. (2004a), there are numerous sectors that would benefit directly from an integrated water cycle observing system. The current observational capabilities and readiness for expanding these applications vary from sector to sector. Furthermore, as indicated in the following paragraphs which summarize Lawford et al. (2004a), a wide variety of measurements are needed to address the needs of these sectors.

8.2.1 Agriculture

Feeding the world's large and rapidly growing population constitutes a major societal challenge. The world's agricultural community is highly dependent upon irrigation for watering crops and on accurate precipitation and temperature predictions for planning cropping schedules. Forecasting agricultural yields based on precise precipitation and temperature information could benefit production planning and the agricultural commodities markets. Factors such as crop progress, condition and production are directly dependent on weather and climate and can be effectively monitored using a combination of water cycle data, satellite data and crop models. Timing of precipitation is also critical information for assessing crop productivity, while soil moisture is a highly desirable variable for many applications. Local-scale information for field management, based on hydrometeorological data, weather forecasts (including seasonal) and high-technology telemetered *in situ* soil moisture monitoring for fine scale irrigation application scheduling are now available in the developed world.

8.2.2 Water Management and Sustainable Development

Water management involves balancing the demands for water with its availability in a way that ensures equitable, socially acceptable and economically prudent decisions. Time series of ground-based hydrometeorological data are the most commonly used observations to assess water supply. Regional supply applications rely on more or less standardized water balance schemes of varying sophistication. While climate change will alter the supply side of this balance over time, water managers spend the vast majority of their time coping with variability in the water supply on the daily to interannual time scales. Our state of readiness to deal with this variability currently depends, in great measure, on the level of investment in *in situ* monitoring. At the national level this is highly correlated with the level of economic development. There is a pressing need for consensus on methods for producing and applying operational assimilated and integrated hydrometeorological products. Based on the primary applications of these data, an emphasis on variability and extremes—as opposed to average conditions—is warranted.

Vorosmarty et al. (2000) have shown that population growth rather than climate will be the major cause of change in the long-term supply/demand balance. Data, from various sources, have been used to establish demand statistics such as household water use, industrial withdrawal for processing and cooling, and agriculture. In the developing world these data are not regularly available but are sometimes collected through special studies of water use. In well-monitored parts of the world, these data can be reliable, although some administrative entities do not readily share this information. Indicators of water stress such as relative water scarcity, coping capacity against periodic or sustained water shortages, the Water Poverty Index (Sullivan et al., 2003), etc., are derived variables based on the co-location of measured or estimated water demand and availability statistics, together with socioeconomic information.

8.2.3 Land Use and Planning

As populations increase, there are pressures to use more marginal lands for agriculture and to allocate some of the more productive agricultural lands to urban development. There is a close correspondence between land stewardship and the terrestrial water cycle, as land use practices and planning, which are important for water quality, could benefit greatly from ready access to new data products, especially if these products could encourage harmonization of land use and water management plans.

Readiness for regional scale mapping activities using remote sensing data not only is very high, but there are also a number of global land-use/cover products available. However, some land-use and land-suitability mapping applications require a level of detail not yet available through remote sensing; consequently, they rely on *in situ* observations, aerial photography and documentary data. The availability of such data tends to be highly variable across the globe, largely reflecting economic and political factors. As a result, land use planning methodologies range from very sophisticated in some areas to non-existent in others.

8.2.4 Ecosystems and Water Quality Assessment

Rapid urban development is increasing the demand for clean water at the same time as it increases the pressure on sewage and water treatment systems. For most of the world, water quality monitoring and assessment is very inadequate. In the developed world, individual focused studies and routine monitoring are respectively better. A broad spectrum of variables such as suspended solids, dissolved nutrients, metals, chlorophyll, organic loading and acidity/alkalinity are monitored through point-scale river chemistry sampling. Given the strong link between primary productivity and the state of water, it is possible to monitor inland water bodies (e.g., lakes) for manifestations of productivity (e.g., eutrophication) using optical sensors on satellites. Other satellite-based monitoring tools are needed to enhance global monitoring.

8.2.5 Global Biogeochemistry

Biogeochemical cycling is closely linked to the cycling of water. Models are typically used to estimate biogeochemical signals associated with terrestrial and ocean productivity. Field campaigns (e.g., the Large-scale Biosphere-Atmosphere Experiment in the Amazonia (LBA)) have provided some regional data bases, as have the Long Term Ecological Research sites. However, data from widespread, routine terrestrial monitoring have not been available on an operational basis. An integrated water cycle/biogeochemical cycle information system is needed.

8.2.6 Fisheries and Habitat Management (Aquatic, Terrestrial)

Overfishing and water contamination have reduced the number of fisheries during the past two decades, although better stock management and aquaculture have made some species of fish more abundant. Broad application of satellite remote sensing for fisheries and habitat management currently exists. Optical and microwave remote sensing, both satellite-based and airborne, are used in habitat monitoring. Fish population estimates and habitat measures are derived from *in situ* measurements. In large inland water bodies, fish can be detected and populations estimated by sonar. However, most inland water bodies are relatively small and generally need airborne, high-resolution remote sensing information, which is typically costly. Operational applications have not yet been sufficiently refined.

8.2.7 Human Health

Many world health issues are directly traceable to anomalies in precipitation and other components of the water cycle. For example, infectious and vector-borne diseases, such as malaria, rift valley fever, west Nile virus, encephalitis and others

can be correlated to environmental factors, including precipitation, flooding and humidity. Ponds and standing water resulting from excessive precipitation are particularly favorable for disease vectors (e.g., mosquitoes). Additionally, extreme weather events such as flash floods, hurricane-induced floods and excessive runoff can create sewage overflows and lead to health problems related to pathogens, biotoxins and sewage pollutants. Preliminary evaluations have established relationships between environmental factors like precipitation/excess water and outbreaks of diseases. Prototype operational applications of remote sensing are being used to map inundated areas for malaria habitat assessment and control. With further research, improved observations of precipitation could provide information needed by the health community to (a) identify weather and climate patterns associated with disease outbreaks, and (b) provide advance warnings of outbreaks, thereby enabling preventative measures such as vaccination and vector control.

8.2.8 Flood Forecasting

Floods arise from a number of causes, including prolonged rainstorms over large basins, heavy winter snow with rapid spring melt, heavy thunderstorms over small basins, rain on snow events and ice jams in northern rivers. They continue to be one of the costliest and deadliest natural hazards worldwide. In general, forecast information is required before a flood event to indicate where it will occur and how severe it will be. Information is also required on the state of reservoirs and soil moisture, since these will determine the potential water retention capacity for flood waters. During the flood, information is needed on water levels for emergency operations, while after the flood the inundated areas must be delineated for clean-up operations. Flood warning and protection systems have incorporated geostationary satellite precipitation fields in combination with hydrologic models. Such operational systems often are calibrated to particular locations based on empirical models. Linked sub-basin responses constitute a flood warning system, with flood waves tracked as they travel down monitored rivers. Flood warning systems in developing countries often do not have this level of sophistication. There is a great deal of potential for using water cycle measurements more extensively in flood defense.

8.2.9 Drought Monitoring and Prediction

Many drought monitoring systems depend on data from polar orbiting and geostationary satellites, as well as *in situ* information. Some drought monitoring systems use indexing schemes, while satellite data provide Leaf Area Indices (LAI) and greenness indices. Groundwater levels in wells and lake levels have also been used to monitor drought. Monitoring water available from snow packs is also important for determining whether there is sufficient spring moisture available to recharge soil moisture and groundwater reserves and to replenish lakes and reservoirs.

Satellite remote sensing is a particularly important technology for augmenting information from ground-based observational systems and for increasing our level of readiness to deal with the impacts of droughts. Reanalysis using Numerical Weather Prediction (NWP) models can provide a time series of drought variables and thus the probability statistics of drought. Systems that combine satellite and *in situ* data can also support the operational monitoring of progressive drought severity (i.e., non-rain events, surface temperature and radiation).

8.2.10 Other Water Cycle Hazards

Extreme events, such as high intensity precipitation events, mudflows and debris flows, are expected to increase as the climate changes. Rapid slope movements (e.g., avalanches, mudslides and debris flows) pose significant risks for people and structures in susceptible areas. Mudslides and debris flows generally start on steep hillsides during periods of intense rainfall or rapid snowmelt. Often, unwise intensification of land-use and human occupation of questionably stable ground cause or exacerbate mudflow and debris-flow problems. Data are required to support the identification of areas vulnerable to land slippage and to provide early warnings of increases in landslide risks.

Typically, avalanche forecasting is accomplished by conducting regular snow stability tests and combining test results with meteorological information. Most snow stability tests are simple mechanical tests of snow layer failure. The most reliable avalanche predictions require a detailed diagnosis of the snow pack structure. Avalanche prediction is aided by Geographical Information Systems (GIS) that can map avalanche probability based on topographic analysis and weather data, as well as new data gathering technologies such as frequency modulated, continuous wave (FMCW) and satellite microwave radiometry.

8.3 Review of the Existing Systems and the Potential of Science and Technology to Provide a Basis for Monitoring Surface Waters

In order to monitor global change for the world's water resources, it is necessary to have data sets that are global and long term. *In situ* data are the most reliable source of long-term records but they do not provide uniform global coverage. Satellites do provide uniform global coverage but their records are generally too short for climate trend analysis. As Maurer (2003) describes, some of the problems associated with the maintenance of uniform *in situ* networks around the globe arise because some nations:

1. do not have adequate funds or the will to give priority to observing networks,
2. are unable to adequately quality control and archive observations, and
3. are reluctant to share their data with others.

There are a number of issues that affect the rate at which monitoring programs for surface waters improve. The lack of technology suitable for overcoming the limitations of some nations to mount observing programs is being addressed. In particular, the developments of space-based remote sensing techniques now are being applied to monitor changes in runoff (Alsdorf and Lettenmaier, 2003) and groundwater (Tapley et al., 2004) on a global basis.

Observational programs must deal effectively with scale issues. The internal variability of water cycle variables occur over a wide range of space and time scales. For example, precipitation phenomena vary over scales of 10s of meters to 100s of kilometers. Knowledge of this spatial variability is a central requirement for planning observational networks. In some cases, water cycle processes are binary (e.g., rain/no rain) and exponential and interact in non-linear ways that must be accounted for in models and observational programs. Atmospheric processes are influenced by atmospheric turbulence, which is a function of air stability and wind speed. Clouds and, in turn, precipitation phenomena have characteristic scales that are dependent on whether the cloud is the result of convective processes or large-scale dynamic systems. Even within the same precipitation event, small pockets of high precipitation intensity may exist and affect the accumulation patterns at the surface. It is this accumulation pattern that drives the streamflow, soil moisture and infiltration into the groundwater system; however, the runoff and soil moisture spatial scales are also influenced by the underlying topography and physiography. For example, runoff is affected by the slope and aspect of the underlying surface and structure of the river network. Soil moisture is influenced by the nature of the underlying surface, the vegetation cover and the hydrologic properties of the soil.

The implementation of new observational programs generally is a challenge because new measurements must be validated in areas where *in situ* calibration data do not exist. Furthermore, poor planning often reduces or eliminates the overlap needed between different observation types that allows for modern records to be merged with traditional data bases or with older satellite records.

The status of measurements of different water cycle variables differs among variables and applications. For some variables, such as precipitation, extensive *in situ* networks exist and observations have been taken for 100 years or more. For other variables, such as radiation, the measurements are complicated and the number of stations around the world that can take the measurements are limited. Table 8.1 provides a limited set of requirements that were compiled from interactions with users (Lawford et al., 2004a).

Before looking at specific variables, it is useful to comment on the integrated water cycle as simulated by models and reanalysis products. One type of analysis has been carried out by Roads et al. (2002) using the National Centers for Environmental Prediction (NCEP) Reanalysis II and another by Trenberth et al. (2007) using the European Centre for Medium-range Weather Forecasts (ECMWF) reanalysis products. Both of these studies show that while models are improving in their ability to simulate water cycle processes, substantial research is required to make the models good enough to serve as tracking tools for all components of the water cycle.

Table 8.1 List of observational requirements for water cycle variables

Variable	Hor. Res.	Temp. Res.	Accuracy
Precipitation	4–5 km	3 hr	0.1 mm/h
Soil Moisture	10–100 km	1–10 days	5%
Streamflow	1–10 km for basins	1–10 days	5%
Lake Levels	1–10 km	1 wk – 1 mo	5%
Snow Cover	1–10 km	24 hr	10%
Clouds	100 m–10 km	3 hr	5%
Water Vapor	10–100 km	3 hr	5%
Surface Fluxes	10–100 km	3 hr	5%
Short Wave	10–100 km	3 hr	5 w/m ²

8.3.1 Precipitation

At present, precipitation is observed through a combination of observations from a wide variety of instruments and systems, some of which include: precipitation gauges, surface-based rain radars, observations of passive microwave radiance from Low Earth Orbit (LEO) satellites and visible and infrared radiance observations of clouds from both LEO and geostationary satellites. These observations are combined in different ways, depending upon the required scales and accuracies and on the type of observations available.

Satellites provide the data input for global products such as the GPCP products. Initially these products, which are produced by combining data from a global network of rain gauges, geostationary satellite infrared and passive microwave observations, were available at $2.5^\circ \times 2.5^\circ$ and monthly resolution (Huffman et al., 1997; Adler et al., 2003). A product with similar characteristics and data sources but utilizing a different approach known as the National Oceanic and Atmospheric Administration (NOAA) Climate Prediction Center (CPC) Merged Analysis of Precipitation (CMAP), was developed by Xie and Arkin (1997). These products have been used in studies of Extremes (Curtis et al., 2007) and tropical rainfall (Gu et al., 2006). However, in both cases hydrologic users have clearly stated that they are seeking data sets with high spatial resolution for their models. GPCP responded by developing and implementing products with near-global coverage and much finer spatial and temporal resolution, (i.e., $1^\circ \times 1^\circ$ and daily; Huffman et al., 2001). Even this resolution is not adequate for many purposes, and so GPCP has begun experimental production of a product on $0.25^\circ \times 0.25^\circ$ and three-hourly scales. New products based on TRMM high resolution data processing procedures such as the Artificial Neural Network (ANN), used to generate the PERSIANN products (Sorooshian et al., 2000), are also becoming available. It is anticipated that GPM will eliminate the need for interpolation systems and provide products with global extent on a three-hourly basis (Smith et al., 2006).

8.3.2 Stream Discharge

Surface runoff was affected by the construction of dams and reservoirs during the 20th century. These reservoirs have generally been constructed to supply water for

irrigation, urban water demands and hydroelectricity and to control flood waters and to modify the seasonal and interannual variability of the flow. The trends seen in runoff data have to be interpreted in terms of changes in the distribution and storage of water as well as changes in precipitation patterns arising from climate change. In general, there are major challenges in acquiring data in near-real time, especially in developing countries (Maurer, 2003). Even in regions with traditionally extensive hydrological monitoring networks, a net loss of recording stations continues to take place (IAHS, 2001). Although there are estimates of the surface storage in lakes, wetlands and river channels, the capacity to inventory the amounts in these stores on a regional basis needs to be developed. Satellite-based sensors offer an alternative for near real-time data for lake/river stage and river discharge for applications at continental and global scales. For example, determination of river stage and flow estimations when ice is present remains a challenge.

In addition to the use of better and more extensive hydrometric measurements where available, the mapping of runoff is now being expanded through the use of other technologies such as acoustical means for measuring river level. While these measurements offer more precision at a point, they do not provide the global coverage that satellite data offer. Hydrologic altimetry is notionally based on a radar remote sensing system, with day/night and all-weather capability for river and lake stages (Alsford and Lettenmaier, 2003). These satellite data often provide spatial averages but lack the horizontal resolution to give river heights except for the largest rivers. As for other variables, it is believed that the best results will be obtained when the measurement system combines information from very accurate and precise *in situ* measurements with the larger spatial scale measurements available from satellite.

8.3.3 Soil Moisture

Soil moisture information is critical for understanding the global water and energy cycles, for predicting precipitation and for advisory services for local water resource managers. Research by Koster et al. (2004) and others has shown that soil moisture contributes to the monthly and seasonal predictability of precipitation in some continental areas. Soil moisture data sets are also important for improving numerical weather forecasts (Drusch, 2007). Remote sensing of surface layer soil moisture, or “soil wetness,” has been studied extensively in the course of numerous field and/or airborne campaigns (Jackson et al., 2002). The use of remote sensing for soil moisture has been convincingly demonstrated in terrain covered by thin or moderately dense vegetation (e.g., typical crops), using passive microwave emission radiometry at low microwave frequencies (1.4 to 3 GHz).

The European Space Agency (ESA) is currently implementing the Soil Moisture and Ocean Salinity (SMOS) mission for measurement of soil moisture and ocean salinities. A follow-on mission with the goal of a 10-km spatial resolution, regarded as the “fingerprint” spatial scale of soil-moisture heterogeneity for land/boundary-layer interactions and increased temporal coverage, could augment this initial mission. These space-based data sources combined with data assimilation systems will

make it possible to contribute to the monitoring of soil moisture at finer scales compatible with the needs of hydrometeorology.

8.3.4 Surface Water Storage

Surface water storage is an important variable for many applications. Surface water can be stored in permanent or semi-permanent reservoirs such as lakes, reservoirs and wetlands and in seasonal reservoirs such as the snow pack. Wetlands have large variability and many of them are vulnerable to droughts and other human interventions such as drainage. In general, measurement of the levels and volumes of lakes and wetlands is not done systematically on a global basis, although regional data bases do exist. Remote sensing provides a technique for greatly expanding data from these important ecological reserves.

Snow on the ground is a cold season water reservoir that becomes accessible during spring melt. Climate modelers are very concerned about the area of snow cover, which has important albedo effects and is very sensitive to global warming. Water resource managers generally are more interested in the water content of the snow pack. Snow cover measurements are used to initialize forecast models for weather and hydrologic prediction. Satellite data, primarily from polar orbiting and geostationary satellites (e.g., LandSat, Moderate Resolution Imaging Spectroradiometer (MODIS), Goddard Earth-Observing System (GEOS), Advanced Very High Resolution Radiometer (AVHRR)), are the only sources of comprehensive high-resolution data for many key regions. In addition, passive microwave measurements provide a basis for reliable snow-pack estimates of water equivalent in areas with dry snow and short vegetation cover.

In situ measurements have been developed for different aspects of the snow pack. Snow pillows weigh the overlying snow pack while snow boards and snow rulers provide data on the depth of the snow pack. However, the heterogeneity of snow depth can make *in situ* measurements at a point irrelevant for non-representative areas where local snow processes such as drifting and blowing are large enough to change the snow retention in a very short period. Furthermore, these data are usually available for a limited number of critical locations but are not dense enough to provide reliable snow maps.

Both remote sensing and *in situ* measurements are used to define the distribution of permafrost. In the past, the main source of information about permafrost came from temperature profiles in boreholes in permafrost regions. Some *in situ* networks with soil temperature profiles are useful for monitoring ground frost. Lower frequency satellite measurements can provide useful freeze/thaw products because of their improved ability to penetrate vegetation.

8.3.5 Water Quality

The quality of water in lakes, rivers and reservoirs is affected by increasing industrialization in areas where environmental standards are neither developed nor enforced.

A number of case studies of water quality trends associated with industrial development and river cleanup are given in the World Water Assessment Report (WWAP, 2003). Climate change is expected to lead to warmer water temperatures, which will enhance the growth of algae and have an adverse effect on oxygen levels in the water. Water quality measurements are needed to provide assessments of the status of water quality in lakes and reservoirs for management purposes. Typically this information is needed by municipal drinking and sanitation utilities, as well as agriculture, recreation, industry and ecological managers seeking to maintain standards for human health and biological integrity. *In situ* water quality monitoring programs have been maintained for several decades in many developed countries, frequently relying on grab samples and laboratory analyses. Traditional water-quality sampling and analysis is time consuming, expensive and only provides information about a single location at one point in time. Satellites may provide a partial alternative to the monitoring of ambient water quality. Furthermore, the lack of technical, institutional and financial resources, discontinuity of historic records, political instability and ineffective and slow dissemination of data are obstacles to proper water-quality assessment in many countries. Currently water quality data are archived in the Global Environmental Monitoring System (GEMS) water quality data base, operated by the United Nations Environmental Program (UNEP). GEMS acquires *in situ* data on water quality from stations around the world for use in global environmental assessments.

Remote sensing could provide global coverage for a limited number of parameters. These observations could be of particular value in countries where *in situ* measurements are sparse or nonexistent. The majority of these have focused on clarity, chlorophyll, suspended solids, color and temperature. Future satellite sensors should be hyperspectral, have high signal-to-noise ratios and large dynamic ranges that do not saturate over cloud or coastal features.

8.3.6 *Evaporation*

If the global water cycle intensifies under global change, then the latent heat flux can be expected to increase on a global basis. Surface fluxes are directly measured only at eddy flux towers, which are operated on an experimental basis in many countries. Although remote sensing techniques cannot measure evaporation or evapotranspiration (ET) directly, techniques have been developed to estimate ET from the energy balance equation (Nishida et al., 2003; Diak et al., 2004). These techniques are also critical in estimating carbon uptake, since ET determined from satellite observations is related to biomass production (Moran et al., 1995) and carbon sequestration. Typical differences between remote sensing estimates and observed values are within 10%. Stable isotopes such as ^{18}O and ^2H provide an alternative method for deriving evaporation rates.

Over the oceans, information about the energy balance is needed to refine our knowledge of the “atmospheric demand” for water and heat and to develop more accurate estimates of large-scale air-sea fluxes. Measurements of ocean-surface

wind-velocity data, atmospheric temperature and humidity profiles, ocean-surface temperature and total precipitable water measurements from satellite and buoys provide the information needed to compute this flux. The SEAFLEX project (Curry et al., 2004) brings together various data sets to produce a range of air-sea interaction products, including the latent heat flux.

8.3.7 Groundwater

As society increasingly turns to groundwater to meet its water shortages, caused by periodic droughts and the over-allocation of surface waters, it will be increasingly important to inventory and monitor groundwater availability. Groundwater measurements are generally collected at the state or province level. Furthermore, the observation and data processing methods have not been standardized to the same level as surface hydrology. In view of the limited *in situ* groundwater observations available in central archives, attention is being given to the estimation of groundwater from time-variant space-based measurements of the gravimetric anomalies. These anomalies result from changes in ground and surface water mass. The Gravity Recovery and Climate Experiment (GRACE) mission uses high-precision, satellite-to-satellite tracking to measure changes in mass distribution equivalent to $\pm 1\text{cm}$ variation in water storage over a $500 \times 500 \text{ km}^2$ area (Tapley et al., 2004). Because the method is essentially gravimetric, no discrimination is possible between changes in water stored in various reservoirs (e.g., snow pack, soil moisture and groundwater), so additional modeling and analysis is required (Rodell et al., 2004). Data from permanent scatterers with European Remote Sensing Synthetic Aperture Radars have demonstrated the possibility of detecting land-surface movements arising from the depletion of groundwater aquifers.

8.4 Moving Forward

In order to comprehensively assess these needs in a coordinated fashion and to develop strategies for influencing them, several initiatives focusing on Earth observations and the water cycle have been launched. In the 1990s, the Global Observing System panels were established to address the needs of different communities to study observational systems. These included the Global Climate Observing System (GCOS), Global Terrestrial Observing System (GTOS) and Global Ocean Observing System (GOOS). The GCOS plan (GCOS, 2003) deals with many of the issues that concern the water cycle community. These were followed by the formation of the Integrated Global Observing Strategy Partnership (IGOS-P) in the late 1990s and the Group on Earth Observations (GEO) in 2004. While the activities of the global observing programs are well known, the later two programs are newer and described here in more detail. In addition, GEWEX, which supports these observation coordination programs, is briefly described.

8.4.1 *The Integrated Global Observing Strategy*

In 1998, the Committee on Earth Observing Systems (CEOS) joined with global environmental programs to form the IGOS-P. IGOS-P launched the preparation of a number of theme reports and established working groups to oversee their implementation. As part of this effort, the Integrated Global Water Cycle Observations (IGWCO) theme was developed and approved in 2004. To improve the relevance of Earth observations to water cycle needs, IGWCO has developed initiatives in a number of areas, including the observation of priority cycle variables, the integration of data sets of different types and the use of information in meeting the demands of users. IGWCO activities focus on strategies rather than the design and development of observational and information systems. Some IGWCO activities related to water cycle variables are briefly described below.

1. **Precipitation:** IGWCO, in collaboration with the International Precipitation Working Group and the GEWEX, is involved in the development of an Integrated Precipitation Product that will bring together the diverse precipitation measurements available through gauges, radar and satellites. An integrated product will be developed after an initial assessment of the quality of the high resolution global precipitation products currently available.
2. **Soil Moisture:** IGWCO is coordinating its soil moisture activities with the Global Climate Observing System (GCOS) Implementation Plan. GCOS plans will enable scientists to bring the best available *in situ* observations together with SMOS and other satellite data and modeling and data assimilation capabilities to produce an experimental integrated soil moisture product.
3. **Water Quality:** IGWCO is assessing the potential of remote sensing data to evaluate water quality in areas where environmental stress is high so that guidance can be given for targeted comprehensive surface-based monitoring activities. IGWCO is working with GEO to explore these opportunities in more depth.
4. **Streamflow and Groundwater:** Plans for the integration of runoff and groundwater are under development. The runoff project will take advantage of the research activities supporting the development and evaluation of the WaTER mission (Alsdorf and Lettenmaier, 2003). GEO also is developing proposals to strengthen the hydrometric network.

Other IGWCO activities of a more integrative nature involve IGWCO collaboration with ground water activities the Coordinated Energy and water cycle Observation Project (CEOP) (see Koike, 2004), the Global Water System Project (GWSP) (see GWSP, 2005) and Capacity Building activities. IGWCO has benefited from the data systems in CEOP developed in conjunction with the CEOS Working Group on Information Systems (WGISS). Recently, two capacity building workshops were held in Buenos Aires, Argentina and Bangkok, Thailand in collaboration with GEO. Both of these workshops drew participants from humid areas who elaborated the requirements for Earth observation systems to support flood forecasting and monitoring as well as other regional water cycle phenomena.

8.4.2 *The Group on Earth Observations*

GEO is an Intergovernmental Group composed of more than 70 nations and more than 43 participating international organizations that have joined to implement the Global Earth Observation System of Systems (GEOSS) over the next 10 years. GEO is working towards a global, coordinated, comprehensive and sustained system of Earth observing systems. This Group was formally established at the Third Earth Observation Summit in 2004. Its primary objectives are: 1) Build a sustainable, comprehensive, coordinated GEOSS, 2) Provide open and easy access to data anytime, anywhere, and 3) Increase the use of Earth observations. GEO has established nine Societal Benefit Areas, namely: 1) Reduction and prevention of disasters, 2) Human health, 3) Energy management, 4) Climate change, 5) Water management, 6) Weather forecasting, 7) Ecosystem, 8) Agriculture, and 9) Biodiversity. Both the Water Management and Climate Societal benefit areas include a number of goals that advance the use of Earth observations in water cycle monitoring. The plans for GEO are documented in its ten-year implementation plan (GEO, 2005). Plans to merge the IGOS-P themes unto the GEO programme are now being implemented.

8.4.3 *GEWEX*

The GEWEX project was initiated under the World Climate Research Programme (WCRP) in 1988 to utilize the growing capabilities of Earth observing systems in understanding the climate system. Given the progress of GEWEX in developing the capabilities of using satellite data, the GEWEX mission could be defined functionally as “*the development and application of planetary Earth science, observations and models to climate and hydrology.*” In fulfilling this mission, GEWEX addresses its central science objectives dealing with global energy and water budgets. It has developed more than 40 coordinated projects and activities that involve global and regional data sets and products, climate system analyses, model development, predictability studies, field campaigns, process studies and applications (Sorooshian et al., 2005). GEWEX has developed a number of long-term climate data sets from satellite data for clouds, precipitation, water vapor, radiation and aerosols. The GEWEX Hydrometeorology Panel (GHP) which has recently merged with the Coordinated Enhanced Observing Period to form the Coordinated Energy and water cycle Observation Project (CEOP) and the GEWEX Modeling and Prediction Panel (GMPP), which oversee GEWEX field campaigns and continental-scale studies, use satellite data to evaluate the results of regional models and to understand regional processes (Lawford et al., 2004b). GEWEX also initiated CEOP (Koike, 2004), which brings together *in situ* and satellite data and model output to address critical science issues related to Water and Energy Simulation and Prediction (WESP) and monsoons.

8.5 Summary and Conclusions

Many of the techniques that support monitoring of global change and its impacts also facilitate the realization of societal benefits of Earth observations. There are many potential applications of Earth observations that could bring large benefits to society if they were fully implemented. Some of these benefits are being realized in the climate area where long-term (25+) year records derived from satellite data are now available. Others are being realized in the water management area, where better forecasts are being produced as a result of the assimilation of satellite data. Currently the rate of development is limited by society's investment in these techniques, rather than the existence of the enabling technologies themselves.

However, there are also potential applications that are not being fully exploited. These arise because not all nations have access to the funds to maintain effective observational networks, and the capacity to fully utilize the new satellite products, nor do all nations share their data. In areas such as global change monitoring, where there are widespread public concerns but few advocates for a specific technology, these deficiencies limit the effectiveness of global assessments of environmental change. New programs established to coordinate the development of observational systems may help address these problems. In the near term, GEO may have the best potential because of the political support it has garnered for its activities.

References

- Adler, R.F., G.F. Huffman, A. Chang, R. Ferraro, P. Xie, J. Janowiak, B. Rudolf, U. Schneider, S. Curtis, D. Bolvin, A. Gruber, J. Susskind, and P. Arkin, 2003: The Version 2 Global Precipitation Climatology Project (GPCP) Monthly Precipitation Analysis (1979-present). *Journal of Hydrometeorology*, 4(6), 1146–1167.
- Aldorf, D.E., and D.P. Lettenmaier, 2003: Tracking Fresh Water from Space. *Science*, 301, 1491–1494.
- Barry, R.G., 2006: The Status of Research on Glaciers and Global Glacier Recession: A Review. *Progress in Physical Geography*, 30(3), 285–306.
- Curry, J.A., A. Bentamy, M.A. Bourassa, D. Bourras, E.F. Bradley, M. Brunke, S. Castro, S.H. Chou, C.A. Clayson, W.J. Emery, L. Eymard, C.W. Fairall, M. Kubota, B. Lin, W. Perrie, R.R. Reeder, I.A. Renfrew, W.B. Rossow, J. Schulz, S.R. Smith, P.J. Webster, G.A. Wick, and X. Zen, 2004: Seaflux. *Bulletin of the American Meteorological Society*, 85(3), 409–424.
- Curtis, S., A. Aalahuddin, R.F. Adler, G.F. Huffman, G. Gu, and Y. Hong, 2007: Precipitation extremes estimated by GPCP and TRMM: ENSO Relationships, runoff and groundwater Accepted, *Journal of Hydrometeorology*. (Accepted for publication).
- Dettinger, M.D. and D.R. Cayan, 1995: Large-scale atmospheric forcing of recent trends toward early snowmelt in California. *Journal of Climate*, 8, 606–623.
- Diak, G.K., J.R. Mecikalski, M.C. Anderson, J.M. Norman, W.P. Kustas, R.D. Torn, and R.L. Wolfe, 2004: Estimating Land Surface Energy Budgets from Space. *Bulletin of the American Meteorological Society*, 85(1), 65–78.
- Drusch, M., 2007: Initializing numerical weather prediction models with satellite derived surface soil moisture: Data assimilation experiments with ECMWF's Integrated Forecast System and the TMI soil moisture data set. In press, *Journal of Geophysical Research*.

- Fort, D.D., 2003: Water policy for the West: Who makes it? What is it? Will it lead us to a sustainable future? (In R.G., Lawford, D. Fort, H. Hatmann, and S. Eden, (Eds.), *Water: Science, Policy and Management*). Water Resources Monograph No. 16, American Geophysical Union, Washington, DC, 123–141.
- Global Climate Observing System (GCOS), 2003: The Second Report on the Adequacy of the Global Observing Systems for Climate in Support of the UNFCCC. GCOS, Geneva, Switzerland.
- Global Water System Project (GWSP), 2005: The Global Water System Project: Science Framework and Implementation Activities. Earth System Science Partnership, ESSP Report No. 3, GWSP Report No. 1, 76 p.
- Gu, G., R. Adler, G. Huffman, and S. Curtis, 2006: Tropical Rainfall Variability on Interannual-to-Interdecadal/Longer-Time Scales Derived from the GPCP Monthly Product. Submitted, *Journal of Climate*.
- Henderson-Sellers, A., T.B. Durbridge, A.J. Pitman, R.E. Dickinson, P.J. Kennedy, and K. McGuffie, 1993: Tropical Deforestation: Modelling Local to Regional Scale Climate Change. *Journal of Geophysical Research*, 98, 7289–7315.
- Hornberger, G.M., J.D. Aber, J. Bahr, R.C. Bales, K. Bevan, E. Foufoula-Georgiou, G. Katulo, J.L. Kinter III, R.D. Koster, D.P. Lettenmaier, D. McKnight, K. Miller, K. Mitchell, J.O. Roads, B.R. Scanlon, and E. Smith, 2001: *A Plan for a New Science Initiative on the Global Water Cycle*. U.S. Water Cycle Study Group of the U.S. Global Change Research Program (USGCRP), USGCRP Program Office, Washington, DC.
- Huffman, G.J., R.F. Adler, P. Arkin, A. Chang, R. Ferraro, A. Gruber, J. Janowiak, A. McNab, B. Rudolf, and U. Schneider, 1997: The Global Precipitation Climatology Project (GPCP) Combined Precipitation Data Set. *Bulletin of the American Meteorological Society*, 78(1), 5–20.
- Huffman, G.J., R.F. Adler, M.M. Morrissey, D.T. Bolvin, S. Curtis, R. Joyce, B. McGavock, and J. Susskind, 2001: Global Precipitation at One-Degree Daily Resolution from Multisatellite Observations. *Journal of Hydrometeorology*, 2(1), 36–50.
- International Association of Hydrological Sciences (IAHS), 2001: Global Water Data: A Newly Endangered Species. *EOS, Trans Am Geophysical Union*, 82(5), p. 54, 56, 58.
- Intergovernmental Panel on Climate Change (IPCC), 2001: *Climate Change 2001: The Scientific Basis*. Cambridge University Press.
- Jackson, T.J., A.Y. Hsu, and P. O'Neill, 2002: Surface Soil Moisture Retrieval and Mapping Using High-Frequency Microwave Satellite Observations in the Southern Great Plains, *Journal of Hydrometeorology*, 3(6), 688–699.
- Kabat, P. et al. (Eds.), 2004: *Vegetation, Water, Humans and the Climate*. Springer, Heidelberg.
- Koike, T., 2004: The Coordinated Enhanced Observing Period – An Initial Step for Integrated Global Water Cycle Observation. *WMO Bulletin*, 53(2) 7, 115–121.
- Koster, R.D., P.A. Dirmeyer, Z.-C. Guo, G. Bonan, E. Chan, P. Cox, C.T. Gordon, S. Kanae, E. Kowalczyk, D. Lawrence, P. Liu, C.-H. Lu, S. Malyshev, B. McAvaney, K. Mitchell, D. Mocko, T. Oki, K. Oleson, A. Pitman, Y.C. Sud, C.M. Taylor, D. Verseghy, R. Vasic, Y. Xue, and T. Yamada, 2004: Regions of strong coupling between soil moisture and precipitation. *Science*, 305, 1138–1140.
- Lawford, R., K. Nakamura, P. Arkin, M. Bonell, E. Herland, H. Hoff, T. Koike, P. Aggarwal, S. Benedict, P. Dirmeyer, S. Eden, S. Greb, D. Hinsman, J. Huang, P. Houser, T. Maurer, W. Rossow, G. Stephens, S. Unninayar, and C. Vorosmarty, 2004a: A global water cycle theme for the IGOS Partnership. European Space Agency, the Netherlands, 100 p.
- Lawford, R.G., R. Stewart, J. Roads, H.-J. Isemer, M. Manton, J. Marengo, T. Yasunari, S. Benedict, T. Koike, and S. Williams, 2004b: Advancing Global- and Continental-scale Hydrometeorology: Contributions of the GEWEX Hydrometeorology Panel (GHP). *Bulletin of the American Meteorological Society*, 85(12), 1917–1930.
- Maurer, T., 2003: Challenges in transboundary and transdisciplinary environmental data integration I in a highly heterogeneous and rapidly changing world – a view from the perspective of the Global Runoff Data Center. In N.B., Harmancioglu, S.D., Ozkul,

- O., Fistikoglu, P., Geerders, (Eds.), *Integrated Technologies for Environmental Monitoring and Information Production*. Proc. NATO Advanced Research Workshop, 10–14 September 2001, Marmaris, Turkey, NATO Science Series IV, Vol. 23, Kluwer Academic Pub. McDonald, 1998.
- Meybeck, M., and C.J. Vorosmarty, 2004: The Integrity of River and Drainage Basin Systems: Challenges from Environmental Change. In Kabat et al. (Eds.), *Vegetation, Water, Humans in Climate*. Springer, Heidelberg.
- Moran, M.S., S.J. Maas, and P.J. Pinter Jr., 1995: Combining remote sensing and modeling for estimating surface evaporation and biomass production. *Remote Sens. Rev.*, 12, 335–353. National Research Council, 1997.
- Nishida, K., R.R. Nemani, R.S.W. Running, and J.M. Glassy, 2003: An Operational Remote Sensing Algorithm of Land Surface Evaporation. *Journal of Geophysical Research*, 108(D9), 4270, doi:10.1029/2002JD002062.
- Peterson, B.J., R.M. Holmes, J.W. McClelland, C.J. Vorosmarty, R.B. Lammers, A.I. Shiklomanov, I.A. Shiklomanov, and S. Rahmstorf, 2002: Increasing river discharge to the Arctic Ocean. *Science*, 298, 2171–2173.
- Roads, J., M. Kanamitsu, and R. Stewart, 2002: CSE Water and Energy Budgets in the NCEP-DOE Reanalysis II, *Journal of Hydrometeorology*, 3(3), 227–248.
- Rodell, M., J.S. Famiglietti, J. Chen, S. Seneviratne, P. Viterbo, S. Holl, and C.R. Wilson, 2004: Basin Scale Estimates of Evapotranspiration using GRACE and Other Observations. *Geophysical Research Letter*, 31(L20504), doi:10.1029/2004GL.
- Smith, E.A., G. Asrar, Y. Furuhashi, A. Ginati, R. Adler, V. Casse, J. Durning, J. Entin, P. Houser, T. Iguchi, R. Kakar, J. Kaye, M. Kojima, C. Kummerow, V. Levizzani, M. Luther, A. Mehta, P. Morel, A. Mugnai, K. Nakamura, T. Nakazawa, S. Neeck, R. Oki, G. Raju, M. Shepherd, J. Simpson, E. Stocker, and J. Testud, 2006: International Global Precipitation Measurement (GPM) Program and Mission: An Overview, Measuring Precipitation from Space: EURAIN-SAT and the Future. In V. Levizzani, P. Bauer, and F.J. Turk, (Eds.), *Kluwer Publishers*, (In Press).
- Sorooshian, S., K. Hsu, X. Gao, H.V. Gupta, B. Imam, and D. Braithwaite, 2000: Evaluation of PERSIANN System Satellite-Based Estimates of Tropical Rainfall, *Bulletin of the American Meteorological Society*, 81(9), 2035–2046.
- Sorooshian, S., R. Lawford, P. Try, W. Rossow, J. Roads, J. Polcher, G. Sommeria, and R. Schiffer, 2005: Water and Energy Cycles: Investigating the Links. *WMO Bulletin*, 54(2), 58–64.
- Sullivan, C.A., J.R. Meigh, and A.M. Giacomello, 2003: The Water Poverty Index: Development and Application at the Community Scale. *Natural Resources Forum*, 27(3), 189–199.
- Tapley, B.D., S. Bettadpur, J.C. Ries, P.F. Thompson, and M.M. Watkins, 2004: GRACE Measurements of Mass Variability in the Earth System. *Science*, 305, 503–505.
- Trenberth, K.E., L. Smith, T. Qian, A. Dai, and J. Fasullo, 2007: Estimates of the global water budget and its annual cycle using observational and model data. *Journal of Hydrometeor* (Accepted for publication).
- Vorosmarty, C.J., P. Green, J. Salisbury, and R. Lammers, 2000: Global water resources: Vulnerability from climate change and population growth, *Science*, 289, 284–288.
- WMO (World Meteorological Organization), 1997: *Comprehensive Assessment of the Freshwater Resources of the World*. Stockholm Environment Institute.
- World Water Assessment Programme (WWAP), 2003: *Water for People, Water for Life*, World Water Development Report, UNESCO, Paris, p. 576
- Xie, P., and P. Arkin, 1997: Global Precipitation: A 17-year monthly analysis based on gauge observations, satellite estimates, and numerical model outputs. *Bulletin of the American Meteorological Society*, 78, 2539–2558.

Chapter 9

Remote Sensing of Terrestrial Snow and Ice for Global Change Studies

Richard Kelly and Dorothy K. Hall

Abstract Snow and ice play a significant role in the Earth's water cycle and are sensitive and informative indicators of climate change. Significant changes in terrestrial snow and ice water storage are forecast, and while evidence of large-scale changes is emerging, *in situ* measurements alone are insufficient to help us understand and explain these changes. Imaging remote sensing systems are capable of successfully observing snow and ice in the cryosphere. This chapter examines how those remote sensing sensors, that now have more than 35 years of observation records, are capable of providing information about snow cover, snow water equivalent, snow melt, ice sheet temperature and ice sheet albedo. While significant progress has been made, especially in the last 5 years, a better understanding is required of the records of satellite observations of these cryospheric variables.

9.1 Introduction

The cryosphere exists at all latitudes of the Earth and has significant impacts on water resources, transportation and agriculture and related socio-economic activities in many countries of the world (Slaymaker and Kelly, 2007). It also plays a significant role in climate and is a sensitive and informative indicator of its change. Extended regional snow cover influences the global heat budget (Robinson and Kukla, 1985; Foster and Chang, 1993) and has strong feedbacks with the planetary albedo and outgoing longwave radiation (Groisman et al., 1994). Temperature change in high latitudes is strongly influenced by the albedo-temperature feedback process. Snow is one of the key variables in global change (Walsh, 1991), thus, changes in global snow have direct consequences on energy and water cycle variabilities.

Clear signs are emerging that change is occurring in the cryosphere due to global temperature changes (Duguay and Pietroniro, 2005): spring snow cover extent is decreasing and the timing of melt is changing, with melt occurring earlier; lake and river ice freeze-up dates occur later and break-up dates earlier; globally, mountain glaciers are retreating; ice sheet dynamics appear to be changing; the duration of seasonally-frozen ground is decreasing; permafrost temperatures are increasing and, in many areas, permafrost is thawing. In addition, northern hemisphere sea-ice extent is at record minima and thinning, though the extent of the sea ice in the

Southern Ocean is increasing slightly. Field measurements have provided evidence for the observed changes for much of our early understanding of cryosphere dynamics but the decline of *in situ* measurements over the last 20 years has left important geographical gaps in observation networks. Remote sensing, therefore, is a vital tool for monitoring the impacts of global climate change on the cryosphere since together with environmental models, it can fill the temporal and geographical gaps in the field measurement record.

This chapter discusses the use of imaging remote sensing systems for observing two key parts of the cryosphere, namely terrestrial seasonal snow and high latitude glaciers and ice sheets. The focus falls particularly on the northern hemisphere. These cryospheric elements are highly significant indicators of climate change yet our understanding of their role in the Earth system is only gradually being understood as the scientific and technical capability to quantify these systems develops. Historical records have provided powerful ways of analyzing the cryosphere and the organization of distributed but linked data centres containing *in situ* measurements of cryospheric variables is facilitating the analysis of local to regional scale environmental cryospheric issues.

Global organizations, such as the United Nation's Global Observing Systems comprise the Global Climate Observing Network (GCOS), the Global Terrestrial Observing Network (GTOS) and the Global Oceanic Observing Network (GOOS) enable improved understanding of the cryosphere. For example, evidence for a shortening of the snow season duration in the northern hemisphere has now been found in the *in situ* measurement record especially in the spring time (Brown, 2000; Robinson and Frei, 2000). *In situ* measurements of snow and ice over Greenland are used to explain local mass balance variations and to help constrain and force energy and mass balance models. As a result of these coordinated measurements, especially when they are coupled with remote sensing observations, our understanding of the mass balance of Greenland is now at a defining stage with scientific results agree that the ice sheet mass balance is negative, but still unable to specify with certainty the magnitude of changes.

Remote sensing is an increasingly important tool for our understanding of complex cryosphere environments since the quantification of terrestrial snow and ice at the local to regional scale requires the use of synoptic-scale measurements. Remote sensing imaging instruments provide important measurements in this regard. In both snow and ice environments, remote sensing systems are vitally important for the provision of direct evidence of change and for providing data that can be used in models that estimate and predict change.

In this chapter, imaging systems refer to remote sensing instruments that are used to provide low or high spatial resolution instantaneous field of view area coverage rather than linear profilers. The wavelengths used by imaging systems, generally in the visible to infrared (IR) and microwave parts of the electromagnetic spectrum (ES), enable the observation of surface and volume properties of snow and ice. In the case of snow cover, this includes the presence or absence of snow and the water equivalent of a snowpack. For ice sheets it includes the surface temperature of the snow/ice and the snow/ice albedo, as well as surface and subsurface melt extent. The chapter does not cover non-imaging remote sensing measurement techniques

which are also an important approach for ice sheet observations to estimate surface-elevation changes. For detail on non-imaging remote sensing systems, the reader is directed to the excellent text by Bamber and Payne (2004). This is an important distinction because two new generation instruments, the Ice Cloud and land Elevation Satellite (ICESat), launched by the National Aeronautics and Space Administration (NASA) in 2003, and Cryosat-II due for launch by the European Space Agency (ESA) in 2008, are nadir-pointing, linear along-track profiling instruments that are capable of precise measurements along a the sub-satellite track but do not provide local to regional synoptic-scale swath coverage. To date the majority of the remote sensing measurements for long term studies, however, come from imaging systems and these are the focus of our attention.

The remainder of this section briefly describes key measurable snow and ice processes used in global change studies and the basic remote sensing principles that apply to observe snow and ice. The chapter is then separated into three further sections: first a synthesis of remote sensing techniques applied to the estimation of snow and ice, then a description of how these observations have contributed to our understanding of snow and ice in global change, and last we identify key themes in remote sensing and Earth system science that are evolving to help us gain an improved understanding of snow and ice dynamics. The emerging themes have developed from our current understanding and capabilities of the application of remote sensing techniques and will rely on the development of new technologies and the implementation of cutting-edge remote sensing and modeling methods.

9.1.1 Measurable Snow and Ice Processes: The Role of In Situ Measurements

In situ, or ground measurements are available for global change studies of seasonal snow and glacier ice. While the description here of these data is brief, it is recognized that there is a strong heritage of in situ measurements of these environments and much of the early discovery of global change in the cryosphere came from field measurements. Furthermore, these measurements often are used to test and validate satellite estimates and therefore, they maintain an important role in understanding the uncertainties related to remote sensing estimates of these environments. The reader is directed to Slaymaker and Kelly (2007) for more extensive survey of in situ measurements of snow and ice.

9.1.1.1 Seasonal Snow

Snow is one of the most dynamically varying components of the global water cycle. Its extent varies from $46 \times 10^6 \text{ km}^2$ of the land surface in the northern hemisphere in mid winter to $4 \times 10^6 \text{ km}^2$ in mid summer (Frei and Robinson, 1999), making the regional effect of snow mass on basin hydrology substantial. The key variables of interest for snow mapping are primarily the presence or absence of snow or snow

cover extent (hereafter referred to as SCE) and the bulk snow properties of snow depth (in cm) or snow water equivalent (SWE) which is the amount of water stored in a column (usually in mm) should the snow melt. By measuring snow depth or SWE, the presence of snow is detected, *de facto*.

Snow is a porous, permeable aggregate of ice grains (Bader, 1962) that begin their growth at sub-zero temperatures in clouds. Geometric differences in snow crystals result from variations in the temperature, wind and humidity throughout the atmosphere at the time of ice crystal formation (Male, 1980). Freshly-fallen snow almost immediately begins to compact and metamorphose, initially preserving the original shape of the snow crystal. Over time the snowpack metamorphoses and a complex stratigraphy often develops as a result of heat and energy exchanges in the pack; a seasonal snowpack might have average grain sizes ranging from 0.1 to 0.5 mm throughout the season although depth hoar (large crystals in the pack) can grow to much larger sizes of up to tens of mm. Average snow densities range from 0.1 to 0.3 g cm⁻³ throughout the pack. Average snow depths at the planetary scale are of the order of 50 to 100 cm although there is a large variability especially in mountain terrain where snow depths can reach upwards of 300 cm or more.

While the measurement of snow on the ground is relatively straightforward at the local scale, representing snow depth or snow water storage distribution accurately at regional scales is not. Studies have shown that the scale of spatial variability of snow accumulation ranges from a few metres to perhaps a few hundred metres. In principle, the local nature of the variability is controlled by hydrologic processes such as local temperature and vapor gradients in both vertical and horizontal dimensions (Colbeck, 1982). At regional scales these variations scale up and are controlled by hydroclimatology processes. Snow depth and SWE spatial variability has been analyzed by several authors (e.g. Atkinson and Kelly, 1997; Bloschl, 1999; Fassnacht et al., 2003) who have found that in general they are controlled by landscape and hydrometeorological conditions such as vegetation cover type, topographic complexity and energy and mass exchanges driven by thermal and vapor gradients in the pack, and of course regional temperature and precipitation patterns. In places where the landscape is flat and has low stand vegetation, hydrometeorology alone tends to control the spatial variability while in complex landscapes with mountains, forests and lakes, snow properties are often heterogeneous. Our estimation capability of snow characteristics in more complex landscapes is usually uncertain because the number and coverage of in situ snow measuring stations is biased to low latitude and low elevation terrain (Brown and Braaten, 1998). In situ measurements have to be used carefully from such regions and should be combined with remote sensing and hydrologic energy balance models (Davis et al., 2001).

9.1.1.2 Glaciers and Ice Sheets

For global change studies, of key interest is the mass balance of mountain, or alpine glaciers and large continental ice sheets (Meier, 1998). These long-term water stores constitute an important water supply for many parts of the world, especially where summer precipitation is scarce. Additionally, the world's small glaciers in particular act as harbingers of change as their movements and mass-balance trends

are influenced by changes in regional climate. The continental ice sheets store enough water that if melted, would cause significant sea level rise. The Greenland Ice Sheet, for example, contains enough water to produce a rise in eustatic sea level of ~ 7.0 m if the ice were to melt completely (Gregory et al., 2004). However, even small increases (centimeters) in sea level are important, with implications for the hundreds of millions of people who live on islands, in deltaic environments, and low-lying coastal plains.

The accurate estimation of how a glacier's water equivalent mass or volume is changing is important for our understanding of how these water stores contribute to global change including sea level. Determination of glacier and ice sheet state is conducted through the measurement of mass balance. Paterson (1994) defines the mass balance as "the change in mass (expressed as the equivalent volume of water) per unit area relative to the previous summer surface." Braithwaite (2002) gives an excellent summary of approaches to glacier mass balance measurements over the last 50 years. In situ measurements attempt to capture changes in mass over the glacier or ice sheet surface by measuring accumulation and ablation at discrete places, ideally over the entire surface. Changes in the Greenland Ice Sheet have been documented in recent years through a combination of in situ measurements and aircraft and satellite remote sensing observations (Krabill et al., 2000 and 2004; Abdalati & Steffen, 2001; Nghiem et al., 2001; Steffen et al., 2004; Steffen & Huff, 2005 <http://cires.colorado.edu/science/groups/steffen/greenland/melt2005/>; Comiso, 2006; Hall et al., 2006; Rignot & Kanagaratnam, 2006). It is clear that for full ice sheet and mountain glacier mass balance estimate, remote sensing can contribute critical measurements needed to improve our understanding of the state and prognosis of these "water towers."

9.1.2 Principles of Remote Sensing of Snow

Two wavebands of the ES are commonly used for imaging remote sensing systems for snow mapping. First, the visible and near-IR part provides the potential to determine SCE and albedo of a snow cover, and sometimes snow depth can be inferred in instances when snow covers vegetation of a known height. IR sensors can provide snow surface temperature which may be useful for hydrologic modeling and for determining imminent melt. Second, at microwave wavelengths, active (backscatter) or passive (emission) signals respond to the bulk properties of a snowpack as well as to variations in surface and subsurface features in the snow. This capability of microwaves to penetrate a snow cover enables the estimation of snow depth and SWE to be made when the snowpack is dry. Under wet snow conditions, the depth or SWE cannot be estimated directly by microwaves although the wetness can be estimated. A key difference between optical and microwave observations is that microwave observations can be made under nearly all weather and lighting conditions. The advantage of using both optical and microwave observations is that optical measurements can provide high-resolution SCE and albedo, while microwave sensors provide SCE and SWE albeit at a lower resolution but under all weather and lighting conditions. This powerful synergy between observation

approaches can be exploited to derive comprehensive, daily snow maps useful for operations and modeling. This chapter covers only these basic aspects of remote sensing of snow; for more detail, the reader is directed to Hall et al. (2005).

9.1.2.1 Optical Properties of Snow

The spectral albedo of a surface is the upflux divided by the downflux of radiation at a particular wavelength (Warren, 1982), while the broadband albedo is the reflectance across the reflective part of the solar spectrum. The spectral albedo of fresh snow in the visible region of the spectrum remains high (Fig. 9.1), and decreases slowly as snow ages, but in the near-IR the spectral albedo of aging snow decreases considerably as compared to fresh snow (O'Brien and Munis, 1975; Warren and Wiscombe, 1980). The near-IR albedo of snow is especially sensitive to snow grain size and the visible albedo is less so, but is affected by snow impurities. Warren and Wiscombe (1980) demonstrated that small, highly absorbing particles can lower the snow albedo in the visible part of the spectrum by 5–15% compared with pure snow. Broadband albedo decreases when grain size increases as the snow ages (Choudhury and Chang, 1979), and melting causes snow grains to grow and bond into clusters (Dozier et al., 1981; Grenfell et al., 1981; Warren, 1982). New snow can have an albedo of 0.85 or greater (Warren, 1982), however, snow albedo may decrease by >25% within just a few days as grain growth proceeds (Nolin and Liang, 2000). Even small changes in the surface albedo can increase the amount of energy absorbed by the snowpack significantly. Hansen and Nazarenko (2004) calculated that anthropogenic soot emissions have reduced snow and ice albedos by up to 3% in northern hemisphere land translating to a climate forcing of +0.3 Wm⁻² in the northern hemisphere, thus soot contributes to global warming.

The spectral albedo of snow is characterized by a high albedo across the visible part of the spectrum and a decrease through the near IR (Fig. 9.1). Snow, which is composed of ice crystals, is highly reflective in the visible and highly absorptive in the IR part of the ES (Warren and Wiscombe, 1980) and this, in general, explains the shape of the spectral curve. For different grain sizes of crystals, these spectral curves vary, with larger grains causing moderate lowering of the reflectance across the visible part and significant lowering in the near-IR part of the spectrum. This is an important characteristic because snowpack metamorphism generally increases the snow grain size and thus the spectral response across the visible and near infrared part of the ES.

The albedo of a snow cover is also influenced by the presence of land cover, especially vegetation and trees. Even tree shadows can affect the spectral response of snow depending on the solar zenith angle at time of observation. Accurate land cover maps help to identify regions where such effects might influence the reflectance of snow. Furthermore, if the vegetation canopy is closed, remote sensing instruments cannot usually observe the under-storey snow. However, in such cases, snow might accumulate in the canopy, especially shortly after a snowfall event, and a remote

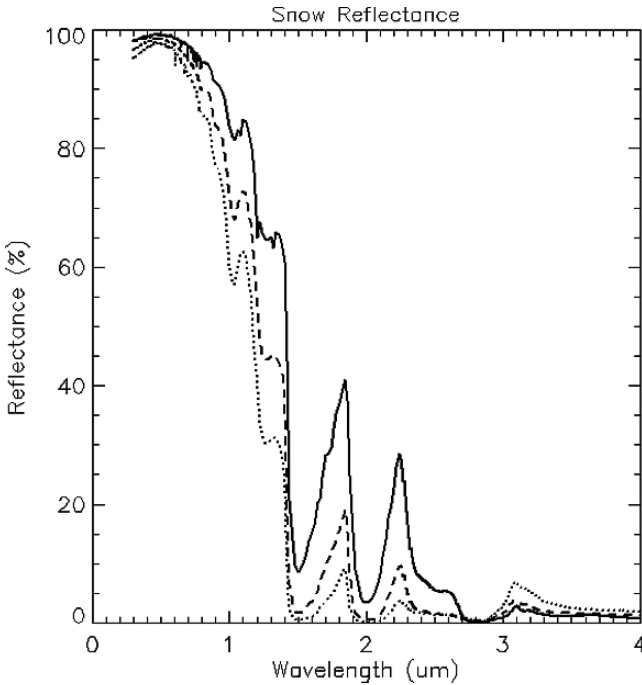


Fig. 9.1 Reflectance properties of snow in the visible and IR part of the electromagnetic spectrum. The solid line represents fine snow (24 μm effective grain size), the dashed line represents medium grained snow (82 μm) and the dotted line represents coarse grained snow (178 μm). [Data source: John Hopkins University IR Spectroscopy Lab]

sensing instrument will observe this snow cover assuming the extent is sufficient with respect to the instrument's instantaneous field of view.

9.1.2.2 Microwave Properties of Snow

Microwave remote sensing instruments that observe in the 300 to 1 GHz (1 mm to 30 cm wavelength) range, measure naturally-emitted radiation with a radiometer or measure the intensity of the return (in decibels) of a signal sent by a radar. Several factors control the microwave response from snow and while there are similarities between the physical processes affecting active and passive microwave responses from snow, generally, for applications, the two approaches are separated for convenience. This is because active microwave systems historically have operated only at the lower frequency ranges (<10 GHz) while passive microwave systems make observations between 6 and 90 GHz.

The dielectric properties of snow control the microwave absorptive and scattering processes and are affected by the relative proportion of air, liquid and solid water in the snow by volume. In the case of dry snow, a mixture of air and ice, the dielectric constant of air is 1.0 and ice 3.17 \pm 0.07 for frequencies from 1 MHz to well

above the microwave region (Evans, 1965). The combined dielectric constant of snow, therefore, generally lies between 1.2 and 2.0 when the snow densities range from 0.1 to 0.5 g/cm³ (Hallikainen and Ulaby, 1986). If a dry snowpack contains large enough grain sizes relative to the microwave wavelength, volume scattering will occur. Otherwise, the signal is returned mainly from the ground/snow interface. In the case of snow that contains a liquid water (>5% by volume), the dielectric constant is high (>35 below 20 GHz) relative to that of dry snow. In this case scattering processes are negligible and absorptive processes dominate.

The mass or volume of snow also affects its microwave response. In practical terms, the microwave emission from a layer of dry snow consists of an emission component from the snow volume and an emission by the underlying ground. Both contributions are governed by the transmission and reflection properties of the air-snow and snow-ground interfaces and by the absorption/emission and scattering properties of the snow layer determined by the snowpack stratigraphy (Stiles et al., 1981). Furthermore, many other physical parameters affect the emission and backscatter, probably most importantly, the presence of vegetation such as forests and low stand shrubs (Hall et al., 1982; Derksen et al., 2002). As an electromagnetic wave emitted from the underlying surface propagates through a snowpack, it is scattered by the randomly-spaced snow particles in all directions. For active systems, the transmitted radiation will be scattered in all directions away from the field of view. Increased loss of radiation occurs with increased snow depth due to scattering, and the emission/backscatter of the snowpack is further reduced, thus lowering the brightness temperature or the backscatter from the field of view. The deeper the snow the more crystals are available to scatter the microwave energy, and the magnitude of this loss forms the basis for the estimation of SWE.

If snow is wet, the physical interaction processes are very different. For passive microwave radiation, a wet snowpack approximates a blackbody radiator at the physical temperature of the snow layer, and becomes indistinguishable from snow-free soil (Kunzi et al., 1982). For active microwave radiation, wet snow is a very strong absorber with the backscattered emission very much reduced compared with dry snow (which is transparent to low frequency microwaves) or snow free ground. Critically, the dielectric constants of water, ice and snow are different enough so that even a little surface melting causes a strong microwave response (Schanda et al., 1983; Foster et al., 1987). The scattering loss decreases drastically with increasing liquid water content (free water) and becomes negligible for values above about 1% (Hallikainen, 1984).

The above factors (dielectric behaviour of snow (wet and dry), and the scattering response from snow) have been exploited to develop microwave retrievals of SWE and snow wetness. For dry snow, low frequency (<10 GHz) existing radar systems are generally not capable for estimating snow mass or SWE. The size of snow particles is much smaller than the size of the wavelength and there is little chance for a microwave signal to be attenuated and scattered by the relatively small ice crystals comprising a snowpack (Waite and MacDonald, 1970; Ulaby and Stiles, 1980 and 1981). Low frequency microwaves travel almost unaffected through dry snow and are not useful directly for detecting and mapping SWE. Passive microwave instruments, however, can be used to estimate SWE because observations

are made at frequencies greater than 10 GHz for which scattering processes are important. For a snowpack with SWE greater than 5–10 mm, scattering processes by snow grains dominate the microwave emission signal and can be detected at frequencies greater than about 20 GHz (e.g., Chang et al., 1987). Figure 9.2 shows the brightness temperature response from the Advanced Microwave Scanning Radiometer – EOS (AMSR-E) over a snow covered site in the Canadian prairies in November 2002 and February, 2003. The decreased brightness temperature differences at 36 and 89 GHz (both at vertical and horizontal polarizations) on 20 February 2003 are the result of a thicker snowpack at this time compared with the November data. For SWE less than 5–10 mm, passive microwave observations are less effective at estimating SWE because the thin layer is almost transparent. If the SWE exceeds 300 mm, sensitivity to SWE is lost as the observed signal saturates. This means that passive microwave observations are useful for measuring SWE at between 10 and 300 mm.

In the case of wet snow direct observations are best made using low frequency radar systems (Stiles and Ulaby, 1980; Ulaby and Stiles, 1980; Rott, 1984; Ulaby et al., 1986). When at least one layer of a snowpack (within the penetration depth of the radar signal) becomes wet (4–5% liquid water content), the penetration depth of the radar signal is reduced to about 3–4 cm (Mätzler and Schanda, 1984). The wet snow transmitted signal is absorbed producing a low backscatter. Thus, a high contrast between snow-free ground and wet snow-covered ground can be observed making it possible to distinguish wet and dry land or snow when imaged with low frequency radar (see, for example, Rott and Nagler, 1993; Shi et al., 1994).

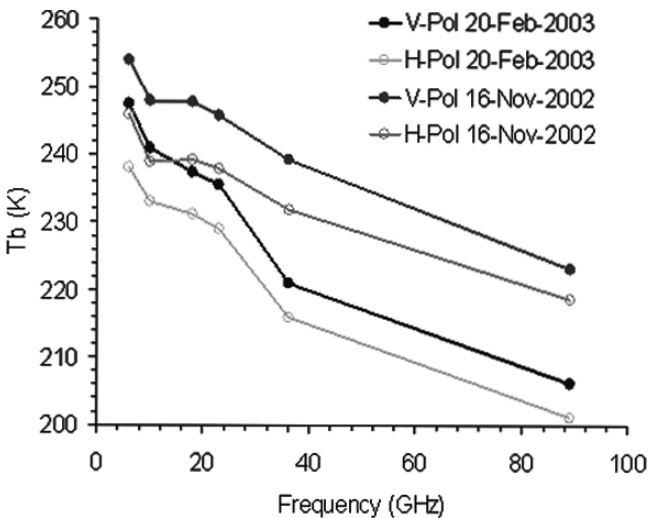


Fig. 9.2 Brightness temperatures at 6.9, 10.3, 18, 23, 36 and 89GHz for both vertical polarization (V-POL) and horizontal polarization (H-POL) at a location in the Canadian Prairies on 16 November, 2002 and 20 February, 2003. The measurements were made by the Advanced Microwave Scanning Radiometer – EOS

9.2 Application of Remote Sensing for Terrestrial Snow and Ice: Heritage and Current Approaches

9.2.1 Snow Cover Extent

Though ground- and aircraft-based photographs had been used to map areal extent of snow cover, a major step forward in snow mapping came with the advent of satellites (Singer and Popham, 1963). Primarily due to its high albedo, snow was observed even in the first images obtained from the Television Infrared Operational Satellite-1 (TIROS-1) meteorological satellite on 1 April 1960. With increasingly sophisticated instruments having increasingly higher spatial and spectral resolution, our ability to map SCE has improved dramatically through the years since the early Earth-observing satellites. Major advances have taken place due to increasing spatial resolution, the ability to discriminate snow and clouds and the ability to estimate SWE and snow melt onset. From a climatological standpoint, interpretation of the 40+ year record of SCE has provided invaluable information for global-change studies.

9.2.1.1 NOAA Operational Snow Maps

The National Oceanic and Atmospheric Administration (NOAA) began to generate operational Northern Hemisphere Weekly Snow and Ice Cover analysis charts in November 1966 from NOAA satellite data, at a spatial resolution of 190 km (Matson et al., 1986). Geostationary Operational Environmental Satellite (GOES) data and Very High Resolution Radiometer (VHRR), and Advanced Very High Resolution Radiometer (AVHRR) data from polar-orbiting satellites have been used extensively by NOAA to produce operational snow products (Matson et al., 1986; Carroll, 1995; Ramsay, 1998) since 1966. Through the years, improvements in snow mapping came about due to improved sensor resolution and the use of more consistent mapping techniques. In 1997, the NOAA Interactive Multisensor Snow and Ice Mapping System (IMS) was initiated to produce operational products daily at a spatial resolution of about 25 km, utilizing a variety of satellite data (Ramsay, 1998). Improvements in the spatial resolution of the IMS product in February 2004 resulted in increased resolution of the snow maps to 4 km resolution. NOAA now produces daily maps from a variety of visible satellite imagery, estimates of snow extent derived from microwave satellite data, and station-mapped products.

The AVHRR instrument on NOAA platforms has been an important source for satellite snow cover observations globally. The first AVHRR was a four-channel radiometer and was launched on TIROS-N in October 1978. A five-channel version of the instrument (AVHRR/2) was launched on NOAA-7 in June 1981. The latest instrument version is AVHRR/3, with six channels, and was launched aboard NOAA-15 in May 1998. This last version is the most significant for snow mapping applications because its six channels include a snow-cloud discrimination channel at 1.6 μm which is the wavelength at which snow and clouds exhibit maximum

spectral separability; Figure 9.1 shows very low reflectance of snow in this wavelength range but clouds have a high reflectance at the same wavelength.

The weekly visible-wavelength satellite-derived dataset consisting of maps of northern hemisphere snow cover produced by NOAA is the longest satellite-derived environmental dataset (Robinson, 1993). However, since the production of the maps was not conceived as a long-term dataset at the outset of the mapping program, various techniques have been used to develop the maps over the decades, and many of the early techniques were not well-documented. To address this, a reanalysis effort at the Rutgers University Global Snow Lab (RUGSL) produced a new set of snow maps covering the period from late 1966 through 1971 (Robinson and Frei, 2000).

The data set at RUGSL archives the weekly and monthly snow cover extent data back to 1966 (<http://climate.rutger.edu/snowcover/>). The weekly and monthly data are consistent and can be used for research into snow cover extent climatology since the continuous NOAA snow cover extent data set now constitutes the longest satellite snow cover record available stretching back over 40 years.

The National Operational Hydrologic Remote Sensing Center (NOHRSC) snow-cover maps generated by National Weather Service (NWS) NOHRSC hydrologists are distributed electronically in near-real time, to local, state and federal users during the North America snow season (Carroll et al., 2001). The NOHRSC 1 km digital maps provide the areal extent of snow cover for the conterminous United States, Alaska, and parts of southern Canada. Through their extensive website <http://www.nohrsc.nws.gov/>, NOHRSC also produces snow products and a myriad of information that include estimates of: SWE, snow depth, snowpack temperatures, sublimation, evaporation, estimates of blowing snow, modeled and observed snow information, airborne snow data, satellite snow cover, historic snow data, and time series for selected modeled snow products.

9.2.1.2 MODIS-Derived Snow Maps

With the launch of NASA's Terra satellite, snow maps have been produced globally, using automated algorithms from the Moderate Resolution Imaging Spectroradiometer (MODIS) instrument since 24 February 2000. The 2002 launch of the Aqua satellite provided a second MODIS, and more snow-mapping opportunities each day. The MODIS snow products [<http://modis-snow-ice.gsfc.nasa.gov/>], are provided in a variety of different spatial and temporal resolutions and projections to serve different user groups (Riggs et al., 2006; Hall and Riggs, 2007). Daily, 8 day and monthly composite snow maps with fractional snow cover are available at 500 m and 0.05° resolution, and daily albedo is mapped at 500 m resolution. For modelers, and others interested in a coarser-resolution product, a 0.25° resolution product is also available.

The MODIS snow mapping approach is fully automated and uses the Normalized Difference Snow Index (NDSI) approach to estimate daily snow cover extent at 500 m resolution. There is a long heritage for mapping snow using the normalized difference of visible and near-IR channels from aircraft- and satellite-borne

instruments (Bunting and d’Entremont, 1982; Crane and Anderson, 1984; Dozier, 1989; Hall and Riggs, 2007). The efficacy of the NDSI for snow mapping was demonstrated on a satellite by the Landsat-5 Thematic Mapper (TM) instrument which had a 1.6 μm channel on board (Dozier, 1989). The MODIS Snow Products Guide (Riggs et al., 2006) documents the details of the algorithmic approach. In essence, snow covered area is mapped if NDSI is greater than 0.4 and near-IR reflectance is greater than 0.11 and band 4 is greater than 0.10. Many other spectral tests are also applied. For example, if dense vegetation is present, a criteria test using NDSI and the normalized difference vegetation index (NDVI) of $((\text{band } 2 - \text{band } 1) / (\text{band } 2 + \text{band } 1))$ is applied to pixels that have an NDSI value in the range of 0.1 to 0.4. Work by Klein et al. (1998) demonstrated that using the combined NDSI and NDVI, detection of more snow is possible in densely vegetated areas. The MODIS cloud mask, MOD35_L2, is an input to the snow algorithm. Figure 9.3 is an example of a global 8 day composite MODIS snow cover map on the climate modeling grid for 6–13 April 2000.

9.2.2 Snow Water Equivalent

Beginning with the launch of the Nimbus-5 Electrically-Scanned Microwave Radiometer (ESMR) in 1972, and continuing with the Nimbus-7 Scanning Multichannel Microwave Radiometer (SMMR), launched in 1978, the subsequent launch of the Defense Meteorological Satellite Program’s Special Sensor Microwave Imager (SSM/I) and most recently, NASA’s Advanced Microwave Scanning Radiometer – EOS (AMSR-E), space-borne passive microwave instruments have been measuring the natural upwelling microwaves from the Earth for 35 years. Table 9.1 shows the frequency bands and spatial resolution of the passive microwave instruments plus

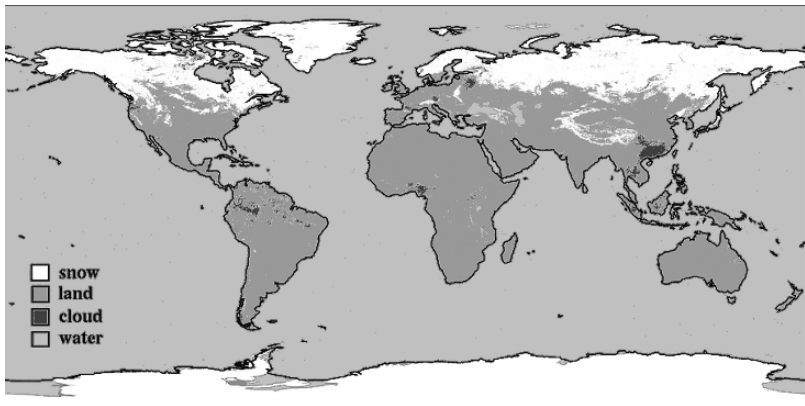


Fig. 9.3 Moderate-Resolution Imaging Spectroradiometer (MODIS) 8 day snow map for the period April 6–13, 2000 (MOD10C2) (From Hall and Riggs, 2007). The product is georeferenced to the 0.05° climate modeling grid

Table 9.1 Key sensor characteristics for the AMSR-E, SSM/I and SMMR instruments

AMSR-E	Center Freq (GHz)	6.9	10.7	18.7	23.8	36.5	89.0
	Sensitivity (K)	0.3	0.6	0.6	0.6	0.6	1.1
	IFOV (km × km)	76 × 44	49 × 28	28 × 16	31 × 18	14 × 8	6 × 4
SSM/I	Center Freq (GHz)			19.35	22.235	37.0	85.5
	Sensitivity (K)			0.8	0.8	0.6	1.1
	IFOV (km × km)			69 × 43	60 × 40	37 × 29	15 × 13
SMMR	Center Freq (GHz)	6.6	10.7	18.0	21.0	37.0	
	Sensitivity (K)	0.9	0.9	1.2	1.5	1.5	
	IFOV (km × km)	156 × 156	97 × 97	60 × 60	60 × 60	30 × 30	

the sensitivity of each channel measurement. The record for 18–19 GHz, 21–23 GHz and 36–37 GHz is continuous back to 1979.

As previously noted, in general, for snow covered terrains, the strength of higher frequency scattering signal from snow is proportional to the SWE or snow depth, and it is this relationship that forms the basis for estimating the water equivalent. Several algorithms for the retrieval of SWE or snow depth have been proposed in the literature, such as those by Chang et al. (1987), Hallikainen and Jolma (1992), Grody and Basist (1996) and Tait (1998), to name a few. Foster et al. (1997) reviewed and updated the Chang et al. (1987) algorithm, to account for forested areas. Recent studies have also been conducted by Goita et al. (2003), Goodison and Walker (1995) and Tedesco et al. (2004), for providing improved the estimates of SWE at regional scales and through the use of numerical techniques for the inversion of semi-empirical relationships. Also, Derksen et al. (2003) describe a regional approach to estimate SWE in discrete Canadian regions using satellite passive microwave observations from the SSM/I. This product is available operationally through Environment Canada (see <http://www.ccin.ca>).

Recently, a dynamic algorithm based on the original baseline algorithm has been proposed by Kelly et al. (2003). Here the authors show that a dynamic approach is able to improve the performance of the retrieval with respect to the static algorithm (Chang et al., 1987 and Foster et al., 1997), when the evolution of grain size and density is modeled along the snow season by means of exponential functions. Grippa et al. (2004) developed a dynamic algorithm to estimate seasonal SWE in Siberia, although this approach is more for climatological rather than hydrology application studies. Recent work by Derksen et al. (2005) in the Canadian boreal forest/tundra transition zone demonstrated that a regional approach to SWE retrievals, based on dominant landscape characteristics, can yield representative results. They found that a large range of measured SWE values exist on the ground within each of many satellite footprints. Statistical comparisons showed that a high percentage of satellite SWE estimates fell within 20 mm of the median ground measurement values. This regional approach, that is empirically derived but calibrated by careful field campaigns demonstrates great promise for practical estimates of SWE.

Daily global maps of snow water equivalent from AMSR-E are available through the National Snow and Ice Data Center (<http://www.nsidc.org>). The retrieval is

performed using AMSR-E/Aqua L2A Global Swath native resolution and spatially resampled brightness temperature (T_b) measurements (Kelly et al., 2004). Snow depth retrievals are performed on the instantaneous field of view samples and then accumulated within a $25\text{ km} \times 25\text{ km}$ Equal-Area Scalable Earth Grid (EASE-Grid) projection that encompasses 721×721 pixels per north and south hemisphere. Figure 9.4 shows an example of the 5 day maximum SWE for the northern hemisphere in March 2006. A daily SWE product is also available along with a monthly average SWE.

While satellite passive microwave measurements used for snow monitoring typically have spatial footprints ranging from 12 km to 40 km, these measurement scales are not capable of resolving local, hydrologic process-controlled variations of SWE that are evident at scales less than 100 m. Furthermore, the passive microwave approach has particularly large uncertainties in mountainous areas and in heterogeneously-vegetated landscapes where SWE variability is controlled strongly by the landscape character typically over distances of less than 100 m. For these reasons, use of these observations is best undertaken for climatological studies at average monthly timescales until these uncertainties are resolved. To this end, a snow climatology data set at the monthly scale has been developed at the National Snow and Ice Data Center by Armstrong et al. (2005). Based on an adjusted algorithm of Chang et al. (1987), the approach uses SSM/I estimates of SWE and computes monthly averages. These data are gridded to the EASE grid polar projection and are beginning to be used by scientists to understand SWE trends.

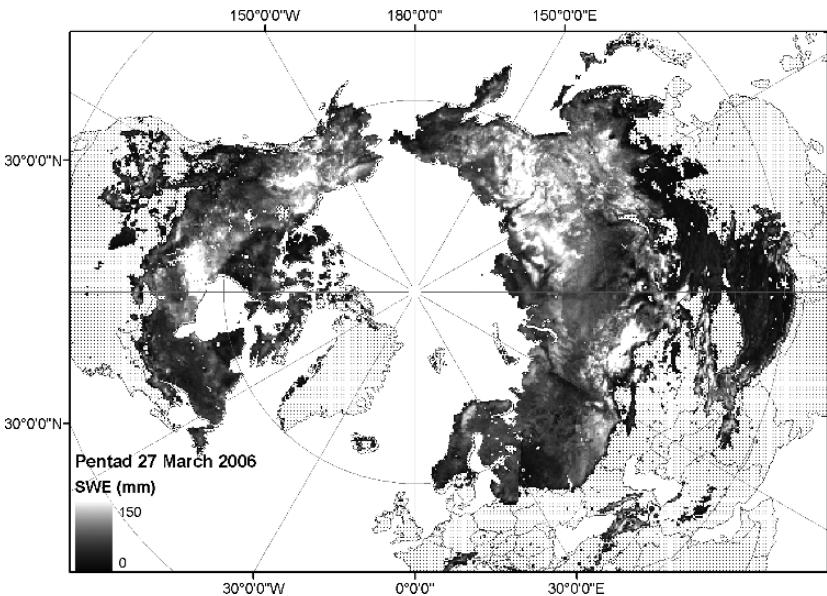


Fig. 9.4 Five day maximum SWE from AMSR-E. From Kelly et al., 2004

9.2.3 Snow Wetness

Passive microwave algorithms have exploited the fact that the presence of liquid water within the snowpack increases the absorption, reducing the penetration depth. As a consequence the brightness temperatures at 19 and 37 GHz become similar and the values of SWE retrieved are not representative in wet snow conditions. It is important to distinguish between dry and wet snow conditions, to exclude those pixels containing wet snow in order to reduce the uncertainty in SWE retrievals. Thus, knowledge of surface or air temperature might not be enough: melting can indeed occur also from the bottom of the snowpack because geothermal heat fluxes and air and snow temperatures can be different. Walker and Goodison (1993) reported a wet snow discrimination technique based on the 37 GHz polarization differences; Sun et al. (1996) used a neural network to determine snow wetness in vegetated terrain. Both techniques were developed and calibrated for specific regions and require tuning when applied to different regions.

A more promising approach for wet snow mapping comes from the use of active microwave instruments, especially SAR and scatterometer systems. To date, most satellite-based SAR systems have been designed to operate at the low frequency range of the ES, and especially at the 5 GHz range (C-band). These instruments, such as ERS-1/ERS-2, Envisat, and Radarsat, while lacking in the number of frequency bands, are capable of observing wet snow at the spatial scale of tens of metres. The backscatter response is far less than from surrounding non-snow surfaces and can be detected by simple multi-temporal image segmentation (Nagler and Rott, 2000; Koskinen et al., 1997).

Though the focus of this chapter is to discuss the imaging techniques, it is important to mention that non-imaging active microwave sensors such as scatterometers, also provide important contributions to snow studies. For example, QuikSCAT Sea-winds scatterometer data at 13.4 GHz are capable of detecting snow melt regions in snow-covered areas including over the Greenland Ice Sheet (Nghiem et al., 2001), thus augmenting data from imaging sensors.

9.2.4 Ice Sheet Surface Temperature and Albedo

Remote sensing techniques have been developed to measure albedo and surface temperature from spaceborne instruments. Both variables are important for the 'balance' processes of ablation and accumulation. The surface temperature, T_s , and albedo of the Greenland Ice Sheet are important parameters to study for monitoring the ice-sheet mass balance, and are amenable to study using satellite data. The T_s of the Greenland Ice Sheet is influenced strongly by near-surface air temperature, and sustained changes in air temperature of $\geq 0^\circ\text{C}$ will lead to a negative ice-sheet mass balance. The study of ice sheet albedo is important because albedo influences the energy absorption, and some factors which cause a lowering of the surface albedo (e.g., introduction of soot into the surface layers of snow) may cause accelerated melting.

9.2.4.1 Ice Sheet Surface Temperature and Melt Characteristics

Surface temperatures on the Greenland Ice Sheet have been studied both on the ground using automatic weather station (AWS) data from the Greenland-Climatic Network (GC-Net) (Steffen and Box, 2001; Box, 2002), and from analysis of sensor data from satellites (see for example, Key and Haeffliger, 1992; Haeffliger et al., 1993; Stroeve and Steffen 1998; Comiso, 2006; Hall et al., 2006). Stroeve and Steffen (1998) presented monthly-mean temperature maps of the Greenland Ice Sheet from 1989–1993 using AVHRR data. Also using AVHRR weekly IR surface-temperature maps at 6.25 km resolution, Comiso (2006) showed an increase in T_s of Greenland of 1.19°C per decade, or an average of $\sim 0.12^\circ\text{C a}^{-1}$, between 1981 and 2005, with a possible 3+ day increase in the length of the melt season during the same period. Hall et al. (2006) used MODIS surface-temperature data products at 5 km resolution (8 day averages) to show the relationship between T_s and ice-sheet mass balance. The mean T_s of the Greenland Ice Sheet during the melt season was highest in 2002 and 2005 (Hall et al., 2006) in agreement with Steffen et al. (2004) and Steffen and Huff (2005) (<http://colorado.edu/steffen/greenland/melt2005>) who noted unusually-extensive melt of the ice sheet in 2002 and 2005 as a result of their analyses of passive and active microwave data. In addition, Hall et al. (submitted) calculated daily, monthly and annual mean T_s of the Greenland Ice Sheet under clear-sky conditions, from 2000 to 2006 using MODIS IR data products, and quantified the trend of increasing T_s over the Greenland Ice Sheet.

9.2.4.2 Ice Sheet Albedo

Snow can be one of the most reflective materials on the Earth's surface, thus reflecting much of the incident solar radiation back to space. A great deal of work has been accomplished to study the albedo, and changes in the albedo of the Greenland Ice Sheet using AVHRR data (see for example, Stroeve and Steffen, 1998; Knap and Oerlemans, 1996; Nolin and Stroeve, 1997; Stroeve et al., 1997; Greuell and Knap, 2000; Comiso, 2001; Stroeve et al., 2001), and MODIS data (Greuell and Oerlemans, 2005; Liang et al., 2005; Stroeve et al., 2006).

While large changes in albedo are possible to observe on a seasonal and inter-annual basis, long-term albedo changes, which can now be measured using satellite data, will require much work to understand precisely. Satellite data already provide temporally and spatially consistent estimates of the albedo of the Greenland Ice Sheet (Stroeve et al., 2001). Recent work by Stroeve et al. (2001) analyzed the AVHRR Polar Pathfinder (APP) data over Greenland. These data provide a long-time series (1981 to present) of consistent, calibrated surface albedo and surface temperature data. They compared the APP-derived surface albedo product at 1.25 km grid cell size with measurements made at 14 automatic weather stations (AWS) around the Greenland ice sheet from January 1997 to August 1998. They noted that while satellite-derived surface albedo values were 10% less than those measured by the AWS stations, the AWS measurements tend to be biased high and that after corrections the APP underestimates albedo by 6%. They also noted that

where the natural albedo variability is small, the APP estimation uncertainty exceeds the natural variability suggesting further work is needed to improve the APP albedo estimates. However, spatially and temporally, Stroeve et al. (2001) noted that the data provide consistent estimates of the Greenland Ice Sheet albedo.

Intercalibration of different sensors must be done to ensure a high-quality dataset for analysis especially intercalibration of the longer-term AVHRR- with the more-recent and better-calibrated MODIS-derived albedo data.

9.2.4.3 Mapping the Movements of the Earth's Small Glaciers

The Earth's small glaciers are retreating in response to global warming. Globally, small glaciers have lost significant mass and the rate of recession has generally been increasing in the last two decades (Dyurgerov and Meier, 2000). Small glaciers are sensitive indicators of regional climate and climate change, and they are also important contributors to sea level, though the potential of sea-level rise (<0.5 m) is by far less than that of the Greenland (~7 m) and Antarctic (~70+ m) ice sheets. The total area and volume of mountain glaciers and ice caps outside Greenland and Antarctica, hereafter referred to as the Earth's "small glaciers," is $512 \times 10^6 \text{ km}^2$ and $33.1 \times 10^6 \text{ km}^3$, respectively (Ohmura, 2006). Recent recession of the Earth's approximately 160,000 small glaciers has been documented in the last decade in the scientific literature (see for example, Dyurgerov and Meier, 1997; Arendt et al., 2002; Kargel et al., 2006).

In the European Alps, many glaciers have been retreating since the end of the Little Ice Age which occurred around 1850 in Europe. Glacier recession in the Alps has accelerated in recent decades (Paul et al., 2004) as seen, for example, on the Pasterze Glacier, in Austria, which has been receding for over 100 years (Hall et al., 2003). In Scandinavia, most glaciers advanced from around the 1970s to the mid-1990s or the turn of the century, and then began to retreat. In fact in Norway, all monitored glaciers have shown a large mass loss in recent years (Andreassen et al., 2005). Glaciers in the Polar Ural Mts. in Russia also experienced large negative mass balance in the latter part of the last century, and into the 21st century (Kononov et al., 2005). Tropical glaciers at high elevations are also in recession (Ceballos et al., 2006) and many other well-documented studies of glacier recession and mass loss in various other parts of the world have been documented.

High-resolution data such as from the Landsat instruments, and ASTER (Advanced Spaceborne Thermal Emission and Reflection Radiometer) aboard the Terra satellite play a key role in monitoring changes of small glaciers. Beginning in 1972 with the launch of the Landsat-1 satellite, data have been collected every 16 or 18 days (cloud-cover permitting) of every part of the Earth, providing a valuable database for changed detection of glacier area. Though the earlier Landsat imagery from the Multispectral Scanner (MSS) had a spatial resolution of ~80 m, and the TM through ETM+ imagery provides a higher resolution (15–30 m), an invaluable database was established beginning with the launch of Landsat-1. ASTER data, with its 15 m resolution, also provides an excellent source of data for monitoring glaciers, though the acquisition of the ASTER data is not as frequent as was the case using

Landsat instruments. The 2003 failure of the Landsat-7 scan-line corrector has acted as a warning that our critical database of global change may not continue. Efforts to provide follow-on sensors that will allow glacier-change measurements to continue are underway, but should be hastened to avoid data gaps that can never be recovered.

In conjunction with non-imaging data such as from the ICESat, and from aircraft lidars (see Krabill et al., 2000; Arendt et al., 2002), it should be possible to derive good estimates of mass balance of many of the Earth's small glaciers and ice caps. In addition, Gravity Recovery And Climate Experiment (GRACE) satellite data provide novel and important data for measuring changes in the mass of glaciers and ice sheets (Luthcke et al., 2006). Combining sensors from different parts of the ES provides important measurements on glacier mass balance, and, used alone, the various sensors provide independent confirmation of global glacier shrinkage.

9.3 Snow and Greenland Ice Sheet Global Change Status from Imaging Remote Sensing Observations

Remote sensing is an important part of Earth system science especially related to cryospheric processes. Near real time systems now exist for mapping snow cover extent (MODIS and AVHRR) and for estimating SWE (AMSR-E). Furthermore, long term records are now available for the analysis of snow cover (NOAA AVHRR) and SWE (SMMR, SSM/I and AMSR-E) during the satellite measurement period. Seasonal snow melt estimates from satellite instruments are under development but it will not be long before these data too will become available to the research community for use in global change studies. With respect to the Greenland Ice Sheet analysis of surface temperature, melt and albedo trends have also been conducted using remote sensing observations.

The following three sections report on how imaging remote sensing measurements have contributed to our understanding of seasonal snow dynamics and to albedo and surface ice temperature/melt dynamics over Greenland. For mature analyses, imaging remote sensing observations are generally combined with in situ estimates or other remote sensing measurements.

9.3.1 Snow Cover Extent

The latter half of the 20th century shows a decline in snow-covered area in the northern hemisphere (IPCC, 2001). Northern hemisphere as shown in Figure 9.5 annual SCE has been monitored continuously using visible and near-IR satellite data since 1966 as discussed earlier. Since 1979, passive-microwave observations have been made, creating an independent record of SCE. Robinson (1997) shows that, since 1966, the SCE in the Northern Hemisphere has decreased $\sim 10\%$, largely due to decreases in spring and summer since the mid-1980s over both the Eurasian and American continents (Frei and Robinson, 1999). Winter and autumn SCE show no statistically significant change. Using passive-microwave data, Armstrong and

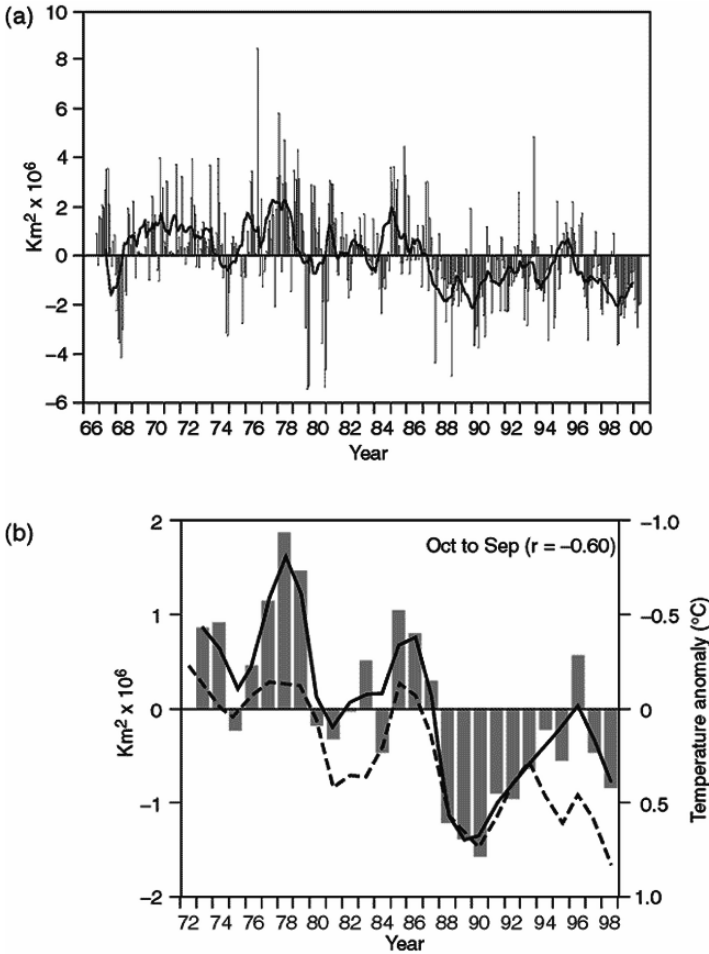


Fig. 9.5 Source: IPCC (2001). (a) NOAA snow map anomalies of monthly SCE over the northern hemisphere between November 1966 and May 2000. The black line is the twelve-month running anomalies of hemispheric snow extent, plotted on the seventh month of a given interval. The mean hemispheric snow extent is 25.2 million km² for the full period of record. (b) Seasonal snowcover anomalies (in million km²) and temperature anomalies (in °C). Both SCE (NOAA snow maps) and temperature (Jones data set) anomalies are area averages over the region for which climatological values of seasonal snow-cover frequency (based on the 1973 to 1998 period) are between 10 and 90%. The bar graph indicates time-series of SCE anomalies. The solid black line is the nine-point weighted average of snow-cover anomaly and the dashed black curve represents the nine-point weighted average of area average temperature anomaly. The correlation coefficient (r) between seasonal snow cover anomalies and temperature anomalies is indicated in parentheses. (Figure contributed by David A. Robinson and Anjali Bamzai, Rutgers University to the 2001 IPCC report)

Brodzik (2001) also show a reduction of about 2 percent a^{-1} from 1978–1999. These independent satellite-derived results are supported by ground measurements. Brown (2000) studied longer regional time-series based on station records; his reconstructions suggest that Northern Hemisphere spring and summer SCEs in the past decade have been at their lowest values in the past 100 years. Over Canada, there has been a general decrease in snow depth since 1946, especially during spring, in agreement with decreases in SCE (Brown and Braaten, 1998).

As mentioned, the snow cover extent record from the NOAA record is used to construct this long-term trend. There are, however, still uncertainties in the data that comprise this trend. Recently, Wang et al. (2005) found that the NOAA record consistently overestimates the duration of snow cover extent in the Arctic by up to four weeks. They attributed errors in the data to persistent cloud cover and the consequent low frequency of data coverage over higher latitudes. They urge caution when using these data for the analysis of seasonal snow cover climatology.

9.3.2 Snow Water Equivalent

Despite the 35 year record of passive microwave observations of snow, only recently have efforts been made to analyze the full satellite passive microwave record of SWE. Colton and Poe (1999) found that the stability of the SSM/I sensor series is high signaling the possibility of long-term studies of snow for the cryospheric research community.

The National Snow and Ice Data Center (NSIDC) at the University of Colorado has successfully developed a SMMR and SSM/I Level 3 Pathfinder data set for the period 1978 to 2005. This 27 year, consistently processed time series of brightness temperatures is projected to the EASE-Grid and is used to estimate mean monthly SWE in the northern and southern hemispheres. The data are input into a passive microwave algorithm which is based on the algorithm of Chang et al. (1987) and Foster et al. (1997). Forest corrections are made with up to a maximum factor of two applied for forest fractional coverage within a grid cell greater than 50%. Retrievals less than 7.5 mm, are considered unreliable and estimates are flagged as zero. SWE over ice sheets is not estimated since the algorithm of Chang et al. (1987) is known to be physically inappropriate in these regions. Figure 9.6 shows the monthly estimates for the SMMR period: the upper panel is the monthly climatology for the SMMR era (1979–1987) and the lower panel is the monthly climatology for the SSM/I era (1987–2003).

With respect to SWE time trends from satellite passive microwave observations, Derksen et al. (2004) conducted an analysis of SWE from SMMR and SSM/I along a longitudinal transect in North America derived from a consistent algorithm. The first outcome of note was that SMMR estimates of SWE required adjustment to ensure that biases and uncertainty characteristics (errors) were the same as the SSM/I estimation record (1987–2002). Similar to Armstrong and Brodzik (2001), Derksen et al. (2004) also found that the passive microwave estimates systematically underestimated SCE relative to the NOAA snow map record, especially in early winter.

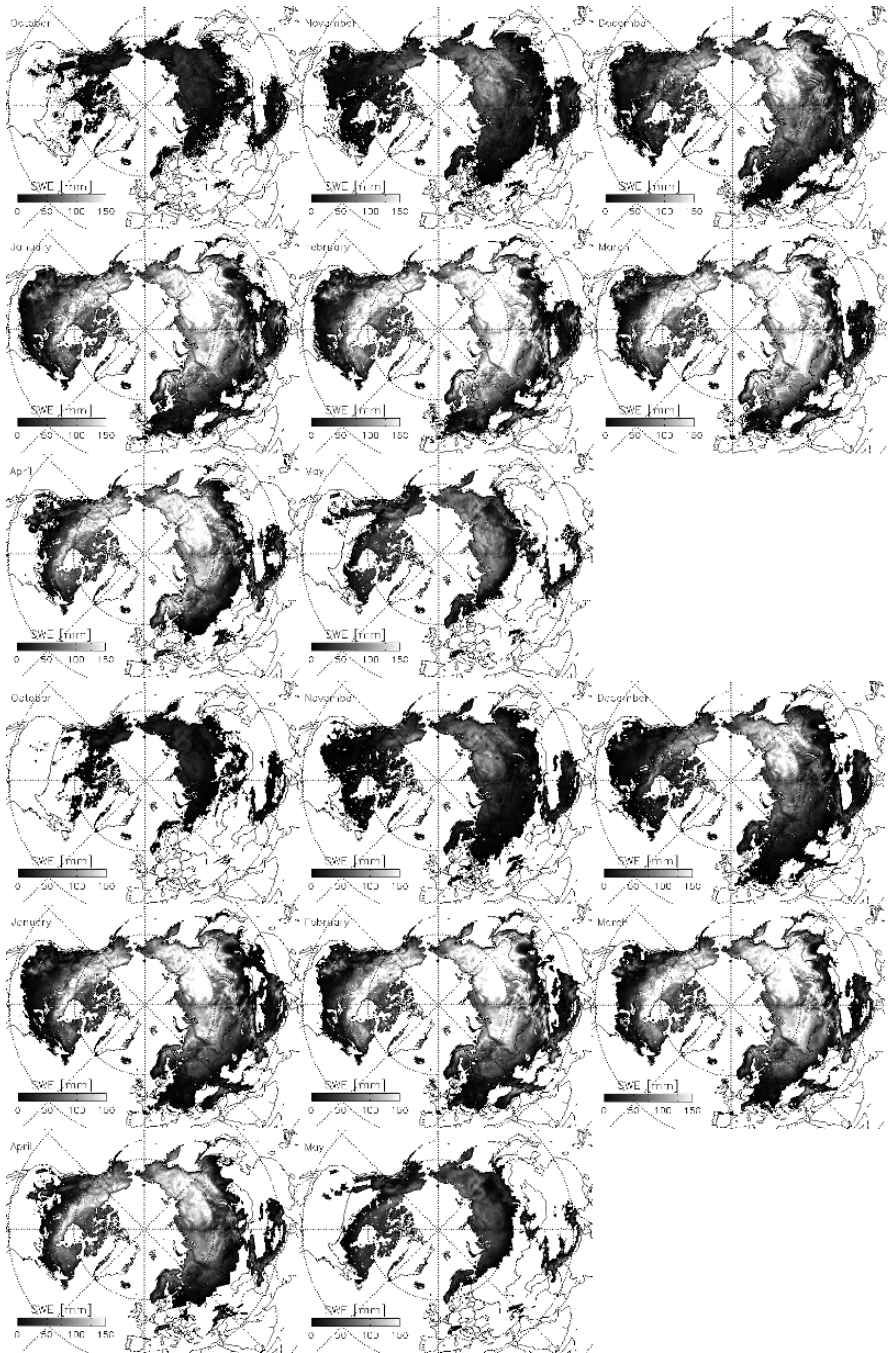


Fig. 9.6 Monthly (October through May) northern hemisphere SWE climatology from SMMR SWE estimates from 1978–1987 (upper panel) and from SSM/I estimates from 1987–2003 (lower panel). The averages includes snow cover extent from AVHRR which is used to observe shallow snow when the snowpack is too shallow to be observed by passive microwave observations (especially from October to December). Source, Armstrong *et al.* (2005).

Most interestingly, the passive microwave data were successfully merged with historical *in situ* snow survey data and analysis of SWE and SCE time series for the months of December through March 1915–2002 yielded no evidence of significant trends in either variable over the 88 year period. Anomalies observed during the relatively recent period of passive microwave data acquisition did not exceed the range of anomalies observed in the historical data record. It should be noted, however, that these data were for a longitudinal transect and more work needs to be done to assess other areas.

9.3.3 Greenland

It is possible to monitor decade-scale changes of the Greenland Ice Sheet from 1981 to present using satellite data. Using passive-microwave data, ice sheet melting has been measured and using data from the visible through near-IR parts of the ES, surface albedo has been measured (Stroeve et al., 2001). IR data have provided decade-scale surface temperature measurements (Comiso, 2006). In short, sensors from various parts of the ES are consistent in their findings that the Greenland Ice Sheet melting and surface temperature have been increasing in recent years. Furthermore, the velocity of outlet glaciers has increased, especially in the southeastern part of the ice sheet, and this has been accompanied by accelerated thinning and retreat of those glaciers (Rignot and Kanagaratnam, 2006). If the velocity of the outlet glaciers continues to increase, the contribution of the Greenland Ice Sheet to near-term sea-level rise may well be far greater than expected.

There appears to be a near-consensus from recent work that shows a small mass loss of the Greenland Ice Sheet, with a thinning at lower elevations ($\sim <2000$ m) and a thickening at the higher elevations (>2000 m), with the southeastern parts of the ice sheet experiencing the greatest mass loss. This is confirmed by data from sensors that record energy from different parts of the electromagnetic spectrum. And if the well-documented warming continues in the Arctic (ACIA, 2005; Richter-Menge et al., 2006), melting of the Greenland Ice Sheet will likely accelerate, contributing further to sea-level rise.

9.4 Future Directions

9.4.1 Combined Remote Sensing Approaches

Remote sensing has been very important in developing our understanding of cryospheric processes. Instruments such as AVHRR, MODIS, SSM/I and AMSR-E are now used to deliver daily snow estimates at the regional to global scale. It is also recognized that each instrument has its own estimation uncertainty whether it is through the effect of cloud cover on the mapping capability or the effect of snowpack physical property on a SWE retrieval. The combination, however, of

different remote sensing instruments can provide synergy for the estimation of snow properties from space and can reduce the overall mapping uncertainties to which individual sensors are subject. Visible and IR instruments are capable of mapping SCE at 500 m with the MODIS instrument on a daily basis using automated algorithms. This measurement scale is close to the natural hydrologic process scale of variability for snow. However, cloud cover obscures snow from MODIS. Passive microwave observations, while coarser in resolution, can provide daily estimates of SWE under almost all cloud cover conditions and SAR observations have been used for mapping wet snow under cloud. Combining these remote sensing methods has been a challenging undertaking but important advances in comprehensive snow-cover mapping are likely to be realized.

Tait et al. (2000) demonstrated the successful combination of the NOAA AVHRR and GOES snow charts with SSM/I estimates for global snow mapping. Armstrong and Brodzik (2001) also demonstrated the utility of combining microwave estimates of SCE with VIS-IR estimates. Tait et al. (2001) developed this combined approach by using MODIS snow maps, rather than low resolution NOAA maps to augment and improve the global snow mapping capability. With the availability of AMSR-E observations at finer spatial resolution measurements than the SSM/I (see Table 9.1), there is scope for further improvements to the combined sensor mapping approach.

9.4.2 New Imaging Remote Sensing Approaches

Radar remote sensing systems can measure snow at the hydrologic process scale. This is one of the fundamental challenges to passive microwave remote sensing instruments that measure brightness temperatures at kilometer scales. At C-band frequencies (5 GHz) Radarsat, ERS-1 and 2 and Envisat have spatial resolution capabilities between 10–30 m. Unfortunately, as previously discussed, C-band radiation does not interact with snowpacks in a way that can be used to measure snow water storage and these instruments are generally restricted to mapping snow wetness in the upper layers (Shi and Dozier, 1995). The optimal active microwave frequency range with the necessary sensitivity to volumetric snowpack properties, and hence to estimate SWE, lies between 8–18 GHz (X- and Ku-bands; 2–4 cm wavelengths) or even at Ka-band frequencies (36 GHz). Theoretical and empirical work from modeling and field studies have demonstrated the sensitivity of the Ku-band frequency range to SWE (e.g. Mätzler and Schanda, 1984; Ulaby et al., 1986; Marshall et al., 2004). However, no airborne or satellite imaging radar systems are currently available for the development of Ku- and X-band retrieval methods at the hydrologic scale. Whilst analyses have been conducted using a Ku-band radar altimeter on the Topex/Poseidon mission (Papa et al., 2002) and a Ku-band scatterometer on the QuikSCAT system (Rawlins et al., 2005), in both cases the measurement spatial resolutions are coarse (1–25 km) and are not focused at the snow hydrology process scale (less than 100 m). The development of Ku- and X-band radar-based SWE estimation methods at the snow hydrology process scale is emerging as a crucial technology, therefore, for quantifying local to regional snow distributions.

This higher frequency radar technology has been recognized at NASA and ESA as a key technology for cryospheric science. With the development of Cryosat-II, a Ku-band interferometric altimeter and the concept development of the Cold Regions Hydrology (CoReH2O) mission with a dual frequency (Ku- and X-band) SAR, there is much interest in these technologies not least because they could provide the measurements at the snow hydrologic process scale and when combined with the 35 year record of passive microwave observations, could be used to further reduce uncertainties in the passive observation SWE record.

9.4.3 Combining Remote Sensing and Hydrologic Models to Estimate Snow State Variables

Kelly et al. (2003), Derksen et al. (2005) and others have shown that coarse spatial resolution satellite passive microwave measurements from the SSM/I and AMSR-E can capture regional-scale SWE features but may underestimate local scale SWE patterns or deep snow accumulations. Dominant physical environment processes (at scale lengths less than 100 m), such as vegetation-snow energy interactions or snowpack metamorphism, complicate the microwave emission behaviour from snow and degrade the accuracy of the passive microwave retrievals (Kelly et al., 2003). Moreover, passive microwave observations tend to under-measure snow extent in the early and late part of the winter when snows are shallow or wet. At the point process spatial scale, energy and mass balance models, such as SNTherm (Jordan, 1991) or the Utah Energy Balance (UEB) model (Tarboton and Luce, 1996) have demonstrated successfully the simulation of snowpack energy flux exchanges and are capable of estimating SWE from high quality meteorological input data (Tribbeck et al., 2004). The most comprehensive snow state modeling and mapping system is the US National Snow Analysis (NSA) system developed at NOHRSC. The NSA uses in situ meteorological measurements from up to 30000 sites, downscaled numerical weather prediction data, multi-instrument remote sensing observations and in situ snow state measurements to drive a snow energy and mass balance model and a snow data assimilation system at 1 km grid scale for the USA (Carroll et al., 2006). Examples of the NSA snow state estimates include SWE, snow depth, snow temperature, snow melt and sublimation. It should be noted that in situ snow and meteorological measurements are included in the SWE state analysis which contributes to the accurate performance in many areas of the USA. However, it is unknown how well the system performs in regions where few or no in situ measurements are available, such as in remote mountain or high latitude regions.

For predictive land surface models, such as the Canadian Land Surface Scheme, the effective representation of SWE is also achieved through a snow energy balance model that is driven by in situ meteorological measurements, i.e. net solar and longwave radiation, air temperature and relative humidity and wind speed (Brown et al., 2006). However, Versegny (2000) indicated that it is unclear how well these

models will perform in regions where in situ observations for model forcing are few or unavailable. Until this performance is better understood it is important that multi-scale satellite remote sensing retrieval schemes and technologies be developed and improved to enhance our observational capabilities of snow. Furthermore, without in situ measurements of snow state variables in remote regions, remote sensing measurements of snow offer the best hope of mapping SCE and estimating SWE in combination with snow energy and mass balance models to estimate snow variables. With the current International Polar Year (2007–2009) highlighting science and societal issues in the polar regions (www.ipy.org), there will be several opportunities to develop combined remote sensing and modeling approaches; this is an exciting time for global change studies of snow and ice.

References

- Abdalati, W. and K. Steffen, 2001. Greenland ice sheet melt extent: 1979–1999. *Journal of Geophysical Research*, 106(D24): 33: 983–989.
- ACIA, 2005. Arctic climate impact assessment. Cambridge, U.K. Cambridge University Press, 1042pp.
- Andreassen, L.M., H. Elvehoy, B. Kjollmoen, R.V. Engeset and N. Haakensen, 2005. Glacier mass-balance and length variation in Norway. *Annals of Glaciology*, 42: 317–325.
- Arendt, A.A., K.A. Echelmeyer, W.D. Harrison, C.S. Lingle and V.B. Valentine, 2002: Rapid wastage of Alaska glaciers and their contribution to rising sea level, *Science*, 297: 382–386.
- Armstrong, R.L., and M.J. Brodzik, 2001. Recent Northern Hemisphere snow extent: A comparison of data derived from visible and microwave sensors. *Geophysical Research Letters*, 28(19): 3673–3676.
- Armstrong, R.L., M.J. Brodzik, K. Knowles, and M. Savoie. 2005. *Global monthly EASE-Grid snow water equivalent climatology*. Boulder, CO: National Snow and Ice Data Center. Digital media.
- Atkinson, P.M. and R.E.J. Kelly, 1997. Scaling-up point snow depth data in the U.K. for comparison with SSM/I imagery, *International Journal of Remote Sensing*, 18(2): 437–443.
- Bader, H., 1962. *The Physics and Mechanics of Snow as a Material*, Cold Regions Research and Engineering Laboratory, Hanover, NH, Report II-B, p.1.
- Bamber, J.L. and A.J. Payne, eds. 2004. Mass balance of the cryosphere: Observations and modelling of contemporary and future changes. Cambridge: Cambridge University Press.
- Bloschl G. 1999. Scaling issues in snow hydrology, *Hydrological Processes*, 13(14–15): 2149–2175.
- Box, J.E. 2002. Survey of Greenland instrumental temperature records: 1873–2001. *International Journal of Climatology*, 22(15): 1829–1847.
- Braithwaite, R.J. 2002. Glacier mass balance: The first 50 years of international monitoring. *Progress in Physical Geography*, 26(1), 76–95.
- Brown, R., P.Bartlett, M.MacKay and D.Versegny, 2006. Evaluation of snow cover in CLASS for SnowMIP, *Atmosphere-Ocean*, 44: 223–238.
- Brown, R.D. and R.O. Braaten. 1998. Spatial and temporal variability of Canadian monthly snow depths, 1946–1995. *Atmosphere-Ocean*, 36, 37–45.
- Brown, R.E. 2000. Northern Hemisphere snow cover variability and change, 1915–1997. *Journal of Climate*, 13, 2339–2355.
- Bunting, J.T. and R.P. d'Entremont, 1982. Improved cloud detection utilizing defense meteorological satellite program near infrared measurements, Air Force Geophysics laboratory, Hanscom AFB, MA, AFGL-TR-82-0027, Environmental Research Papers No. 765, 91p.

- Carroll, T.R., 1995. Remote sensing of snow in the cold regions, *Proceedings of the First Moderate Resolution Imaging Spectroradiometer (MODIS) Snow and Ice Workshop*, 13–14 September, 1995, Greenbelt, MD, NASA Conf. Pub. 3318, pp.3–14.
- Carroll, T., D. Cline, G. Fall, A. Nilsson, L. Li and A. Rost, 2001. NOHRSC operations and the simulation of snow cover properties for the coterminous U.S., *Proceedings of the 69th Western Snow Conference*, 16–19 April, 2001, Sun Valley, Idaho.
- Carroll, T., D.Cline, C.Olheiser, A.Rost, A.Nilsson, G.Fall, C.Bovitz and L.Li, 2006. NOAA's National Snow Analysis, *Proceedings of the 74th Western Snow Conference* Las Cruces, NM April 17–20 2006.
- Ceballos, J.L., C. Euscategui, J. Ramirez, M. Canon, C. Huggel, W. Haeberli and H. Machguth, 2006. Fast shrinkage of tropical glaciers in Columbia, *Annals of Glaciology*, 43: 194–206.
- Chang, A.T.C., J.L. Foster and D.K. Hall, 1987. Nimbus-7 SMMR derived global snow cover parameters, *Annals of Glaciology*, 9: 39–44.
- Choudhury, B.J. and A.T.C. Chang, 1979. Two-stream theory of reflectance of snow, *IEEE Transactions on Geoscience and Remote Sensing*, GE-17(3): 63–68.
- Colbeck, 1982. An overview of seasonal snow metamorphism, *Reviews of Geophysics and Space Physics*, 20(1): 45–61.
- Colton M.C., and G.A. Poe, 1999. Intersensor calibration of DMSP SSM/T's: F-8 to F-14, 1987–1997, *IEEE Transactions on Geoscience and Remote Sensing* 37(1): 418–439.
- Comiso, J. 2001. Satellite-observed variability and trend in sea-ice extent, surface temperature, albedo and clouds in the Arctic, *Annals in Glaciology*, 33: 457–473.
- Comiso, J.C. 2006. Arctic warming signals from satellite observations. *Weather*, 61(3): 70–76.
- Crane, R.G. and M.R. Anderson, 1984. Satellite discrimination of snow/cloud surfaces, *International Journal of Remote Sensing*, 5(1): 213–223.
- Davis, R. E., R. Jordan, S.F. Daly, G. G. Koenig, 2001. Validation of snow models, In M.G. Anderson and P.D. Bates, Eds, *Model validation: Perspectives in hydrological science* (pp. 261–292). John Wiley & Sons Ltd.
- Derksen, C., A. Walker, E. LeDrew and B. Goodison, 2002. Time-series analysis of passive-microwave-derived central North American snow water equivalent imagery, *Annals of Glaciology*, 34: 1–7.
- Derksen, C., R. Brown and A.E. Walker, 2004. Merging conventional (1915–1992) and passive microwave (1978–2002) Estimates of snow extent and water equivalent over Central North America. *Journal of Hydrometeorology*, 5(5) DOI: 10.1175/1525–7541(2004)005.
- Derksen, C., A. Walker, B. Goodison, and J. W. Strapp. 2005. Integrating in situ and multi-scale passive microwave data for estimation of sub-grid scale snow water equivalent distribution and variability. *IEEE Transactions on Geoscience and Remote Sensing*. 43(5): 960–972.
- Dozier, J., S.R. Schneider and D.F. McGinnis, Jr., 1981. Effect of grain size and snowpack water equivalence on visible and near-infrared satellite observations of snow, *Water Resources Research*, 17: 1213–1221.
- Dozier, J., 1989. Spectral signature of alpine snow cover from the Landsat thematic mapper, *Remote Sensing of Environment*, 28: 9–22.
- Duguay, C.R. and A. Pietroniro, 2005. *Remote sensing in northern hydrology: Measuring environmental change*. Geophysical monograph 163, Washington D.C.: American Geophysical Union, 160 pp.
- Dyurgerov, M .B. and M. F. Meier. 1997. Year-to-year fluctuation of global mass balance of small glaciers and their contribution to sea level changes. *Arctic and Alpine Research* 29(4): 392–401.
- Dyurgerov, M. and M. Meier, 2000: Twentieth century climate change: evidence from small glaciers., *Proceedings of the National Academy of Sciences of the United States of America*, 1406–1411.
- Evans, S., 1965. The dielectric properties of ice and snow – A review, *Journal of Glaciology*, 5: 773–792.

- Fassnacht, S.R., K.A. Dressler, R.C. Bales, 2003. Snow water equivalent interpolation for the Colorado River Basin from snow telemetry (SNOTEL) data, *Water Resources Research*, 39(8): doi:10.1029/2002WR001512.
- Foster, J.L., D.K. Hall and A.T.C. Chang, 1987. Remote sensing of snow, *EOS Transactions, American Geophysical Union*, 68(32): 681–684.
- Foster, J. L. and A. T. C. Chang, 1993. Snow cover. In R. J. Gurney, C. L. Parkinson, and J. L. Foster, Eds, *Atlas of satellite observations related to global change* (pp. 361–370). Cambridge, U.K.: University of Cambridge Press.
- Foster, J.L., A.T.C. Chang and D.K. Hall, 1997. Comparison of snow mass estimates from a prototype passive microwave snow algorithm, a revised algorithm and snow depth climatology, *Remote Sensing of Environment*, 62: 132–142.
- Frei, A., and D.A. Robinson. 1999. Northern Hemisphere snow extent: Regional variability 1972–1994. *International Journal of Climatology* 19: 1535–1560.
- Goodison, B., and A. Walker, 1995. Canadian development and use of snow cover information from passive microwave satellite data. In B. Choudhury, Y. Kerr, E.Njoku, and P. Pampaloni Eds, *Passive Microwave Remote Sensing of Land-Atmosphere Interactions* (pp 245–262). Utrecht, Netherlands, VSP BV.
- Goita, K., A.E. Walker and B.E. Goodison, 2003. Algorithm development for the estimation of snow water equivalent in the boreal forest using passive microwave data, *International Journal of Remote Sensing*, 24(5): 1097–1102.
- Gregory, J.M., P. Huybrechts and S.C.B. Raper. 2004. Threatened loss of the Greenland ice sheet. *Nature*, 428:616 (8 April 2004).
- Grenfell, T.C, D.K. Perovich and J.A. Ogren, 1981. Spectral albedos of an alpine snowpack, *Cold Regions Science and Technology*, 4: 121–127.
- Greuell, W. and J. Oerlemans. 2005. Validation of AVHRR- and MODIS-derived albedos of snow and ice surfaces by means of helicopter measurements, *Journal of Glaciology*, 51(172): 37–48.
- Greuell, W. and W.H. Knap. 2000. Remote sensing of the albedo and detection of the slush line on the Greenland ice sheet, *Journal of Geophysical Research*, 105(D12): 15: 567–576.
- Grippa, M., N. Mognard, T. Le Toan, and E.G. Josberger, 2004. Siberia snow depth climatology derived from SSM/I data using a combined dynamic and static algorithm, *Remote Sensing of Environment*, 93: 30–41.
- Grody, N. and A. Basist, 1996. Global identification of snowcover using SSM/I measurements, *IEEE Transactions on Geoscience and Remote Sensing*, 34(1): 237–249.
- Groisman, P. Y., T. R. Karl, and R. W. Knight, 1994. Changes of snow cover, temperature, and radiative heat balance over the northern hemisphere. *Journal of Climate*, 7: 1633–1656.
- Haefliger, M., K. Steffen and C. Fowler. 1993. AVHRR surface temperature and narrow-band albedo comparison with ground measurements for the Greenland ice sheet. *Annals of Glaciology*, 17: 49–54.
- Hall, D.K., J.L. Foster and A.T.C. Chang, 1982. Measurement and modeling of microwave emission from forested snowfields in Michigan, *Nordic Hydrology*, 13: 129–138.
- Hall, D.K, R.E.J. Kelly, J.L. Foster and A.T.C. Chang, 2005. Estimation of snow extent and snow properties. In Anderson, M.G., Ed, *Encyclopedia of Hydrological Sciences*, Chichester: John Wiley and Sons, Ltd., Volume 2, pp.811–830, ISBN: 0-471-49103-9.
- Hall, D.K., K.J. Bayr, W. Schöner, R.A. Bindschadler and J.Y.L. Chien, 2003. Consideration of the errors inherent in mapping historical glacier positions in Austria from the ground and space (1893–2001), *Remote Sensing of Environment*, 86: 566–577.
- Hall, D.K., R.S. Williams, Jr., and N.E. DiGirolamo, submitted: Greenland ice sheet surface-Temperature and Melt Variability: 2000–2006.
- Hall, D.K., R.S. Williams, Jr., K.A. Casey, N.E. DiGirolamo and Z. Wan. 2006. Satellite-derived, melt-season surface temperature of the Greenland Ice Sheet (2000–2005) and its relationship to mass balance. *Geophysical Research Letters*, 33:L11501, doi:10.1029/2006GL026444.
- Hall, D.K. and G.A. Riggs, 2007. Accuracy assessment of the MODIS snow-cover products, *Hydrological Processes*, in press.

- Hallikainen, M., 1984. Retrieval of snow water equivalent from Nimbus-7 SMMR data: effect of land-cover categories and weather conditions, *IEEE Journal of Oceanic Engineering*, OE-9(5): 372–376.
- Hallikainen, M. and F.T. Ulaby, 1986. Dielectric and scattering behaviour of snow at microwave frequencies, *Proceedings of the International Geoscience and Remote Sensing Symposium*, 8–11 September 1986, Zurich, Switzerland, pp. 87–91.
- Hallikainen M. and P. Jolma 1992. Comparison of algorithms for the retrieval of snow water equivalent from NIMBUS-7 SMMR data in Finland. *IEEE Transactions on Geoscience and Remote Sensing*, **30**: 124–131.
- Hansen, J. and L. Nazarenko, 2004. Soot climate forcing via snow and ice albedos, *Proceedings of the National Academy of Sciences*, 101(2): 423–428.
- IPCC, 2001. Climate Change 2001. The scientific basis. In J.T. Houghton, Y. Ding, D.J. Griggs, M. Noguer, P.J. van der Linden, X. Dai, K. Maskell, and C.A. Johnson Eds, *Contribution of working group I to the third assessment report of the intergovernmental panel on climate change* (881 pp). Cambridge University Press, Cambridge, United Kingdom and New York, NY, USA.
- Jordan, R. 1991. A one-dimensional temperature model for a snow cover, Special Report 91–16, U.S. Army Corps of Engineers, Cold Regions Research and Engineering Laboratory, Hanover, New Hampshire, 1989.
- Kargel, J.S. and 16 others, 2005. Multispectral imaging contributions to global land ice measurements from space, *Remote Sensing of Environment*, 99: 187–219.
- Kelly, R.E.J., A.T.C. Chang, L. Tsang, and J.L. Foster, 2003. Development of a prototype AMSR-E global snow area and snow volume algorithm, *IEEE Transactions on Geoscience and Remote Sensing*, **41**(2): 230–242.
- Kelly, R. E. J., A. T. C. Chang, and J. L. Foster. 2004. updated daily. *AMSR-E/Aqua daily L3 global snow water equivalent EASE-Grids V001*, March to June 2004. Boulder, CO, USA: National Snow and Ice Data Center. Digital media.
- Key, J. and M. Haefliger. 1992. Arctic ice surface temperature retrieval from AVHRR thermal channels. *Journal of Geophysical Research*, 97(D5): 5885–5893.
- Klein, A.G., D.K. Hall, and G. Riggs, 1998. Improving snow-cover mapping in forests through the use of a canopy reflectance model, *Hydrological Processes*, 12: 1723–1744.
- Knap, W. H., J. Oerlemans. 1996. The surface albedo of the Greenland ice sheet: satellite-derived and in situ measurements in the Søndre Strømfjord area during the 1991 melt season. *Journal of Glaciology*, **42**(141): 364–374.
- Kononov, Y. M., M.D. Ananicheva and I.C. Willis, 2005. High-resolution reconstruction of Polar Ural glacier mass balance for the last millennium, *Annals of Glaciology*, 42(1): 163–170.
- Koskinen J.T., J.T. Pulliainen, and M.T. Hallikainen, 1997. The use of ERS-1 SAR data in snow melt monitoring. *IEEE Trans. Geosc. Rem. Sens.*, 35(3): 601–610.
- Krabill, W., E. Hanna, P. Huybrechts, W. Abdalati, J. Cappelen, B. Csatho, E. Frederick, S. Manizade, C. Martin, J. Sonntag, R. Swift, R. Thomas, W. and J. Yungel. 2004. Greenland Ice Sheet: Increased coastal thinning, *Geophysical Research Letters*, 31, L24402, doi:10/1029/2004GL021533.
- Krabill, W., W. Abdalati, E. Frederick, S. Manizade, C. Martin, J. Sontag, R. Swift, R. Thomas, W. Wright and J. Yungel. 2000. Greenland ice sheet: High-elevation balance and peripheral thinning. *Science*, 289: 428–430.
- Kunzi, K.F., S. Patil and H. Rott, 1982. Snow-cover parameters retrieved from Nimbus-7 Scanning Multichannel Microwave Radiometer (SMMR) data, *IEEE Transactions on Geoscience and Remote Sensing*, GE-20(4): 452–467.
- Liang, S., J. Stroeve, and J.E. Box, 2005. Mapping daily snow/ice shortwave broadband albedo from Moderate Resolution Imaging Spectroradiometer (MODIS): The improved direct retrieval algorithm and validation with Greenland in situ measurement. *Journal of Geophysical Research*, 110, D10109, doi:10.1029/2004JD005493.
- Luthcke, S.B., H.J. Zwally, W. Abdalati, D.D. Rowlands, R.D. Ray, R.S. Nerem, F.G. Lemoine, J.J. McCarthy and D.S. Chinn. 2006. Recent Greenland ice mass loss by drainage system from satellite gravity observations. *Science*, 19 October 2006, 10.1126/science.1130776.

- Male, D.H., 1980. The seasonal snowcover. In S. Colbeck, Ed, *Dynamics of snow and ice masses* (pp. 305–395). New York: Academic Press.
- Marshall, H.P., G. Koh, and R. Forster. 2004. Ground-based frequency-modulated continuous wave radar measurements in wet and dry snowpacks. Colorado, USA: An Analysis and Summary of the 2002–03 NASA CLPX Data. *Hydrological Processes*, 18(18): 3609–3622.
- Matson, M., C.F. Roepewski and M.S. Varnadore, 1986. *An Atlas of satellite-derived northern hemisphere snow cover frequency* (75 pp). Washington D.C.: National Weather Service.
- Mätzler, C. and E. Schanda, 1984. Snow mapping with active microwave sensors, *International Journal of Remote Sensing*, 5(2): 409–422.
- Meier, M.F. 1998. Monitoring ice sheets, ice caps and glaciers. In W. Haeberli, M. Hoelze and S. Suter, Eds, *Into the second century of Worldwide Glacier Monitoring – prospects and Strategies* (No. 56, pp. 209–214). UNESCO, Studies and reports in hydrology.
- Nagler T. and H. Rott, 2000. Retrieval of wet snow by means of multitemporal SAR data, *IEEE Transactions on Geoscience and Remote Sensing*, 38(2): 754–765.
- Nghiem, S., K. Steffen, R. Kwok and W.-Y. Tsai. 2001. Detection of snowmelt regions on the Greenland ice sheet using diurnal backscatter change. *Journal of Glaciology*, 47(159): 593–547.
- Nolin, A.W. and J.C. Stroeve. 1997. The changing albedo of the Greenland ice sheet: Implications for climate modeling, *Annals of Glaciology*, 25: 51–57.
- Nolin, A.W. and S. Liang, 2000. Progress in bi-directional reflectance modeling and applications for surface particulate media: snow and soils, *Remote Sensing Reviews*, 18: 307–342.
- O'Brien, H.W. and R.H. Munis, 1975. Red and near-infrared spectral reflectance of snow, Operational Applications of Satellite Snowcover Observations, a workshop held in South Lake Tahoe, CA, 18–20 August, 1975, NASA SP-391.
- Ohmura, A., 2006. Changes in mountain glaciers and ice caps during the 20th century, *Annals of Glaciology*, 43: 361–368.
- Paterson, W.S.B. 1994. *The Physics of Glaciers*, 3rd edn. London: Pergamon press.
- Papa F., B. Legrésy, N. Mognard, E.D. Josberger and Rémy, F. 2002. Snow depth estimations with the Topex-Poseidon altimeter and radiometer, *IEEE Geoscience and Remote Sensing*, 40(10): 2162–2170.
- Paul, F., A. Kääb, M. Maisch, T. Kellenberger and W. Haeberli, 2004. Rapid disintegration of Alpine glaciers observed with satellite data, *Geophysical Research Letters*, 31, L21402, doi:10.1029/2004GL020816, 2004.
- Ramsay, B., 1998. The interactive multisensor snow and ice mapping system, *Hydrological Processes*, 12: 1537–1546.
- Rawlins, M.A., K.C. McDonald, S. Froking, R.B. Lammers, M. Fahnestock, J.S. Kimball, and C.J. Vorosmarty, 2005. Remote sensing of snow at the pan-Arctic scale using the SeaWinds scatterometer. *Journal of Hydrology*, 312: 294–311.
- Richter-Menge, J. and 24 others, 2006. State of the Arctic Report. NOAA OAR Special Report, NOAA/OAR/PMEL, Contribution No. 2952 from NOAA, Pacific Marine Environmental Laboratory, Seattle, WA, 36 p.
- Riggs, G.A., D.K. Hall and V. Salomonson, 2006. MODIS Snow Product User Guide to Collection 5, NASA Goddard Space Flight Center, <http://modis-snow-ice.gsfc.nasa.gov/> 80pp.
- Rignot, E. and P. Kanagaratnam. 2006. Changes in the velocity structure of the Greenland Ice Sheet. *Science*, 311: 986–990.
- Robinson, D.A., 1993. Hemispheric snow cover from satellites, *Annals of Glaciology*, 17: 367–371.
- Robinson, D.A. 1997. Hemispheric snow cover and surface albedo for model validation. *Annals of Glaciology*, 25: 241–245.
- Robinson, D.A. and A. Frei, 2000. Seasonal Variability of Northern Hemisphere Snow Extent Using Visible Satellite Data. *Professional Geographer*, 51: 307–314.
- Robinson, D.A. and G. Kukla, 1985. Maximum surface albedo of seasonally snow covered lands in the Northern Hemisphere. *Journal of Climate and Applied Meteorology*, 24: 402–411.

- Rott, H., 1984. The analysis of backscattering properties from SAR data of mountainous regions, *IEEE Journal of Oceanic Engineering*, OE-0: 347–355.
- Rott, H. and T. Nagler, 1993. Capabilities of ERS-1 SAR for snow and glacier monitoring in alpine areas, In *Proceedings of the Second ERS-1 Symposium*, 1–6, ESA SP-359.
- Schanda, E., C. Mätzler and K. Künzi, 1983. Microwave remote sensing of snow cover, *International Journal of Remote Sensing*, 4(1): 149–158.
- Shi, J., J. Dozier and H. Rott, 1994. Snow mapping in alpine regions with synthetic aperture radar, *IEEE Journal of Geoscience and Remote Sensing*, 32(1): 152–158.
- Shi, J.C. and J. Dozier, 1995. Inferring snow wetness using SIR-C C-band polarimetric synthetic aperture radar, *IEEE Transactions on Geoscience and Remote Sensing*, 33(4): 905–914.
- Singer, F.S. and R.W. Popham, 1963. Non-meteorological observations from weather satellites, *Astronautics and Aerospace Engineering*, 1(3): 89–92.
- Slaymaker, H.O. and R.E.J. Kelly, 2007. *The Cryosphere and Global Environmental Change*, Oxford: Blackwell Publishing, 272pp.
- Steffen, K., S.V. Nghiem, R. Huff, and G. Neumann. 2004. The melt anomaly of 2002 on the Greenland Ice Sheet from active and passive microwave satellite observations. *Geophysical Research Letters*, 31, L20402, doi:10.1029/2004GL020444.
- Steffen, K. and R. Huff, 2005. Greenland melt extent: 2005, <http://colorado.edu/steffen/greenland/melt2005>
- Steffen, K. and J. Box. 2001. Surface climatology of the Greenland ice sheet: Greenland climate network 1995–1999. *Journal of Geophysical Research*, 106(D24): 33: 951–964.
- Stiles, W.H. and F.T. Ulaby, 1980. The active and passive microwave response to snow parameters – 1. Wetness, *Journal of Geophysical Research*, 85(C2): 1037–1044.
- Stiles, W.H., F.T. Ulaby and A. Rango, 1981. Microwave measurements of snowpack properties, *Nordic Hydrology*, 12: 143–166.
- Stroeve, J. and K. Steffen. 1998. Variability of AVHRR-derived clear-sky surface temperature over the Greenland ice sheet. *Journal of Applied Meteorology*, 37: 23–31.
- Stroeve, J., A. Nolin and K. Steffen. 1997. Comparison of AVHRR-derived and in situ surface albedo over the Greenland Ice Sheet, *Remote Sensing of Environment*, 62: 262–276.
- Stroeve, J., J.E. Box, C. Fowler, T. Haran, and J. Key, 2001. Intercomparison between in situ and AVHRR polar Pathfinder-derived surface albedo over Greenland. *Remote Sensing of Environment*. 75: 360–374.
- Stroeve, J., J.E. Box and T. Haran, 2006. Evaluation of the MODIS (MOD10A1) daily snow albedo product over the Greenland ice sheet, *Remote Sensing of Environment*, 105: 155–171.
- Sun, C.Y, C.M.U. Neale and J.J. McDonnell, 1996. Snow wetness estimates of vegetated terrain from satellite passive microwave data. *Hydrological Processes*, 10: 1619–1628.
- Tait, A. 1998. Estimation of snow water equivalent using passive microwave radiation data. *Remote Sensing of Environment*, 64: 286–291.
- Tait A.B., D.K. Hall, J.L. Foster, and R.L. Armstrong, 2000. Utilizing multiple datasets for snow-cover mapping *Remote Sensing of Environment* 72(1): 111–126.
- Tait A.B., J.S. Barton and D.K. Hall, 2001. A prototype MODIS-SSM/I snow-mapping algorithm *International Journal of Remote Sensing* 22(17): 3275–3284.
- Tarboton, D. and C.Luce, 1996. Utah Energy Balance snow accumulation and melt model (UEB), Computer model technical description and users guide, Utah Water Research Laboratory and USDA Forest Service Intermountain Research Station.
- Tedesco M., J. Pulliainen, P. Pampaloni and M. Hallikainen, 2004. Artificial neural network based techniques for the retrieval of SWE and snow depth from SSM/I data, *Remote Sensing of Environment*, 90(1): 76–85.
- Tribbeck, M., R. Gurney, E. Morris and W. Pearson, 2004. A new Snow-SVAT to simulate the accumulation and ablation of seasonal snow cover beneath a forest canopy, *Journal of Glaciology*, 50: 171–182.
- Ulaby, F.T. and W.H. Stiles, 1980. The active and passive microwave response to snow parameters 2. water equivalent of dry snow, *Journal of Geophysical Research*, 85(C2): 1045–1049.

- Ulaby, F.T. and W.H. Stiles, 1981. Microwave response of snow, *Advanced Space Research*, 1: 131–149.
- Ulaby, F.T., R.K. Moore and A.K. Fung, 1986. Microwave remote sensing, active and passive, Vol. 3, From Theory to Applications, Reading, MA, Addison-Wesley Publishing Co., p. 2162
- Verseghy, D., 2000. The Canadian Land Surface Scheme (CLASS): Its history and future, *Atmosphere-Ocean*, 38: 1–13.
- Waite, W.P. and H.C. McDonald, 1970. Snowfield mapping with K-band radar, *Remote Sensing of Environment*, 1: 143–150.
- Walker, A.E. and B.E. Goodison, 1993. Discrimination of a wet snow cover using passive-microwave satellite data, *Annals of Glaciology*, 17: 307–311.
- Walsh, J. E., 1991. Operational satellites and the global monitoring of snow and ice, *Global Planetary Change*, 90(1–3): 219–224.
- Wang L.B., M. Sharp, R. Brown, C. Derksen and B. Rivard, 2005. Evaluation of spring snow covered area depletion in the Canadian Arctic from NOAA snow charts, *Remote Sensing of Environment*, 95 (4): 453–463.
- Warren, S. 1982. Optical properties of snow. *Reviews of Geophysics and Space Physics*, 20: 67–89.
- Warren, S.G. and W.J. Wiscombe, 1980. A model for the spectral albedo of snow, II: Snow containing atmospheric aerosols, *Journal of the Atmospheric Sciences*, 37: 2734–2745.

Index

- ADEOS, 61, 71, 73
Advanced Microwave Scanning Radiometer (AMSR-E), 37, 155, 200
Advanced Spaceborne Thermal Emission and Reflection Radiometer (ASTER), 34, 36, 41, 112, 130, 205
Advanced Very High Resolution Radiometer (AVHRR), 111, 152, 180, 198, 204–206, 210–211, 452
Advanced wide-field sensor (AWiFS), 33
Africa, 17, 51, 85, 91–93, 97–98, 100–102, 104, 109, 120
Agriculture – Croplands, 100–106
Albedo, 25, 52, 86, 124, 180, 189, 190, 193–194, 198–199, 203–206, 210
Algorithm Theoretical Basis Documents (ATBD), *see* Earth Observing System (EOS)
Along Track Scanning Radiometer (ATSR), 52, 112, 153
Altimeter, 160–164
Antartic, 69, 75
Aqua, 33–34
Asia, 11, 85, 97, 120, 165
Atmospheric Infrared Sounder (AIRS), 37
Aura, 25, 38, 74, 79

Biomass, 109–131
Biomass burning, 109–131
Burn scars, 128, 130
Burn severity, 113, 122, 126, 131

CALIPSO, 25
Carbon, 6, 11, 17, 24–25, 36, 52, 56–57, 66, 86, 110, 126, 181
CEOS (Committee on Earth Observation Satellites), 10, 45, 51
Change detection, 94, 125
Classification, 80, 88–89, 94–95, 98–99, 101, 104, 111, 114–115

Climate change, 2, 5, 15, 24, 41, 51, 52, 62, 86, 110–111, 126, 143–144
Cloud, 25, 33, 34, 36–38, 43–44, 71, 98, 99, 119, 122, 177, 181, 191, 198, 200, 205, 208, 211
Clouds and Earth Radiant Energy System (CERES), 25
Cloudsat, 25
CO₂, 1, 6, 52, 62, 145, 150
Coastal Zone Color Scanner (CZCS), 152
Committee on Earth Observing Systems (CEOS), 183
Cryosphere, 189, 190, 191

Data access, 39–41
Defense Meteorological Satellite Program (DMSP), 43–44, 121, 200
Deforestation, 57, 85, 92, 93, 95–100, 105, 110, 111, 121, 170
Distributed Active Archive Center (DAAC), 34, 40, 43
Drought, 5, 100, 104, 165, 170, 175–176, 180, 182

Earth Observing System (EOS), 9, 23–25, 27, 33, 39–41, 45, 84, 121, 155, 180, 183–184
Earth Observing System Data and Information System (EOSDIS), 40
Earth Radiation Budget Satellite (ERBS), 38
The Earth System Science Partnership (ESSP), 10–16
Ecosystems, 1–2, 5–6, 9, 10, 12, 17–19, 24, 27, 41, 89, 92–93, 96, 100, 106, 109, 134
El Niño Southern Oscillation (ENSO), 5, 144
Emissions, 19, 51, 54, 56–57, 61, 86, 109, 110, 114, 116, 118, 121, 123, 125–128, 131, 194
Enhanced Thematic Mapper (ETM), 31, 32, 39, 98, 101, 104, 107, 123, 126, 130, 205

- ENVISAT, 49, 52, 55, 61, 75–76, 112, 120, 125, 152, 158, 161, 203, 211
 EO-1, 25, 38, 39
 ERS, 61, 75, 112, 120, 124, 153, 158, 161, 203, 211
 Erythemic Radiation, 80–81
 Europe, 148, 149, 150, 205
 European Space Agency (ESA), 49, 75–76, 91, 120, 124–125, 152, 179, 191
 Evaporation, 181–182
 Evapotranspiration, 86, 113, 118, 170, 172, 181

 Fire, 109–131
 Fisheries, 151, 164, 165, 174
 Flood, 5, 88, 92, 94, 170–171, 175, 179, 185
 Forest inventory, 56–57
 Fuel moisture content (FMC), 113, 114, 116–118, 128
 Fuel type, 113, 114–116

 GBA2000, 124, 130–131
 Geostationary Operational Environmental Satellite (GOES), 42, 198, 211
 Geostationary satellites, 42, 118–119, 131, 175, 178, 180
 Glacier, 24, 52, 86, 149, 162, 171, 190–193
 The Global Earth Observation System of Systems (GEOSS), 10, 184
 Global land cover (GLC2000), 85, 88, 90–92
 Global Monitoring of Environment and Security (GMES), 50, 106
 Global Observation of Forest Cover – Global Observation of (GOF-C-GOLD), 106
 Global Ozone Monitoring by Occultation of Stars (GOMOS), 61, 76–79
 Global Ozone Monitoring Experiment (GOME), 61, 75
 GLOBACARBON, 52, 54, 125
 GLOBSCAR, 124, 130, 131
 Gravity Recovery And Climate Experiment (GRACE), 182, 206
 Great Conveyor Belt (GCB), 148–150
 Greenhouse gases, 1, 24, 51–52, 143, 145, 169
 Greenland, 5–6, 144, 148–149, 162–163, 190, 193, 203–206, 210
 Groundwater, 175, 177, 182, 183

 Heat Capacity Mapping Mission (HCMM), 30
 Human health, 11, 174–175, 181, 184
 Hyperion, 38, 126

 Ice, 189–213
 ICESat, 38–39, 116, 191, 206

 Ice sheets, 24, 38, 52, 189–193, 205–206, 208, 210
 Ikonos, 112
 The Integrated Global Observing Strategy (IGOS), 9–10, 15, 182, 183
 Integrated Global Water Cycle Observations (IGWCO), 183
 Intergovernmental Panel on Climate Change (IPCC), 6, 14–16, 24, 144, 149–150
 International Geosphere-Biosphere Programme (IGBP), 11, 14–15, 89, 91, 119
 International Human Dimensions Programme on Global Environmental (IHDP), 10, 12–14
 International Programs, 6–9
 Invasive species, 2, 12

 Jason, 161, 166

 Kyoto Protocol, 19, 56–57

 Land cover/use, 85–107
 Land-cover dynamics, 92–106
 Landsat, 25, 30–33, 34, 39, 41, 45, 87–89, 91, 94, 96, 98, 101, 104, 115, 117, 123, 126, 130, 180, 200, 205–206
 Latin America, 97
 LIDAR, 18, 38, 61, 113, 115–116, 128, 131

 Manned missions, 28–30
 Measurements of Pollution in The Troposphere (MOPITT), 34, 36–37
 MERIS, 52, 91, 125, 152, 155, 166
 METEOSAT, 49–50
 METOP, 43, 158
 Moderate Resolution Imaging Spectroradiometer (MODIS), 25, 34, 61, 88, 91, 112, 117–118, 120–122, 124–125, 130–131, 152, 165, 180, 199–200, 204–206, 210–211
 Montreal Protocol, 61
 Multi-Angle Imaging Spectroradiometer (MISR), 34, 36–37

 National Aeronautics and Space Administration (NASA), 23–45
 National Oceanic and Atmospheric Administration (NOAA), 32, 37, 38, 41–45, 61, 88, 111, 153, 178, 198–199, 208, 211
 National Polar Orbiting Operational Environmental Satellite System (NPOESS), 44–45
 Nimbus, 38, 60–61, 69–71, 73, 200
 NOAA satellite, 38, 42–43, 111, 198

- Normalized Difference Snow Index (NDSI), 199–200
- Normalized Difference Vegetation Index (NDVI), 43, 117–118, 128, 200
- Ocean circulation, 145–150
- Ocean colour, 52, 54, 151, 152
- Ocean Conveyor Belt (OCB), 146
- Ocean eddies, 147–148
- Oceans, 143–166
- Optical depth, 72
- Orbiting Carbon Observatory (OCO), 25
- Ozone, 24, 38, 42, 44, 59–83
- Ozone Monitoring Instrument (OMI), 38, 74, 79
- PARASOL, 25
- Pathfinder AVHRR Land (PAL), 41, 42, 123
- Permafrost, 162, 171, 180, 189–190
- Photography, 28–31, 88, 104, 173
- Pollution, 2, 36, 65
- Population growth, 1, 19, 99–100, 172–173
- Precipitation, 24, 37, 149, 169–172, 174–179, 183–184, 192
- Quickbird, 112
- QuikSCAT, 38, 158–159, 203, 211
- RADAR, 29, 30, 113, 115, 117, 131
- Reservoir, 119, 169–170, 175, 178, 180–182
- Runoff, 170–171, 175, 177, 178–179, 183
- SAC-C, 25
- Salinity, 146, 150–151, 155–156
- Science Partnership, 10–16
- Sea level, 143, 148, 162–164, 166, 193, 205, 210
- Seasat, 30
- SeaWiFS, 152, 166
- Shifting cultivation, 110
- Shuttle Imaging Radar (SIR), 29–30
- Skylab, 28–30, 161
- Snow, 30, 37, 44, 52, 85–86, 144, 171, 175–176, 180, 189–213
- Snow Cover Extent (SCE), 189, 192–193, 198–200, 206–208, 210–211, 213
- Snow water equivalent (SWE), 189, 192, 200–202, 208–210
- Soil Moisture and Ocean Salinity (SMOS), 151, 155–156, 179, 183
- Space Shuttle, 28–30, 38
- SPOT, 32, 88, 90–91, 112, 118, 123–124, 130
- SPOT VGT, *see* VEGETATION
- Television and Infrared Observational Satellite-1 (TIROS-1), 28, 198
- Temperature, 9, 25, 30, 37, 42, 44, 52, 59, 62, 63, 66–68, 70, 78, 113, 116–119, 131, 143–146, 148–151, 153, 155–156, 162, 171–172, 176, 180–182, 189–190, 192–193, 196–197, 199, 203–204, 206, 210–212
- Terra, 25, 33–34, 36–37, 39, 43–44, 74, 112, 121, 199, 205
- Thematic Mapper (TM), 31, 88–89, 98, 101, 104, 111, 200, 205
- Thermohaline circulation (THC), 146, 148–150
- Total Ozone Monitoring System (TOMS), 44, 60, 61, 64, 69–75, 78–79
- Tropical Rainfall Measuring Mission (TRMM), 34, 120, 172, 178
- United National Environment Programme (UNEP), 12, 91, 181
- Urban – Habitat, 110, 173, 174
- Validation (accuracy assessment), 25, 27, 36, 41, 44, 78–79, 83, 85, 89, 94–95, 106, 115–116, 118, 121, 128–130, 160
- VEGETATION, 52
- Visual analysis, 61, 94, 96, 98–99, 101–102, 104
- Water Management, 169–185
- The World Climate Research Programme (WCRP), 11, 15–16, 184